Rethinking plant protein extraction

Interfacial and foaming properties of mildly derived plant protein extracts

Jack Yang

Propositions

1. The degree of purification controls the interfacial and foaming properties of plant protein ingredients.
   (this thesis)

2. Non-linear rheology and microstructure imaging should be standard in characterising the mechanical properties of interfacial films.
   (this thesis)

3. Academic inflation is driven by the high requirements of academic institutions.
   (Yi, G. & Mcmurtrey, M. (2013). The impact of academic inflation on the labour market: if everyone has a PhD, who will be the custodian?, International Journal of Electronic Finance, 7(3/4), 1-13)

4. The reproducibility issues of studies involving people, as highlighted by Aarts, et al., are in fact due to geographical differences.
   (Aarts, A.A. et al. (2015). Estimating the reproducibility of psychological science. Science, 349(6251), 1-7)

5. Sustainability claims are valid only after a comprehensive quantitative analysis, where causality is incorporated.

6. Becoming a true expert in a given field must involve inspiration from other fields.

Propositions belonging to the thesis, entitled

Rethinking plant protein extraction - Interfacial and foaming properties of mildly derived plant protein extracts

Jack Yang

Wageningen, 18 June 2021

Rethinking plant protein extraction

Interfacial and foaming properties of mildly derived plant protein extracts

Jack Yang

Thesis committee

Promotor

Dr L.M.C. Sagis
Associate professor, Physics and Physical Chemistry of Foods
Wageningen University & Research

Co-promotors

Dr C.C. Berton-Carabin
Associate professor, Food Process Engineering
Wageningen University & Research

Dr K. Nikiforidis
Associate professor, Biobased Chemistry and Technology
Wageningen University & Research

Prof. Dr E. van der Linden
Professor of Physics and Physical Chemistry of Foods
Wageningen University & Research

Other members

Prof. Dr R.M. Boom, Wageningen University and Research
Dr V. Garbin, Technical University Delft
Dr G. Waschatko, Cargill R&D Centre Europe, Vilvoorde, Belgium
Prof. Dr S. Drusch, Technical University of Berlin, Germany

This research was conducted under the auspices of Graduate School VLAG
(Advanced Studies in Food Technology, Agrobiotechnology, Nutrition and Health Sciences).

Rethinking plant protein extraction

Interfacial and foaming properties of mildly derived plant protein extracts

Jack Yang

Thesis

submitted in fulfilment of the requirements for the degree of doctor

at Wageningen University & Research

by the authority of the Rector Magnificus,

Prof. Dr A.P.J. Mol,

in the presence of the

Thesis Committee appointed by the Academic Board

to be defended in public

on Friday 18 June 2021

at 4.00 pm in the Aula.

Jack Yang
Rethinking plant protein extraction - Interfacial and foaming properties of mildly derived plant protein extracts
210 pages

PhD thesis, Wageningen University, Wageningen, the Netherlands (2021)
With references, with summary in English

ISBN: 978-94-6395-747-2
DOI: https://doi.org/10.18174/543524

Contents

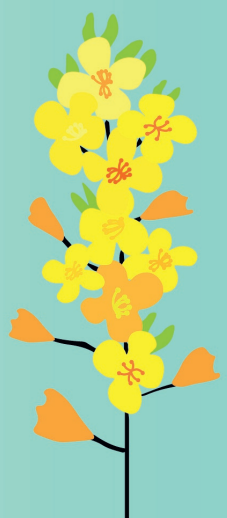

Chapter 1

Introduction and thesis outline

1.1 The plant protein transition

Sustainable food production is currently of global importance to meet the increasing demand for food due to a growing world population, estimated to become 9.6 billion in 2050[1]. In addition to food availability, the environmental impact of food production is also a key topic. Food production was estimated to generate a quarter of global greenhouse gas emissions[2], consume about two-thirds of world freshwater supplies[3], and require half of the world's habitable land[4]. The food industry is a large contributor to climate change, which could even further increase as the agricultural output has to substantially increase by 2050 to meet the increasing demands for food[5]. Therefore, it is a necessity to reduce the environmental impact of food production[6], and one of the main responses is the protein transition from animal-derived to plant-derived sources[7]. The large-scale utilisation of plant-based proteins is a crucial step in reducing the environmental impact of food production, as the primary production of plant proteins has a lower CO_2 and water footprint, and lower land use compared to animal protein production. At the same time, crop cultivation also generates a massive CO_2 uptake, while a large negative output of livestock farming is the increased emission of greenhouse gases, such as methane and nitrous oxide[8]. Changing our diets towards plant-based diets will thus yield climate benefits. However, effective implementation of plant proteins in food production can only be achieved after overcoming one of the major challenges, which is the plant protein extraction process. To better understand the challenges in designing such processes, it is necessary to evaluate the relationship between processing and composition of the plant protein extracts. Additionally, the composition- and structure-function relationships of these extract can be determined. Such an approach would allow the correlation of the plant protein extraction process to the functional properties of the final extract.

1.2 Plant crop composition

Examples of commonly used sources of plant proteins are soybean, pea and lupine. There is an emerging market for rapeseed (*Brassicaceae Cruciferae*) as a plant protein source, which will be studied in this thesis. Rapeseed is the second most grown oilseed in the world[9] and is primarily cultivated for its oil, as the oil content of the seeds is between 40 – 50%[10,11]. The second component, content-wise, is protein, as rapeseed contains between 17 – 26% protein, depending on the breed type and environmental conditions during growth[10]. Rapeseed is also rich in phenols, which are known to induce drawbacks for plant protein extraction[12,13]. Nonetheless, rapeseed possesses the potential as a source for nutritional and functional plant-based ingredients.

1.2.1 Proteins

The majority of proteins in plant crops are storage proteins, which play an essential role in germination, such as an amino acid source or defence proteins. Many types of storage proteins exist, leading to different protein structures and properties among plant sources. Plant proteins are commonly classified based on their solubility using the Osborne classification[14]. Storage proteins can be classified into water-soluble (albumins), dilute saline solution-soluble (globulins), alcohol-soluble (prolamins), and dilute acid or alkali solution-soluble (glutelins). Oilseeds and legumes contain mainly albumins and globulins, with globulins often as the most abundant protein class[15]. Both proteins are separated based on their solubility, as globulins of various plant sources have an isoelectric point (**pI**) between pH 4 – 5[16,17], while albumins remain soluble at an extensive pH range between 2 – 12[18,19]. Plant globulins possess a complex quaternary structure, as they can exist in monomeric, trimeric, hexameric, or even larger conformations, depending on concentration, pH, and ionic strength[20]. The main globulin in rapeseed is called cruciferin (schematic overview in Figure 1.1) and represents about 60% of the total seed protein. The monomer of cruciferin has a molecular weight of about 50 kDa and comprises an α- and β polypeptide chain of 32 and 20 kDa, respectively[21]. The native quaternary protein structure of cruciferin was found to be hexameric and could fall apart into trimers or monomers at lower pH[18]. Albumin is used as a group name to label the water-soluble proteins, and the main albumin in rapeseed is called napin. Napin has a molecular weight of around 18 kDa and consists of two polypeptides of 7 and 11 kDa, which are interlinked by disulphide bonds[18].

1.2.2 Oleosomes

Oil is another major component in oilseeds, such as rapeseed. Plant oil is stored in structures called oleosomes, also known as oil bodies or lipid droplets, with diameters between 0.2-10 µm. Oleosomes are natural oil droplets with a triacylglycerol (**TAG**) core surrounded by a monolayer of phospholipids with anchored proteins (schematic overview in Figure 1.1)[22–24]. The phospholipids and proteins in the membrane interact strongly through hydrophobic and electrostatic interactions, which results in a protective membrane around the TAG core. The membrane was proven to provide high physical and chemical stability against, for instance, lipid oxidation and droplet coalescence[25–28]. Oleosomes can be disrupted by mechanical pressing or using organic solvents, such as hexane, which is commonly applied in plant oil extraction. On the other hand, intact oleosomes can also be obtained by aqueous extraction, as the oleosome surface is hydrophilic[29]. Extracted oleosomes have been extensively studied as natural oil droplets, and may be directly applied in food or cosmetics.

1.2.3 Phenols

Phenols are secondary metabolites in plants and play an important role, such as natural pesticides and protective agents against UV-light[30]. The chemical structure of phenols

contains an aromatic ring with hydroxyl groups, and other functional side groups. Phenols are classified into different groups based on their molecular structure, such as simple phenols, hydroxycinnamic acid derivatives, flavonoids, and tannins. Rapeseed may contain up to 3% phenols[11], with sinapic acid (molecular structure in Figure 1.1) as the most abundant one. These components are generally undesired in foods, as they contribute to a bitter taste and astringency, loss of protein digestibility, and alteration of colour[12,31,32]. Another adverse effect is the binding of phenols on proteins, affecting protein functionality, e.g., solubility, gelation and emulsification[30,33]. Therefore, it is essential to remove phenols in the protein extraction process to obtain protein extracts with high functionality.

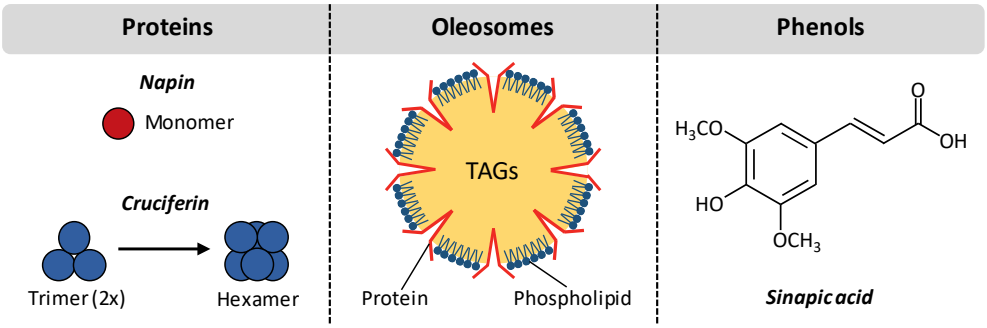

Figure 1.1. Schematic overview of the major rapeseed components: proteins, oleosomes and phenols. Illustrations are not to scale.

1.3 Plant protein extraction

The food industry aims to remove non-proteinaceous impurities in order to produce protein extracts with high predictability of their functional properties. As a result, an extensive extraction process is required to obtain well-standardised protein extracts of high purity (>80%), which are convenient to utilise on an industrial scale. A commonly applied method is an extensive aqueous extraction process, and an overview of such a process is shown in Figure 1.2[34].

The first step is pre-processing the plant crops, often (oil)seeds or beans, by dehulling, milling, and defatting. The defatting step is achieved by a combination of pressing and solvent defatting. The oil industry generally performs pre-processing to obtain plant oils and a side-stream called defatted meal, which is rich in proteins, carbohydrates, and phenols. The soluble proteins and other soluble components are then extracted by dispersing the meal in an alkaline solution in a pH range from 8 to 13[34], as the protein solubility increases at a pH that is further from the pI. The next step is removing insoluble components, followed by an isoelectric point precipitation step, with typically ranges between pH 4–5. Plant globulins often have their pI in this pH range, causing these proteins to precipitate[16,17], which allows them to be separated from the mixture, using techniques such as centrifugation or

filtration. The supernatant is considered a waste-stream and contains solutes (e.g. sugars, minerals, and phenols). Additionally, the waste-stream contains albumin proteins, which often remain soluble in the isoelectric point precipitation step[35–37]. The pellet is recovered and sometimes further purified into a protein extract with high purity.

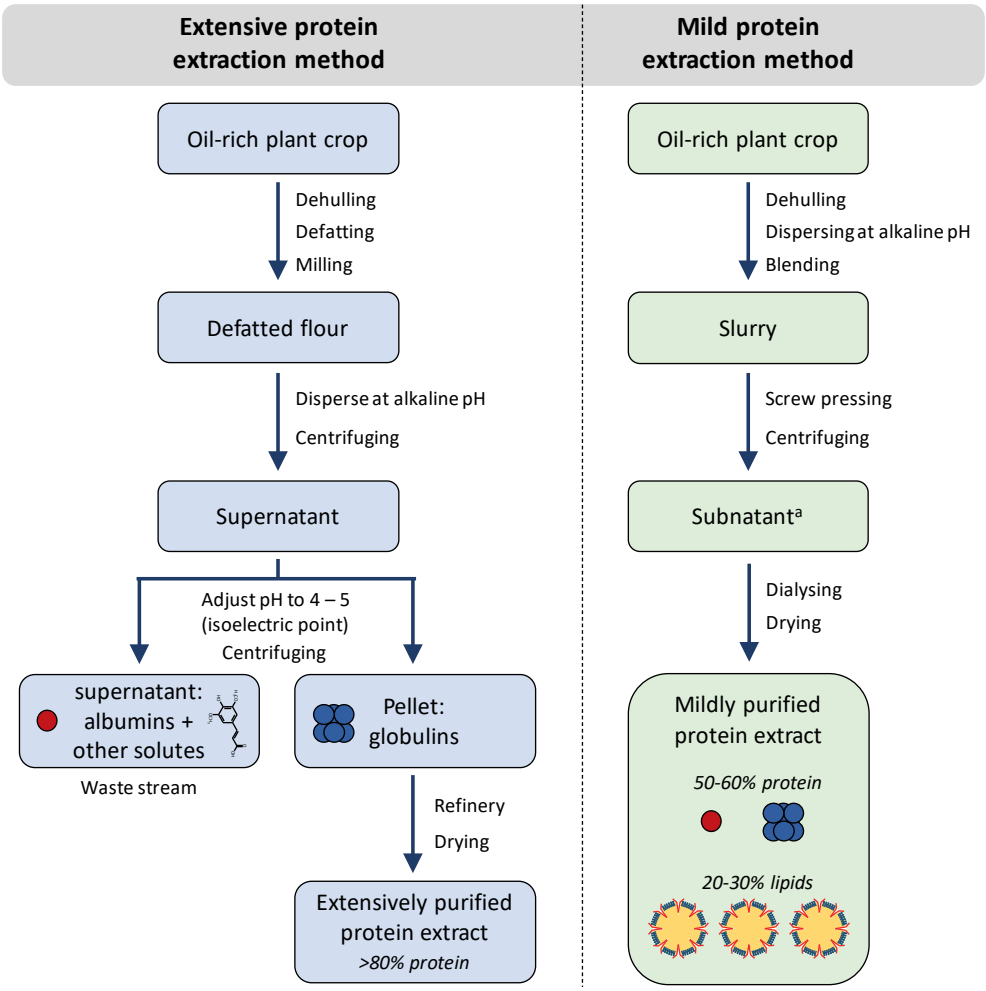

Figure 1.2. A schematic overview of an extensive and mild protein extraction method on an oil-rich plant crop. Legend of illustrations: red sphere = napin, blue sphere = cruciferin, yellow sphere = oleosome, and chemical structure = sinapic acid. [a] The subnatant is the middle layer between the pellet and cream layer.

An extensive protein extraction process has several disadvantages, such as in terms of sustainability. An inefficient plant protein extraction method can vastly reduce its environmental advantage compared to animal-derived proteins. Milder protein extraction methods could be exploited to reduce the number of processing steps, thus reducing the required amounts of water and energy, and reducing the generation of waste streams.

Another drawback is the alteration of the native protein properties, as protein conformation and hydrophobicity are affected by the isoelectric point precipitation step. Such alterations may lead to protein aggregation, as demonstrated for soybean and pea[38,39], and could affect protein functional properties, such as gelation and emulsification[39–42].

Therefore, the interest in mild protein extraction processes has been increasing. The process is mild from a sustainability point aspect, due to the requirement of fewer resources, and from a functionality aspect, as protein nativity is more retained using such type of processs[40,43–45]. An example of such a mild extraction process is illustrated in Figure 1.2[43]. A blending step substitutes the defatting and milling steps in the extensive process, and the isoelectric point precipitation step is excluded. Non-proteinaceous solutes are removed by dialysis or diafiltration. Finally, the mild extraction process yields a mildly derived protein extract with both albumins and globulins. An obvious drawback is a lower protein purity (50 – 60%) in the extract, which contains substantial amounts of non-proteinaceous components, such as lipids, phenols and carbohydrates. Such impurities could result in detrimental effects on the protein functional properties, thus limiting the application of mildly derived protein extracts. Lipids and phenols are notorious for hampering protein functionality, which will be elaborately discussed in further sections.

1.4 Protein functionality: a multi-length scale approach

This thesis focuses on the foaming properties of mildly derived protein extracts. To fully understand the foaming properties of such complex mixtures, a multi-length scale approach must be applied (overview in Figure 1.3). Three length scales are defined, starting with the smallest one, the molecular length scale. At this length scale, the physicochemical properties of components in the bulk are studied, such as chemical structures, surface hydrophobicity, and intermolecular interactions. The largest scale is the macroscopic length scale, where the foam stabilising properties are assessed in terms of foamability and stability. The molecular and macroscopic length scales are bridged by an intermediate one, also known as the mesoscopic length scale or mesostructure. For such systems, the intermediate length scale would be the air-water interfacial layer stabilised by adsorbed components from the bulk.

Commonly used methods to study the interfacial layer are rheology and microstructure imaging. Often, the type and strength of intermolecular interactions at the interface, and the type of formed interfacial layer can be correlated to the molecular properties. Also, the interfacial properties can help to understand the macroscopic foaming properties. Therefore, the extensive and accurate characterisation of the air-water interfacial layer is a crucial link in the multi-length scale approach. This approach is key in linking the plant protein extract's composition and structural properties to the plant protein functional properties. As the protein extract composition is determined by the purification process, the multi-length scale

approach allows an accurate correlation between the plant protein purification process and the functional properties of the produced protein extracts.

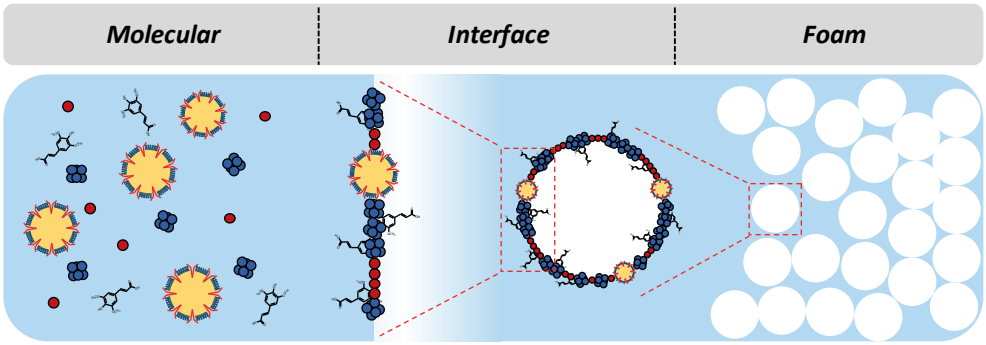

Figure 1.3. Overview of a multi-length scale approach. Legend of illustrations: red sphere = napin, blue sphere = cruciferin, yellow sphere = oleosome, and chemical structure = sinapic acid.

1.5 Interfacial properties of proteins

1.5.1 Interfacial rheology

Proteins are widely applied as functional ingredients to stabilise interfaces in foams and emulsions[46,47]. The efficiency of interface stabilisation by proteins results from two factors: 1. the ability to adsorb at the interface, also known as the adsorption behaviour, and 2. the ability to interact among adsorbed proteins[48]. Additionally, the hydrodynamic conditions play an important role in adsorption behaviour, as pure diffusion-based adsorption could yield a different type of interface compared to a more convection-based interface. This is especially true in mixed systems, where components with a lower surface activity could be more rapidly transferred to the interface in a convection-based system. The adsorption behaviour is also dictated by several protein molecular properties, such as size, charge, and the distribution of hydrophobic and hydrophilic regions on the protein surface[49–51]. Smaller proteins with a low electrostatic net charge can overcome the adsorption barrier of the interface more easily compared to larger aggregated proteins. Also, smaller protein sizes would result in a more efficient packing of the interface, especially in combination with low protein charges, leading to lower repulsive forces between adsorbed proteins. An efficient packing would allow proteins to closely approach each other, and increase the interaction junctions[52]. Thereby, the aforementioned protein properties determine the molecular interactions at the protein interface, thus influencing the mechanical properties of the interfacial protein layer.

Another commonly accepted idea on protein behaviour upon adsorption is the unfolding of protein secondary and tertiary structure[48,53]. Globular proteins in a polar solvent are folded in an effective way to bury a majority of the hydrophobic regions in the protein core, while more hydrophilic regions remain on the surface. Upon adsorption, the proteins are proposed

to unfold and redirect the hydrophobic regions towards the hydrophobic air or oil phase, and the hydrophilic regions towards the water phase[48,54]. Protein unfolding at the interface is claimed to be a long-term process[49], as their surface pressure isotherms often show a long time-tail, where the surface pressure slowly increases, even up to 12 hrs[55]. Constant rearrangements of protein structure seem unlikely, as similar time-tails were previously shown for heated systems, where the proteins denatured and formed aggregates[56]. Other processes could play a more substantial role, which will be elaborately discussed in this thesis.

The adsorbed protein layer is often studied by performing interfacial rheology, where the response of the layer upon deformation is monitored. Two types of rheological tests can be performed: 1. dilatational rheology (Figure 1.4A), and 2. surface shear rheology (Figure 1.4B)[52]. In dilatational rheology, the interfacial layer is deformed by an isotropic compression or extension, where the surface area of the interface changes, while the shape is maintained. Dilatational deformation is commonly performed in a Langmuir trough or a droplet tensiometer, and the output signal is the surface tension/pressure. In surface shear rheology, the shape of the surface is altered, while the total interfacial area remains similar. The most commonly used methods involve using a geometry, such as a bi-cone or double-wall ring, coupled to a rheometer, or a magnetic needle driven rheometer. In dilatational and shear rheology, the standard type of applied deformations is oscillatory, leading to an output in an oscillatory fashion. The stress response of the deformations is typically Fourier transformed, and the intensity and phase of the first harmonic are converted into the first harmonic modulus, also known as the fast Fourier transformed (**FFT**) modulus. The modulus can be separated into a storage/elastic and a loss/viscous modulus. The storage modulus represents the elastic contribution of the rheological response, while the loss modulus characterises the viscous portion of the response.

As mentioned in the previous section, the mechanical properties of the interfacial layer are quantified by calculating surface dilatational or shear moduli, which are obtained from the first-order harmonic of the Fourier spectrum after Fourier transforming the stress signal. Using such a first harmonic modulus is meaningful in the linear viscoelastic (**LVE**) regime, where the material response of the interfacial layer is independent of the applied deformation, as the interfacial microstructure should remain intact. However, protein interfaces are complex viscoelastic materials with a short LVE. Additionally, most of the commonly applied deformations are in a regime, where the applied deformation starts breaking down the interfacial microstructure. The LVE regime can be identified by moduli that are independent of a range of applied deformations, while a decline in moduli upon higher deformation amplitudes indicates the breakdown of the structure, also known as the nonlinear viscoelastic (**NLVE**) regime.

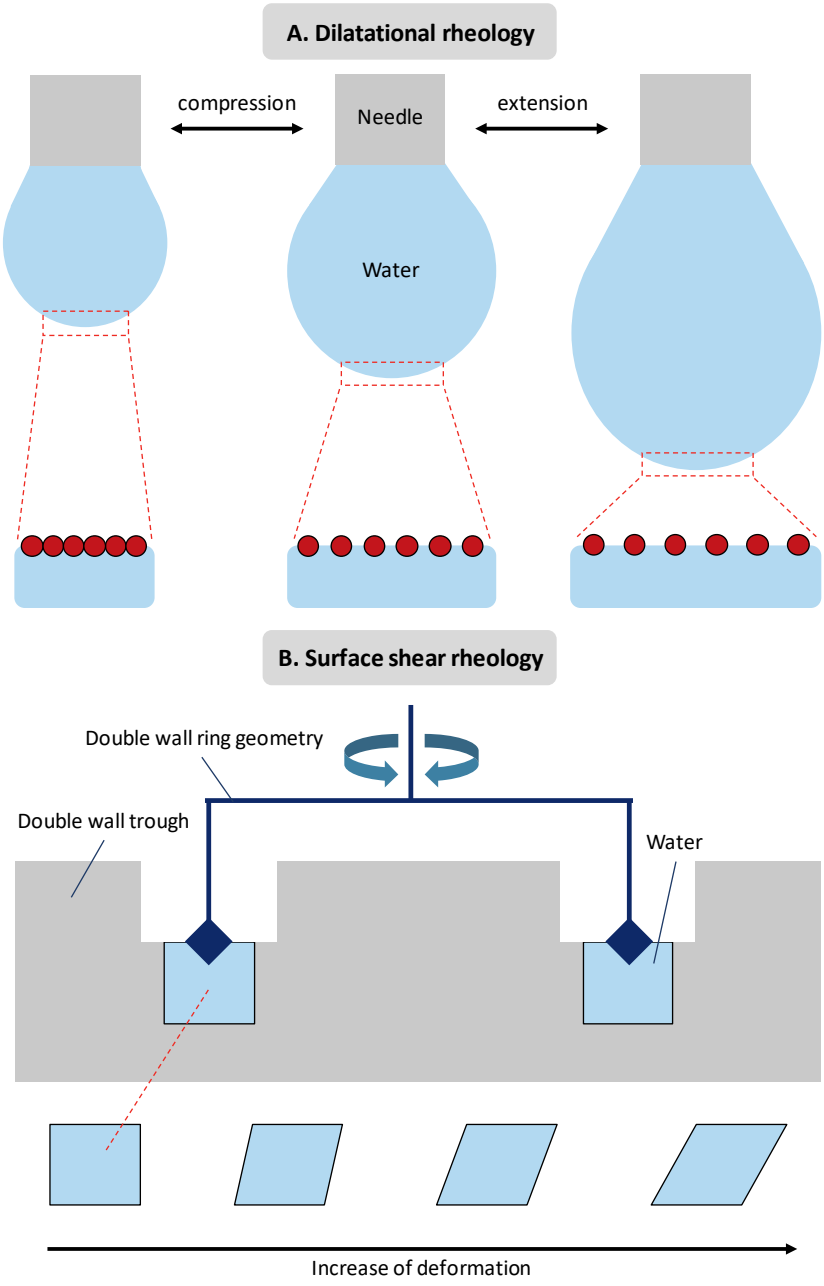

Figure 1.4. Overview of surface dilatational (A) and shear (B) rheology.

The first harmonic moduli are considerably less accurate in the NLVE regime. This inaccuracy is reflected when comparing the original surface pressure signal from an oscillatory dilatational deformation in the NLVE regime with a reconstructed surface pressure signal

from the first harmonic modulus (Figure 1.5). In this comparison, the reconstructed surface pressure signal poorly represents the original signal. Such a mismatch is caused by the disruption of the interfacial microstructure by the applied deformation in the NLVE, and creates nonlinearities in the stress response. This is reflected in the generation of higher-order harmonics in the Fourier spectrum, which are neglected, when only including the first harmonic in the conventional moduli[57,58]. For an accurate analysis of deformations in the NLVE regime, these nonlinearities should be incorporated in the analysis. In most interfacial studies, only one deformation is studied, which is most likely in the NLVE regime. Studying a more extensive range of deformations in the NLVE regime can also yield an additional insight on interactions between stabilisers, thus the type of interfacial layer formed. Unfortunately, such properties cannot be determined accurately with the first harmonic modulus alone, and therefore we will introduce a more effective methodology in the following paragraphs.

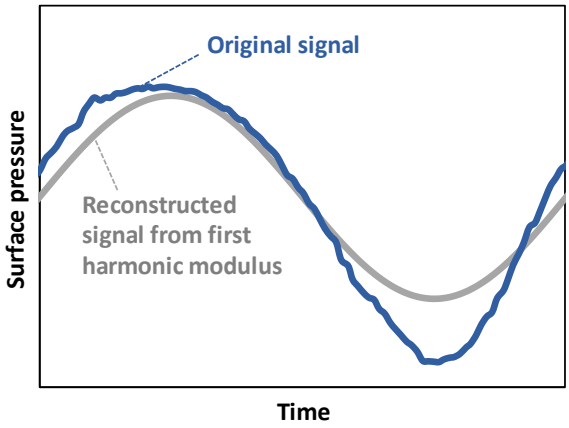

Figure 1.5. Comparison of the original surface pressure signal from an oscillatory dilatational deformation with the reconstructed signal from the first harmonic modulus.

The nonlinearities can be qualitatively analysed by constructing so-called Lissajous plots, where the stress is plotted as a function of the deformation in a cyclic plot (Figure 1.6)[58,59].

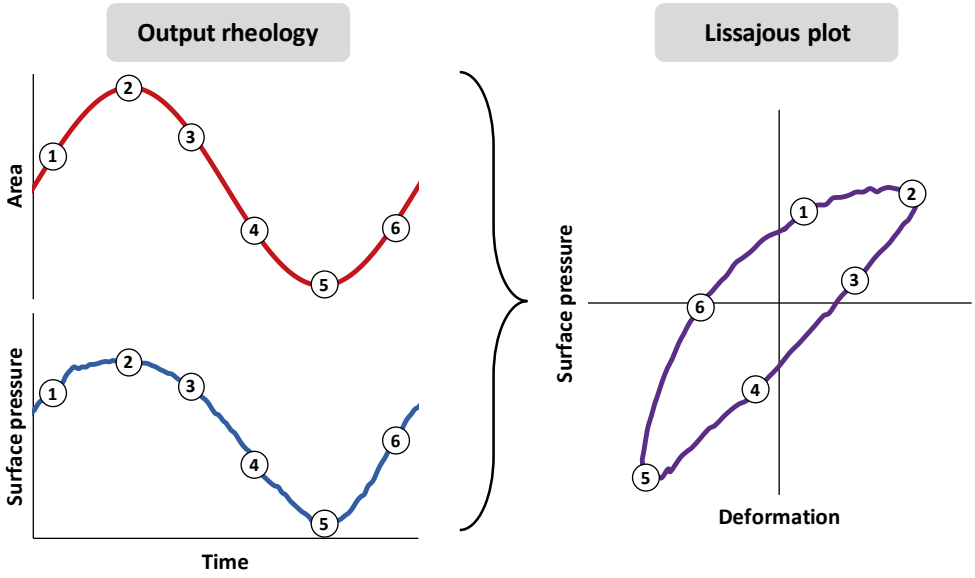

Figure 1.6. An example of transforming the rheological output into a Lissajous plot.

The rheological response of the material upon deformation is reflected in the shape of the Lissajous plots (Figure 1.7).

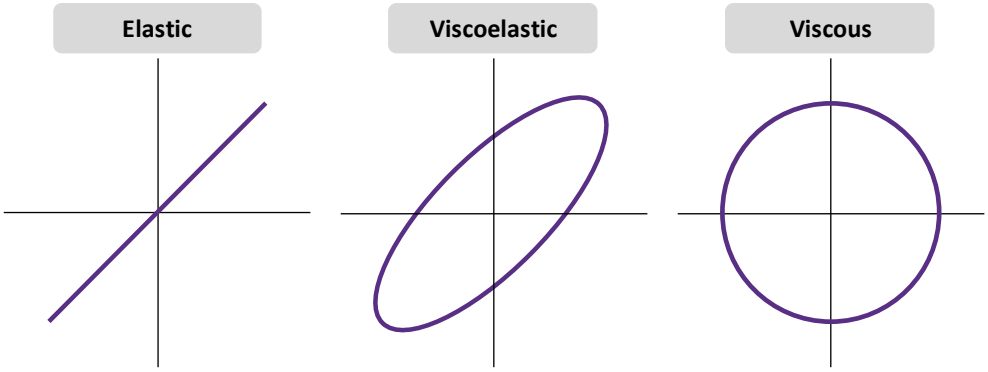

Figure 1.7. Examples of Lissajous plots of surface pressure against deformation.

A pure elastic response is indicated by a straight line, while a pure viscous response is shown as a circle. Most protein-stabilised interfaces form viscoelastic layers, which, in the LVE regime, gives a response in the shape of an ellipse. The wideness of the ellipse is linked to the degree of viscous dissipation in the stress response. Larger deformations often result in

the shift from a predominantly elastic to a more viscous response, leading to a wider Lissajous plot. Another development is the generation of higher even and odd harmonics, which will result in an asymmetric Lissajous plot when comparing the extension and compression part of the cycle (Figure 1.6). Generally, even harmonics are mainly generated in dilatational deformations, since extensions and compressions generate a contribution from the changes of the surface material density, in addition to a contribution from the mechanical properties[60]. Such asymmetries reveal different rheological behaviour in extension or compression of the interfacial layer, which can only be accessed in the Lissajous plots, and are entirely neglected in the first harmonic moduli. Plotting and analysing Lissajous plots was already well-demonstrated and applied to a certain extent in bulk rheology[57,58], while this type of analysis is still upcoming in the field of interfacial rheology. In this thesis, we will perform these analyses and demonstrate the usefulness of Lissajous plots in interfacial science.

1.5.2 Microstructure imaging

Interfacial rheology is an essential tool to characterise the material properties of the interfacial layer. A strong addition to unravelling the interface composition or stabilisation mechanisms is studying the interfacial microstructure by imaging. *In situ* imaging of an interfacial layer is a challenge, and a commonly applied method is Brewster angle microscopy (**BAM**), often combined with a Langmuir trough[61,62]. The Langmuir trough (Figure 1.8) can accurately compress the interfacial layer to a target surface pressure (measured with a Wilhelmy plate), followed by BAM analysis. This microscopy technique introduces polarised light on the surface and analyses the reflection by the surface, which may be converted into images when a particular surface area is scanned. It is a widely applied technique in interfacial science, but a significant drawback is the lateral resolution, as submicron structures cannot be analysed.

The submicron range structures can be analysed by applying other techniques, such as scanning electron microscopy (**SEM**) or atomic force microscopy (**AFM**). However, these techniques require that the sample is deposited onto a solid substrate, which can be done by applying deposition methods in the Langmuir trough. Several types of deposition methods exist, and this work focuses on the Langmuir-Blodgett (**LB**) deposition (Figure 1.8). The LB deposition is performed by perpendicularly inserting a substrate into the subphase of the Langmuir trough. Afterwards, the proteins or other surface-locating compounds are introduced by spreading on the surface or injecting at the bottom of the trough[63,64].

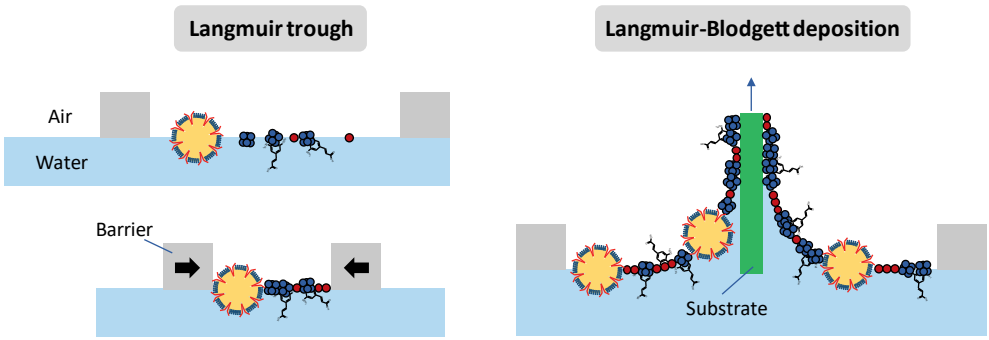

Figure 1.8. Schematic overview of a Langmuir trough and Langmuir-Blodgett deposition. Legend of illustrations: red sphere = napin, blue sphere = cruciferin, yellow sphere = oleosome, and chemical structure = sinapic acid.

In the spreading method, all compounds are forced to locate at the surface of the subphase, which is an advantage, as film formation is relatively fast (<1 hr). Also, a trough area expressed over interfacial compound concentration can be calculated, as a known amount was spread. Spreading might be a suitable method to study a single-component system, but the spreading method forces all components of a mixture onto the surface. This method gives a less accurate representation of a diffusion-based interfacial layer, which are generally formed in rheological experiments. When studying mixtures, injecting the sample at the bottom of the trough is more appropriate, as this method allows the stabilisers to diffuse and adsorb at the interface, thus competing for it. A slight drawback of this method is a long waiting time (>3 hrs) to allow adsorption of sufficient material.

After interfacial layer formation, the Langmuir trough compresses the layer to a targeted compression state, often defined by surface pressure, where the LB deposition starts by slowly drawing up the solid substrate. The substrate is dried to create an LB film and studied by microscopy. SEM is an accurate method to analyse LB films[65], when structures provide a sufficient difference in structure height, and possess a certain hardness. The components in food are biopolymers, which form relative soft solid structures that are damaged by electrons in SEM, especially when the electron density increases upon scanning in the submicron range. A less invasive method is AFM, especially in tapping mode, where high-resolution topographic images of the surface (in submicron scale) can be obtained[66,67]. In this work, we show how microstructure imaging combined with interfacial rheology is a powerful toolset to unravel the secrets of the interface.

1.6 Influence of non-proteinaceous compounds on protein functionality

Non-proteinaceous components can affect the protein-stabilised interfacial layer. Even in extensively purified protein extracts, impurities can remain with immense consequences for the interfacial and foam properties of the proteins. Two components are well known to affect protein functionality: lipids and phenols. The presence and physical/chemical state of these components are primarily affected by the protein extraction process, which will be further elaborated in the following sections.

1.6.1 Lipid – protein interfaces

In section 1.3, we mentioned that the defatted meal from oilseeds is often processed into an extensively purified protein extract. Generally, the defatting step is performed by solvent extraction, which penetrates the oleosome membrane to extract the oil core. As a result, the oleosome membrane remains in the defatted meal and can also be co-extracted into the extensively purified protein extract. The phospholipids in the membrane can largely influence the protein interface, as they may compete with proteins for the interfacial layer by co-adsorption or even (partial) displacements of adsorbed proteins[68,69]. As a result, the cohesiveness of a protein layer is impaired, leading to film rupture, thus resulting in air bubble and foam destabilisation. In the aforementioned mild purification method in Figure 1.2, the oleosomes are not disrupted, and thus partly end up in the protein extract[43]. Oleosomes are known to adsorb at the air-water interface, followed by rupture of the membrane, resulting in the spreading of TAGs and membrane components[70]. However, the rheological properties of an oleosome-stabilised interface have not received much attention yet and will be addressed in this thesis, especially in mixtures with proteins. Additionally, lipid droplets are notorious anti-foaming components[71,72] and can disrupt protein films around air bubbles effectively by, for instance, bridging two interfaces in a thin film. Such destabilisation mechanisms might also occur for oleosomes.

1.6.2 Phenol – protein-based interfaces

As mentioned in section 1.2.3, phenols are omnipresent in plants and can interact with proteins, leading to alteration of the proteins' functional properties. The ability of phenols to interact with proteins depends on their chemical structure, such as the degree of polymerisation, conformational flexibility, and hydrophobicity[30]. These properties lead to non-covalent or covalent phenol-protein interactions. Non-covalent interactions are the result of hydrogen bonding, van der Waals, electrostatic and hydrophobic forces[73]. Covalent interactions between phenols and proteins occur upon oxidation of phenols, where hydroxyl groups on phenyl rings are converted into quinones by either enzymatic or auto-oxidation[74]. The latter is accelerated at alkaline pH or in the presence of oxidising agents. Quinones are highly reactive electrophilic compounds and can form a covalent bond with free thiols and

amino groups on proteins after a Michael addition reaction. Afterwards, the phenols on the protein-phenol complex are available for a second oxidation step, thus crosslinking another protein, finally forming protein-phenol aggregates[33].

Non-covalent interactions can directly occur upon aqueous dispersion of the plant material, as phenols and proteins are extracted into the solution. The dispersion step is performed at alkaline pH (up to 13) to increase protein solubility. However, an unintended consequence at alkaline pH is the accelerated conversion of phenols to quinones, thus initiating covalent phenol-protein interactions. Both non-covalently and covalently bound phenols were previously proven to be difficult to remove[73], and phenol removal steps were also found to alter the protein structure negatively[75]. Such steps are often not performed and result in (non)covalently bound phenols on the proteins. On the other hand, unbound phenols can be removed. In extensive protein purification methods, the unbound phenols are removed with other solutes in the second centrifugation step. A milder approach could be filtration or dialysis, which is often applied in mild purification methods.

The main influence of phenols on protein functionality is the alteration of molecular properties after phenol-protein interactions. Phenols can influence the protein surface hydrophobicity by either introducing hydrophilic groups from the phenols or by covering hydrophobic residues of proteins[76,77]. Upon binding, phenols may also alter the protein secondary and tertiary structure, and could result in the exposure of buried hydrophobic residues[78–80]. Another major concern is the aggregation of proteins by phenols, which could ultimately result in lower protein solubility[81–83]. Alteration of the surface hydrophobicity, structure and size of the protein can dramatically influence its interfacial and foam stabilising properties. Protein aggregation due to phenols was previously correlated to lower surface activity and interfacial layer strength compared to pure proteins[78,84]. On the other hand, the formation of aggregates could reduce the rate of liquid drainage in foams, due to the blocking of lamellae and plateau borders, which was proposed for phenol-protein and heat-denatured aggregates[78,81,85]. Another study revealed lower protein surface hydrophobicity after non-covalent interactions with phenols, resulting in higher protein solubility, thus a higher foamability and stability[86]. These studies confirm the complexity of phenol-protein mixtures, as the type of phenol and interaction with the protein determine the interface- and foam-stabilising properties. Therefore, we will focus on the influence of rapeseed phenols on protein interfacial and foaming properties.

1.7 Research aim and outline of this thesis

The thesis aimed to investigate the contribution of non-proteinaceous components to the interfacial and foaming properties of mildly derived plant protein extracts. We used a multi-length scale approach to link the molecular properties of the different components to the macroscopic foam properties by characterising the intermediate mesoscopic length scale, the air-water interface. A two-way approach was performed by purifying the complex plant protein extract and mixing pure components in model systems. Our approach provides insights on the effect of impurities in protein extracts, thus providing design rules in (mild) plant protein extraction methods. The thesis outline is shown in a graphical overview in Figure 1.9.

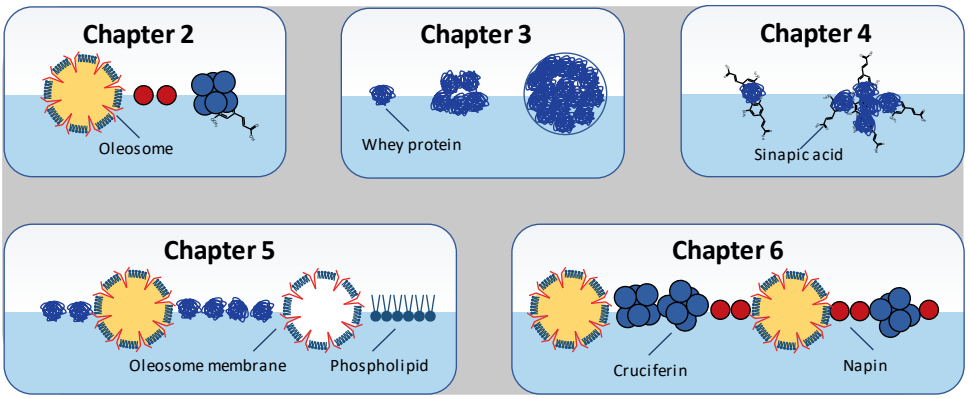

Figure 1.9. Graphical outline of the chapters in this thesis. Legend of illustrations: red sphere = napin, blue sphere = cruciferin, yellow sphere = oleosome, and chemical structure = sinapic acid.

The first step was to produce a mildly derived plant protein extract from rapeseed, which was the model plant source in this thesis. The molecular, interfacial and foaming properties of the rapeseed protein extract were studied in Chapter 2, and the extract was found to contain large amounts of lipids and phenols. In Chapter 2, the influence of lipids was evaluated by defatting the plant protein extract, and comparing its interfacial and foaming properties with the non-defatted one. Before an in-depth study on the non-proteinaceous components, we explored the influence of protein aggregation on interfacial properties in Chapter 3. Protein aggregation is an important parameter, as plant proteins often exist in a highly aggregated state. In Chapter 3 – 5, we switched to a well-characterised model protein, namely whey proteins, as rapeseed proteins were less well characterised in literature, and rather difficult to purify without affecting the nativity of the protein structure. In Chapter 4, whey proteins were mixed with the rapeseed phenol sinapic acid. Non-covalent and covalent phenol-protein interactions were induced to mimic the potential interactions occurring in the plant protein extract. The mixtures were studied for their interfacial and

foaming properties. In Chapter 5, oleosomes were extracted from rapeseeds and mixed with whey proteins to evaluate the influence of oleosomes on protein-stabilised interfaces. Oleosomes were found to form complex multi-component interfaces, and the complexity was reduced by incorporating defatted oleosomes and rapeseed phospholipids into the study. The findings in Chapter 5 were translated into a plant protein system by mixing rapeseed proteins with oleosomes, which yielded Chapter 6. Rapeseed protein and oleosomes were systematically mixed by varying the protein-to-oleosome ratios, and studied for their interfacial and foaming properties. Finally, in Chapter 7, we provide a general discussion of the main findings in Chapter 2 – 6 in perspective to the current protein transition and provide future recommendations for the field of plant protein functionality.

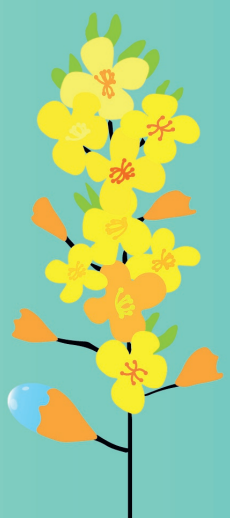

Chapter 2

Interfacial and foaming properties of mildly purified rapeseed proteins

Published as:
Yang, J., Faber, I., Berton-Carabin, C. C., Nikiforidis, C. V., van der Linden, E., & Sagis, L. M. C. (2020). Foams and air-water interfaces stabilised by mildly purified rapeseed proteins after defatting. *Food Hydrocolloids*, *112*, 106270. https://doi.org/10.1016/j.foodhyd.2020.106270

Abstract

Rapeseed protein isolate has promising functional properties (e.g. emulsifying and foaming), but is often extracted with intensive purification steps. This purification process requires a considerable use of resources and damages protein functionality regarding, for instance, foam stabilisation. We studied the interfacial and foaming properties of a mildly obtained rapeseed protein concentrate that contained oleosomes, and of its derived defatted rapeseed protein concentrate after solvent-based defatting. The air-water interfaces were deformed with large amplitude dilatational and shear deformations, which were analysed with Lissajous plots. At low bulk concentrations (0.01% w/w), the rapeseed protein-stabilised interfaces behaved as viscoelastic solids. The interfacial films became weaker and more stretchable at higher concentrations, suggesting that more non-protein components interfere with the intermolecular interactions between the adsorbed proteins at higher bulk concentrations. We confirmed the presence of such non-protein components at the interface by analysing Langmuir-Blodgett films with atomic force microscopy. The stability and air bubble size of foams prepared with either rapeseed protein concentrate or defatted rapeseed protein concentrate were similar. Mild purification of rapeseed resulted in a protein concentrate containing lipids in their native oleosome form, which have a minor destabilising effect on foams. We conclude that mild purification is a suitable method to obtain sustainably produced protein concentrates with promising foaming properties.

2.1 Introduction

Rapeseed (*Brassica napus*) is cultivated worldwide for canola oil extraction, which yields a protein-rich side-product with 35 to 40% (w/w) protein[11]. Currently, the side-product is utilised as animal feed, while it can have a larger added value to human nutrition[87]. Rapeseed proteins are a potential food ingredient, as: (i) the proteins are of high nutritional quality, with a balanced amino acid composition[10]; and (ii) they have good functional properties in forming gels, emulsions and foams[88–94]. The majority of studies dealing with rapeseed protein functionality involve extensive purification steps, including defatting with organic solvents, alkaline extraction of proteins, isoelectric point precipitation, and sometimes further purification using preparative chromatography. This results in materials with high protein purity (>80%), sometimes further separated into albumins and globulins[95,96]. Production of such fractions requires extensive use of energy, water, and chemicals, and on top of this, the additional processing might cause a loss in functionality. For example, defatted oilseed protein mixtures (43-49% w/w protein) have shown better emulsion and foam stability than purified isolates (70-84% w/w protein)[97,98]. Additional processing can change the protein conformation and hydrophobicity, and affect their functionality in interface and emulsion stabilisation[39,40,42]. For pea proteins, it was found that heating upon spray-drying resulted in chemical and structural changes, and decreased emulsifying properties[40,99]. Shifts in pH for soy protein aqueous dispersions also affected the protein hydrophobicity and structure, which resulted in decreased protein solubility and emulsifying properties[39]. With the above in mind, the use of plant protein concentrates obtained via mild processing has gained increasing interest[40,43–45].

Mildly purified plant protein concentrates require fewer purification steps and fewer resources compared to extensive purification, but contain substantial amounts of non-proteinaceous components, such as lipids, phenols, and carbohydrates. One concern is the possible detrimental effect of such components on the functional properties of the concentrate, such as interfacial, emulsifying, and foaming properties. This has not been studied extensively yet. In a yellow pea concentrate produced by aqueous dispersion and centrifugation only, increased emulsion stability was found comparable to commercially available protein isolates[40]. In another example, sunflower seeds, which have been cold-pressed to obtain a sunflower cake, containing proteins, fibres, and residual oil in the form of oleosomes, have successfully been used to prepare emulsions[44]. Nonetheless, little is known about the effect of the non-proteinaceous components in foams. The presence of lipid structures and fibres may have a limited effect on emulsifying properties, but this may differ immensely in foams, where the presence of lipids can be disastrous for foam stability. For example, fatty acids and oil/fat droplets reduce the surface elasticity of protein-stabilised interfaces and thereby increase the chance of bubble coalescence[68,71,72].

In this study, we produced a rapeseed protein concentrate by a mild process involving twin-screw pressing and centrifugation, which only partially removes lipids and insoluble materials. The obtained protein concentrate thus had a considerable fraction of lipids (8.3% w/w). We examined the colloidal state of the lipids and their effect on foaming properties by completely defatting the concentrate to obtain a defatted rapeseed protein concentrate. Both samples were analysed for their physicochemical, interfacial, and foaming properties to evaluate the necessity of lipids removal in such mildly obtained concentrates.

2.2 Experimental section

2.2.1 Materials

Untreated Alizze rapeseeds obtained from a seed producer were used as starting material. All chemicals (Sigma-Aldrich, USA) and the SDS-PAGE materials (Invitrogen Novex, ThermoFisher Scientific, USA) were used as received. Ultrapure water (MilliQ Purelab Ultra, Germany) was used for all experiments.

2.2.2 Sample preparation

Production of mildly purified rapeseed protein concentrate

Mildly purified rapeseed protein concentrate (**mRPC**) was produced using a method described by Ntone et al.[43]. In short, rapeseed kernels were dehulled and soaked at pH 9.0 for 4 hrs in a rapeseed-to-water weight ratio of 1:8. Subsequently, the mixture was blended for 2 min at max speed in a Vita-Prep blender (Vitamix, USA), and solids and supernatant were separated using a twin-screw press. The pH before blending and after screw-pressing was adjusted to 9.0. The supernatant was centrifuged at 10,000xg for 30 min (4 °C), which resulted in a top cream layer, a subnatant containing soluble proteins and other solutes, and a pellet with solids. The subnatant was separated and diafiltrated over a 5 kDa membrane to remove salts and free phenols. Finally, the material was freeze-dried and stored at -20 °C.

Defatting of mildly purified rapeseed protein concentrate

The mRPC was defatted four times by dispersing the concentrate in hexane with a 1:10 (w/v) ratio, followed by 2 hrs stirring at room temperature. The hexane was filtrated using filtration paper and the final retentate was dried overnight under a continuous flow of nitrogen.

Preparation of the soluble fraction

The mRPC and defatted mRPC were further processed by dissolving in a 20 mM sodium phosphate buffer (20 mM, pH 7.0) in a solid-to-water weight ratio of 1:10. The pH was adjusted to 7.0, and the sample was stirred overnight at 4 °C. Subsequently, the samples were centrifuged twice at 16,000xg for 30 min at room temperature to obtain the soluble

fraction (supernatant). The supernatant was freeze-dried for further analysis. The soluble fraction of mRPC is called rapeseed protein concentrate (**RPC**), and the soluble fraction of defatted mRPC is called defatted rapeseed protein concentrate (**DRPC**).

Preparation of protein solutions

All RPC/DRPC solutions in this work were prepared by dissolving RPC/DRPC in a sodium phosphate buffer (20 mM, pH 7.0), unless stated otherwise. The samples were stirred at room temperature for 4 hrs before further studies.

2.2.3 Composition analysis

Protein content was determined by measuring the nitrogen content of triplicates using a Flash EA 1112 Series Dumas (Interscience, The Netherlands). A nitrogen conversion factor of 5.7 was used to calculate the protein content[100]. The oil content of the samples was studied by performing Soxhlet extraction with the solvent petroleum ether for 6 hrs, and the oil content was determined by weighing the starting material and the oil in the collection flasks. All samples were prepared in independent duplicates.

2.2.4 Protein composition by SDS-PAGE

A solution of 0.1% protein (w/w) in water was prepared, and 45 µL were mixed with 6 µL of 500 mM DTT and 7 µL of NuPAGE LDS sample buffer. These samples were heated 10 min for 70 °C and loaded on a 4-12% (w/w) BisTris gel, next to a molecular weight marker in the range of 2.5-200 kDa. The electrophoresis was performed for 30 min at 200 V. Finally, the proteins on the gel were stained with SimplyBlue Safestain, and the gels were scanned using a gel scanner.

2.2.5 Determination of the zeta-potential and the particle size

The zeta-potential and the particle size of the proteins in solution (filtered over 0.45 µm syringe filter) were determined using dynamic light scattering in a Zetasizer Nano ZS (Malvern Instruments, UK). Refractive indices used were 1.45 for the proteins and 1.33 for the continuous phase. All measurements were performed in triplicates at 20 °C.

2.2.6 Alteration of the tertiary structure of proteins

Possible alterations of the tertiary structure of the proteins were probed using intrinsic fluorescence of the tryptophan residues. Protein solutions of 0.01% protein (w/w) were analysed on an LS 50 B luminescence spectrometer (Perkin-Elmer, USA). The excitation and emission slits were set at 5 nm. The excitation wavelength was 295 nm, and the emission spectra were recorded from 300 to 450 nm with steps of 0.5 nm at a scan speed of 120 nm/min. Each sample was measured in duplicate.

2.2.7 Determination of protein thermal stability by DSC

The protein thermal stability was studied by differential scanning calorimetry using a Q100 DSC (TA Instruments, USA). Aliquots of about 50 µL of 10% protein (w/w) solution were weighed in a stainless steel high volume pan. An empty stainless steel pan was used as a reference, and nitrogen was used as a carrier gas during the measurements. Samples were equilibrated at 20 °C for 5 min, followed by a heating step to 140 °C at a rate of 2 °C/min, and finally cooled down to 20 °C with a rate of 10 °C/min. Each sample was prepared in duplicate, and each of these duplicates was measured in duplicate.

2.2.8 Confocal laser scanning microscopy (CLSM)

The RPC and DRPC were dissolved at 15% protein content (w/w) in water for one day at 4 °C. The samples were analysed by confocal laser scanning microscopy (**CLSM**) using a Leica TSC SP8x confocal laser microscope (Leica Microsystems Inc., Germany), which was fitted with a white laser and HyD detector. Lipids and proteins were fluorescently labelled by adding 4 µL 0.1% (w/v) Nile Red and 7 µL 0.1% (w/v) Fast Green per mL of RPC sample. The mixtures were placed on microscope slides and examined with a 63x magnification and a water immersion lens (refractive index = 1.20). Nile Red and Fast Green were excited using a wavelength of 488 and 633 nm, respectively. Images were analysed using the Leica Application Suite X software.

2.2.9 Determination of surface shear properties

Surface shear properties were determined using a magnetic air bearing stress-controlled rheometer (AR-G2, TA Instruments, USA) with a double-wall-ring (**DWR**) geometry. The diamond-edged ring was made of iron and platinum and was positioned at the air-water interface of a protein sample in a double-wall trough. A vapour cap was installed to avoid evaporation, and the sample was pre-sheared for 5 min at a shear rate of 10/s. Afterwards, the interface was equilibrated for 10,800 s, before frequency sweeps were performed with frequencies varying from 0.01 to 10 Hz at a constant amplitude of 1%. Strain sweeps were performed with strains varying from 0.01% to 100% at a constant frequency of 0.1 Hz. All experiments were performed at least in triplicate at 20 °C. The Boussinesq number, which is the ratio between surface and bulk stress, was >1 for all systems studied in our work. This implies that the contribution of the subphase to the stress signal is negligible.

2.2.10 Determination of surface tension and surface dilatational properties

The air-water surface dilatational properties were determined with a drop tensiometer PAT-1M (Sinterface Technologies, Germany). A hanging drop of protein solution was formed at the tip of the needle, with a surface area of 20 mm^2. The surface tension of the drop was calculated by fitting the drop contour with the Young-Laplace equation. The surface tension was monitored for 10,800 s, followed by oscillatory dilatational deformations of the interface.

The deformation amplitude was varied between 3 – 30% at a fixed frequency of 0.02 Hz in so-called amplitude sweeps. Five sinusoidal oscillations were performed at each amplitude. Step dilatation of the interface was done by a sudden extension or compression (step time of 2 s) of the area by 10%. All measurements were performed at least in triplicate at 20 °C.

2.2.11 Rheology data analysis

The oscillatory sweep results (in dilatation) were studied by plotting Lissajous curves of the surface pressure ($\Pi = \gamma - \gamma_0$) versus the deformation ($(A-A_0)/A_0$). Here, γ and A are the surface tension and area of the deformed interface, γ_0, and A_0 are the surface tension and area of the non-deformed interface. The middle three oscillations of each amplitude cycle were processed into plots.

2.2.12 Determination of interfacial layer thickness

The thickness of the air-water interfacial film formed by RPC and DRPC was studied using an imaging nulling ellipsometer EP4 (Accurion, Germany). A 783 cm^2 Langmuir film balance (Langmuir-Blodgett trough, KSV NIMA/Biolin Scientific Oy, Finland) filled with a sodium phosphate buffer (20 mM, pH 7.0) was positioned under the ellipsometer. Protein solution (200 µL of 0.12% (w/w) protein) was spread on the surface using a syringe, and the protein layer was equilibrated for 30 min. Afterwards, it was compressed with barriers moving at 5 mm/min to target surface pressures, as measured by a Wilhelmy plate (platinum, perimeter 20 mm, height 10 mm). At these surface pressures, the interfacial layers were measured over a wavelength range from 499.8 – 793.8 nm of two zones at an angle of incidence of 50 degrees. The ellipsometric parameters δ and ψ were determined for the air-water interface with and without the protein layer. All measurements were performed at room temperature and at least in duplicate. The output was analysed using the software from the supplier (EP4Model v.3.6.1.). The model was created by combining: the ambient medium air, the protein layer, and the substrate buffer. The parameters of the protein layer in the model were fitted using a Cauchy model (Equation 2.1):

$$n(\lambda) = A + \frac{B}{\lambda^2} + \frac{C}{\lambda^4} \qquad (2.1)$$

where n is the refractive index, λ is the wavelength of the polarised light, and A, B, and C are fitting parameters.

2.2.13 Preparation of Langmuir-Blodgett films

Langmuir-Blodgett (**LB**) films of protein-stabilised interfaces were prepared with a 243 cm^2 Langmuir film balance (Langmuir-Blodgett Trough, KSV NIMA/Biolin Scientific Oy, Finland). The balance was filled with sodium phosphate buffer (20 mM, pH 7.0). Protein solution (200 µL, 0.02% (w/w) protein) was spread on the surface using a syringe, and the protein layer

was equilibrated for 30 min. Subsequently, the layer was compressed with barriers moving at 5 mm/min to reach the target surface pressure, as monitored with a Wilhelmy plate (platinum, perimeter 20 mm, height 10 mm). The films were deposited on a freshly cleaved mica sheet (Highest Grade V1 Mica, Ted Pella, USA) at 1 mm/min withdraw speed. The films were produced in duplicate and dried in a desiccator at room temperature.

2.2.14 Determination of the interfacial structure by AFM

The interfacial microstructure was studied using an atomic force microscope (**AFM**, MultiMode 8-HR, Bruker, USA). The AFM images of the LB films were recorded in tapping mode using Scanasyst-air model non-conductive pyramidal silicon nitride probes (Bruker, USA) with a normal spring constant of 0.40 N/m. A lateral scan frequency of 0.977 Hz was employed for all topographical images. The lateral resolution was 512 x 512 pixels^2 in a scan area of 2 x 2 μm^2. At least two locations on the film were scanned to ensure good representativeness. Images were analysed using Nanoscope Analysis 1.5 software (Bruker, USA).

2.2.15 Determination of foam properties

The foams were produced using a Foamscan foaming device (Teclis IT-Concept, France) by sparging nitrogen through a metal frit (27 μm pore size, 100 μm distance between centres of pores, square lattice). A total volume of 40 mL was sparged in a glass cylinder with a diameter of 60 mm at a gas flow rate of 400 mL/min to a maximum foam volume of 400 cm^3. A camera and Foamscan software monitored the foam decay. From this, the foam half-life time was measured, which is the time at which 50% of the initial foam volume had collapsed. Images of the bubbles were taken with a camera and analysed using a custom Matlab script that ran a DIPlip and DIPimage image analysis software. From this, an average bubble size was obtained.

2.3 Results and discussion

2.3.1 Composition

Mild purification resulted in a rapeseed protein concentrate (**RPC**) with a protein content of 71.7% (w/w) and a lipid content of 8.3% (w/w) (Table 2.1). These lipids were likely the natural oil storage organelles of plant seeds, namely the oleosomes (**OS**), also known as oil bodies. OS store lipids, mainly triacylglycerols, surrounded by a membrane consisting of phospholipids and specific proteins called oleosins. These OS exist in sizes ranging from 0.1 to 3 μm depending on the source of seed and environmental factor0,[101]. The presence of OS was confirmed with CLSM imaging, which revealed small spherical lipid structures (Figure 2.1, red colour). The OS in the images were relatively large (a few microns), which is attributed to coalescence during the freeze-drying step (data not shown).

Table 2.1. Protein and lipid content in rapeseed protein concentrate (RPC) and defatted rapeseed protein concentrate (DRPC). The averages and standard deviation were obtained from two replicates.

	RPC	DRPC
Protein	71.7% ± 1.8	81.8% ± 3.5
Oil	8.3% ± 0.2	0.0%

Defatting of RPC was effective, as it resulted in a defatted rapeseed protein concentrate (**DRPC**) with a protein content of 81.8%, and no lipids were found in the lipid content analysis. Despite the defatting step, minor residual fluorescing material (red colour) was observed in the CLSM images (Figure 2.1), which could be membrane polar lipids (phospholipids) or protein hydrophobic domains[102]. SDS-PAGE (Figure 2.1) showed a comparable protein composition for RPC and DRPC with the presence of the two major rapeseed proteins: the water-soluble albumin, called napin, and the salt-soluble globulin, called cruciferin.

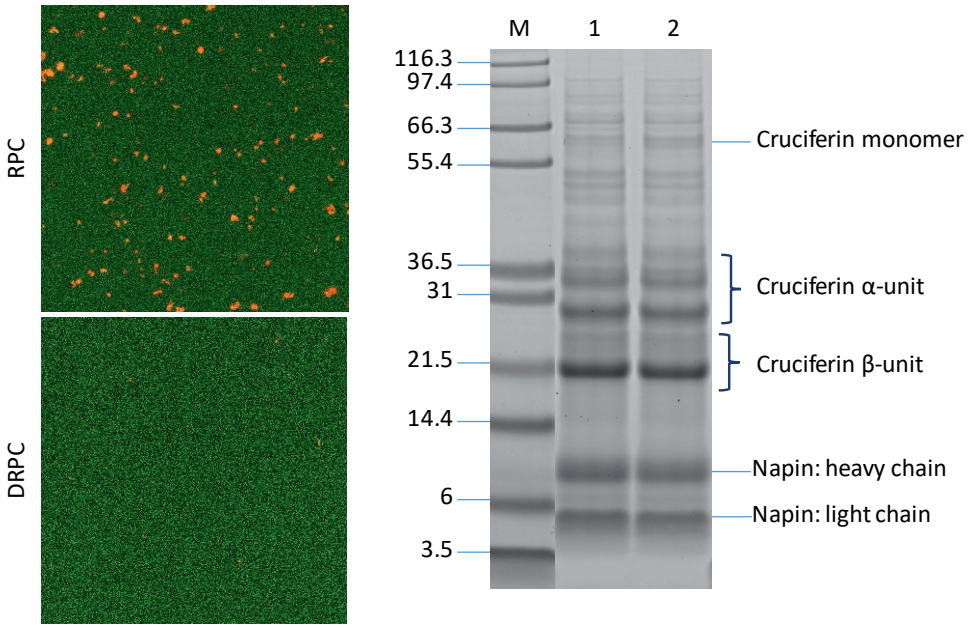

Figure 2.1. (Left) CLSM images of rapeseed protein concentrate (RPC) and defatted rapeseed protein concentrate (DRPC). Red indicates the labelled lipids and green indicates the labelled proteins. (Right) SDS-PAGE profile under reducing conditions containing M (Marker; the corresponding molecular weight are indicated on the left), 1. RPC and 2. DRPC.

2.3.2 Protein structure

Intense processing may alter the protein structure at different scales, and was previously demonstrated for rapeseed proteins after treatments with organic solvents[75]. We will use the same techniques here to evaluate whether changes occurred in the protein structure. First, intrinsic fluorescence was analysed to evaluate the tertiary protein structure (graph A2.1 in the appendix). The emission spectra were similar for both samples, which indicates no alteration of the chemical environment of the fluorescent amino acids, mainly tryptophan. Additionally, proteins were analysed by DSC to probe protein denaturation temperatures and enthalpy (Table 2.2). The thermogram showed two peaks at 89.3-90.0 and 106.7-107.3 °C, which can be attributed to the denaturation temperature of cruciferin and napin, respectively[89]. The comparable denaturation enthalpies and fluorescence spectra for both protein fractions suggest that the protein structure is retained under the defatting procedure. The combination of these measurements allows us to conclude that the protein structure is overall not affected by the additional defatting step.

Table 2.2. Protein denaturation temperature and enthalpy of rapeseed protein concentrate (RPC) and defatted rapeseed protein concentrate (DRPC). The average and standard error were obtained from four replicates.

	Denaturation temperature (°C)		Enthalpy (J/g protein)		
	Cruciferin	**Napin**	**Total**	**Cruciferin**	**Napin**
RPC	90.0 ± 0.7	107.3 ± 0.5	14.6 ± 0.1	6.9 ± 0.1	7.8 ± 0.2
DRPC	89.3 ± 0.0	106.7 ± 0.9	14.1 ± 0.0	6.1 ± 0.1	8.0 ± 0.1

2.3.3 Adsorption behaviour

The adsorption behaviour of the RPC and DRPC at an air-water interface was studied (Figure 2.2), for which the protein bulk concentrations were varied between 0.01 and 1% (w/w). The surface activity was concentration-dependent, i.e., higher bulk concentrations resulted in higher surface pressures even after a substantial adsorption time of 3 hrs. At all concentrations, the RPC gave higher surface pressures compared to DRPC. More specifically, at bulk concentrations of 0.01 and 1% (w/w), the surface pressure for RPC was between 2 and 3 mN/m higher than for DRPC. We observed a more considerable difference at 0.1% (w/w), where RPC had a surface pressure of up to 7 mN/m higher than DRPC. The fact that the presence of OS in the protein concentrate caused a higher surface pressure compared to the defatted protein concentrate suggests that the OS are surface-active. This was also observed in other types of OS. Soy OS can lower the surface tension by adsorbing and unfolding at the air-water interface, forming a mixed phospholipid- and oleosin-stabilised layer[62,70].

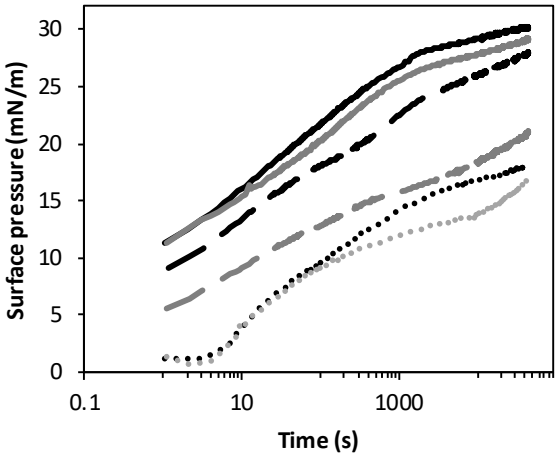

Figure 2.2. Surface pressure as a function of time at air-water interfaces in the presence of rapeseed protein concentrate (RPC, black) and defatted rapeseed protein concentrate (DRPC, grey). The material concentration (w/w) in the aqueous phase was 0.01% (dotted line), 0.1% (dashed line), or 1% (solid line). For clarity, one representative isotherm is shown for each sample, but comparable isotherms were obtained on at least three replicates.

In all protein systems at all concentrations, we observed a relatively rapid increase in surface pressure until roughly 1,000 s, which is often described as a regime where proteins adsorb at the interface[49]. Afterwards, the surface pressure increase was slower, which is often related to rearrangements (e.g., conformational changes or clustering) of the adsorbed proteins[103]. The surface rheology tests described in the next sections should ideally be performed in equilibrium conditions, to limit the influence of the ageing processes. As we do not reach equilibrium conditions, even after 50,000 s, we decided to let all interfacial films age for 3 hrs before subjecting them to deformations.

2.3.4 Surface shear rheology

Frequency sweeps

The rapeseed protein-stabilised interfaces were subjected to oscillatory shear deformations in frequency and strain sweeps (Figure 2.3A), at two different protein bulk concentrations, of 0.01% and 1% (w/w). All interfaces showed a slight frequency dependence in the storage (***G_i'***) and loss moduli (***G_i''***). In all cases, G_i' scaled as $G_i' \sim \omega^{n'}$ and this resulted in n-values of between 0.19±0.02 and 0.23±0.02. This suggests a weak frequency dependency and power-law behaviour, which was also found for gels and soft glassy materials[104]. A combination of power-law behaviour and $G_i' > G_i''$ modulus implies that the rapeseed protein-stabilised interfaces were composed of disordered solid structures, very similar to whey protein-stabilised interfaces[103].

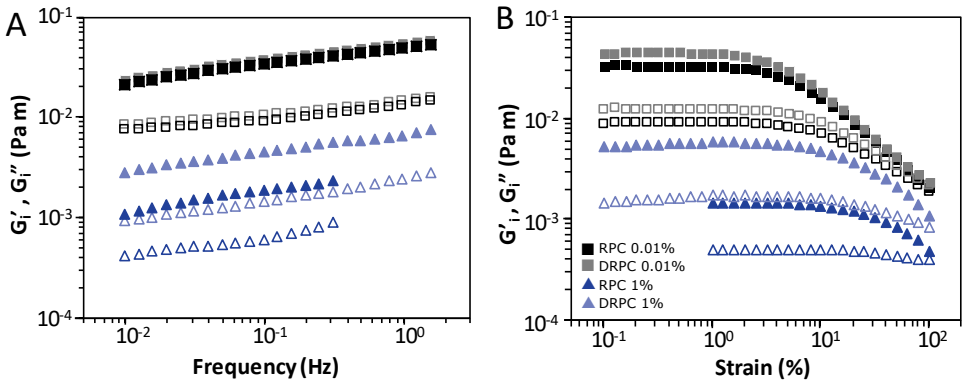

Figure 2.3. The storage (closed symbols) and loss moduli (open symbols) as a function of frequency (A) and strain (B) of air-water interfacial films stabilised by rapeseed protein concentrate (RPC, squares) or defatted rapeseed protein concentrate (DRPC, triangles). The different bulk protein concentrations (w/w) are depicted in the legend. The graphs represent averages obtained from at least three replicates, and the standard deviation for each sample was below 5%.

In the frequency sweeps, the RPC- and DRPC-stabilised interfaces showed comparable moduli at 0.01% (w/w). An increase in bulk concentration to 1% (w/w) gave lower moduli for both samples, of which the decrease was more pronounced for RPC than for DRPC. This may seem surprising, as in pure protein systems, such an increase in bulk concentration results typically in similar or higher moduli, which we showed for interfaces stabilised by whey protein isolate with a bulk concentration of 0.01 or 2% (w/w) (graph A2.2 in appendix). For RPC, a higher protein concentration also resulted in a higher concentration of non-proteinaceous material, such as OS. A higher concentration of the latter would result in more competition with the proteins for adsorption at the interface, and adsorbed OS could reduce the connectivity between adsorbed proteins, thereby reducing the surface shear moduli.

We also observed a modulus decrease for the DRPC-stabilised interface. Oil extraction using hexane removed the oil inside the OS, but some membrane material most likely remained in the DRPC. It is known that milk fat membrane fragments are surface-active and can compete with the proteins for adsorption at the interface[102,105,106]. Therefore, the decrease in moduli for the DRPC may have been caused by the adsorption of membrane material of the OS, thereby again decreasing the connectivity between the adsorbed proteins.

Strain sweeps

In strain sweeps (Figure 2.3B), the G_i' and G_i'' of both protein-based interfacial films at 0.01% (w/w) were also relatively close. At this concentration, the G_i' in the linear viscoelastic (**LVE**) regime were 0.032 and 0.041 Pa·m for RPC- and DRPC-stabilised interfaces, respectively. Increasing the protein bulk concentration to 1% (w/w) resulted in a lower G_i' in the LVE regime, which was found to be 0.0015 and 0.0059 Pa·m for RPC- and DRPC-stabilised interfaces, respectively. All four curves in Figure 2.3B showed an LVE regime, followed by a nonlinear viscoelastic (**NLVE**) regime, where the materials soften at higher deformations. In the whole strain range from 0.1 to 100%, the G_i' was higher than G_i'', suggesting solid-like behaviour, which was also demonstrated by a tanδ (G_i''/G_i') <1 in the LVE regime (0.29 – 0.37 for all interfaces).

The moduli shown in Figure 2.3 are calculated from the intensity and phase shift of the first harmonic of the Fourier transform of the stress signal, while contributions from higher harmonics are neglected. Higher-order harmonics exist in the NLVE regime and result from changes in the interfacial microstructure upon higher deformation. To include these nonlinearities into the analysis, we have plotted the torque against deformation in Lissajous plots[59].

Lissajous plots

The Lissajous plots (Figure 2.4) showed a narrow ellipsoidal shape at strains in the LVE, which suggested viscoelastic behaviour where the elastic component dominated. The plots became wider at higher deformation amplitudes, which indicates an increase of the viscous contribution in the film response. Further into the NLVE regime, the plots started to exhibit a rhomboidal shape, which was clearly present for both rapeseed protein-stabilised interfaces formed from 0.01% (w/w) bulk concentration at 100% strain. In the rhomboidal shape, we observed initially a highly elastic response at the start of the cycle (the lower-left corner of the plot). This was evident from the steepness of the curve in this regime, which indicated high values for the tangential shear modulus (the local slope of the plot). This was followed by a gradual but significant change in the slope. This is typical for (partial) intra-cycle yielding, where a considerable part of the elasticity is lost, and the response becomes dominated by the viscous contribution. The critical stress where this happens is the yield

stress of the interfacial microstructure. It is important to note that intra-cycle yielding is not the same as a macroscopic fracture of the interface. When the deformation continued in the opposite direction, we again observed a highly elastic response, followed by intra-cycle yielding, and a predominantly viscous response of the interface. This suggests that the microstructure of the interface (partially) recovers at both ends of the deformation cycle.

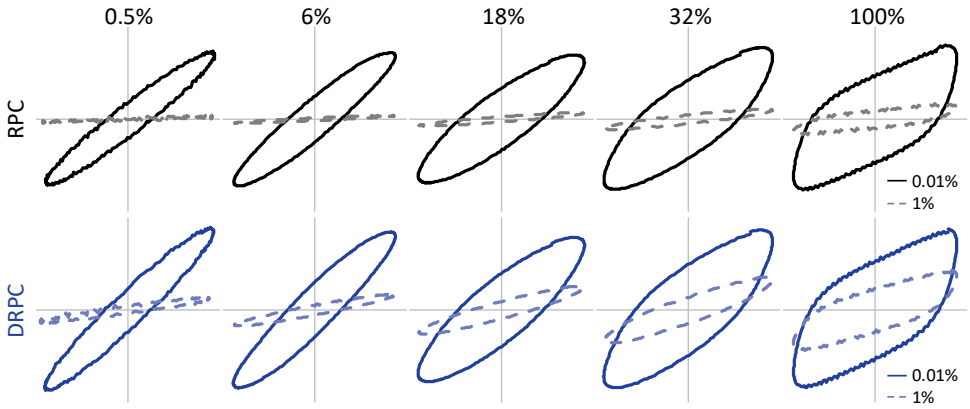

Figure 2.4. Lissajous plots of torque as a function of deformation obtained during strain sweeps of air-water interfacial films stabilised by rapeseed protein concentrate (RPC) and defatted rapeseed protein concentrate (DRPC). The vertical axes were normalised by the maximum torque. The dark solid lines and light dashed lines indicate 0.01 and 1% (w/w) bulk protein concentration, respectively. For clarity, one representative distribution is shown for each sample, but comparable distributions were obtained on at least three replicates.

The Lissajous plots at 100% strain for 0.01% (w/w) bulk protein concentration were comparable for RPC and DRPC, and indicated an interface that behaved like a viscoelastic solid. Increasing the bulk protein concentration to 1% (w/w) resulted in narrower Lissajous plots that were more tilted towards the horizontal axis, which indicates a more dominant elastic contribution in the response and a less stiff interface. Even at 100% deformation, the plots are still nearly ellipsoidal, indicating that response is still close to linear, and the interfacial film has a considerably larger maximum linear strain than 0.01% (w/w) (Figure 2.3B). This concentration dependency was also more pronounced in the RPC-stabilised interface compared to the DRPC-stabilised one. The presence of non-protein components (OS or OS membranes) resulted in the formation of a less stiff and more stretchable interface.

2.3.5 Surface oscillatory dilatational rheology

Amplitude sweeps

The same air-water interfacial films stabilised with rapeseed protein ingredients were studied by performing dilatational deformations in a drop tensiometer. In amplitude sweeps, the RPC-stabilised interface at 0.01% (w/w) bulk concentration showed an amplitude-dependent modulus (Figure 2.5A), as the surface dilatational moduli (E_d') decreased from 70 to 34 mN/m when increasing the amplitude from 3 to 30%. The interfacial layer was increasingly disrupted at higher deformations, suggesting the formation of a solid viscoelastic layer, as observed earlier in the surface shear rheology tests. Just as for these tests, the moduli for the RPC-based layers show a decrease with increasing bulk concentration. The E_d' of an RPC-stabilised interface with 1% (w/w) bulk concentration was around 29 mN/m and independent of the applied amplitude, which suggests a less stiff and more stretchable layer compared to an interface stabilised by the same material at lower bulk concentrations. The same behaviour was observed for the DRPC-stabilised interfaces (Figure 2.5B). At a protein bulk concentration of 1% (w/w), the defatted protein concentrate resulted in a slightly stiffer interface compared to the protein concentrate. The E_d' of the DRPC exhibited a minor degree of amplitude dependence at 1% (w/w) bulk concentration, which was non-existent in the case of RPC. We also studied the nonlinearities in these responses by plotting Lissajous curves.

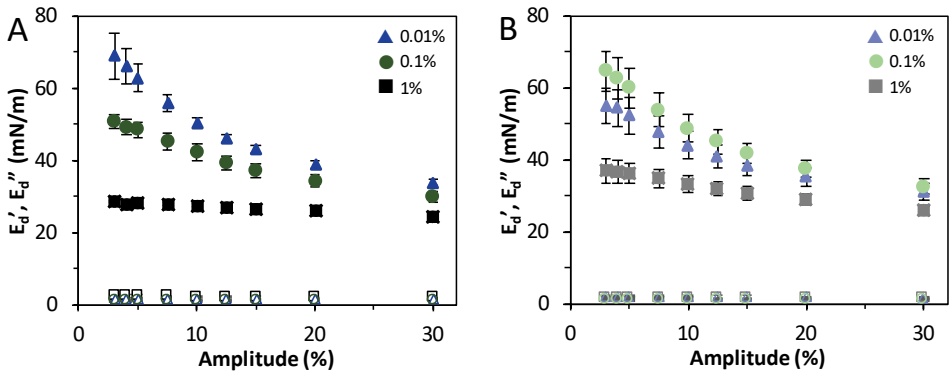

Figure 2.5. Surface elastic (closed symbols) and loss (open symbols) dilatational moduli as a function of deformation amplitude of air-water interfacial films stabilised by rapeseed protein concentrate (RPC, A) or defatted rapeseed protein concentrate (DRPC, B). The different bulk protein concentrations tested (%, w/w) are given in the legend. The graphs represent averages and standard deviations from at least three replicates.

Lissajous plots

The Lissajous plots (Figure 2.6) of RPC- and DRPC-stabilised interfaces at a bulk concentration of 0.01% (w/w) had a symmetric shape at 5% deformation. The plots were becoming less symmetric at higher deformations, which was most pronounced at 30% deformation. In those plots, we observed a relatively steep surface pressure increase from

the left-bottom corner (start of extension of the interface), representing an elastic response, followed by a gradual softening of the interfacial structure. In this part of the cycle, the elastic component of the response diminished, and the viscous contribution increased. The surface pressure reached higher values in maximum compression than in maximum extension, which is an indication for intra-cycle strain hardening. The strain hardening upon compression (at high deformations) most likely resulted from jamming of densely clustered protein regions. These interfaces show the rheological behaviour of viscoelastic solids, and their behaviour is comparable to that of whey protein-stabilised interfaces[103].

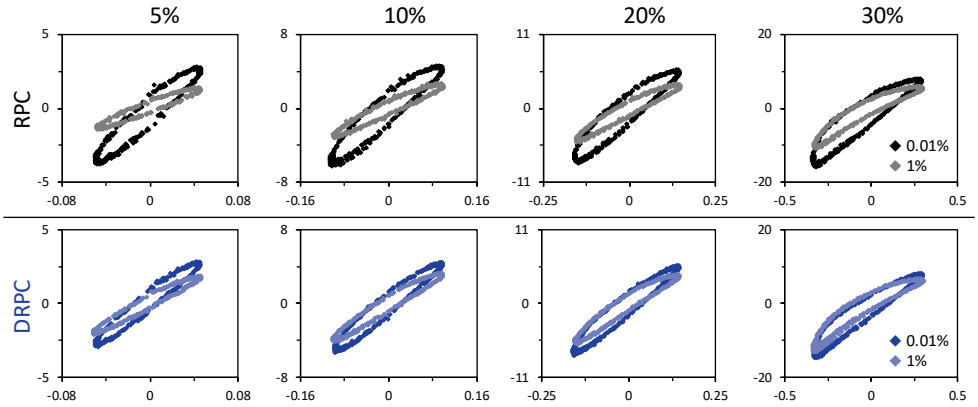

Figure 2.6. Lissajous plots of surface pressure as a function of the applied dilatational deformation, obtained during amplitude sweeps of air-water interfacial films stabilised by rapeseed protein concentrate (RPC) or defatted rapeseed protein concentrate (DRPC). The plots were normalised to the same maximum surface pressure value. The dark lines and light lines indicate 0.01 and 1% (w/w) bulk protein concentrations, respectively. For clarity, one representative distribution is shown for each sample, but comparable distributions were obtained on at least three replicates.

Increasing the protein bulk concentration to 1% (w/w) resulted in narrower Lissajous plots, and also in plots more tilted towards the horizontal axis. These findings, again, suggest the formation of a less stiff and much more stretchable interfacial layer, where the elastic response is more dominant over the whole range of deformations, compared to the interface formed at lower bulk concentrations. The dilatational rheology results thus confirm the shear rheology results, for which we proposed that non-protein components, such as OS and OS-membranes, could hamper the formation of a viscoelastic protein network at the air-water interface.

Understanding the air-water interface stabilising properties of the proteins can contribute to a better insight into the foaming-stabilising properties. Interfacial rheology can be used to evaluate the type of interfacial layer formed, and its strength. It is beneficial to study both dilatational and shear rheology, as both types of deformations could occur in a foam. For instance, the extension of the air bubble upon disproportionation is a dilatational

deformation of the surface, whereas the collision of two bubbles and a possible rupture could have a stronger shear component. Also, in-plane interactions are analysed to a larger extent in shear than in dilatational deformations. We should keep in mind that the interfacial properties alone do not dictate the foaming properties, as the bulk properties, such as viscosity and presence/size of particles, can largely influence foam formation and stability.

2.3.6 Step-dilatation

The interfaces were also subjected to sudden step extensions/compressions, and the resulting relaxation response was fitted with a Kohlrausch-William-Watts (**KWW**) stretch exponential term and a regular exponential (Equation 2.2)[107]. The regular exponential is added to decouple the continuous ageing of the interface from the actual relaxation process.

$$\gamma(t) = ae^{-(t/\tau_1)^{\beta}} + be^{-t/\tau_2} + c \quad (2.2)$$

In Table 2.3, we show the relaxation time τ_1 and stretch exponent β determined for the different systems tested. Parameters τ_2 and constants a, b, and c can be found in Table A2.1 in the appendix.

Table 2.3. β and τ_1 for interfacial films stabilised by rapeseed protein concentrate (RPC) or defatted rapeseed protein concentrate (DRPC) with various bulk concentrations. The averages and standard deviation were obtained from at least three replicates.

		Extension		Compression	
		β	**τ_1**	**β**	**τ_1**
RPC	**0.01%**	0.61 ± 0.03	26.2 ± 4.4	0.58 ± 0.03	24.1 ± 2.3
	0.1%	0.56 ± 0.04	28.0 ± 4.4	0.60 ± 0.05	22.3 ± 3.8
	1%	0.59 ± 0.04	29.4 ± 5.2	0.67 ± 0.04	23.0 ± 1.1
DRPC	**0.01%**	0.59 ± 0.04	31.7 ± 5.2	0.63 ± 0.02	22.4 ± 4.1
	0.1%	0.58 ± 0.06	28.8 ± 4.1	0.60 ± 0.02	23.2 ± 2.7
	1%	0.54 ± 0.06	28.3 ± 6.6	0.66 ± 0.06	25.1 ± 4.9

The KWW is a phenomenological model for describing relaxation processes in disordered systems, which has also been applied for protein-stabilised interfaces[108,109]. The stretch component β<1 reveals dynamic heterogeneity, as it is related to local variations in the relaxation kinetics, and indicates a wide range of relaxation times. The β's of both RPC- and DRPC-stabilised interfaces were 0.54 to 0.61 in extension and 0.58 to 0.67 in compression. In general, compression of the interface resulted in a higher β than an extension of the interface, in line with the asymmetry also observed in the Lissajous plots in Figure 2.6. β-values between 0.42 and 0.73 have been reported for various interfacial layers stabilised by

plant, insect, and milk proteins[108–110]. Such values were also observed in relaxation processes in 3D disordered solids[111]. The relaxation time τ_1 was between 22.3 and 31.7 s for all rapeseed protein-stabilised interfaces. This suggests comparable relaxation processes for interfaces stabilised by both rapeseed protein samples, at bulk concentrations between 0.01 to 1% (w/w).

2.3.7 Ellipsometry

The thickness of the interfacial layer was studied using ellipsometry combined with a Langmuir trough, which allowed us to perform measurements at various surface pressures (Figure 2.7). Both rapeseed protein samples showed a similar interfacial thickness, ranging from 2.1 nm at a surface pressure of 13 mN/m to 3.5 nm at 21 mN/m. At the highest tested surface pressure of 25 mN/m, the DRPC-stabilised interface had a higher thickness (5.1 nm) than that formed with RPC (4.3 nm). This could be related to the stiffer interfacial layer formed by DRPC, as stiffer layers could retain more material at higher compressions. On the other hand, a weaker and more stretchable layer, such as formed with RPC, might result in loss of interfacial material towards the bulk phase at such high compressions. In general, both protein samples gave layers with comparable average thicknesses, while we may have expected an increase in layer thickness for the RPC-stabilised interfaces, as OS were present. Yet, the possible contribution of OS to the interfacial composition and structure may not be captured with this method, as ellipsometry measures the average properties over an area of several square microns. Additionally, large OS subjected to coalescence during extraction might also unfold and disintegrate at the air-water interface, which has already been demonstrated for soybean and sunflower oleosomes[70,102].

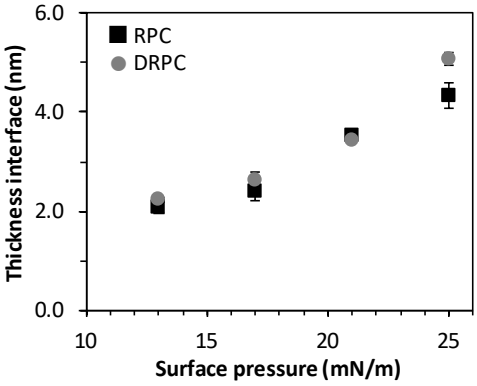

Figure 2.7. The thickness of the interfacial layer as a function of surface pressure for Langmuir films made of rapeseed protein concentrate (RPC, black square) or defatted rapeseed protein concentrate (DRPC, grey circle), measured by ellipsometry. The graph represents averages and standard deviations from at least three replicates.

2.3.8 Interfacial microstructure

We also studied the interfacial microstructure by visualising the topography using AFM on Langmuir-Blodgett films (Figure 2.8), which were produced by transferring a protein film at different surface pressures onto a solid substrate. Surface pressure isotherms obtained upon film compression are shown in graph A2.3 in the appendix. For both RPC- and DRPC-based films at all surface pressures tested, a highly heterogeneous structure was observed with many thicker regions (white dots). The thickness of these regions was between 6 – 8 nm, which is comparable to the protein size measured by dynamic light scattering (8.7 nm, graph A2.4 in the appendix), suggesting that these are protein-dense regions. An increase in surface pressure (and thus higher compression of the film) resulted in more protein-dense regions on the AFM images. Comparable heterogeneity in the interfacial microstructure has also been observed in many other protein-based interfaces[103,112,113]. These protein-stabilised interfaces exhibit solid-like behaviour and form highly disordered structures at the interface, which is also found in three-dimensional gel systems. The dynamic heterogeneity in the step dilatation experiments was suggested to be associated with structural heterogeneity in the interfacial microstructure, which we herein confirm via the AFM images.

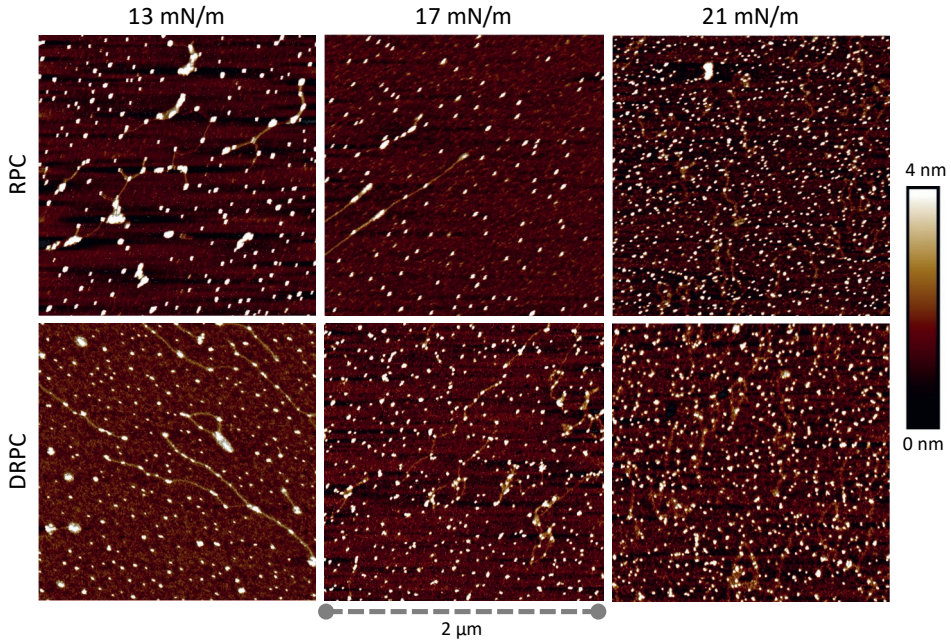

Figure 2.8. AFM images of Langmuir-Blodgett films made from rapeseed protein concentrate (RPC) and defatted rapeseed protein concentrate (DRPC). The surface pressure indicates the conditions during film sampling.

Another interesting observation related to these AFM images was the long strands that were prominently present at 13 mN/m and slightly visible at 17 mN/m. Conversely, at the highest compression of 21 mN/m, where the films are denser, the strands seem to be barely visible. These strands have a thickness of <2 nm, and lengths varying from 0.2 to 2 µm. The strands seem to be close to protein-dense regions and also related to the clustering of these regions. The presence of such strands could have reduced the overall connectivity between the proteins at the interface, which would be in line with the lower moduli at higher concentrations that we observed in shear and dilatation deformation experiments. The exact nature of the strands cannot be established based on AFM images alone, but we can speculate that the strands could be polysaccharides that were not removed during centrifugation. Another explanation for the structures could be membrane fragments of OS, if these would unfold at the air-water interface. We also cannot exclude the possibility that OS is present in a sublayer beneath the scanned interface, as we only studied the topography of the interfaces using AFM. As we also suggested in previous sections, the OS might disintegrate at the interface after adsorption.

2.3.9 Foams

Rapeseed protein-stabilised foams were studied for their average bubble diameter and the foam half-life time, which is the duration for the foam volume to decrease down to half of its original value (Figure 2.9).

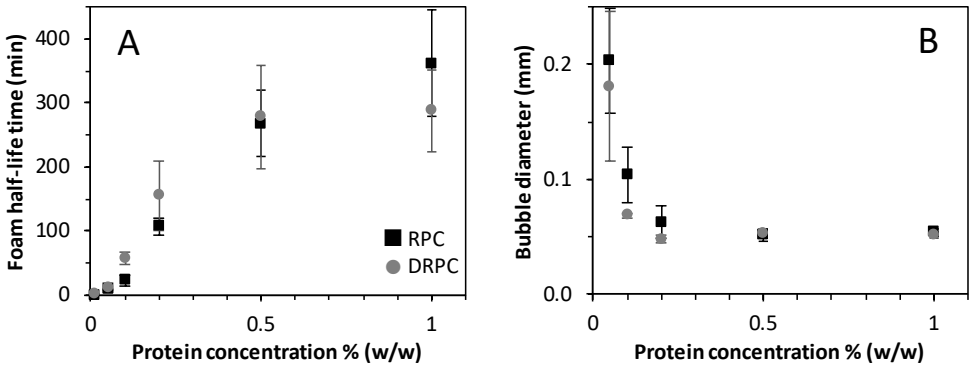

Figure 2.9. The half-life time (A) and bubble diameter (B) of foams stabilised by rapeseed protein concentrate (RPC) or defatted rapeseed protein concentrate (DRPC). The graphs represent averages and standard deviations of at least three replicates.

The RPC-based samples did not reach the set initial volume of 500 cm^3 at a bulk concentration below 0.02% (w/w). Increasing the protein bulk concentration resulted in a higher half-life time of the foam, reaching up to 361±84 and 288±63 min at a concentration of 1% (w/w) for RPC- and DRPC-based foams, respectively. Both protein samples showed comparable foam half-life times over the entire range of protein concentrations between

0.02 to 1% (w/w). The foam stability is closely related to the air bubble size, which decreased with increased protein concentrations. The smallest bubbles can be achieved at concentrations higher than 0.2% (w/w) and are 0.052 mm in diameter for both rapeseed protein samples.

So, the foam stability increased with a higher protein content, while the interfacial properties were affected by the bulk concentration of the different components in RPC or DRPC in the opposite way. A low bulk concentration (0.01% w/w) gave a strong viscoelastic solid-like interface, while a high concentration (1% w/w) resulted in a less stiff and more stretchable interface. The mechanical strength of the interfacial layer is often related to the foam stability, where an increased layer strength would result in higher foam stability. A stronger viscoelastic layer could potentially slow down the bubble rupture. Yet, we did not observe such a relationship here for rapeseed protein-based foams. The increased stability appeared to be more correlated with the smaller bubble size at higher protein concentrations. Although the moduli of the interfacial films obtained with bulk concentrations of 0.01% (w/w) were substantially higher compared to bulk concentrations of 1% (w/w), the adsorption rate in these samples was considerably slower (Figure 2.2), which can be related to lower foamability and larger bubble sizes. Because of the faster adsorption, the foams at higher concentration have a smaller and more homogeneous distributed bubble size and are therefore more stable. The higher stretchability of the corresponding interfaces may also have provided additional protection against the coalescence of the air bubbles. The more brittle interfaces formed at low concentration displayed yielding at large deformations, possibly making the bubbles more prone to coalescence.

With regard to foam formation and stability, we also observed very minor differences between the rapeseed protein concentrate and defatted protein concentrate. The presence of OS in RPC did not appear to negatively influence the foam stability in the tested conditions (pH, ionic strength, and lipid content). Conversely, in many studies, protein-stabilised foams were destabilised due to the presence of fatty acids and oil/fat droplets, as they can decrease surface elasticity, thus increasing the chance for the coalescence of air bubbles[68,71,72,114]. This was not observed in our work, as both RPC and DRPC formed foams with comparable stability. The OS were not detected in AFM images, which could suggest that the OS are indeed not present at the interface as such. However, the OS could in principle be attached to the interfacial film as a sublayer, and therefore invisible for AFM measurements. Based on our data, this cannot be excluded, but even if this would happen, it does not affect the stability of foams in the tested conditions.

2.4 Conclusions

We studied the interfacial and foaming properties of a mildly obtained rapeseed protein concentrate that contained oleosomes, and of its derived defatted protein concentrate after solvent-based defatting. For the concentrate, the air-water interface displayed the behaviour of a disordered viscoelastic solid, and a weakening of the interfacial layer in shear and dilatational rheology was observed for increasing bulk concentration. This suggests that the presence of non-protein components hampered the connectivity of the interfacial layer. In the AFM images, we observed strand-like structures that may cause a weaker interfacial layer at higher concentrations. Removing the non-polar lipids from the concentrate to produce a defatted rapeseed protein concentrate allowed us to study their effects in more detail. The defatted protein concentrate contained only residual oleosome membranes, which consists of proteins and polar lipids. The defatted protein concentrate led to slightly stronger interfacial films compared to the concentrate; in both cases, the interfacial films became weaker with increasing bulk concentrations. This suggests that oleosome membranes influenced the interface stabilization by weakening the interfacial layer. On the other hand, both the rapeseed protein concentrate and defatted rapeseed protein concentrate could form foams with comparable stability. The presence of oleosomes in the concentrate (and at the concentrations studied in this work) did not influence the foam stability. The fact that non-protein components present after mild purification do not negatively influence the macroscopic foam properties, implies rapeseed protein mixtures have promising foam stabilising properties. The findings presented in this manuscript have important implications, since protein mixtures with high functionality can be produced, while reducing the use of water, chemicals, and energy.

2.5 Appendix

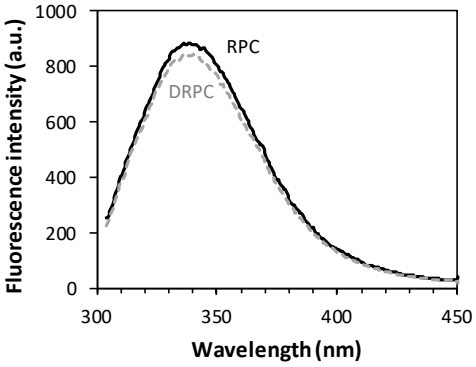

Figure A2.1. Fluorescence emission spectra (λex = 295 nm) of rapeseed protein concentrate (RPC, black solid) and defatted rapeseed protein concentrate (DRPC, grey dotted). Each spectrum represents the average of two replicates.

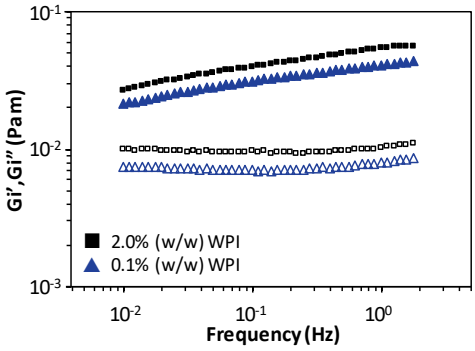

Figure A2.2. Storage (closed symbols) and loss moduli (open symbols) as a function of frequency of air-water interfacial films stabilised by whey protein isolate at pH 7. The different protein bulk concentrations (w/w) are depicted in the legend.

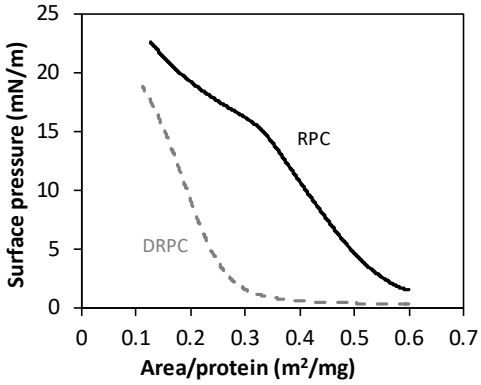

Figure A2.3. Surface pressure isotherms of Langmuir films stabilised by rapeseed protein concentrate (RPIC, solid) and defatted rapeseed protein concentrate (DRPC, dashed). The films were prepared by spreading the protein solution at the surface of the subphase (20 mM PO_4-buffer, pH 7.0) preliminarily placed in the Langmuir trough. Each isotherm represents the average of three replicates.

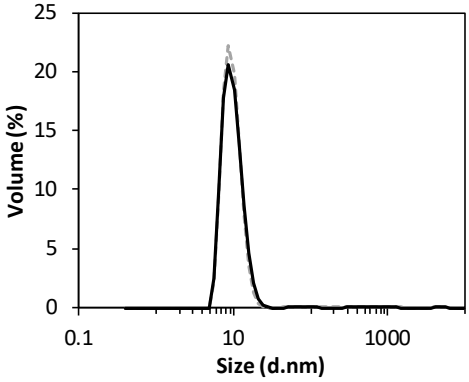

Figure A2.4. Particle size distribution of rapeseed protein concentrate (RPC, solid) and defatted rapeseed protein concentrate (DRPC, dash) in a 20 mM sodium phosphate buffer, pH 7.0, preliminarily filtered over 0.45 µm syringe filter. For clarity, one representative distribution is shown for each sample, but comparable distributions were obtained on two replicates.

Table A2.1. All variables of equation 2.2 for rapeseed protein concentrate (RPC) and defatted rapeseed protein concentrate (DRPC) at various protein concentrations. The averages and standard deviation were obtained from at least three replicates.

	Protein concentration (w/w)	Expansion		Compression	
		RPC	DRPC	RPC	DRPC
β	0.01%	0.61 ± 0.03	0.59 ± 0.04	0.58 ± 0.03	0.63 ± 0.02
	0.1%	0.56 ± 0.04	0.58 ± 0.06	0.60 ± 0.05	0.60 ± 0.02
	1%	0.59 ± 0.04	0.54 ± 0.06	0.67 ± 0.04	0.66 ± 0.06
τ_1	0.01%	26.2 ± 4.4	31.7 ± 5.2	24.1 ± 2.3	22.4 ± 4.1
	0.1%	28.0 ± 4.4	28.8 ± 4.1	22.3 ± 3.8	23.2 ± 2.7
	1%	29.4 ± 5.2	28.3 ± 6.6	23.0 ± 1.1	25.1 ± 4.9
τ_2	0.01%	650 ± 92	668 ± 50	476 ± 54	399 ± 61
	0.1%	649 ± 117	622 ± 40	474 ± 74	512 ± 34
	1%	551 ± 105	648 ± 149	456 ± 103	509 ± 171
a	0.01%	2.2 ± 0.0	2.1 ± 0.1	-2.8 ± 0.1	-2.2 ± 0.4
	0.1%	2.4 ± 0.5	3.1 ± 0.3	-3.7 ± 0.4	-3.0 ± 0.1
	1%	1.4 ± 0.1	2.3 ± 0.3	-1.5 ± 0.1	-1.8 ± 0.1
b	0.01%	1.9 ± 0.1	2.0 ± 0.1	-1.4 ± 0.1	-1.4 ± 0.2
	0.1%	1.5 ± 0.1	2.0 ± 0.1	-2.0 ± 0.3	-1.9 ± 0.1
	1%	0.8 ± 0.0	1.4 ± 0.2	0.8 ± 0.0	-1.3 ± 0.1
c	0.01%	54.9 ± 0.2	54.2 ± 0.3	53.1 ± 1.0	52.5 ± 2.2
	0.1%	47.8 ± 3.0	52.0 ± 0.8	48.4 ± 2.4	48.7 ± 0.5
	1%	41.9 ± 0.3	44.3 ± 0.6	40.6 ± 0.3	42.3 ± 0.3
R^2	0.01%	0.996	0.996	0.991	0.994
	0.1%	0.993	0.994	0.992	0.992
	1%	0.995	0.995	0.995	0.992

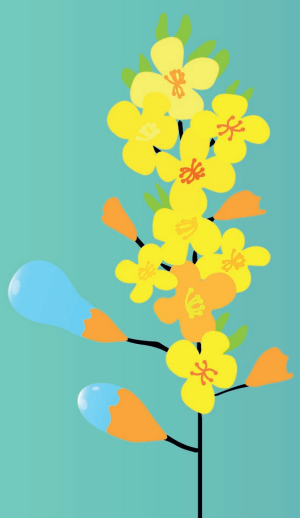

Chapter 3

Interfacial properties of aggregated whey proteins

Published as:
Yang, J., Thielen, I., Berton-Carabin, C. C., van der Linden, E., & Sagis, L. M. C. (2020). Nonlinear interfacial rheology and atomic force microscopy of air-water interfaces stabilized by whey protein beads and their constituents. Food Hydrocolloids, 101, 105466. https://doi.org/10.1016/j.foodhyd.2019.105466

Abstract

In recent years, food-grade Pickering particles have gained considerable interest, because of their ability to form stable emulsions and foams. Such Pickering stabilizers are often produced by aggregation of proteins, which typically results in a mixture of cross-linked particles and unbound proteins (smaller constituents). This study focuses on the possible contribution to the interfacial behaviour of these smaller constituents in whey protein isolate (**WPI**) bead suspensions, which are produced by cold-gelation of WPI aggregates. To understand the interfacial properties of the total mixture, we have studied the involved structures and interactions hierarchically, from native WPI, to aggregates, and finally gel beads. Air-water interfaces were subjected to large amplitude oscillatory dilatation (**LAOD**) and shear (**LAOS**) using a drop tensiometer and a double wall ring geometry. The nonlinear responses were analysed using Lissajous plots. The plots of native WPI- and aggregates-stabilized interfaces showed a rheological behaviour of a viscoelastic solid, while bead-stabilized interfaces tended to have a weaker and more fluid-like behaviour. The interfacial microstructure was analysed by imaging Langmuir-Blodgett films of the protein systems using atomic force microscopy (**AFM**). The native WPI and aggregate films had a highly heterogeneous structure in which the proteins form a dense clustered network. The beads are randomly distributed throughout the film, separated by large areas, where smaller proteinaceous material is present. This smaller and surface-active material present in the bead suspensions plays an important role in interface stabilization, and could also largely influence the macroscopic properties of interface-dominated systems.

3.1 Introduction

Many food systems consist of multiple immiscible phases, such as oil and water for emulsions[46] and air and water for foams[115]. These systems have a large interfacial area between the immiscible phases, which is thermodynamically unfavourable, and are therefore unstable without the presence of interface stabilizers. Conventional interface stabilizers in food are proteins and low molecular weight emulsifiers (**LMWEs**)[116], which are amphiphilic and have the ability to form interfacial layers. Interfaces stabilized by proteins can result in strong viscoelastic films[53,116,117], and differ considerably from interfaces stabilized by LMWEs, as the latter generally form relatively simple fluid-like interfaces[118]. This difference in interfacial microstructure may result in different stability of the macroscopic systems, such as emulsions and foams.

Recently, the interest in food-grade Pickering particles[119] has also been increasing, especially on protein-based stabilizers. Pickering stabilizers are solid colloidal particles, which partially wet both phases, and physically stabilize the interface[120,121]. A layer of particles at the oil-water interface form a mechanical barrier, protecting emulsion droplets against coalescence and Oswald ripening[121]. Several studies describe the ability to form stable emulsions using food-grade protein-based colloids and attribute stability to Pickering stabilization[122–124]. Foams stabilized with protein aggregates or particles may also have considerably increased foam stability compared to foams prepared with native proteins[56,84,125,126]. In fact, these large stabilizers increase the interfacial film thickness and block the liquid from drainage, resulting in stable foams for several days[125]. Although research has been carried out on the macroscopic properties, limited studies exist which investigate the interfacial properties of food-grade Pickering-stabilized interfaces. Studying the interfacial properties of the systems may help us better understand the stabilizing mechanism in macroscopic systems.

Protein-based Pickering stabilizers are often described as nano-particles[122,124,126,127], microgel particles[123,128] or beads[129,130], which are colloids made from cross-linked protein (aggregates). A common method is heat-induced cross-linking of the proteins and yields protein aggregates[56,122,124,127] or a protein gel. The latter requires mechanical disruption to obtain submicron colloids[123,128]. Another method to obtain spherical colloids (beads) requires the formation of a water-in-oil (w/o) emulsion with whey protein isolate (**WPI**) dissolved in the water phase and oil-soluble emulsifiers in the oil phase. The protein is cross-linked by heat-denaturation[122] or by salt-bridge formation, after addition of salt (cold-gelation)[129], and oil is removed by centrifugation.

In these protein particle systems, the presence of smaller constituents is often ignored in studies. However, they can have an enormous contribution to the functionality of cross-linked protein colloids suspensions. Recently, researchers have demonstrated that free

peptides present in soy protein fibril suspensions[131] can outcompete the protein fibrils for the air-water interface and thereby dominate the foam stability of the complete mixture. Another study has shown that the filtrate of WPI microgel particle suspensions exhibits surface activity similar to the complete mixture[123]. The contribution of these smaller constituents to the interfacial properties in mixture with Pickering stabilizers has not received much attention in literature yet.

In this paper, we aim to understand the interfacial properties of spherical WPI beads produced by cold-gelation of WPI heat-denatured aggregates with calcium salt bridges. This multistep process allows us to study the entire hierarchy of structures, starting from the native WPI protein, to the aggregates, and finally the beads. We attempt to study the role of these different colloid structures and sizes (2 – 350 nm) for their interfacial properties. We determine the linear and nonlinear rheological properties of these protein-stabilized air-water interfaces in both shear and dilatation. We examine the rheological properties using large amplitude oscillatory dilatational (**LAOD**) experiments, step dilatational measurements, and small and large amplitude oscillatory surface shear (**SAOS** and **LAOS**) experiments. The LAOD and LAOS measurements are analysed using Lissajous plots, and the dilatational stress-relaxation behaviour is analysed using a Kohlrausch-Williams-Watt stretched exponential function. Finally, we visualize the microstructure by imaging Langmuir-Blodgett films with atomic force microscopy to link the surface rheology behaviour to the interfacial microstructure.

3.2 Experimental section

3.2.1 Materials

Whey protein isolate (**WPI**) consisting of 74% β-lactoglobulin, 12.5% α-lactalbumin, 5.5% bovine serum albumin, and 5.5% IgG1[132] (purity 98%) (Davisco Foods international, France), Calcium chloride dihydrate ($CaCl_2 \cdot H_2O$) (purity ≥ 99%) (Sigma-Aldrich, USA), ethanol absolute (purity ≥ 99.2%) (Merck, Germany), polyglycerol polyricinoleate (**PGPR**) 90 kosher (Danisco, Denmark), and medium-chain triglyceride (MCT) oil (Miglyol 812 N) (Cremer Olea GmbH & Co., Germany) were all used as received. Other chemicals (Sigma-Aldrich, USA) and SDS-PAGE materials (Invitrogen Novex, Thermo Fisher Scientific, USA) were used as received. Solutions were made in ultrapure water (MilliQ Purelab Ultra, Germany).

3.2.2 Sample preparation

Calcium nanocrystals for WPI bead preparation

A 0.1 molal $CaCl_2 \cdot 2H_2O$ solution was prepared in ethanol. After dissolution, the solution was emulsified in MCT containing 2.5% (w/w) PGPR (oil-soluble emulsifier) at 20% (v/v) using

a Sonicator S-250A sonicator (Branson Ultrasonics, USA) for 1 min. The obtained emulsion was heated overnight at 60 °C while stirring to evaporate the ethanol[133].

Preparation of WPI solution

WPI solutions were prepared by dissolving 2.5% (w/w) WPI in a sodium phosphate buffer (20 mM, pH 7) for 4 h and centrifuged at 20,000xg for 30 min. The supernatant was filtered with a syringe filter with a 0.45 µm pore size. The solution was diluted with buffer to 2% (w/w) based on dry matter.

Preparation of WPI aggregates

A 10 % (w/w) WPI solution was stirred for 8 h, and the pH was adjusted to 8 using 1 M NaOH. The solution was heated at 80 °C for 30 min while stirring and afterwards cooled with tap water[129]. Aggregates for analysis were diluted to 2% (w/w) using a sodium phosphate buffer (25 mM, pH 7).

Preparation of WPI beads

The 10% WPI aggregates suspension was added slowly to a 2.5% (w/w) PGPR in MCT oil solution, up to a volume fraction of 10% (v/v), while mixed using a rotor-stator homogenizer (T25 Ultra-Turrax, IKA, GE) at 18,000 rpm. After complete addition, the emulsion was mixed for another 10 min. Calcium nanocrystals were added to the emulsion in a crystal/emulsion volume ratio of 0.72/1, and stored overnight to induce gelation of the proteins in the water droplets. On the following day, the emulsion was subsequently centrifuged at 50,000xg for 1 h. To remove the oil and the PGPR (which is insoluble in water) from the resulting pellet, it was re-dispersed in a 2% WPI solution and homogenised at 150 bar for 5 passes in a Lab Homogenizer (Delta Instruments, BE) followed by centrifugation at 23,500xg for 1 h. This results in a pellet containing the beads and a cream layer with residual oil and PGPR. Removing the oil and PGPR is necessary since they can affect the results of the surface rheology measurements. The pellet was re-dispersed in a 20 mM sodium phosphate buffer and homogenized at 160 bar for 3 passes. The beads were diluted to a 1 % (w/w) suspension based on dry matter.

3.2.3 Determination of the zeta-potential and the particle size

The zeta-potential and the particle size in the different samples were determined using dynamic light scattering in a Zetasizer Nano ZS (Malvern Instruments, UK). Samples were equilibrated for 2 min at 20 °C prior to analysis. The zeta-potential was measured at 20 °C and 40 V with a minimum of 25 individual measurements per determination. The size distribution was determined at 20 °C with 10 scans of 30 s in automatic mode, in which the attenuator and measurement position was selected automatically. The average was

calculated from the 10 scans. All measurements were performed in triplicates for various batches.

3.2.4 Determination of protein composition by SDS-PAGE

Protein samples were dissolved in MilliQ-water at 0.1% protein (w/w). Aliquots of 45 µl were mixed with 6 µl of 500 mM DTT and 7 µl running buffer. The mixtures were heated to 70 °C for 10 min, and 10 µl of the samples were loaded on a 4-12% BisTris gel. A marker of 2.5-200 kDa was included. Electrophoresis was performed for 30 minutes at 200 V. Finally, the gels were stained with SimplyBlue SafeStain and analysed using a gel scanner.

3.2.5 Determination of surface shear properties

The interfacial shear properties were studied using a magnetic air bearing stress-controlled rheometer (AR-G2, TA Instruments, USA) equipped with a double-wall-ring (**DWR**) geometry as described by Vandebril[134]. The DWR is a diamond-edged ring made of platinum and iron. The protein sample was transferred into a double wall trough, and the DWR was positioned at the interface. The trough was covered using a vapour cap to avoid evaporation. The sample was pre-sheared for 5 min at a shear rate of 10/s. After 10,800 s, frequency sweeps were performed with frequencies varying from 0.01 to 10 Hz at a constant amplitude of 1%. Strain sweeps were performed with strains varying from 0.01% to 100% at a constant frequency of 0.1 Hz. All experiments were performed at least in triplicate at 20 °C.

The rheometer provides information on the angle of rotation of the DWR and the torque exerted on the ring. Using this data and the geometrical parameters of the setup, the surface stress and the deformation of the interfacial layer can be determined. The Boussinesq number[134], which is the ratio of surface stress and bulk stress, was much larger than 1 for all protein systems and conditions studied in our work, which implies the contribution of the subphase to the torque signal was negligible.

3.2.6 Determination of surface tension and surface dilatational properties

The interfacial properties in dilatation were analysed using a drop tensiometer PAT-1M (Sinterface Technologies, GE) at 20 °C. A hanging drop with a surface area of 20 mm^2 was formed at the tip of a needle. The drop contour was monitored and fitted with the Young-Laplace equation to obtain the surface tension. The change in surface tension was monitored for 50,000 s. For the oscillatory dilatational measurements, the droplet was subjected to dilatational deformations after a waiting time of 10,800 s. Amplitude sweeps were performed with amplitudes between 2 – 30% at a frequency of 0.02 Hz. Frequency sweeps were performed with frequencies between 0.002 to 0.1 Hz at an amplitude of 3%. The droplet was subjected to five cycles at every amplitude or frequency. Step-dilatations were

performed by a sudden extension or compression (step time 2 s) of the droplet area by 10% and 20%. The measurements were done at least in triplicate.

3.2.7 Rheology data analysis

The results of the amplitude sweeps in dilatation were analysed using Lissajous plots of the surface pressure ($\Pi = \gamma - \gamma_0$) versus the deformation ($(A-A_0)/A_0$). Here γ and A are the surface tension and area of the deformed interface, γ_0 and A_0 are the surface tension and area of the non-deformed interface. Plots were drawn for each deformation from the middle three oscillations. For the quantitative analysis of the curves, four moduli were determined according to Van Kempen, et al.[135]: $E_{L,E}$, the large strain modulus in extension, $E_{M,E}$, the minimum strain modulus in extension, $E_{L,C}$, the large strain modulus in compression, and $E_{M,C}$, the minimum strain modulus in compression. These moduli were used to calculate the stiffening- or S-factors: $S_{exp} = (E_{L,E} - E_{M,E})/E_{L,E}$ for the extension part of the Lissajous plot, and $S_{com} = (E_{L,C} - E_{M,C})/E_{L,C}$ for the compression part.

3.2.8 Preparation of Langmuir-Blodgett films

Langmuir-Blodgett films of the protein-stabilized interfaces were prepared using a 243 mm^2 Langmuir film balance (Langmuir-Blodgett Trough KN 2002, KSV NIMA/Biolin Scientific Oy, Finland) at room temperature. The balance was filled with a sodium phosphate buffer (20 mM, pH 7). Protein layers were formed by spreading protein solution (200 µl, 0.16 mg protein/ml) on the surface using a gas-tight syringe and were equilibrated for 30 min. The surface pressure was monitored using a Wilhelmy plate (platinum, perimeter 20 mm, height 10 mm). The layer was compressed to reduce the surface area of the trough, with barriers moving at 5 mm/min. After reaching a stable surface pressure, the films were transferred on a freshly cleaved mica substrate (Highest Grade V1 Mica, Ted Pella, USA) and 1 mm/min withdraw speed. The films were dried in a desiccator and stored at room temperature until analysis. The films were produced in duplicate.

3.2.9 Determination of the interfacial structure by AFM

The interfacial structure was investigated using an atomic force microscope (**AFM**, MultiMode 8-HR, Bruker, USA). AFM images of the Langmuir-Blodgett films were recorded in tapping mode using Scanasyst-air model non-conductive pyramidal silicon nitride probes (Bruker, USA) with a normal spring constant of 0.40 N/m. A lateral scan frequency of 0.977 Hz was employed for all topographical images. The lateral resolution was set to 512 x 512 $pixels^2$ in a scan area of 2 x 2 μm^2 for WPI films and 10 x 10 μm^2 for aggregate and bead films. At least two locations were visualized for each sample to ensure good representativeness. The AFM images were analysed using Nanoscope Analysis 1.5 software (Bruker, USA).

3.3 Results and discussion

3.3.1 Particle size and charge

First, we have characterized the ζ-potential and particle size distribution of the native whey protein isolate (**WPI**), aggregates, and beads suspensions. The ζ-potential of the different samples is -16.3 ± 2.4 mV for native WPI, -27.4 ± 3.4 mV for aggregates and -29.5 ± 1.9 mV for beads in a 20 mM phosphate buffer at pH 7. A more negative ζ-potential of the aggregates compared to native WPI can be explained by the loss of positively charged groups, which are buried within the hydrophobic regions, upon the aggregation of unfolded proteins, thereby increasing the negative net charge[136]. Similar ζ-potential values are obtained for the aggregates and beads, which is expected as the aggregates are constituents of the beads. These values are comparable to earlier described work[122], where a ζ-potential around the -30 mV is found at pH 7 for WPI beads produced by heating.

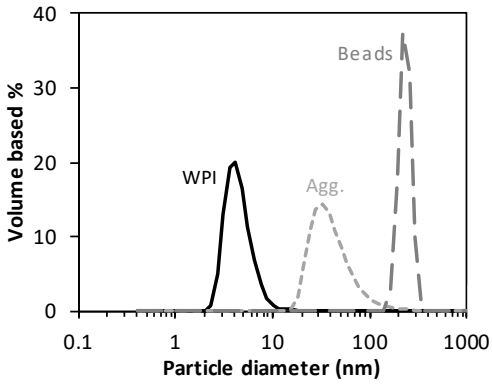

Figure 3.1. Particle distributions in a native WPI solution (solid), aggregates (short dash) and bead (long dash) suspensions in a 20 mM PO4 buffer, pH 7.

The WPI solution shows a particle diameter between 2 and 10 nm with a maximum height of around 4 nm (Figure 3.1). This is the typical size of a β-lactoglobulin dimer[137]. WPI aggregates are larger than the native proteins (20 – 100 nm), as the proteins aggregate upon heat denaturation. Gelation of the aggregates by calcium-salt-bridges results in beads with a size between 150-350 nm with a peak size around 220 nm.

3.3.2 Adsorption behaviour

The adsorption behaviour of the three protein systems (Figure 3.2) is studied using drop tensiometry. The first measurement point at 1 s varies between surface pressure values around 12-22 mN/m, which is followed by a continuous increase over the timescale of the experiment (up to 14 h). The beads increase the surface pressure to a higher extent than both native WPI and aggregates, while the latter has the lowest surface pressure increase over time. We expect lower surface pressures for the aggregates than native WPI, as the

total number of surface-active molecules decreases upon aggregation and the larger size reduces their diffusion rate to the interface[56,126], as the adsorption of the proteins is diffusion-limited in the drop tensiometer.

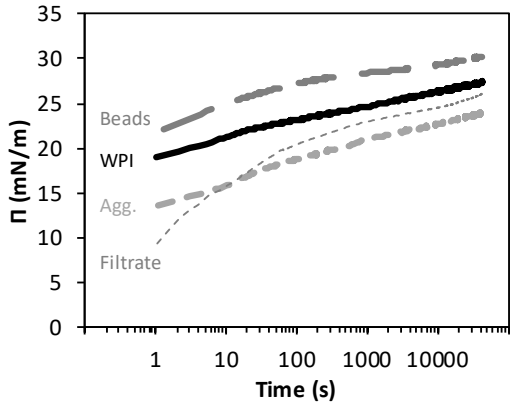

Figure 3.2. The surface pressure as a function of time of an air-water interface stabilized by native WPI (solid), aggregates (short dash) and beads (long dash) in a 20 mM PO4 buffer, pH 7, obtained from the drop tensiometer. The thin line shows the surface pressure isotherm of WPI beads filtrate over a 300 kDa filter.

This size effect is not observed for the larger beads, as these particles increase the surface pressure to the highest extent. Destribats et al.[123] have shown that the filtrate from WPI microgel particle suspensions is remarkably surface-active. For this reason, we have filtered the WPI beads suspension over a 300 kDa filter (Ø = 8.8 nm[138]). The filtrate shows a slow increase of surface pressure from 9 mN/m and reaches a surface pressure comparable to that of native WPI after 14 h of ageing. Due to the size of the filter, only a fraction of the filtrate probably passed the membrane. Based on our observations, we hypothesize that the surface activity of our beads is due to the fast diffusion of small constituents present in the beads suspension. Smaller constituents could consist of non-gelled aggregates and non-aggregated protein[56]. Additionally, we have studied the protein composition of the filtrate using SDS-PAGE, and we have observed similar protein compositions for the native WPI, aggregates, beads, and filtrate of the beads (SDS-PAGE gel can be found in Figure A3.1 in the appendix). This even stronger suggests that the filtrate consists of the smaller constituents of the beads.

For all three protein systems, the surface pressure increases over the timescale of these experiments. No equilibrium is reached, even after 14 h of ageing. The same is observed for the major whey protein β-lactoglobulin after 12 h of ageing by Rühs et al.[55], and the time-tail is often related to long-term rearrangements of protein molecules at the interface[55]. Often, these slow rearrangements are attributed to protein denaturation, which should occur to a higher extent for native WPI, as the aggregates and beads already are (partly) heat-

denatured. Nonetheless, we see a rather similar increase in surface pressure for all protein systems. Other processes besides protein denaturation are likely to be involved at the interface, such as the falling apart of aggregates/beads or in-plane rearrangements, including clustering of the proteins[108,139]. Ideally, when conducting interfacial rheology experiments, the deformations applied to the interface should start after reaching equilibrium. As the protein systems do not reach equilibrium, the surfaces are aged for three hours before starting shear or dilatational deformations, limiting the effect of the ageing processes during the cycles, hence limiting the effect on the moduli values of the interfacial layer.

3.3.3 Surface shear rheology

Frequency sweeps

In the frequency sweeps (Figure 3.3A), we observe that the storage modulus (***G_i'***) is larger than the loss modulus (***G_i''***) for WPI- and aggregate-stabilized interfaces, which is indicative for a predominantly elastic interfacial layer. The G_i' of both films scales with frequency as $G_i' \sim \omega^n$ and yields an n-value of 0.14. The weak frequency dependency and power-law behaviour imply a wide spectrum of relaxation times for the interfacial structure. Gels[140] and soft glassy materials[104,141] exhibit similar power-law behaviour, which is also observed for acacia gum- and bovine serum albumin-stabilized interfaces[104]. The fact that we observe this behaviour for WPI- and aggregate-stabilized interfaces is an indication that these components also form disordered solid structures at the interface.

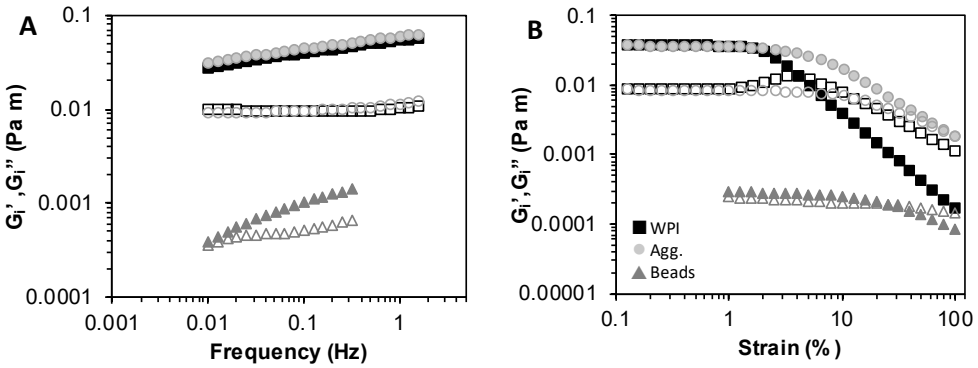

Figure 3.3. (A) G_i' and G_i'' as a function of frequency, with a fixed strain of 1% and (B) G_i' and G_i'' as a function of strain, with a fixed frequency of 0.1 Hz, of native WPI- (black square), aggregate- (grey circle) and bead-stabilized (grey triangle) air/water interfaces in a 20 mM PO4, buffer, pH 7. Closed symbols show the storage modulus G_i' and open symbols show the loss modulus G_i''.

Interfaces stabilized by beads have moduli that are almost two orders of magnitude lower than those of WPI- and aggregate-stabilized interfaces. For bead-stabilized interfaces, we observe a much stronger frequency dependency (n-value = 0.37) compared to WPI and aggregates. Additionally, the cross-over of G_i' and G_i'' for the beads (around 0.01 Hz) occurs

at a higher frequency compared to WPI and aggregates-stabilized interfaces (<0.01 Hz), which implies shorter relaxation times for bead-stabilized interfaces. This suggests the formation of a more mobile interfacial structure by the beads compared to the other materials.

Strain sweeps

Figure 3.3B shows the strain sweeps of all three protein-stabilized interfaces, which have a constant G_i' and G_i'' until a critical strain (5% decrease of G_i' from the max strain) of 1.2% for WPI, 2% for aggregates and 3.5% for beads, which represents the range of the linear viscoelastic regime (LVE). We observe $G_i' > G_i''$ in the LVE regime, suggesting solid-like behaviour. The G_i' in the LVE regime of WPI- and aggregates-stabilized interfaces are comparable, which are 0.035 and 0.041 Pa·m, respectively, and they have a similar tanδ of around 0.24. At strains above the critical strain, G_i' starts to decline with different slopes, and the G_i' of the WPI-stabilized interface has a steeper decrease compared to aggregate-stabilized interfaces. This results in a different strain value for the crossover point, which is 5% for WPI and >100% for aggregates. Additionally, the G_i'' of native WPI has a weak strain overshoot, which is commonly referred to as type III nonlinear behaviour, and is often found for soft solid materials in bulk rheology, such as particle and emulsion gels[57]. It is attributed to the balance between breakdown and formation of network junctions, where new junctions are the result of collisions of clusters. At even higher strains, the clusters break down, which leads to softening behaviour.

The bead-stabilized film shows a G_i' in the LVE regime of $3.8 \cdot 10^{-4}$ Pa·m with a tanδ of 0.84. These moduli are two orders of magnitude lower than the values of WPI- and aggregate-stabilized films. Measurements for this system are close to the machine limits, which is reflected in the first accurate data point of the strain sweep starting at 1%. The bead-stabilized interface is thus clearly weaker and exhibits solid-like behaviour to a lesser extent than the other two systems.

The moduli in Figure 3.3B, are obtained from the first harmonic of the Fourier transform of the stress signal. Nonlinearities in the stress response are the result of changes in the interfacial microstructure induced by the applied deformations, and will generate higher harmonics in the Fourier spectrum. As the moduli in Figure 3.3B are calculated from only the first harmonic, any higher-order harmonics are neglected. Therefore, the accuracy of the moduli determined in the nonlinear viscoelastic (**NLVE**) regime is questionable, as demonstrated by several studies[57,59,142] (which we also demonstrate in Figure A3.2 and A3.3 in the appendix for shear and dilatation). To include the contributions from the higher harmonics, the torque is plotted against the deformation in so-called Lissajous plots[58].

Additionally, we have plotted the decomposition of the torque into its elastic and viscous contribution to further elaborate the intra-cycle behaviour.

Lissajous plots

In the Lissajous plots (Figure 3.4) for native WPI- and aggregate-stabilized interfaces, we observe plots with a narrow ellipse shape for strains <2%, indicating linear viscoelastic behaviour with a predominantly elastic response. This is also reflected in the fact that the torque signal is very close to the dashed curve, representing the purely elastic contribution. At larger deformations, the plots are becoming wider, which indicates a more significant contribution of the viscous response. At 18% strain, the Lissajous plot for WPI-stabilized interfaces takes on a rhomboidal shape, which is an indication of intra-cycle yielding: starting from the lower-left corner of the plot, the initial response of the interface is elastic, until the surface shear stress exceeds the yield stress of the interfacial microstructure, and the interfacial film starts to flow (this should not be confused with macroscopic fracture of the interface). As a result, the yielding is followed by a plateau with a near-zero slope where the response is predominantly viscous. The dashed curves confirmed this for the elastic contribution, which has a slope close to zero, and hence shows a very limited elastic response in this strain range. At maximum positive strain (the upper right corner of the plot), the surface shear rate is zero, and the interfacial microstructure (partially) recovers. Continuing the cycle in the negative strain direction, we first get an elastic response again, followed by yielding and flow. Hence, the rhomboidal shape represents a continuous cycle of yielding and recovery events.

Close to the maximum strain, the dashed elastic contribution curves increase steeply, suggesting intra-cycle strain hardening. A combination of strain softening observed in Figure 3.4 and strain hardening in the Lissajous plots seems contradicting, and is sometimes described as the strain softening/hardening paradox[143]. The observed strain hardening is merely a local effect in the intra-cycle measurements, in a regime where the overall behaviour of the interface is dominated by the viscous contribution, resulting in strain softening. For the aggregate-stabilized interface, the transition to a rhomboidal shape occurs at higher strains and is more gradual. The slope of the plot does not go to zero after yielding, which indicates that the interface retains a considerable degree of elasticity. The plots of the bead-stabilized interfaces reveal wide plots, and show a much more viscous behaviour, which is partially obscured by the noise in the signal because of the low torque stress values generated by these interfaces. Beads form a weak and mobile interface, which is indicative for more fluid-like systems. This could imply that the smaller constituents in the bead suspension play an important part in forming the interfacial layer.

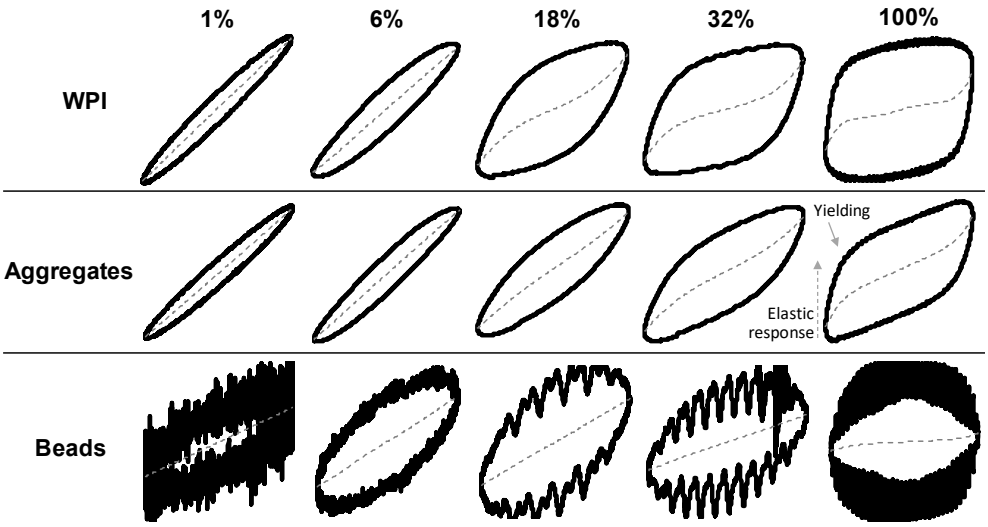

Figure 3.4. Lissajous plots of torque as a function of deformation obtained during strain sweeps of air-water interfaces stabilized by native WPI, aggregates or beads at a frequency of 0.1 Hz. The plots were normalized to their maximum value for the torque. The dotted grey lines show the elastic contribution to the torque.

3.3.4 Oscillatory dilatational rheology

Frequency sweeps

The three WPI-based materials are first studied over a range of frequencies in a frequency sweep (Figure 3.5A).

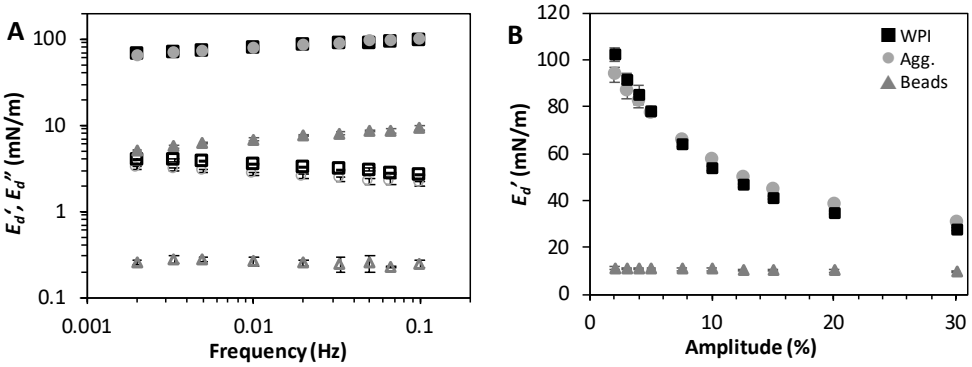

Figure 3.5. (A) The E_d' (closed symbols) and E_d'' (open symbols) over frequency, with a fixed amplitude of 3%; (B) The E_d' over amplitude, with a fixed frequency of 0.02 Hz, for air-water interfaces stabilized by native WPI (black square), aggregates (grey circle) or beads (grey triangle) in a 20 mM PO4-buffer, pH 7.

The three systems show dilatational storage (***E_d'***) and loss moduli (***E_d''***) that are weakly frequency-dependent, and have a low tanδ between 0.02 and 0.06. The complex surface dilatational modulus scales with frequency as $E_d' \sim \omega^n$. According to the Lucassen-Van den

Tempel model[144], a value of n=0.5 indicates that the elasticity of the interface is mainly dominated by the exchange of stabilizer between the bulk and the interface. Here the slope values (n) are 0.11 for WPI, 0.09 for aggregates and 0.15 for beads (± 0.00 for all systems). The n-values are thus much lower than 0.5, indicating that other processes play a more dominant role in the elasticity of the surface, such as in-plane interactions due to rearrangements at the interface, or momentum transfer between bulk and interface[108]. The frequency sweeps in both dilatation and shear (Figure 3.3A & 3.5A) show a weak power-law behaviour for the WPI- and aggregate-stabilized interfaces, which again indicates the formation of disordered gel-like or soft glassy structures.

Amplitude sweeps

Upon increasing the amplitude of the applied dilatational deformation from 2 to 30%, we observe a decrease of E_d' from 102 to 28 mN/m for both native WPI- and aggregates-stabilized interfaces (Figure 3.5B), which reveals that the applied deformation is affecting the interfacial microstructure. On the other hand, the moduli of bead-stabilized interfaces are nearly constant, and thus are in the LVE regime. This implies a weak interface that is more easily stretchable compared to the stronger microstructure of native WPI and aggregates. The studied range of deformations for both WPI- and aggregate-stabilized interfaces are in the NLVE as the E_d' decreases at higher amplitudes, and are also studied with Lissajous plots to include the higher harmonics of the Fourier spectrum.

Lissajous plots

The Lissajous plots (Figure 3.6) of native WPI-stabilized interfaces show a viscoelastic response and become more asymmetric at larger deformations. At 10-30% deformation, we observe a steep surface pressure increase at the start of the extension. The steep increase is followed by a sudden decrease to near-zero slope, which (just as in the surface shear deformations) indicates intra-cycle yielding behaviour of the interfacial structure upon extension. As the interfacial structure is disrupted at large amplitudes, the elastic component in the response diminishes, and results in flow of the system where a viscous response dominates. On the other hand, the Lissajous plots show a steeper surface pressure increase in compression compared to extension, which is known as intra-cycle strain hardening. These large deformations may cause the interface to form densely clustered regions that could start jamming upon compression. The same asymmetry of Lissajous plots has been observed in many interface systems in LAOD experiments[125,131,135,145,146]. In our work, a comparable yielding and flow behaviour is revealed in both dilation and shear (Figure 3.4 & 3.6), which suggests the formation of a solid-like structure by the protein, and results in a contribution of in-plane deviatoric stresses to the surface pressure.

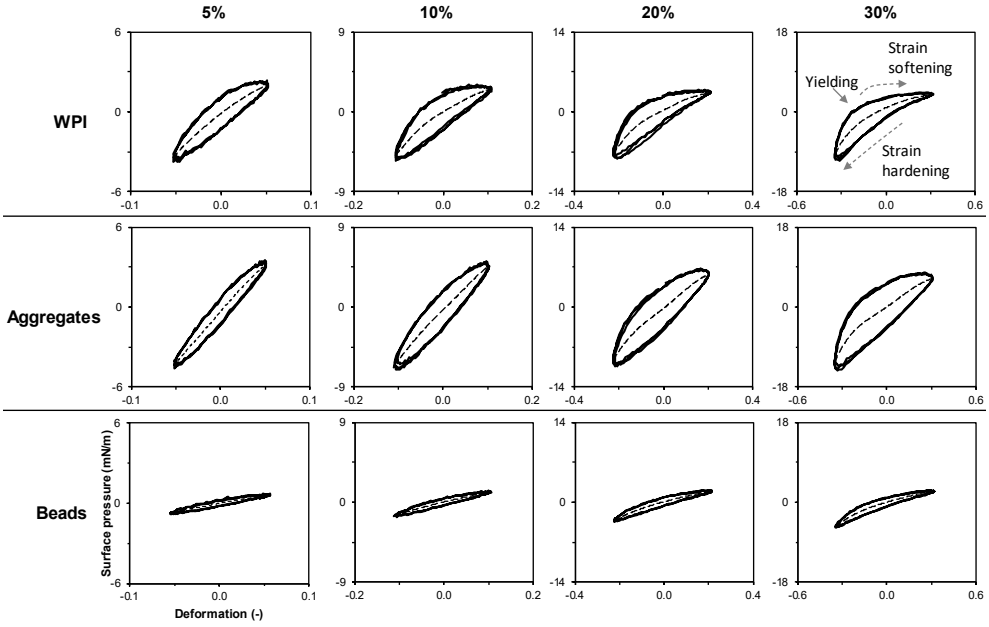

Figure 3.6. Lissajous plots of surface pressure versus deformation obtained during amplitude sweeps of air/water interfaces stabilized by native WPI, aggregates or beads at a frequency of 0.02 Hz

The Lissajous plots of aggregate-stabilized interfaces are wider and more symmetric than those of the WPI-stabilized interfaces. At the highest amplitude they do not display a similarly abrupt yielding as the WPI-stabilized interfaces, but instead, a more gradual strain softening. According to these findings, the microstructure of the aggregate-stabilized interface is less affected by the applied deformation, which can result from the formation of a stronger network by aggregates[147]. These differences in the Lissajous plots are not shown in the E_d' found in Figure 3.5B, demonstrating the limitations of calculating the modulus based on the first harmonic only. The Lissajous plots of the bead-stabilized interface are very narrow and have a relatively low maximum surface pressure. This suggests the formation of a weaker and more stretchable (less brittle) interface compared to native WPI and aggregates, which is in agreement with the moduli reported in Figure 3.5B and supports our assumption that the interface is mainly stabilized by the smaller constituents of the beads suspension.

To quantitatively study the Lissajous plots, we have determined the S-factors (stiffening-factor) in extension and compression for all protein systems (Figure 3.7).

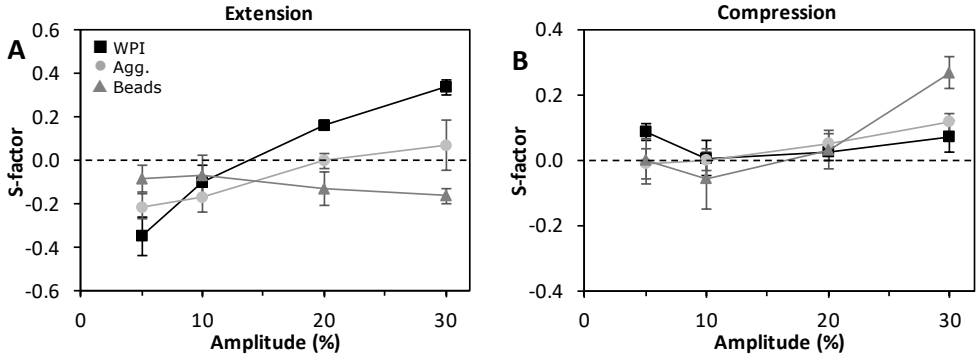

Figure 3.7. The S-factor in extension (A) and compression (B) of air-water interfaces stabilized by native WPI (black square), aggregates (grey circle) or beads (grey triangle) in a 20mM PO4-buffer, pH 7.

The S-factor can be interpreted as follows: for a linear elastic response, S=0; for interfaces displaying strain hardening, S > 0; and for interfaces displaying strain softening, S < 0. Upon extension (Ewoldt et al., 2007), the WPI-stabilized interface shows strain softening at low amplitude. The S-factor increases with increasing amplitude and even becomes positive for 20% deformation and higher. This is the same strain softening/hardening paradox observed in the shear rheology (Figure 3.3B & Figure 3.4). A more linear response of the aggregate-stabilized interfaces can also be observed in extension, where the S-factors are close to zero. For both WPI and aggregates, the interfaces show a mild strain hardening upon compression, which increases slightly at higher amplitudes. Bead-stabilized interfaces show a near linear response in extension and a steep increase from near linear elastic response to strain hardening at higher deformations in compression. At higher compressions, the interfacial stabilizers in the bead suspension could start jamming, which is also observed for the WPI- and aggregate stabilized interfaces.

The differences in the protein systems are in line with earlier work[148], where air-water interfaces stabilized by β-lactoglobulin monomers, peptides or heat-denatured fibrils were studied in LAOD experiments. In that study, the fibril solutions, which contain peptides, were filtered to obtain a supernatant with only peptides. The peptides of β-lactoglobulin showed the rheological properties of a weak and fluid-like film, similar to the behaviour of our WPI beads. Smaller peptides are also described as the main contributor to the interfacial properties in a mixture with soy protein fibrils[131]. This again, even stronger, suggests that smaller constituents predominantly stabilize the interface of the bead system.

3.3.5 Stress-relaxation after step-dilatation

The interfaces are subjected to step-dilatation (i.e. sudden extension or compression of the droplet) to further evaluate the structural properties. The first 1,000 s of the relaxation response are fitted using a combination of a Kohlrausch-William-Watts (**KWW**) stretch exponential term and a regular exponential, which is depicted in Equation 3.1[107]. An example of the step relaxation measurement and its fit is shown in A3.4 in the appendix. The KWW stretch exponential is a phenomenological model for fitting relaxation processes in disordered systems.

$$\gamma(t) = ae^{-(t/\tau_1)^{\beta}} + be^{-t/\tau_2} + c \quad (3.1)$$

In the first term, τ_1 is a relaxation time, and β is the stretch exponent. In the time sweeps of protein interfaces, we observe a surface pressure increase even after 14 hours (Figure 3.2), which is related to slow rearrangements of the proteins at the interface. The second term with characteristic time τ_2 is necessary to decouple the ageing of the interface from the actual relaxation process. Parameters a, b, and c are constants.

Table 3.1. The β and τ_1 for native WPI, aggregate and bead interfaces at 10% and 20% deformations. The remaining variables can be found in Table A3.1 in the appendix.

		Extension		***Compression***	
		10%	***20%***	***10%***	***20%***
β	**WPI**	0.56 ± 0.04	0.54 ± 0.03	0.65 ± 0.01	0.60 ± 0.01
	AGG	0.51 ± 0.02	0.55 ± 0.03	0.56 ± 0.02	0.59 ± 0.02
	Beads	0.52 ± 0.04	0.52 ± 0.03	0.63 ± 0.10	0.58 ± 0.06
τ_1	**WPI**	19.6 ± 1.0	15.8 ± 3.2	20.0 ± 2.2	16.5 ± 1.1
	AGG	21.5 ± 4.4	16.5 ± 1.8	23.8 ± 1.1	17.3 ± 1.9
	Beads	33.2 ± 12	41.6 ± 7.3	16.9 ± 7.2	22.7 ± 8.3

In Table 3.1, we show β-values from 0.56 to 0.65 in compression and from 0.51 to 0.56 in the extension of the interface for all three protein systems. This asymmetry in compression and extension is also present in the Lissajous plots of the LAOD experiments (Figure 3.6). A stretch exponent of $\beta<1$ indicates a phenomenon referred to as dynamic heterogeneity. Dynamic heterogeneity is related to local variances in the relaxation kinetics, which result in a broad spectrum of relaxation times[149]. The values observed here are similar to those of the relaxation processes in 3d disordered solids[108,111,149]. Others have found comparable β-values between 0.50 and 0.66 for β-lactoglobulin- and β-casein-stabilized[110] interfaces upon

compression. The τ_1-values of all three systems are in the same range in compression, which is not the case in the extension of the interface. In extension, the τ_1-values for bead-stabilized interfaces are almost two times higher compared to the other systems, which we will discuss in the following sections.

3.3.6 AFM images of microstructure

Dynamic heterogeneity could be related to the interfacial microstructure, which we have visualized by performing AFM on Langmuir-Blodgett films. In Figure 3.8, we show the topography of such films made by loading the protein film onto a mica substrate at various surface pressures. The surface pressure isotherms during film compression, before loading, can be found in Figure A3.5 in the appendix.

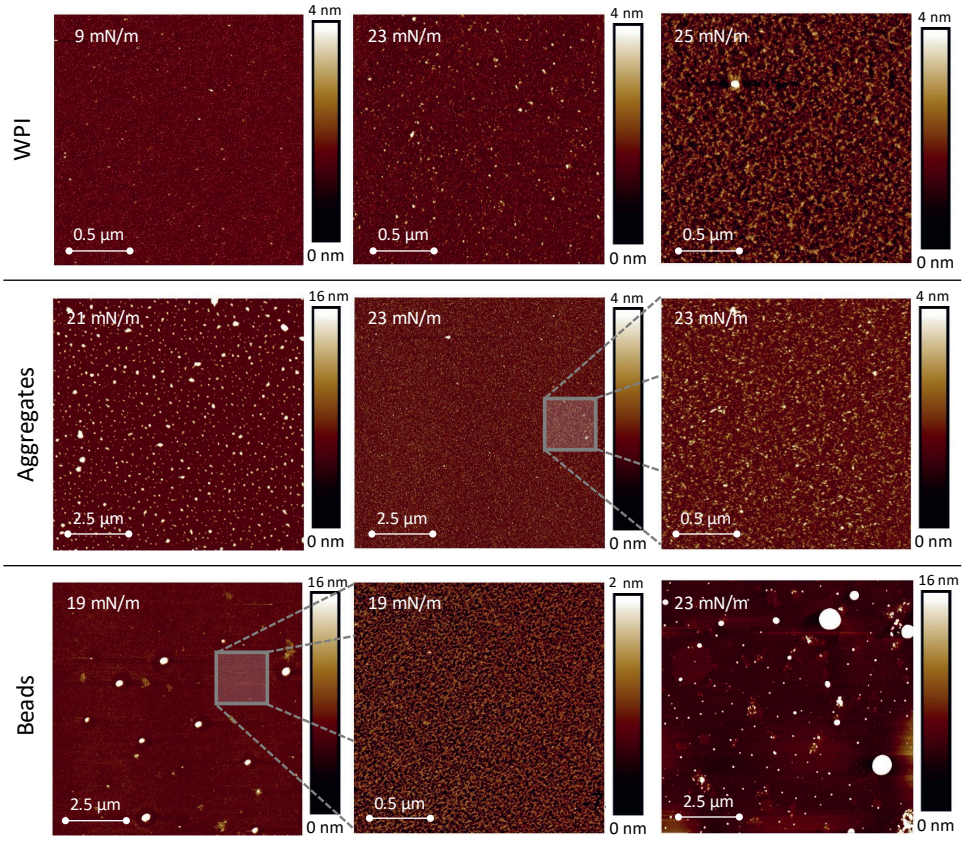

Figure 3.8. AFM images of Langmuir-Blodgett films made from native WPI-, aggregate- and bead-stabilized interfaces. The surface pressure during the film sampling is indicated on the top-left corner.

WPI-stabilized interfaces exhibit a heterogeneous structure with an overall film thickness of ≤4 nm, which is close to the size of proteins (Figure 3.1). At a low surface pressure of 9 mN/m, the film shows thicker regions, which could be more densely clustered regions. At higher surface pressures, the clustered regions are more dense due to higher compression, but still exhibit a heterogeneous structure. Additionally, the film at the highest surface pressure of 25 mN/m closely resembles fractal structures, which are also found in 3D gels. Similar structural heterogeneities can also be observed in AFM images of various protein films, such as β-lactoglobulin[112,148], bovine serum albumin[113,150], and β-casein films[112,150]. Formation of such heterogeneous structures would also explain the weak strain overshoot in the G" of native WPI in the LAOS experiments (Figure 3.3B).

A heterogeneous structure is also found for the aggregate- and bead-stabilized interfaces. The aggregate film at a surface pressure of 21 mN/m is largely covered with aggregates, whereas they largely disappear from the film at a surface pressure of 23 mN/m. If we take a closer look at the interface by scanning a smaller area, we observe a structure similar to highly compressed native WPI interfaces. The absence of the aggregates at the higher surface pressure could suggest the loss of the aggregates at the surface, which does not necessarily suggest the loss of the aggregates from the interface. Aggregates could still remain at the interface, but could be pushed down towards the bulk phase upon compression, which causes them to be invisible for topographical measurements.

WPI beads are present at the interface at a surface pressure of 19 and 23 mN/m. The beads co-exist with aggregates, while thin regions are present between the beads and aggregates, even at higher compression. For these films, we have also scanned a smaller area between the beads, and we reveal a finer and less segregated film compared to the WPI and aggregate films (see cross-sections and height profiles in Figure A3.6 in the appendix). These images give an indication that smaller constituents are present in the bead films, which further supports our hypothesis on their contribution to the interfacial properties, and results in the formation of a weak and mobile interface observed in shear and dilatation. It is important to bear in mind that the films are formed in the Langmuir trough by spreading the material at the interface, which is different compared to the diffusion-based adsorption in the drop tensiometer and rheometer. Interfaces formed by the latter described mechanism might not contain the aggregates and beads, as there could be competition for the interface with the non-aggregated/gelled constituents.

The heterogeneous structures in all three protein films are closely related to the dynamic heterogeneity in the relaxation experiments (Table 3.1). This relationship has been demonstrated extensively by Sagis et al.[108] for fluid interfaces stabilized by a large number of stabilizers, including native proteins, protein aggregates and cross-linked protein particles

from various sources. They have shown that the main process of such relaxation behaviour is the momentum transfer between bulk and interface. Our frequency sweeps for native WPI- and aggregate-stabilized interfaces (Figure 3.3A & Figure 3.5A) also reveal a material with a wide range of relaxation processes, which could be related to the highly disordered structures that are confirmed by AFM.

For the bead-stabilized interface, we observe a different type of interface in the AFM images, which show a fine and dense film mainly covered by the smaller constituents. Frequency sweeps on bead-stabilized interface show a stronger frequency dependency and cross-over point at a higher frequency compared to the other stabilizers, which indicates the formation of a more mobile interfacial layer. Momentum transfer between bulk and interface could be less dominant as a relaxation mechanism for this interface. Additional relaxation mechanisms as mass transfer between bulk and interface, and in-plane reorganization could play a more dominant role for the bead-stabilized interfaces, which could cause slightly higher relaxation times upon extension in the stress-relaxation experiments.

3.4 Conclusion

We have studied the interfacial properties of air-water interfaces stabilized by three WPI-based systems: native WPI, WPI aggregates, and WPI beads. The native WPI- and aggregates-stabilized interfaces show power-law behaviour and weak frequency dependence in frequency sweeps in the LVE regime, suggesting these stabilizers form disordered solid structures. AFM images of the topography of Langmuir-Blodgett films indeed showed structural heterogeneity of the interfacial microstructure, which is intimately related to the dynamic heterogeneity in the stress-relaxation response. In the NLVE regime in both shear and dilatation, the Lissajous plots used to study the nonlinearities of the stress signal, confirm that the WPI- and aggregate-stabilized interfaces have a rheological behaviour of a viscoelastic solid.

WPI bead-stabilized interfaces show a different rheological response with a stronger frequency dependence of the moduli, and form a much weaker interface and more fluid-like behaviour compared to WPI and aggregates. In AFM images, we observe the presence of beads and smaller constituents, of which the latter show remarkable surface activity in time sweeps. The evidence in this study suggests that these smaller constituents in our WPI beads systems are likely to have a major contribution to the rheological properties on the air-water interface. The WPI bead system does not behave as a classical Pickering system, but instead forms mixed interfaces consisting of particles and non-crosslinked proteins.

3.5 Appendix

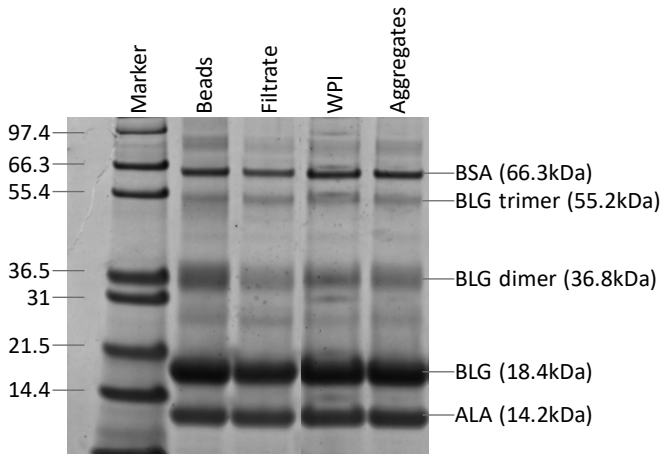

Figure A3.1. An SDS-PAGE gel scan of beads, beads filtrate, WPI and aggregates under reducing conditions. Labels of proteins are indicated on the right.

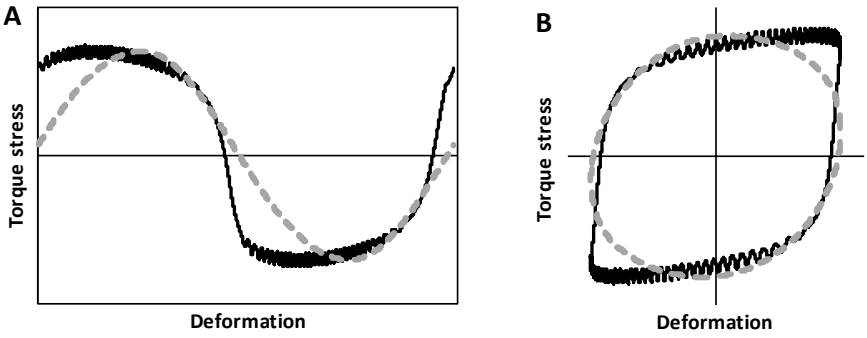

Figure A3.2. (A) The torque versus deformation, and (B) a Lissajous plot of torque over deformation of WPI at 100% strain. The black solid line represents the output of the rheometer, and the dotted grey line represents the torque stress signal of the first harmonic in the Fourier spectrum.

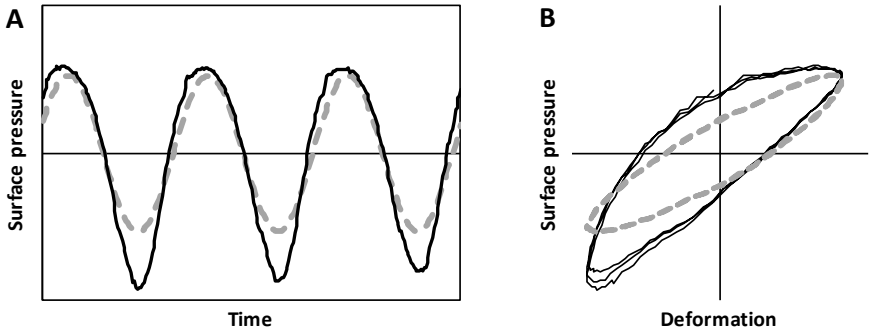

Figure A3.3. (A) The surface pressure over time, and (B) a Lissajous plot of surface pressure over deformation of WPI at 20% amplitude. The solid black line represents the output of the drop tensiometer, and the dotted grey line represents the surface pressure signal of the first harmonic in the Fourier spectrum.

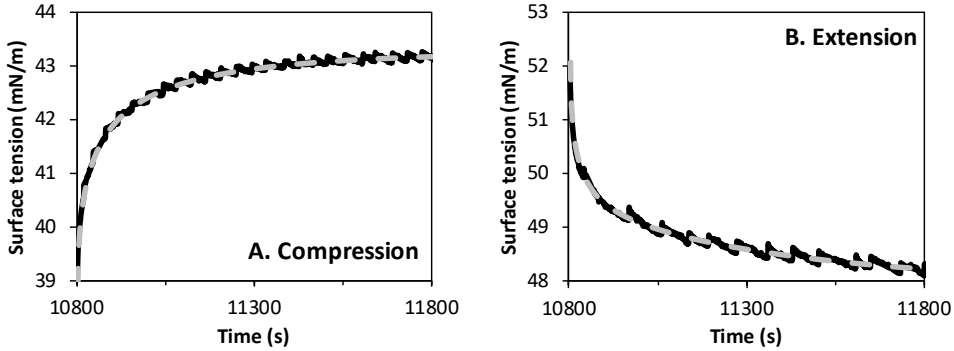

Figure A3.4. The surface tension over time of the first 1,000 s of the relaxation step in the step-dilatation experiments upon compression (A) and extension (B) of a WPI-stabilized interface. The solid black line shows the data, and the dotted grey line shows the fit of Equation 3.1.

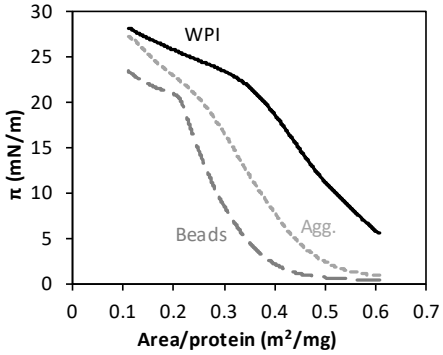

Figure A3.5. Surface pressure isotherms of protein films made from WPI (solid), aggregates (short dashed) and beads (long dashed) by spreading the protein at the interface in a 20mM PO_4-buffer, pH 7, in the Langmuir trough.

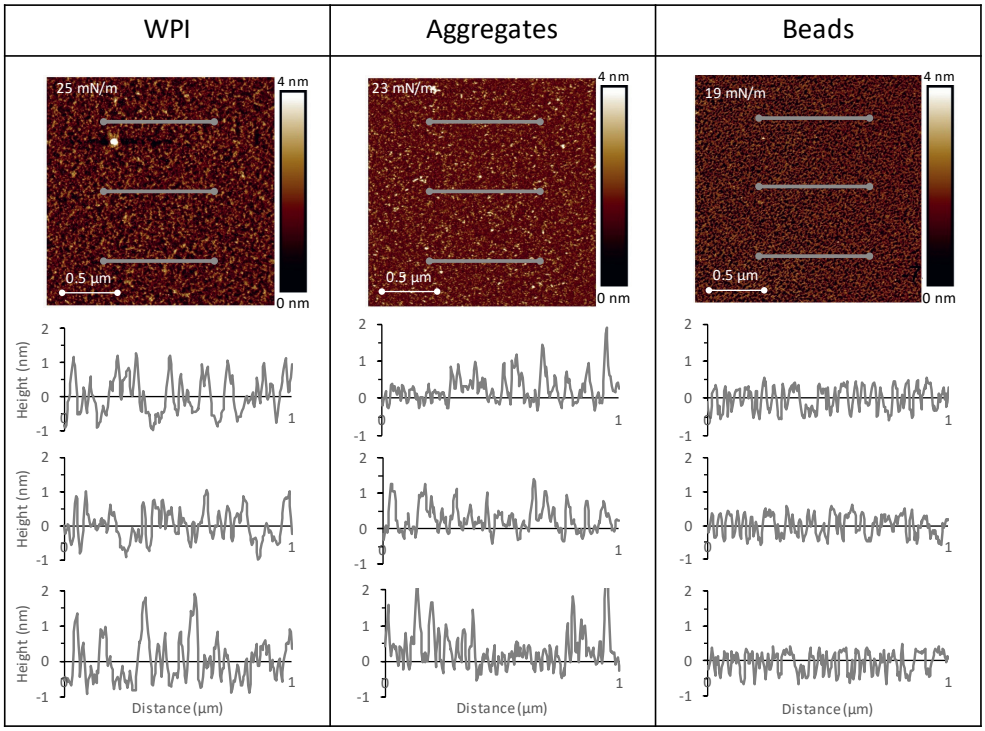

Figure A3.6. The cross-sections of AFM images of the protein films. The lines in the AFM image correspond to the analysed section.

Table A3.1. All variables of equation 3.1 for native WPI, aggregates and beads at 10% and 20% deformations.

		Expansion		*Compression*	
		10%	***20%***	***10%***	***20%***
β	WPI	0.56 ± 0.04	0.54 ± 0.03	0.65 ± 0.01	0.60 ± 0.01
	AGG	0.51 ± 0.02	0.55 ± 0.03	0.56 ± 0.02	0.59 ± 0.02
	Beads	0.52 ± 0.04	0.52 ± 0.03	0.63 ± 0.10	0.58 ± 0.06
τ_1	WPI	19.6 ± 1.0	15.8 ± 3.2	20.0 ± 2.2	16.5 ± 1.1
	AGG	21.5 ± 4.4	16.5 ± 1.8	23.8 ± 1.1	17.3 ± 1.9
	Beads	33.2 ± 12	41.6 ± 7.3	16.9 ± 7.2	22.7 ± 8.3
τ_2	WPI	633 ± 83	647 ± 172	357 ± 23	356 ± 32
	AGG	590 ± 92	494 ± 42	587 ± 48	456 ± 46
	Beads	1908 ± 1246	482 ± 262	173 ± 50	391 ± 140
a	WPI	3.0 ± 0.4	3.8 ± 0.2	-3.5 ± 0.5	-5.9 ± 0.2
	AGG	3.7 ± 0.2	4.1 ± 0.2	-3.9 ± 0.1	-5.3 ± 0.2
	Beads	0.9 ± 0.1	1.2 ± 0.1	-0.7 ± 0.2	-1.1 ± 0.2
b	WPI	1.5 ± 0.2	1.7 ± 0.1	-2.2 ± 0.4	-2.3 ± 0.2
	AGG	1.6 ± 0.2	1.8 ± 0.2	-2.2 ± 0.2	-2.5 ± 0.2
	Beads	0.3 ± 0.1	1.0 ± 0.1	-0.2 ± 0.1	-0.4 ± 0.1
c	WPI	48.0 ± 1.2	48.8 ± 0.9	46.1 ± 1.0	45.5 ± 0.6
	AGG	50.2 ± 1.3	52.4 ± 1.7	47.4 ± 1.1	46.4 ± 0.8
	Beads	42.8 ± 0.2	42.1 ± 1.0	42.1 ± 0.5	41.5 ± 0.8
R^2	WPI	0.987	0.992	0.991	0.993
	AGG	0.988	0.994	0.992	0.993
	Beads	0.916	0.969	0.954	0.984

Chapter 4

Influence of phenol sinapic acid on whey protein foaming properties

Published as:
Yang, J., Lamochi Roozalipour, S. P., Berton-Carabin, C. C., Nikiforidis, C. V., van der Linden, E., & Sagis, L. M. C. (2021). Air-water interfacial and foaming properties of whey protein - sinapic acid mixtures. *Food Hydrocolloids*, *112*, 106467. https://doi.org/10.1016/j.foodhyd.2020.106467

Abstract

Phenols are widely present in plants and often are co-extracted in plant protein extracts, while such components could influence the protein's interface and foam stabilising properties. In this study, the influence of rapeseed phenol sinapic acid (**SA**) on the interfacial and foaming properties of a well-characterised model protein, whey protein isolate (**WPI**), was investigated. WPI formed strong viscoelastic interfacial layers, and the addition of SA reduced the surface dilatational modulus by 25%. Turning SA into its active oxidised form in the WPI-SA mixtures led to protein aggregation, resulting in a further decrease of the modulus by 40%. Removal of unbound phenols induced a slight increase of the dilatational modulus, but the interfacial layer strength did not fully recover to that made with pure WPI. This suggests binding of phenols to proteins, and thus influencing the protein interface stabilising properties. Foams stabilised by WPI-SA mixtures had a shorter foam half-life time (130-180 min) than foams stabilised by pure WPI (260 min). Our data are thus in line with the observation that a lower surface dilatational modulus leads to lower foam stability. Yet, the foam stability did not recover to the original values of pure WPI-stabilised foams after the removal of unbound phenols. In conclusion, the presence of SA resulted in a decrease in interfacial layer strength and foam stability. We conclude that in producing protein extracts from rapeseed or other phenol-rich plant sources, the presence and oxidation of phenols should thus be considered.

4.1 Introduction

One of the challenges in utilizing plant protein extracts as functional food ingredients is the naturally present phenols. For example, rapeseed proteins have promising emulsifying[43,91,151], foaming[96,152], and gelling properties[153], but rapeseed may contain up to 3% of phenols[11]. Rapeseed phenols are known to contribute to a bitter taste and astringency in foods, loss of protein digestibility, and also colour changes of the protein extracts[31,32,154]. The effects of rapeseed phenols on protein functionality (e.g., gelling, emulsifying, and foaming properties) are not yet well understood. At the same time, it is key to understand such interactions in the utilization of phenol-rich plant sources in food systems. This work focuses on the main phenol present in rapeseed, which is sinapic acid (**SA**, Figure 4.1), and its influence on interfacial and foaming properties of proteins. Instead of rapeseed proteins, whey protein isolate (**WPI**) was chosen as a model protein system. Whey proteins were already included as model proteins in previous protein-phenol studies, and has well known interfacial properties[79,81,84,86,155–157]. Additionally, the removal of phenols from rapeseed proteins requires multiple washing steps with organic solvents, resulting in a 75-90% phenol removal and unknown effects on the protein structure and properties[75,158].

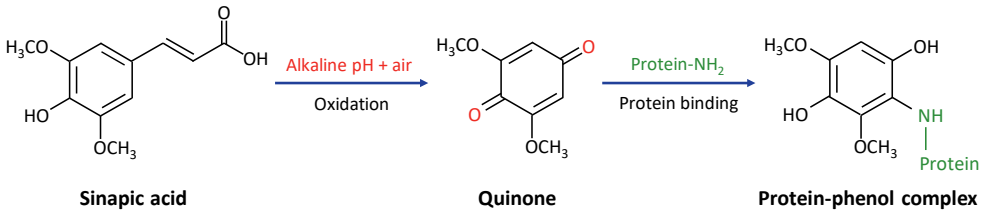

Figure 4.1. A simplified mechanism of sinapic acid oxidation and covalent binding with proteins.

Protein-phenol interactions are dictated by the chemical structure of the phenols, such as the degree of polymerization, conformational flexibility, and hydrophobicity[30,159], which can lead to non-covalent and/or covalent interactions with the proteins. The non-covalent interactions may occur via hydrogen bonding, van der Waals forces, electrostatic and hydrophobic interactions[160]. Xu et al. showed that 50% of rapeseed phenols interacted non-covalently with rapeseed proteins at pH 12. Another 40% exist as unbound phenols in the aqueous solution, and the remaining 10% of the phenols interact covalently with the proteins[73]. Covalent interactions between phenols and proteins usually occur upon oxidation of the phenols. Hydroxyl groups on phenyl rings can be converted into quinones by enzymes or auto-oxidation, and the latter is accelerated at alkaline pH or in the presence of oxidizing agents[33,74]. A similar reaction was also found for SA, as the carboxyl and hydroxyl groups were ionized at a pH above 7. Two oxidised SA could form the molecule thomasidioic acid and can be further converted into quinones[31] (Figure 4.1). Quinones are electrophilic

compounds that are stabilised by their conjugated cyclic dione structure, and thus very reactive towards free thiol and amino groups on the proteins. After a Michael addition reaction, a covalent bond between quinone and protein is formed (Figure 4.1). The phenols on the protein-phenol complex can be oxidised a second time, thereby crosslinking another protein, and could ultimately lead to the formation of protein-phenol aggregates[33,161]. Such complexation into aggregates was demonstrated for several protein sources, and often resulted in a decreased protein solubility[76,81–83].

Both non-covalent and covalent phenol-protein interactions can largely influence the protein structure and thus protein functionality. First of all, bound phenols might influence the protein surface hydrophobicity by several mechanisms, such as introducing hydrophilic groups from the phenol or the covering of hydrophobic residues on the protein[76,77]. Additionally, phenol interaction could alter protein structure, and thereby exposing hydrophobic residues. A decrease of protein surface hydrophobicity was shown for whey proteins upon interaction with phenols[78,79,86,155]. The alteration of protein structure is another major change in proteins upon phenol binding, which was also confirmed for milk proteins, as non-covalent interactions with phenols resulted in an increase of unordered secondary protein structures[78–80].

Alteration of a protein's surface hydrophobicity, structure, and size may considerably influence its interface and foam stabilising properties. For instance, phenols that were able to induce aggregation of WPI, resulted in lower surface activity and dilatational moduli compared to pure WPI[78,84]. Even though the interfacial properties were affected negatively, the foam stability increased, which was probably related to the blocking of lamellae and plateau borders of the foam by aggregates, which reduced the rate of liquid drainage[78,81,125]. Another work showed that lower protein surface hydrophobicity after non-covalent interaction with phenols resulted in higher protein solubility, and thus an increase in foam height and stability[86]. These studies again confirm the complexity of phenol-protein mixtures, as the type of phenol and interaction with the protein determine the interface and foam stabilising properties of the mixtures. Also, the influence of SA on proteins with regards to protein functionality (e.g. stabilisation of interfaces and foams) has not been reported yet.

Therefore, the objective of this work was to determine the effect of SA on interface and foam stabilising properties of WPI. Based on earlier reports on protein-phenol studies, non-covalent interactions between the WPI and SA were expected, and covalent interactions were also induced in this study by incubation at pH 10. An insight into these interactions and the link to protein functionality is also useful with regard to the processing of plant proteins, as non-covalent interactions between phenol and protein occur directly upon

solubilisation of the plant material. A conventional protein extraction step is adjusting the pH to alkaline conditions (8-10) to increase protein solubility, but also induces covalent interactions. This study can give an in-depth understanding of the influence of such processing steps on the protein functionality, of which air-water interfacial and foaming properties were studied in this work. The air-water interfacial properties were studied using large amplitude oscillatory dilatation (**LAOD**). The protein structures were evaluated using differential scanning calorimetry (**DSC**). The foaming properties of the WPI/SA mixtures were analysed by monitoring the foam stability and bubble size distribution.

4.2 Experimental section

4.2.1 Materials

Whey protein isolate (**WPI**) consisting of 74% β-lactoglobulin, 12.5% α-lactalbumin, 5.5% bovine serum albumin, and 5.5% IgG1[132] (purity 98%) (Davisco Food International, France), sinapic acid (**SA**, 3,5-dimethoxy-4-hydroxy-cinnamic acid) (Sigma-Aldrich, USA), and other chemicals (Sigma-Aldrich, USA) were all used as received. The samples were prepared in ultrapure water (MilliQ Purelab Ultra, Darmstadt, Germany).

4.2.2 Sample preparation

Preparation of WPI solution

WPI was dissolved at 2.5% (w/w) in a sodium phosphate buffer (20 mM, pH 7.0) for 4 hrs at room temperature and centrifuged at 16,000xg for 30 min. The supernatant was filtered over a 0.45 µm syringe filter, and the filtrate was diluted based on dry matter.

Preparation of sinapic acid solution

A stock solution of 2% (w/w) sinapic acid (SA) was prepared in a buffer. The pH was corrected with NaOH to pH 7.0 and stirred for 4 hrs at room temperature. The pH was adjusted to 7.0 every 15 min, which was necessary for the first hour of dissolving. The SA solution was filtered over a 0.45 µm syringe filter after complete dissolution.

Preparation of WPI and SA mixtures

A WPI solution with a fixed concentration of 0.2% (w/w) was mixed with a SA solution varying from 0.04 to 2% (w/w) in a 1:1 (v/v) ratio, which resulted in a final concentration of 0.1% (w/w) WPI. This non-oxidised WPI-SA mixture is abbreviated as **WS**. The WS sample was oxidised by adjusting the pH to 10.0 with NaOH, followed by incubation overnight (16 hrs) while stirring slowly at room temperature. The pH was adjusted to 7.0 on the following day, and this solution is the oxidised sample (**WSox**). SA was also oxidised separately using the earlier mentioned method (16 hrs incubation at pH 10) and mixed with WPI at pH 7.0, which yielded the separately oxidised sample (**WSsepox**). A schematic overview of different samples and their preparation is depicted in Figure 4.2.

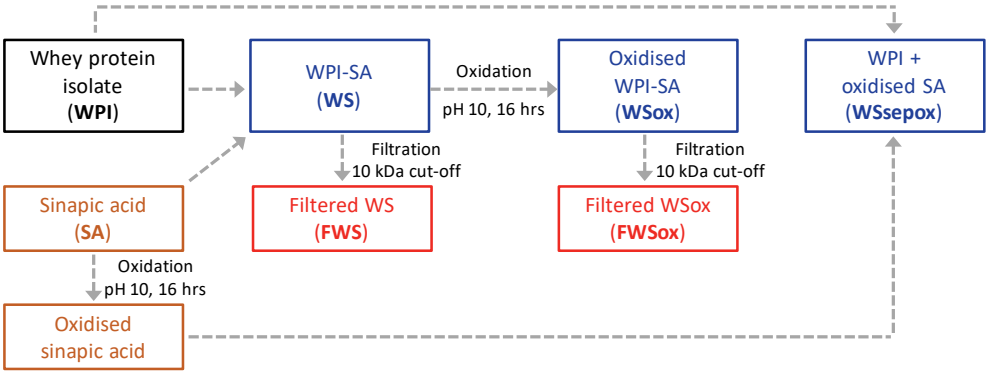

Figure 4.2. Explanation scheme of prepared mixtures and abbreviations.

Filtration of the mixtures to remove unbound phenols

Selected WS and Wsox mixture solutions were ultra-filtrated with an Amicon stirred cell (Merck, Germany) equipped with a 10 kDa-pore size membrane to remove unbound phenols. An initial volume of 160 mL WPI-SA mixture was concentrated to 20 mL, which was diluted again with 140 mL of buffer, followed by another filtration step to 20 mL of the retentate. The retentate was diluted and filtered a total of four times. After three dilutions, the conductivity of the filtrate remained constant. The filtration step resulted in approximately 5% protein loss due to loss on the filtration membrane, and therefore the final retentate was diluted with buffer to 95% of the initial volume (152 mL).

4.2.3 Determination of protein thermal stability by DSC

The protein thermal stability was studied by differential scanning calorimetry (**DSC**) using a Q100 DSC (TA Instruments, USA). About 50 µL of the solution was weighed in a stainless steel high volume pan. All mixtures contained a fixed WPI concentration of 10% (w/w) and 1% (w/w) of SA. An empty stainless-steel volume pan was used as a reference, and nitrogen was used as the carrier gas. Samples were equilibrated for 5 min at 20 °C, which was followed by heating to 120 °C at a rate of 5 °C/min. Possible refolding of the proteins was evaluated by a cooling step from 120 to 20 °C at a rate of 10 °C/min. Samples were prepared in duplicate, and each of these duplicates was measured twice.

4.2.4 Determination of surface tension and surface dilatational properties

The interfacial properties were studied with a drop tensiometer PAT-1M (Sinterface Technologies, Germany) at 20 °C. The hanging drop method was performed by forming a drop of sample solution with a surface area of 20 mm^2 at the tip of a needle. The droplet shape was monitored for 10,800 s and fitted with the Young-Laplace equation to obtain the surface tension. After this waiting time, the droplet was subjected to dilatational deformations. Amplitude sweeps were performed with amplitudes ranging from 3 to 30% at

a fixed frequency of 0.02 Hz. The droplet was subjected to five cycles at every amplitude. Step-dilatations were performed by a sudden extension or compression (step time of 2 s) of the area by 10%. All measurements were performed at least in triplicate at 20 °C.

4.2.5 Rheology data analysis

The results of the oscillatory amplitude sweeps in dilatation were analysed using Lissajous plots of the surface pressure ($\Pi = \gamma - \gamma_0$) versus the deformation ($(A-A_0)/A_0$). Here γ and A are the surface tension and area of the deformed interface, γ_0 and A_0 are the surface tension and area of the non-deformed interface. Plots were generated for each deformation from the middle three oscillation cycles[135].

4.2.6 Preparation of Langmuir-Blodgett films

Langmuir-Blodgett films of the protein-stabilised interfacial films were prepared using a 243 mm^2 Langmuir film balance (Langmuir-Blodgett Trough KN 2002, KSV NIMA/Biolin Scientific Oy, Finland) at room temperature, which was filled with sodium phosphate buffer (20 mM, pH 7.0). Protein-phenol mixtures with a 1:10 (w/w) ratio were diluted to a 0.02% (w/w) protein content, and 200 µL of the sample was spread on top of the surface using a gas-tight syringe and were equilibrated for 30 min. The surface layer was compressed at a barrier moving speed of 5 mm/min, while the surface pressure was monitored with a Wilhelmy plate (platinum, perimeter 20 mm, height 10 mm). After reaching a stable surface pressure, the protein layer was transferred on a freshly cleaved mica substrate (Highest Grade V1 Mica, Ted Pella, USA) at 1 mm/min withdraw speed. The films were dried in a desiccator, and produced in duplicate.

4.2.7 Determination of the interfacial structure by AFM

The interfacial structure of the Langmuir-Blodgett films was studied using an atomic force microscope (**AFM**, MultiMode 8-HR, Bruker, USA). Images were recorded in tapping mode using the Scanasyst-air model non-conductive pyramidal silicon nitride probe (Bruker, USA) with a normal spring constant of 0.40 N/m. A lateral scan frequency of 0.977 Hz was employed for all topographical images. The lateral resolution was set to 512 x 512 $pixels^2$ in a scan area of 2 x 2 μm^2. Duplicates of the Langmuir-Blodgett films were scanned for at least two locations to ensure good representativeness. The AFM images were analysed using Nanoscope Analysis 1.5 software (Bruker, USA).

4.2.8 Determination of foam properties

Foams were produced using a Foamscan foaming device (Teclis IT-Concept, France) by sparging nitrogen through a metal frit (27 µm pore size, 100 µm distance between centres of pores, square lattice). Aliquots of 40 mL sample were sparged in a glass cylinder (ø = 60 mm) at a gas flow rate of 400 mL/min to a foam volume of 400 cm^3. A camera monitored

the decay of foam volume, and from this, the foam half-life time was measured, which is the time required for the foam volume to reduce by 50%. The morphology of foam bubbles was captured with a camera, and analysed using a custom Matlab script that used DIPlip and DIPimage image analysis software to obtain an average bubble size. All experiments were performed at least in triplicate at 20 °C.

4.3 Results and discussion

4.3.1 Evaluation of protein denaturation properties by DSC

The interactions between sinapic acid (**SA**) and whey protein isolate (**WPI**) were initially evaluated by probing the protein denaturation temperatures and enthalpy using differential scanning calorimetry (**DSC**) (Table 4.1). An overview of the samples and abbreviations is given in Figure 4.2. The DSC showed the main denaturation peak for WPI (see Figure A4.1 in the appendix), corresponding to a temperature at 74.4 ± 0.1 °C, and a denaturation enthalpy of 13.6 ± 0.7 J/g protein. The whey protein isolate used in this study is a mixture of proteins with β-lactoglobulin (74%) and α-lactalbumin (12.5%) as the most abundant ones. The denaturation peak is mainly dominated by the denaturation of β-lactoglobulin. Additionally, a small shoulder peak is present due to α-lactalbumin, with a denaturation temperature of around 65 °C[162].

Table 4.1. Protein denaturation onset and peak temperatures and enthalpy of WPI and WPI-SA mixtures dissolved in a 20 mM PO_4 buffer, pH 7.0. The averages and standard deviations were obtained from four replicates.

	WPI	WS	WSox	WSsepox
T_{onset} (°C)	60.0 ± 0.7	59.9 ± 0.9	54.5 ± 1.3	61.4 ± 0.3
T_{peak} (°C)	74.4 ± 0.1	73.9 ± 0.1	67.5 ± 0.7	74.4 ± 0.2
Enthalpy (J/g protein)	13.6 ± 0.7	13.2 ± 0.9	5.9 ± 0.4	12.2 ± 0.1

Addition of SA to a WPI solution at pH 7.0 (**WS**) resulted in a denaturation peak temperature of 73.9 ± 0.1 °C and a denaturation enthalpy of 13.2 ± 0.9 J/g protein. These values for WS were comparable to those of pure WPI (Table 4.1). Non-covalent interactions between the compounds were expected, as reported for bovine serum albumin (**BSA**)[74,156]. SA has a hydroxycinnamic-acid-like structure containing a phenyl ring connected to a carboxyl group by a double covalent bond (Figure 4.1), thereby forming a conjugated system[31]. The interactions between BSA and SA were expected to be mainly hydrophobic due to the interaction between the hydrophobic phenyl group and hydrophobic domains on the surface of the protein. A similar interaction mechanism was confirmed for hydroxycinnamic acid derivatives caffeic and ferulic acid and the main whey protein β-lactoglobulin[155]. Binding of these molecules on the hydrophobic domains of the protein surface was confirmed using NMR spectroscopy, and resulted in a decrease of protein surface hydrophobicity up to 35%.

Another major alteration of the protein was the secondary protein structure, as the percentage of β-sheets decreased and unordered structures increased. Coinciding findings on structure and surface hydrophobicity were also observed when epigallocatechin, chlorogenic, caffeic, ferulic, or coumaric acid was introduced to whey proteins[78,79,86]. Based on these previous studies, we expect the SA to bind non-covalently via hydrophobic interactions of the phenyl-ring with hydrophobic domains on the protein surface. This interaction would probably also lead to decreased surface hydrophobicity, and an increase in unordered secondary protein structures. This alteration of secondary protein structure was not reflected in the DSC results, as WS and pure WPI showed comparable thermal stability. However, the comparable thermal stability of a protein before and after the addition of phenols does not necessarily indicate an unaffected protein structure, which was also shown for BSA and biochanin-A mixtures[163]. The secondary structure of the BSA was found to be altered after non-covalent interaction with phenols, as a decrease of α-helix and β-sheet domains was observed.

Subsequently, to induce covalent interactions between SA and WPI, the WS mixtures were oxidised by overnight incubation at pH 10.0, and the pH was adjusted back to 7.0, which yielded **WSox**. The WSox sample exhibited a slight increase in turbidity (based on visual observation) compared to WPI and WS, and a substantial decline of the denaturation peak, which was not observed for pure WPI (see Table 4.1 and Figure A4.1 in appendix). The peak enthalpy diminished by more than half, and the peak temperature also shifted slightly to lower values, close to the T_{peak} of α-lactalbumin. This could suggest the loss of the initial structure for β-lactoglobulin, while the structure of α-lactalbumin seems to be (partially) present. The substantial decrease in protein denaturation enthalpy could be related to the formation of phenol-protein aggregates. As mentioned in earlier sections, SA is converted into quinones at alkaline pH, which can covalently bind to proteins, and thus cross-linking multiple proteins into aggregates. The formation of larger aggregates was also observed for WPI-epigallocatechin mixtures after inducing covalent interactions by overnight oxidation at alkaline pH[81]. We also included a negative control, where WPI was given the overnight alkaline pH treatment (to pH 10.0), and we obtained similar results in DSC as non-treated WPI (see Table A4.1 in appendix).

To further understand the properties of the WSox mixture, SA was first oxidised separately and then added to WPI (**WSsepox**). The resulting WSsepox mixture had a lower denaturation peak with a roughly 10% decrease in enthalpy compared to WPI. Oxidising WPI and SA together led to a much larger change in protein denaturation temperatures and enthalpy than adding pre-oxidised SA to WPI. One explanation could be the polymerization of quinones with each other in the absence of proteins, and this could result in less effective bridging to the proteins[30]. Another explanation could be the difference in pH of the reaction

between SA and WPI, as phenols are more reactive at alkaline pH[31]. In WSox, the WPI and SA coexist at pH 10.0, where the phenols are potentially more reactive than the pre-oxidised phenols in WSsepox, as WPI and pre-oxidised phenols are only mixed at pH 7.0 in WSsepox. The difference in reactivity and possible pre-polymerization probably resulted in less aggregation of proteins for the WSsepox compared to the WSox. Please note that the ratio of WPI:SA was 10:1 (w/w) for the DSC experiments, which is different from the experiments in further sections. This ratio was chosen, since a high concentration of WPI (10%) was required for the DSC measurements, and the dissolution of higher concentrations of SA was not feasible. Other experiments required lower WPI concentrations that allowed us to go to WPI:SA ratios with higher SA contents. In the next sections, we focus on the interface stabilising properties of the WPI-SA mixtures.

4.3.2 Surface oscillatory dilatational rheology

Non-oxidised mixtures

The surface activity of WPI and WS mixtures with WPI:SA ratios between 5:1 to 10:1 (w:w) was assessed using a drop tensiometer (Figure 4.3A). WPI exhibited an immediate increase in surface pressure within a few seconds, and the surface pressure increased continuously to 19.0 mN/m after three hours of adsorption. The addition of SA resulted in a surface pressure increase over the whole time range with an additional 1.5 mN/m at the highest SA concentrations. The surface-active phenols (Figure 4.3A) contributed to increased surface activity of the WS mixtures, which could suggest the co-adsorption of SA and WPI on the air-water interface. The nature of the stabilised interfacial layer can be further investigated by performing deformations at a range of amplitudes (3-30%) in amplitude sweeps.

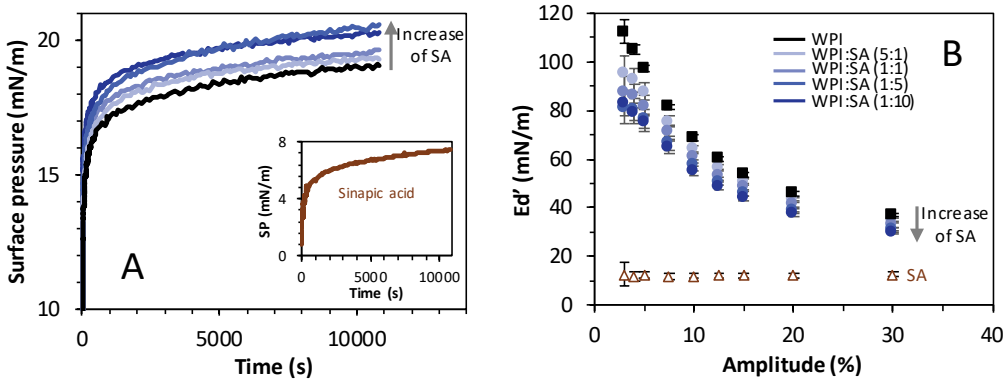

Figure 4.3. (A) Surface pressure as a function of time at air-water interfacial films stabilised by WPI (black) and WPI-SA mixtures with a WPI:SA 5:1 to 1:10 (w/w) ratio (blue lines). A darker blue colour indicates a higher concentration of SA compared to WPI. The WPI concentration was 0.1% (w/w) in all samples. An insert of the same graph for 1% (w/w) sinapic acid (brown) can be found in the bottom-right corner. The surface pressure isotherms represent an average from at least three replicates. The standard deviation was below 5%. (B) The surface elastic dilatational modulus as a function of deformation amplitude of the same interfacial films as described in graph A (fixed frequency 0.02 Hz). The average and standard deviations are the result of at least three replicates.

The WPI-stabilised interface exhibited high dilatational elastic moduli (***E_d'***) above 100 mN/m at deformations below 5% and a decrease to 37 mN/m at 30% deformation (Figure 4.3B). The amplitude-dependency of the elastic modulus reveals that the interfacial microstructure is affected by the applied deformation[103]. SA-covered interfaces showed an E_d' around 12 mN/m, independent of strain amplitude, which indicated a less stiff and more stretchable interfacial layer. Mixing WPI and SA resulted in less stiff interfaces than the pure WPI-stabilised interface, and the elastic moduli decreased with increasing SA concentrations. At a WPI:SA ratio of 1:10 (w:w), the E_d' of the interface declined by between 20-26% over the whole amplitude range compared to WPI. Several studies also demonstrated a weakening in interfacial layer strength of β-lactoglobulin upon the addition of green-tea polyphenols[84,157]. Another study revealed the same effect for WPI upon the addition of gallic acid and epigallocatechin[78]. The response to the deformations can be analysed more accurately using Lissajous plots, since the moduli in Figure 4.3B are based only on the intensity and phase of the first harmonic of the Fourier transform of the surface stress, and any nonlinearities in the response are neglected. Higher-order harmonics are present, as the modulus is amplitude-dependent, and implies that the deformations were in the nonlinear viscoelastic regime (**NLVE**). These nonlinearities can be included by plotting the surface pressure against the deformation in Lissajous plots[59].

The Lissajous plots of a WPI-stabilised interface (Figure 4.4) at 5% deformation showed a narrow and symmetric ellipse. This indicates linear viscoelastic behaviour with a dominant elastic component, and implies the formation of a viscoelastic solid-like layer, as shown in earlier work[103]. The shape of the plots became wider and asymmetric at 30% deformation, which is far into the NLVE. At the start of the extension (bottom-left corner), we can observe a steep surface pressure increase that indicates a predominantly elastic response. Afterwards, the elastic component started to diminish, which was reflected in a gradual decrease in the slope of the surface pressure curve. This is related to a gradual loss of cohesiveness of the interfacial microstructure, and an increase in the viscous contribution to the total surface pressure response. This phenomenon upon extension of the interface is called intra-cycle strain softening. The opposite can be observed upon compression, namely intra-cycle strain hardening, as the maximum surface pressure reached much higher values compared those reached in extension. In earlier work, we attributed this phenomenon to the jamming of densely clustered protein regions at the interface[103]. From the Lissajous plots, we can conclude that WPI can form stiff and cohesive interfaces with the rheological behaviour of a viscoelastic two-dimensional solid, as described in several studies[55,103,109].

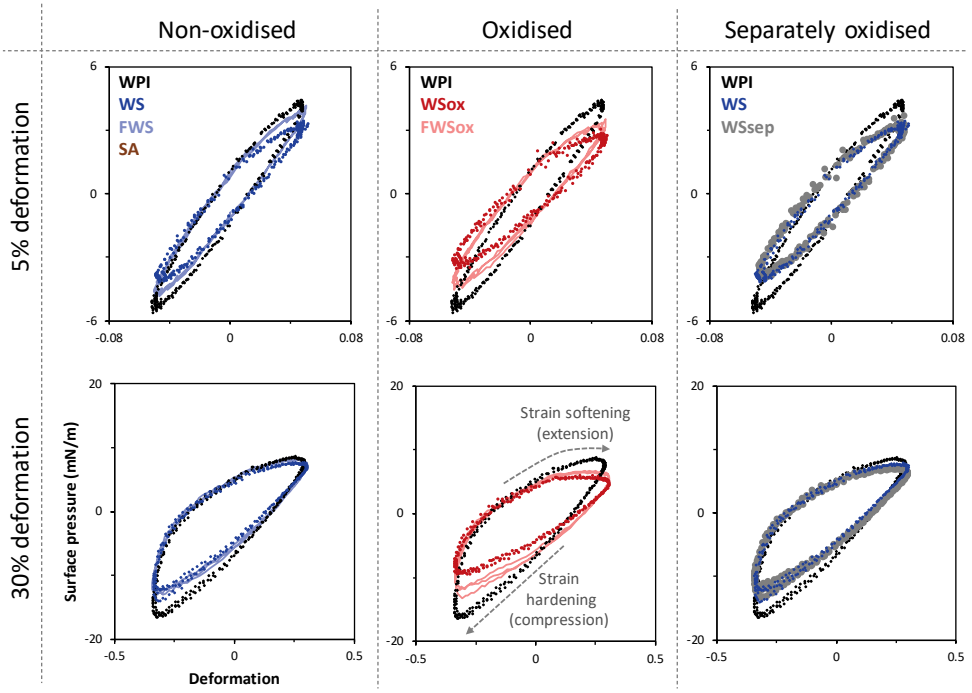

Figure 4.4. Lissajous plots of surface pressure as a function of the applied deformation, obtained during amplitude sweeps of air-water interfacial films stabilised by WPI and WPI-SA mixtures at a 1:10 (w/w) ratio. Lissajous plots of a 1% (w/w) SA solution was also included. For clarity, one representative plot is shown for each sample, but comparable plots were obtained on at least three replicates.

On the other hand, the Lissajous plots of SA had a narrow shape, and were more tilted towards the horizontal axis. From this, we can conclude that SA formed very weak interfaces compared to WPI. The Lissajous plots of WS-stabilised (WPI:SA ratio 1:10) interfaces (Figure 4.4, left) at 5% deformation had a similar shape as WPI-stabilised interfaces, but the plots of WS were more tilted towards the horizontal axis, which indicates a weaker network. A more pronounced difference can be observed at 30% deformation, where the strain hardening at compression became less evident compared to WPI, as the maximum surface pressure value in compression decreased from -17 mN/m (WPI) to -13 mN/m (WS). This could be due to the presence of SA at the interface, as a reduction of strain hardening would imply that first the SA is expelled from the interface into the bulk. Afterwards, the WPI starts jamming and again showed a steep increase in surface pressure at the start of the extension. At 30% deformation, both WPI and WS showed a comparable strain-softening behaviour upon extension, as the curves overlap in extension. This suggests that the WPI in a mixture with SA still interacts to form a cohesive interfacial network similar to the pure WPI interface. Upon extension, a comparable protein network would imply that the strain hardening in compression is due to the desorption of phenols from the interface towards the bulk phase,

followed by jamming of the proteins. We should also keep in mind that the SA interacts with the WPI by hydrophobic interactions. As a result, hydrophobic regions on the surface of the proteins will be reduced, and less hydrophobic interactions would occur between the proteins on the air-water interface. To summarise, the addition of SA to WPI resulted in an increase in surface activity and a decrease in interfacial layer strength (Figure 4.3A & B). A WPI:SA ratio of 1:10 gave the most pronounced difference compared to WPI alone. Therefore, we chose to continue with this ratio in all further experiments.

Oxidised mixtures

Oxidised WS (**WSox**) mixtures were more surface-active compared to the non-oxidised WS (Figure 4.5A). Additionally, the E_d' decreased by 11-18% over the whole amplitude range after oxidation (Figure 4.5B).

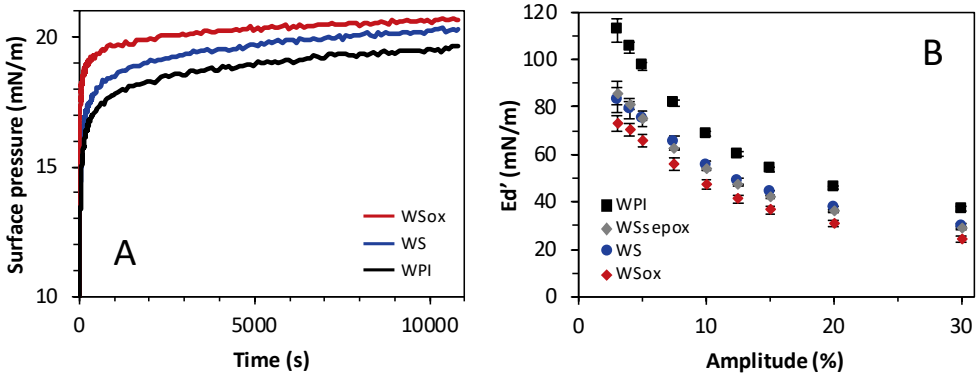

Figure 4.5. (A) Surface pressure as a function of time at air-water interfacial films stabilised by WPI and WPI-SA mixtures. The surface pressure isotherm represents an average from at least three replicates. The standard deviation was below 5%. (B) The surface elastic dilatational modulus as a function of deformation amplitude of interfacial films stabilised by WPI and WPI-SA mixtures at a 1:10 ratio (fixed frequency 0.02 Hz). The different samples are given in the legend. The average and standard deviations are the result of at least three replicates.

The Lissajous plots of WSox-stabilised interfaces at 30% deformation (Figure 4.4, middle) showed even less strain hardening in compression compared to WS, implying that phenols were also adsorbed at the interface, and desorbed into the bulk before the WPI started jamming. In the extension part, we can observe a lower surface pressure increase for WSox than WPI, and the curve for WSox even starts flattening, which indicates increased strain-softening of the interfacial layer. This would imply a reduced resistance of the interfacial network against extensional deformations, thus altering the interactions between proteins at the interface. The proteins in WSox were found to be aggregated, which could explain a weaker interfacial network compared to WPI and WS, as fewer proteins are available to interact at the interface. A negative control, where WPI was given the same pH-shift treatment, was included and gave identical results as untreated WPI in the drop tensiometer (see Figure A4.2 in appendix). The effect of phenol oxidation related to interfacial properties

was further studied by separately mixing oxidised SA with WPI (**WSsepox**), which revealed a similar surface rheological behaviour as non-oxidised WS (overlapping moduli and Lissajous plots, Figure 4.4 & 4.5B). This proves that the oxidation of WPI and SA together at pH 10.0 had a more significant impact on the interfacial properties than the addition of separately oxidised SA.

Removal of unbound phenols

As mentioned in earlier sections, only a fraction of SA is bound non-covalently or covalently to the proteins, which implies an unbound fraction of phenols[82]. To remove SA that is not interacting with WPI, the WS and WSox mixtures were filtered to obtain filtered WS (**FWS**) and filtered WSox (**FWSox**), respectively. Both filtered and non-filtered samples had a comparable surface activity (see Figure A4.3 in appendix). A larger difference was demonstrated in the interfacial layer stiffness (Figure 4.6).

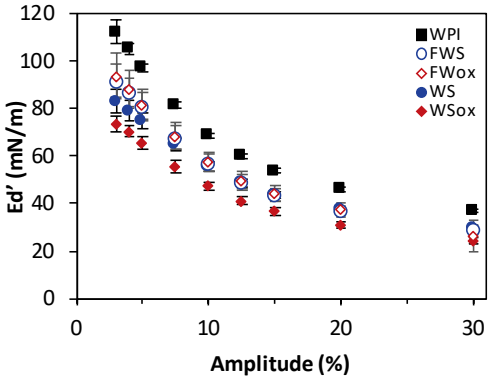

Figure 4.6. Surface elastic dilatational modulus as a function of deformation amplitude of interfacial films stabilised by WPI, WPI-SA mixtures, and filtered WPI-SA mixtures at a 1:10 ratio (fixed frequency 0.02 Hz). The different samples are given in the legend. The average and standard deviations are the result of at least three replicates.

Interfacial films stabilised by FWS revealed a slight increase of E_d' below 10% deformation compared to WS, but both FWS and WS had overlapping E_d' at higher deformations. This is also reflected in the Lissajous plots (Figure 4.4), as an FWS-stabilised interface showed an increase of maximum surface pressure at 5% deformation, and a similar Lissajous plot at 30% deformation compared to WS. The FWSox-stabilised interface had a comparable rheological behaviour as the FWS-stabilised interface, which implied a sizable increase of E_d' after unbound phenol removal compared to WSox. The Lissajous plot (Figure 4.4) of the FWSox-stabilised interface also exhibited more strain hardening than WSox, suggesting fewer phenol molecules at the interface. Unbound SA seems to play a larger role in interfacial properties after oxidation together with protein. Oxidised SA was also studied separately for the interfacial properties, which coincided with the non-oxidised version (see Figure A4.4 in

appendix). The strain-softening in extension in the 30% Lissajous plot of FWSox was coinciding with the plot of WSox, and implies that the proteins show less resistance to extension compared to pure WPI, and thus the interactions between the proteins became weaker.

After the removal of unbound phenols, the samples FWS and FWSox still showed a higher surface activity and a decrease of elastic moduli compared to pure WPI. This would imply the non-covalent interaction with phenols affected the proteins by reducing the protein surface hydrophobicity, and induces changes in protein secondary structure. This was reflected in weaker interfaces for WS compared to WPI. Oxidation of the phenols resulted in WSox, which showed an even less stiff layer than WS, which could be related to the formed protein-phenol aggregates. Still, the removal of unbound phenols resulted in a slight increase in moduli, indicating that some unbound phenols could be present at the interfacial layer. Additionally, we should keep in mind that traces of unbound phenols might still be present after extensive filtration. Besides, non-covalently bound phenols could be released from the proteins, when the phenol concentration in the bulk decreases, and thereby still co-adsorb at the interface.

4.3.3 Interfacial microstructure

We also evaluated the interfacial microstructure by transferring the interfacial film at a surface pressure of 15 or 25 mN/m onto a solid substrate (Langmuir-Blodgett deposition) and analysing the topography of the dried film using atomic force microscopy (**AFM**) (images in Figure 4.7). A heterogeneous structure was observed for the WPI-stabilised films at 15 mN/m, where thicker regions were present. The thicker regions could be densely clustered proteins that are even more densely compressed at a higher surface pressure of 25 mN/m. At this surface pressure, a heterogeneous structure was still present, as was also demonstrated by others[55,112], and related to the rheological nature of the WPI-stabilised interface[103], which behaved as a heterogeneous viscoelastic solid. The WS mixture exhibited a similar heterogeneous structure, and this structure remained after filtration for FWS.

Oxidation of SA showed changes in microstructure, as the WSox-stabilised interface at 15 mN/m showed the presence of larger structures. These structures could be the previously mentioned aggregates that are cross-linked by quinones. The aggregates were still intact and present in the film after filtration. The addition of separately oxidised SA (WSsepox) resulted in more clustered areas compared to pure WPI, but they were not as large as the aggregates in WSox and FWSox. This suggests that conditions (pH & reaction time) between phenol and WPI are key parameters to influence the interaction between phenols and proteins. The aggregates are not present at a surface pressure of 25 mN/m, which was also observed for interfaces stabilised by heat-denatured WPI aggregates[103]. In that study, it was shown that the aggregates were pushed out of the interface into the bulk phase upon compression in the Langmuir trough. It should be noted that the Langmuir-Blodgett films are produced by spreading the material at the interface, and may result in a different microstructure compared to an interfacial layer formed by spontaneous diffusion of surface-active material, such as those formed in the drop tensiometer. At a surface pressure of 25 mN/m, we observed a similar heterogeneous interface for all samples, which we could relate to the rheological behaviour at higher deformations, as the moduli of all samples started to overlap at 30% deformation in the amplitude sweeps (Figure 4.3, 4.5, and 4.6). This would suggest that WPI still forms a heterogeneous viscoelastic layer at the interface in the presence of SA.

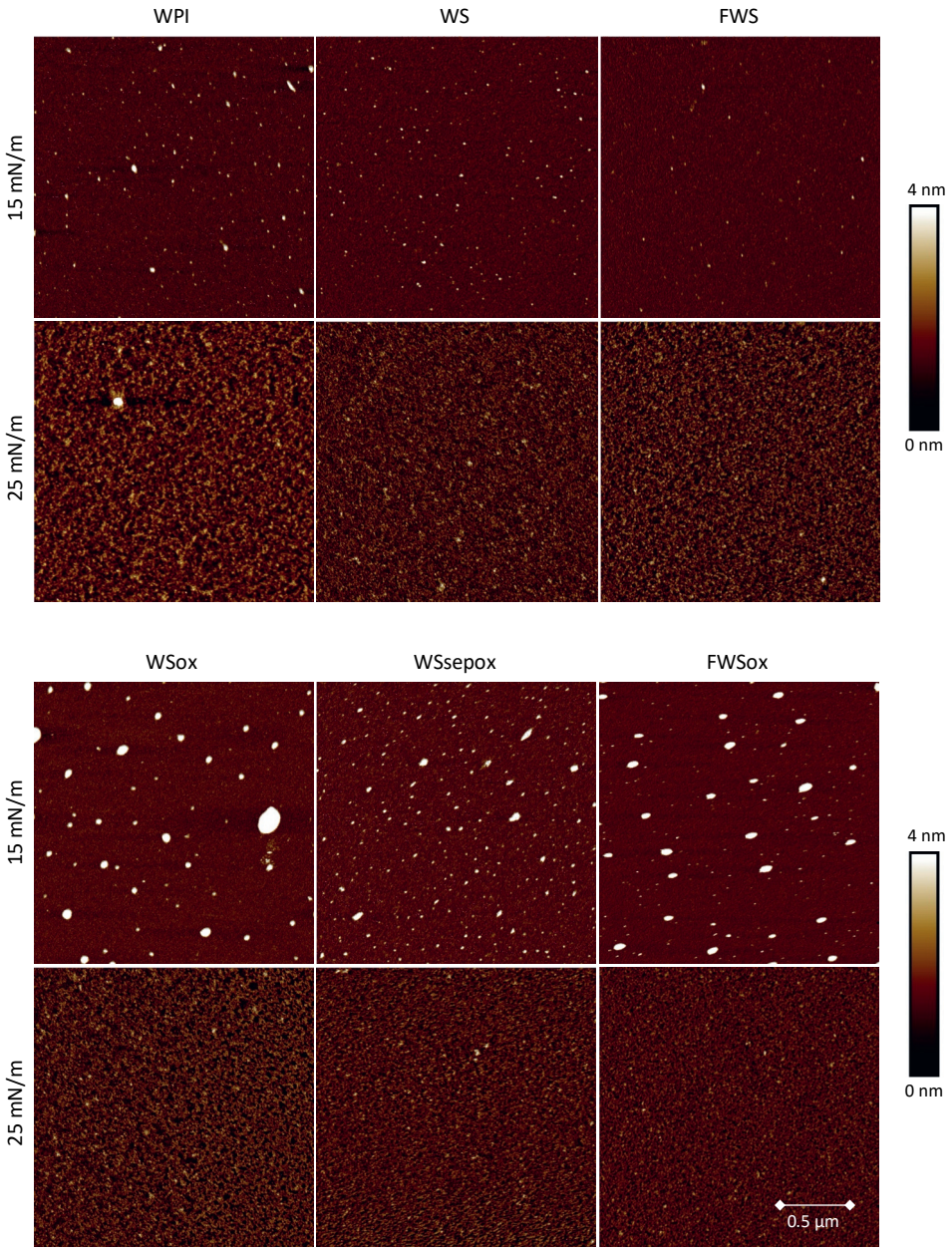

Figure 4.7. AFM images of Langmuir-Blodgett films made from WPI- and WPI-SA mixtures-stabilised interfaces. The surface pressure indicates the conditions during film sampling.

4.3.4 Step-dilatation experiments

The structural heterogeneity of the WPI- and WPI-SA mixture-stabilised interfaces were further investigated by performing step-dilatations in the drop tensiometer (example in Figure A4.5 in the appendix). The relaxation response was characterised by a combination of a Kohlraus-William-Watts (**KWW**) stretch exponential and a regular exponential term (Equation 4.1)[107].

$$\gamma(t) = ae^{-(t/\tau_1)^{\beta}} + be^{-t/\tau_2} + c \quad (4.1)$$

The stretch exponent β and relaxation time τ_1 in the equation are presented in Table 4.2. The characteristic time of the second term τ_2 and fitting parameters a, b, and c can be found in Table A4.2 in the appendix.

Table 4.2. The stretch exponent β and relaxation time τ1 for WPI and WPI-SA mixtures obtained from the step-dilatation experiments. The averages and standard deviations are the result of at least three replicates.

	Extension		Compression	
	β	τ_1	β	τ_1
WPI	0.51 ± 0.05	25.9 ± 2.3	0.56 ± 0.01	27.4 ± 6.7
WS	0.54 ± 0.01	23.0 ± 3.9	0.59 ± 0.03	26.5 ± 1.5
WSox	0.50 ± 0.04	23.7 ± 3.6	0.59 ± 0.04	19.7 ± 2.3
WSsepox	0.51 ± 0.02	23.1 ± 2.4	0.62 ± 0.03	24.2 ± 7
FWS	0.56 ± 0.01	25.9 ± 2.1	0.60 ± 0.02	26.6 ± 2.1
FWSox	0.53 ± 0.03	22.2 ± 3.4	0.55 ± 0.02	21.6 ± 3.6

The KWW model was applied previously to characterise the relaxation behaviour of WPI-stabilised interfaces[103,108,109], which was described by the first term of the equation. The regular exponential term was included to separate the ageing of the interface from the relaxation process. All interfaces showed β's between 0.50-0.56 for extension and 0.55-0.62 for compression, and relaxation times (τ_1) between 19.7 and 27.4 seconds. A value of $\beta<1$ is an indication of dynamic heterogeneity, and reveals the presence of local variations in the relaxation kinetics, and is also common in disordered solids[111,149]. This dynamic heterogeneity could be the result of the structural heterogeneity that was revealed in the interfacial microstructure (Figure 4.7). The β- and τ_1-values of all interfaces were in a comparable range, which was also expected, as all AFM images at a surface pressure of 25 mN/m gave comparable heterogeneous structures. The addition of SA to WPI leads to a similar relaxation behaviour of the interfaces, which shows that the WPI in the presence of SA still forms solid-like structures at the air-water interface, as also demonstrated in the amplitude sweeps, and AFM images.

4.3.5 Foams

Foams were produced by N_2-gas injection and were monitored for the foamability and stability, which were expressed by the average bubble size, and foam half-life time, where half of the foam volume collapsed (Figure 4.8).

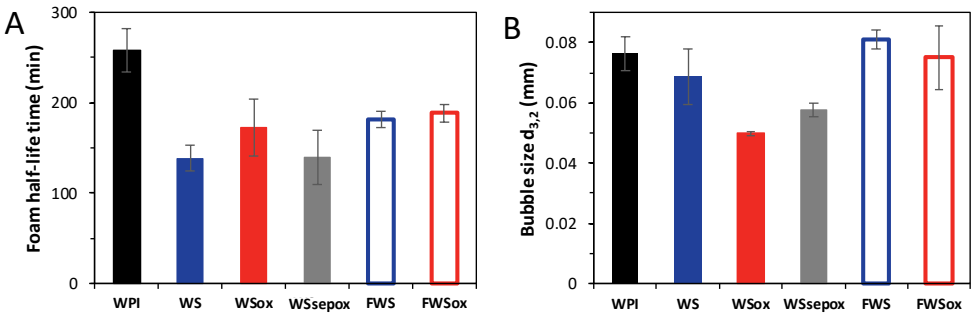

Figure 4.8. The half-life time (A) and bubble diameter (B) of foams stabilised by WPI and WPI-SA mixtures. Averages and standard deviations are the result of at least three replicates.

WPI is often described as an excellent foaming agent with high foam stability[78,164]. In our work, WPI exhibited a high foam half-life time of 258 ± 24 min. The presence of SA (WS, WSox, WSsepox) diminished the half-life time to 138 – 172 min. This lower foam stability could be related to the surface dilatational elastic modulus decrease (Figure 4.3, 4.5, and 4.6), as the strength of the interfacial layer around the air bubble is often related to foam stability[53]. The increased surface activity after the addition of SA resulted in a smaller air bubble size (Figure 4.8B). WSox-stabilised foam showed a slightly longer half-life time compared to WS and WSsepox, which is probably due to the smaller bubble size of WSox, and can be linked to its higher surface activity. Additionally, the formation of aggregates/particles could increase foam stability, as was demonstrated for casein micelles and β-lactoglobulin aggregates[56,125]. These studies suggested that these colloids had little contribution to the air bubble surface, but that the micelles/aggregates were trapped in the lamellae and plateau borders of the foam, and slowed down the drainage of liquid from the foam. Nevertheless, the less stiff interfacial layer of WSox compared to WPI seems to be more detrimental for foam stability.

Removal of unbound phenols (FWS and FWSox) resulted in larger bubble sizes, comparable to that obtained with pure WPI, and in a slight increase of the foam half-life time to 181-188 min. FWS and FWSox still formed less stable foams than WPI (258 min), which aligned with the lower surface elastic modulus of films formed by FWS and FWSox compared to pure WPI (Figure 4.6). The presence of unbound phenols and the bound phenols on proteins led to the formation of weaker interfacial layers, and thus a less stable foam compared to pure WPI. Generally, previous studies also showed an increase in foamability after adding phenols

to protein, which was related to the co-adsorption of phenols and proteins, and an alteration of the protein structure and surface hydrophobicity[78,81,86]. The type of interaction also influenced the foam stability, as the formation of protein aggregates seemed to increase foam stability due to blockage of the lamellae and plateau borders in the foams[81,84]. This phenomenon was slightly present in WSox foams, as the stability was higher than WS foams, but still lower than pure WPI. The aggregate size is largely determining the effectiveness in lamellae and plateau border blockage[56], which suggests that the aggregate size in WSox was not optimal compared to those in the earlier reported works[81,84]. Other works also demonstrated an increase in foam stability, as the protein solubility increased due to a decrease in surface hydrophobicity upon addition of phenols[78,86]. This cannot occur in our work, as we prepare the WPI solutions by centrifugation and filtration to obtain a soluble fraction. Therefore, we can largely attribute the foaming properties to the studied interfacial properties.

4.4 Conclusions

Interfacial and foaming properties of whey protein isolate were studied in the presence of sinapic acid. A schematic overview of the proposed interfacial microstructure stabilised by WPI-SA mixtures can be found in Figure 4.9. Whey protein isolate forms a strong viscoelastic solid-like layer at the air-water interface (Figure 4.9A), and thereby exhibits high foam stability. The addition of sinapic acid results in weaker interfacial layers (Figure 4.9B), and oxidation of the phenols further enhances this effect. Oxidation of sinapic acid increases the reactivity of sinapic acid towards proteins and cross-links WPI into aggregates (Figure 4.9C), as shown by AFM. Removal of unbound phenols caused a slight recovery in interfacial layer strength and foam stability, but it was still less compared to whey protein. From this, we suggest that the unbound phenols and proteins are both present at the air-water interface, and form a weaker interfacial layer than pure protein (Figure 4.9B). Additionally, phenols are bound to the proteins, and could presumably induce changes to surface and structural properties of the proteins, which should be addressed in further research. The phenol sinapic acid can negatively influence the functionality of (whey) proteins, and this negative effect is further enhanced upon oxidation of the phenols. The presence of phenols and the possible oxidation upon protein extraction (at alkaline conditions) should be considered in the production of plant protein extracts from phenol-rich plant sources, and also in the utilization of these sources in our food systems.

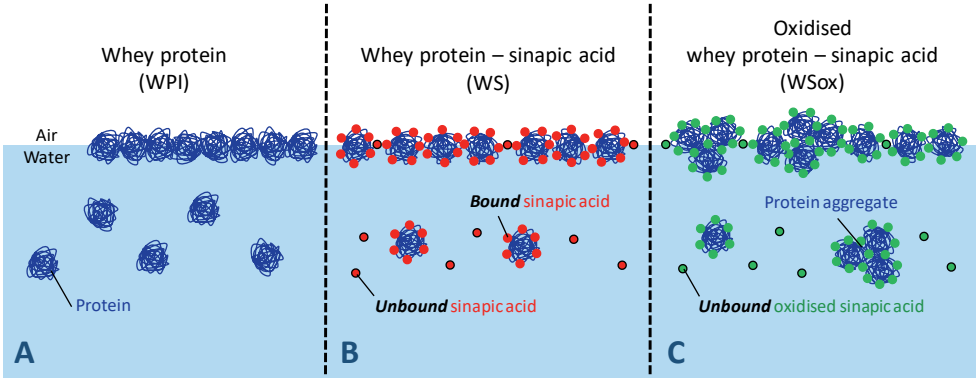

Figure 4.9. Schematic overview of the proposed interfacial composition of WPI-SA mixtures. The illustrated molecules are not on scale.

4.5 Appendix

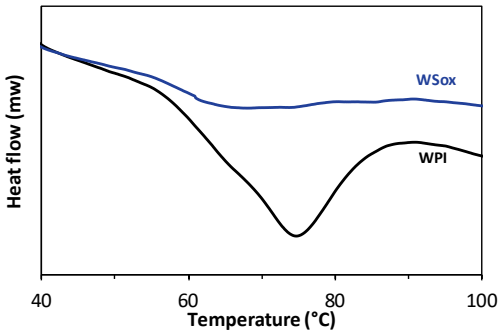

Figure A4.1. DSC raw data: heat flow over temperature of WPI and WSox.

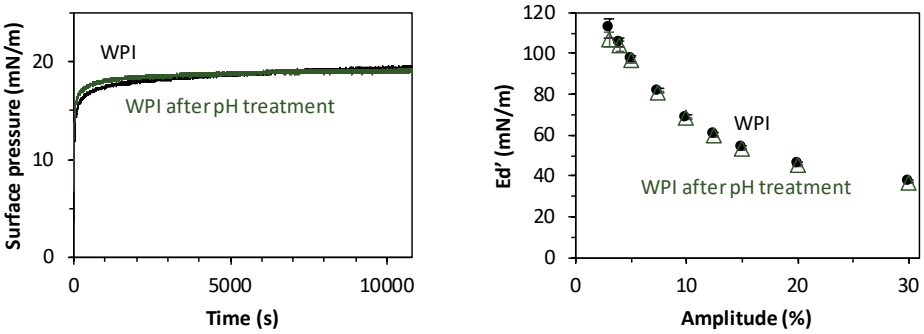

Figure A4.2. Left, surface pressure as a function of time at air-water interfacial films stabilised by WPI, and WPI after overnight pH treatment at pH 10.0. The surface pressure isotherms represent an average from at least three replicates. Right, surface elastic dilatational modulus as a function of deformation amplitude of interfacial films stabilised by WPI, and WPI after overnight pH treatment at pH 10.0 (fixed frequency of 0.02 Hz). The average and standard deviations are the result of at least three replicates.

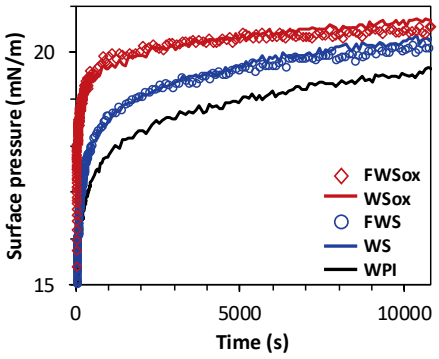

Figure A4.3. Surface pressure as a function of time for air-water interfacial films stabilised by WPI, WS, FWS, WSox, and FWSox. The surface pressure isotherms represent an average of at least three replicates.

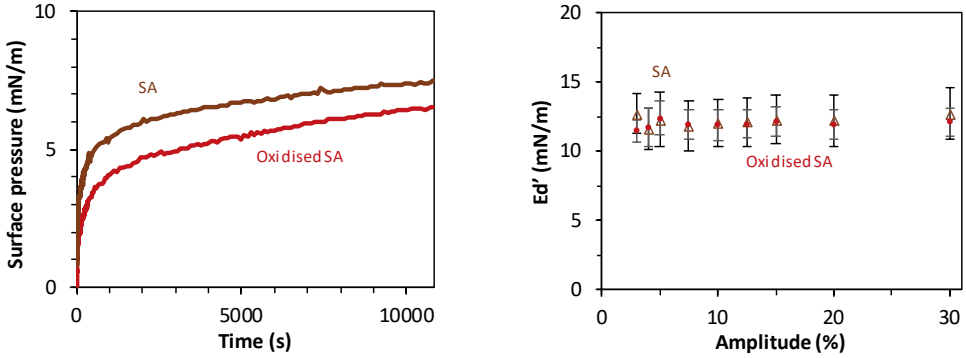

Figure A4.4. Left, surface pressure as a function of time for air-water interfacial films stabilised by sinapic acid (SA) and oxidised sinapic acid. The surface pressure isotherms represent an average of at least three replicates. Right, surface elastic dilatational modulus as a function of deformation amplitude of interfacial films stabilised by SA and oxidised SA (fixed frequency of 0.02 Hz). The average and standard deviations are the result of at least three replicates.

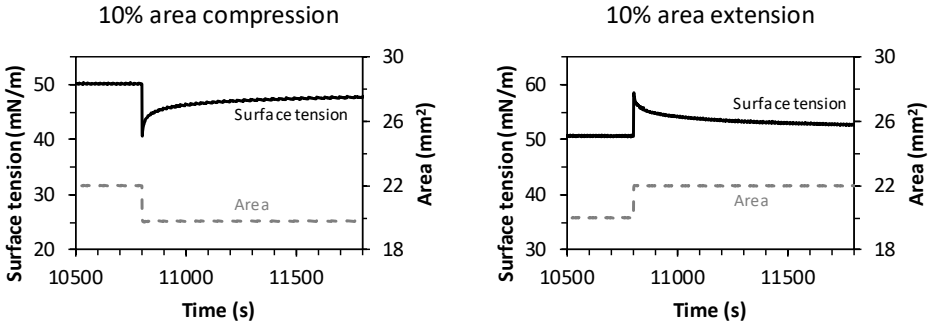

Figure A4.5. An example of a step-dilation experiment in both 10% compression or extension in surface area.

Table A4.1. Protein denaturation onset and peak temperatures and enthalpy of WPI, and a treated WPI sample that was given an overnight alkaline pH treatment (to pH 10.0), and afterwards adjusted to pH 7.0. The averages and standard deviations were obtained from four replicates.

	WPI	Treated WPI
T_{onset} (°C)	60.0 ± 0.7	60.5 ± 0.8
T_{peak} (°C)	74.4 ± 0.1	74.9 ± 0.4
Enthalpy (J/g protein)	13.6 ± 0.7	13.5 ± 0.5

Table A4.2. All variables of equation 4.1 for WPI, and the WPI-SA mixtures. The average and standard deviations are the result of at least three replicates.

		β	τ_1	τ_2	a	b	c
Expansion	WPI	0.51 ± 0.05	25.9 ± 2.3	526 ± 39	-4.8 ± 0.2	-2.3 ± 0.0	48.3 ± 0.1
	WS	0.54 ± 0.01	23.0 ± 3.9	468 ± 30	-4.4 ± 0.4	-2.3 ± 0.1	46.9 ± 0.2
	WSox	0.50 ± 0.04	23.7 ± 3.6	443 ± 82	-4.1 ± 0.5	-1.8 ± 0.1	48.4 ± 0.2
	WSsep	0.51 ± 0.02	23.1 ± 2.4	428 ± 31	-3.6 ± 0.2	-2.0 ± 0.2	47.5 ± 0.3
	FWS	0.57 ± 0.01	25.9 ± 2.1	474 ± 19	-4.0 ± 0.2	-2.2 ± 0.1	47.8 ± 0.0
	FWSox	0.53 ± 0.03	22.2 ± 3.4	493 ± 83	-5.3 ± 0.2	-2.7 ± 0.2	48.9 ± 0.6
Compression	WPI	0.56 ± 0.01	27.4 ± 6.7	638 ± 175	5.0 ± 0.7	2.3 ± 0.2	53.1 ± 0.4
	WS	0.59 ± 0.03	26.5 ± 1.5	645 ± 48	3.8 ± 0.3	2.0 ± 0.1	50.6 ± 0.2
	WSox	0.59 ± 0.04	19.7 ± 2.3	845 ± 278	2.5 ± 1.0	0.8 ± 0.1	48.8 ± 0.4
	WSsep	0.62 ± 0.03	24.2 ± 7	641 ± 204	3.6 ± 0.3	1.4 ± 0.1	49.6 ± 0.2
	FWS	0.60 ± 0.02	26.6 ± 2.1	386 ± 221	3.9 ± 0.0	1.9 ± 0.1	50.9 ± 0.3
	FWSox	0.55 ± 0.02	21.6 ± 3.6	504 ± 45	4.5 ± 0.3	1.6 ± 0.2	51.3 ± 0.2

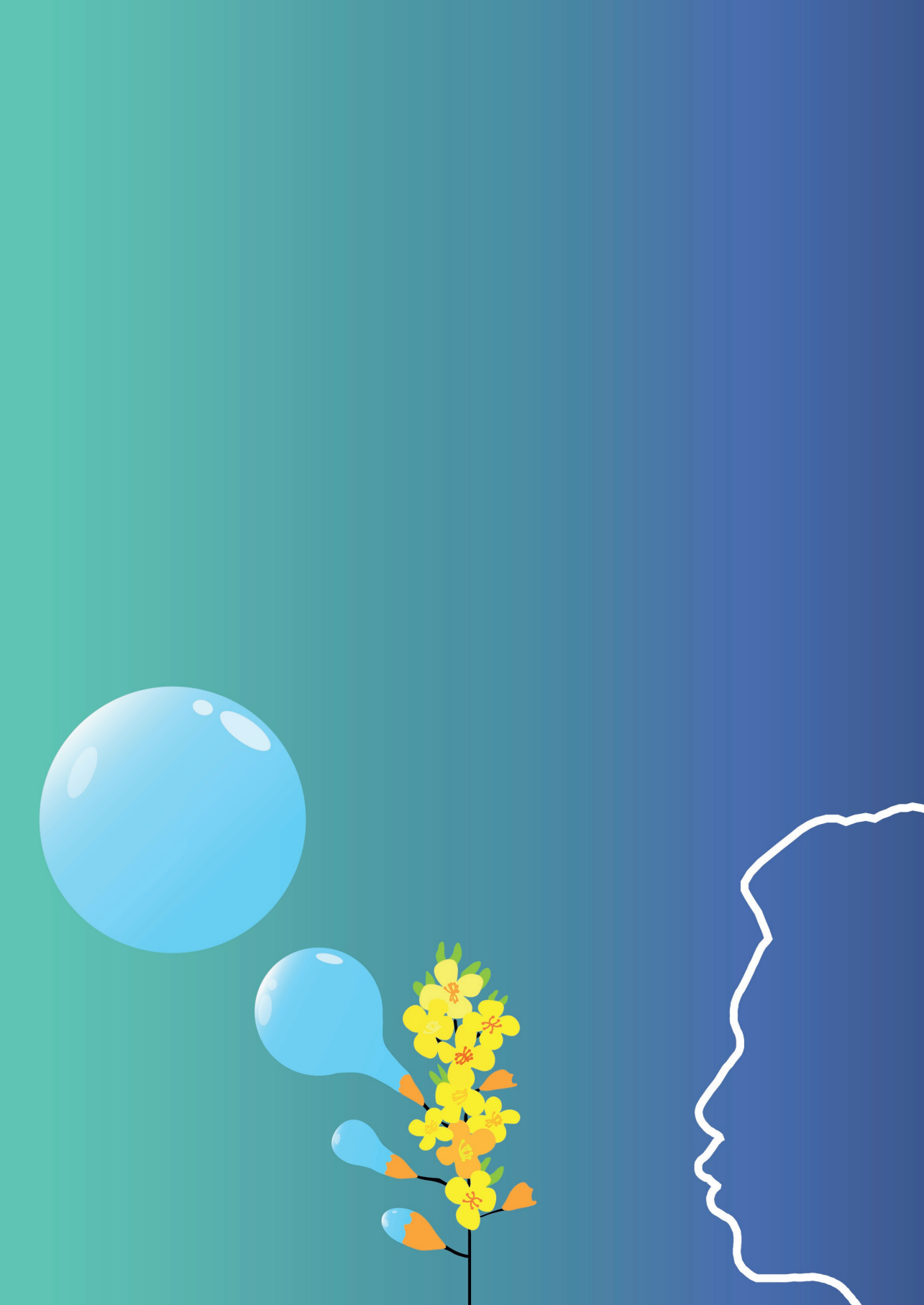

Chapter 5

Mixed interfaces stabilised by

whey protein – rapeseed lipid mixtures

Submitted as:
Yang, J., Waardenburg, L. C., Berton-Carabin, C. C., Nikiforidis, C. V., van der Linden, E., & Sagis, L. M. C. Air-water interfacial behaviour of whey protein and rapeseed oleosome mixtures.

Abstract

Plant seeds store lipids in oleosomes (also known as oil bodies or lipid droplets), which are spherical storage organelles with a triacylglycerol (**TAG**) core surrounded by a phospholipid monolayer and proteins. Due to their membrane components, oleosomes have an affinity for the air/oil-water interface and have potential as food ingredients. In this study, we mixed rapeseed oleosomes with a well-characterised model protein, whey protein isolate (**WPI**), and evaluate their air-water interfacial properties. Oleosomes were found to disrupt after adsorption at the interface. AFM images of the interfacial microstructure showed TAG/phospholipid-rich regions and membrane fragments, forming a weak and mobile interfacial layer. Mixing oleosomes with WPI resulted in an interface with TAG/phospholipid-rich regions surrounded by whey protein clusters. To understand the contribution of the different oleosome compounds on the interfacial properties, oleosome membrane components (obtained after oleosome solvent defatting) or rapeseed phospholipids (lecithin) were mixed with WPI. The result was an interface where WPI molecules aggregated into small WPI domains, surrounded by a continuous phase of membrane components or phospholipids. Upon compression, it seems that phospholipids are pushed out of the interface, and the WPI molecules interact with each other. Such behaviour was not observed for the WPI-oleosome membrane component interfaces, as the adsorbed defatted oleosome phase showed high resistance against the applied deformation, probably due to attractive forces between membrane proteins and phospholipids. Mixing WPI and rapeseed oleosomes resulted in mixed interfaces, which is an important finding for the utilisation of oleosomes as an emulsifier in mixed systems.

5.1 Introduction

Plant oilseeds, such as soybeans, rapeseeds, and sunflower seeds, are cultivated worldwide for their oils. In plant oilseeds, lipids are present in storage organelles, called oleosomes (**OS**, also known as oil bodies or lipid droplets)[165]. OS are natural oil droplets with a triacylglycerol (**TAG**) core that is surrounded by a monomeric membrane layer, consisting of a phospholipid monolayer with anchored proteins[22–24] (Figure 5.1). The diameter of OS ranges from 0.2 to 10 µm, depending on the plant source and environmental conditions during cultivation[22,166]. Currently, OS are disrupted with mechanical treatments and organic solvents to extract the TAG core for the production of plant oils for food purposes. A side product from the oil production are phospholipids, which are commercially known as lecithin. Phospholipids are widely applied as emulsifiers to stabilise oil droplets or other colloidal structures in the food, cosmetical, and pharmaceutical industry[167]. A new upcoming trend is the so-called minimal processing of ingredients to decrease the environmental impact of the purification process[45,152,168]. Pure phospholipids are obtained through extensive refinery and thus is not environmentally friendly. In contrast, the direct use of natural oil droplets, OS, would be much more environmentally friendly than pure phospholipids.

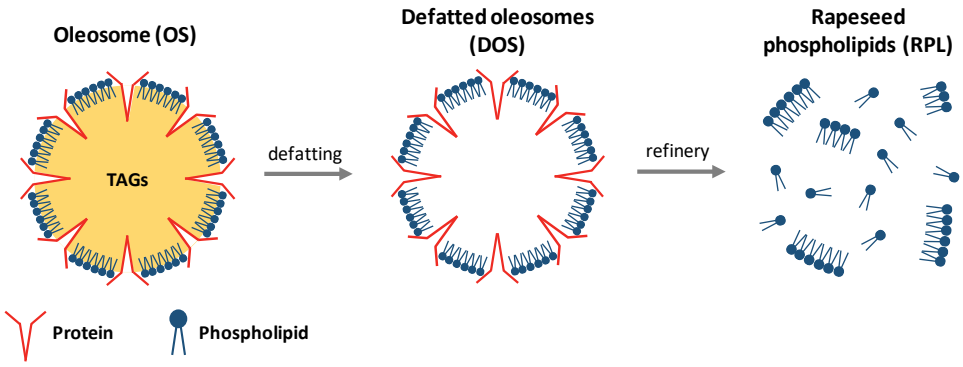

Figure 5.1. A schematic structure of the studied materials in this work: oleosomes, dried and defatted oleosomes, and rapeseed phospholipids. The components of the illustrations are not to scale.

OS has several other promising features, such as a high physical and chemical stability against lipid oxidation and droplet coalescence[25–28] due to the protective protein-phospholipid membrane, where surface proteins and phospholipids interact through hydrophobic and electrostatic forces. The most abundant phospholipids in plant OS membranes are phosphatidylcholine and phosphatidylserine[166]. Next to phospholipids, three types of membrane proteins are found in the interface of OS, which are oleosins, caleosins, and steroleosins, with oleosin being by far the most abundant one[23,165]. The outer surface of the OS is hydrophilic, due to the polar phospholipid headgroups and membrane protein hydrophilic domains being directed outwards[24]. The overall hydrophilicity of the OS' surface

allows an aqueous extraction from plant material, which is often performed by soaking, and disruption of cell walls, followed by separation of solids from the aqueous phase[29,169,170].

Many functionality studies have been performed on OS as a natural oil droplet with high chemical and physical stability[25,26,102,171]. Another potential application could be the role of emulsifier/surfactant, which was demonstrated by several studies for OS from different sources. Ishii et al. showed the possibility to stabilise oil droplets using soybean OS as an emulsifier[169]. The same was also demonstrated for sunflower seed OS, which was disrupted upon homogenisation, and fragments of membrane material formed an interfacial layer around the oil droplets[102]. The unfolding of soybean OS at the air-water interface was investigated by Waschatko et al.[62,70], and revealed rupture of the OS after adsorption, which is presumably followed by structural rearrangement of the interfacial components (phospholipids, membrane proteins, and TAGs) over time. Furthermore, Deleu et al. revealed that both phospholipids and OS proteins play an important role in emulsion stabilisation, as phospholipids were able to form small oil droplets and prevent flocculation due to a high negative surface charge. Additionally, the presence of membrane proteins provided oil droplet stability against coalescence[172].

The interface stabilising properties of the OS and their membrane components is not well understood yet. Therefore, we extracted OS from rapeseeds, which are one of the most cultivated oilseeds worldwide and contain about 40% (w/w) oil[173], and investigated their interfacial properties. To further investigate their interfacial stabilisation mechanisms, the OS were defatted to obtain OS membranes. Additionally, we included a commercially available rapeseed phospholipid extract (lecithin), which was derived from the OS membranes of defatted seeds. As foods are complex multi-component systems, other surface-active components will co-exist with OS, possibly influencing the interfacial layer formation. An example is proteins, a commonly used emulsifier, which could influence the interface stabilising behaviour of OS, and vice versa[48]. To specifically address this matter, the OS were mixed with a model whey protein isolate (**WPI**) system, as the structural and functional (interfacial) properties of these proteins are well characterised[103,174].

In summary, we first studied the air-water interface stabilising properties of the rapeseed phospholipids (**RPL**), followed by those of a less refined system, the defatted oleosomes (**DOS**), and finally of the OS. The components were mixed with WPI to assess the interfacial properties of the mixtures. The interfacial properties were evaluated using large amplitude oscillatory dilatational (**LAOD**) and shear (**LAOS**) rheology. The topography of the interfacial films was characterised by atomic force microscopy (**AFM**) on Langmuir-Blodgett films. Our work provides valuable insights into the interface stabilising mechanism of OS and mixtures of OS and exogenous proteins. The findings in this work allow the further exploitation of

oleosomes as a food ingredient and interface stabiliser in multiphase food systems, such as foams and emulsions.

5.2 Experimental section

5.2.1 Materials

Alizze rapeseeds were obtained from a European seed producer. Rapeseed phospholipids (**RPL**, commercial lecithin) (Emulpur RS Lecithin, Cargill, France), whey protein isolate (**WPI**) (BiPro, Davisco Food International, France), and other chemicals (Sigma-Aldrich, USA) were all used as received. Ultrapure water (MilliQ Purelab Ultra, Germany) was used for all experiments.

5.2.2 Sample preparation

Oleosomes extraction

The oleosome extraction method was based on previous work by Romero-Guzmán et al., with several adaptations[175]. Rapeseeds were dispersed in ultrapure water at a 1:10 (w/v) ratio. The pH was adjusted to 9.0 with 1 M NaOH, and the dispersion was stirred for 4 hrs, while constantly adjusting the pH to 9.0. After soaking, the dispersion was blended for 1 min at maximum speed in a kitchen blender (Waring Commercial, 400 W, USA). The slurry was passed through a cheesecloth to remove the solids. The pH of the filtrate was adjusted to 9.0, and the filtrate was centrifuged at 10,000xg at 4 °C for 30 min. The cream layer was collected and re-suspended in ultrapure water at a 1:5 (w/v) ratio. The dispersion was stirred for 15 min and centrifuged at 10,000xg at 4 °C for 30 min. The washing step and centrifugation step were once more repeated with buffer (sodium phosphate, 20 mM, pH 7.0) instead of ultrapure water. The oleosome extract was diluted with buffer based on dry matter content and used in experiments for a maximum of 5 days with the addition of sodium azide and storage at 4 °C.

Defatting of oleosomes

Oleosomes were diluted in ultrapure water in a 1:10 (w/v) ratio, frozen using liquid nitrogen, and freeze-dried. The freeze-dried oleosomes were defatted by adding hexane in a 1:10 (w/v) ratio, followed by 2 hrs stirring at room temperature and filtering over filtration paper. The defatting steps were repeated three more times. The final residue was dried overnight in a desiccator while constantly being flushed with nitrogen gas.

Protein content

The protein content was determined by measuring the nitrogen content using a Flash EA 1112 Series Dumas (Interscience, The Netherlands). The nitrogen content was converted into a protein content with a conversion factor of 5.7[100].

Lipid content

The lipid content of the oleosomes was determined by solvent (petroleum ether) extraction using a Soxhlet. The oleosomes were dried overnight at 60 °C, followed by solvent extraction for 6 hrs. The lipid content was determined by weighing the initial sample and the lipids in the collection flasks. The measurements were performed in duplicate.

Dissolving samples

Whey protein isolate (WPI) was dissolved at 2.5% (w/w) in buffer (sodium phosphate, 20 mM, pH 7.0) for 4 hrs and centrifuged at 16,000xg for 30 min. The supernatant was passed through a 0.45 µm syringe filter, and the filtrate was diluted based on the dry matter content. Rapeseed phospholipids (commercial lecithin) and defatted oleosomes were dispersed in the buffer by stirring the sample for 2 hrs at room temperature, followed by high speed mixing in an Ultra-Turrax (IKA, USA) at 8,000 rpm for 10 s, and hydrated overnight at 4 °C.

Preparation of mixtures

For the majority of the experiments, a WPI solution with a fixed concentration of 0.2% (w/w) was mixed with a 0.2% (w/w) oleosome, defatted oleosome, rapeseed phospholipid suspension in a 1:1 (v/v) ratio, which resulted in a final concentration of 0.1% (w/w) of all components. When concentrations deviated from this, it will be mentioned in the following sections.

5.2.3 Determination of droplet size distribution

The droplet size distribution of the oleosomes dispersions was characterised by static laser light scattering using a Mastersizer 2000 equipment (Malvern Instruments, UK). The refractive indices were 1.469 for the dispersed phase (oleosomes) and 1.330 for the dispersant (water). Potential flocculation was assessed by diluting the sample in a 1:1 (v/v) ratio with a 1% (w/w) sodium dodecyl sulphate (**SDS**) solution. Two independent oleosome batches were produced, and each sample was measured three times.

5.2.4 Determination of adsorption behaviour and surface dilatational properties

Adsorption behaviour, frequency sweeps, and step dilatation

The interfacial properties of the air-water interface, stabilised by the various components, and their mixtures, were studied with drop tensiometry. Time sweeps, frequency sweeps, and step-dilatations were performed in a PAT-1M drop tensiometer (Sinterface Technologies, Germany). The protein solution was injected through a hollow needle to create a hanging droplet (area of 20 mm^2) at the tip of a needle. The contour of the droplet was fitted with the Young-Laplace equation to obtain the surface tension. Before deformations, the droplet

was equilibrated for 3 hrs while monitoring the surface tension. Frequency sweeps were performed by varying the oscillatory frequency from 0.002 – 0.1 Hz with an amplitude of 3%. Each frequency cycle was performed with 5 sinusoidal oscillations followed by a rest step with the duration of a full oscillation. Step dilatation experiments were performed by extending or compressing the interfacial area by 10% with a step time of 2 s. All measurements were performed at least in triplicate at 20 °C.

Amplitude sweeps

Amplitude sweeps of the interfacial layer were performed using an ADT (Teclis, France), which was operated similarly to the PAT. The main difference was the droplet size (area of 15 mm^2) and the needle type (G18). After 3 hrs of waiting time, the droplet was subjected to various amplitudes (3-50%) at a frequency of 0.02 Hz. Each amplitude cycle was performed with 5 sinusoidal oscillations followed by a rest step of 50 s. All measurements were performed at least in triplicate at 20 °C.

Analysis of large amplitude oscillatory dilatational experiments

The amplitude sweep data were visualised by plotting Lissajous curves of the surface pressure ($\Pi(t) = \gamma(t)-\gamma_0$) versus deformation ($(A(t)-A_0)/A_0$). Here, $\gamma(t)$ and $A(t)$ are the surface tension and area of the deformed interface at time t, and γ_0 and A_0 are the surface tension and area of the non-deformed interface. Lissajous plots were made from the middle three oscillations of each amplitude cycle.

5.2.5 Determination of surface shear properties

The surface shear properties of the interfaces were determined using a double-wall-ring (**DWR**) geometry coupled to an AR-G2 rheometer (TA Instruments, USA). The diamond-edged ring of the DWR was positioned at the air-water interface of the sample in a double-wall Teflon trough and covered with a vapour cap to limit evaporation. The interface was pre-sheared for 5 min at a shear rate of 10/s, and equilibrated for 3 hrs before a strain or frequency sweep. The strain sweeps were performed with strains varying from 0.01-100% at a frequency of 0.1 Hz, and the frequency sweeps were performed with frequencies varying from 0.01 to 10 Hz at a strain of 1%. All experiments were performed in triplicate at 20 °C. In all our studied systems, the contribution of the subphase to the stress signal is negligible, as the Boussinesq number (ratio between surface and bulk stress) was >1[134].

5.2.6 Preparation of Langmuir-Blodgett films

Protein/lipid-stabilised interfaces were deposited on solid substrates to produce Langmuir-Blodgett (**LB**) films in a Langmuir trough (KSV NIMA/Biolin Scientific Oy, Finland). Samples of pure WPI, oleosome, rapeseed phospholipid, and defatted oleosome contained 0.1%

(w/w) material. The WPI-lipid mixtures contained 0.05% (w/w) protein (WPI), and 0.05% (w/w) lipids based on dry matter.

The mixtures of protein with lipid had a protein content of 0.05% (w/w), and lipid content of 0.05% (w/w). The Langmuir trough was filled with buffer (sodium phosphate, 20 mN, pH 7.0), and 200 µL of the sample were injected in the subphase using a syringe. The samples were allowed to adsorb and equilibrate at the interface for 3 hrs, while the surface pressure was monitored using a Wilhelmy plate (platinum, perimeter 20 mm, height 10 mm). After equilibration, the interfacial layer was compressed with barriers moving at a speed of 5 mm/min to target surface pressures. The interfacial layer was deposited on a freshly cleaved mica sheet (Highest Grade V1 Mica, Ted Pella, USA) at a 1 mm/min withdrawal speed. The LB films were dried in a desiccator at room temperature, and all films were produced in duplicate.

5.2.7 Determination of interfacial microstructure by AFM

The topography of the interfacial microstructure was analysed using atomic force microscopy (**AFM**, MultiMode 8-HR, Bruker, USA). The LB films were analysed in tapping mode using a Scanasyst-air model non-conductive pyramidal silicon nitride probe (Bruker, USA) with a normal spring constant of 0.40 N/m and a lateral scan frequency of 0.977 Hz was applied on all images. The scan area was 2 x 2 μm^2 and 10 x 10 μm^2 with a lateral resolution of 512 x 512 $pixels^2$. The films were scanned for at least two locations to ensure good representativeness, and the images were analysed using Nanoscope Analysis v1.5 software (Bruker, USA).

5.3 Results and discussion

5.3.1 Physico-chemical properties of oleosomes

The aqueous extraction method yielded rapeseed oleosomes (**OS**) with 88.5 ± 3.8 % (w/w) lipids, 7.2 ± 0.3% protein, and the remaining 4.3% should mainly consist of phospholipids and minerals. We should also keep in mind that the phospholipids might also be partially extracted with the lipid content determination method. The OS suspension had a broad size distribution at pH 7.0, ranging from 2 to 300 µm with a $d_{3,2}$ of 7.97 ± 0.20 µm (Figure 5.2A). Sodium dodecyl sulphate (**SDS**) was added to break up aggregated droplets and revealed smaller droplets ranging from 0.2 to 20 µm with a $d_{3,2}$ of 0.81 ± 0.02 µm. Comparable OS composition and droplet sizes were also demonstrated by Romero-Guzmán et al. for rapeseed oleosomes extracted at a pH value of 7.0[175], where the formation of large flocculates was attributed to the low surface charges and the presence of storage proteins[29].

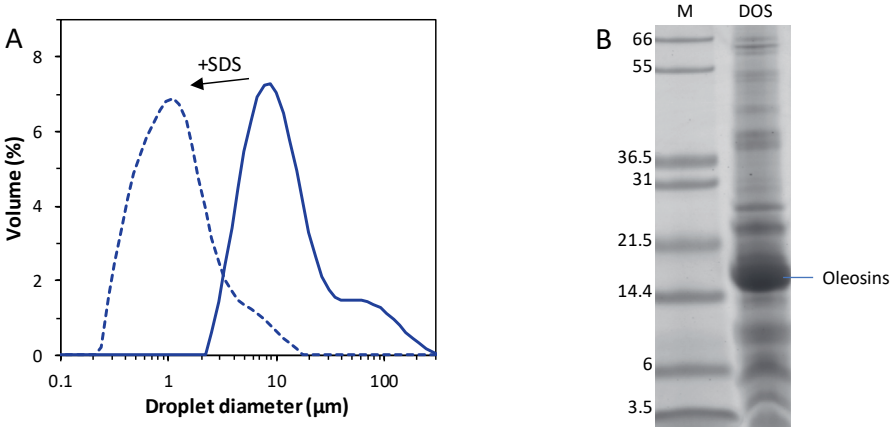

Figure 5.2. (A) The volume-based size distribution of oleosomes (solid line) in buffer (20 mM PO_4, pH 7.0). SDS was added to break up possible aggregates to obtain the single droplet size of the oleosomes (dashed line). (B) SDS-PAGE under reducing conditions containing marker with the corresponding molecular weight in kDa on the left and the defatted oleosomes (DOS) on the right.

Defatted oleosomes (**DOS**) were analysed using SDS-PAGE (Figure 5.2B) to investigate the efficiency of the OS purification step and the possible presence of rapeseed storage proteins. The thickest band in the scan is around 16 kDa, which corresponds to the oleosome membrane protein oleosin[166]. The rapeseed storage protein napin and cruciferin were previously found to form bands between 6-10 and 18-28 kDa, respectively[176]. As only light bands are shown in these molecular weight regions, we do not expect the storage proteins to play a major role in the interfacial composition and properties.

5.3.2 Whey protein – rapeseed phospholipid mixtures

Adsorption behaviour of whey protein – rapeseed phospholipid mixtures

First, we studied the interfacial properties of rapeseed phospholipids (**RPL**) from a commercial lecithin, which were extracted from the oleosome membrane as a side product of plant oil extraction. During oil extraction, the triacylglycerol (**TAG**) core was extracted using organic solvents, and the remaining membrane is often refined by the removal of the proteins to obtain a pure phospholipid extract (lecithin). The removal of protein is also reflected in the low protein content of 6.9 ± 1.1 % (w/w). We should keep in mind that the main phospholipid in the OS membrane, phosphatidylcholine, possesses a choline group, which can contribute to the nitrogen-based protein content. Nonetheless, the protein content gives us a rough estimation of the difference in protein content between the RPL, DOS, and OS. The surface activity of RPL, whey protein isolate (**WPI**) and a WPI-RPL mixture at a 1:1 (w/w) ratio is shown in Figure 5.3.

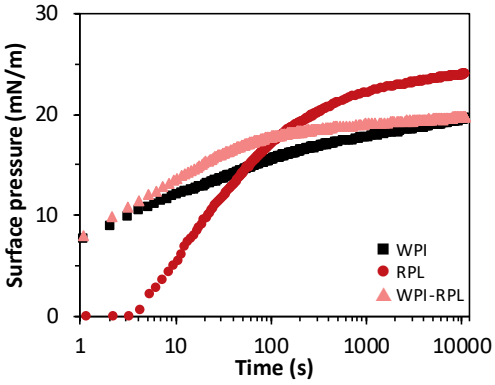

Figure 5.3. Surface pressure as a function of time of interfacial films stabilised by WPI (black square), RPL (dark red circle), and WPI-RPL mixtures (light red triangle) in buffer (20 mM PO4, pH 7.0). The surface pressure isotherms represent an average from at least three replicates. The standard deviation was below 5%.

RPL had a lag time of 2 s before the material started to increase the surface pressure. An explanation could be the low solubility of RPL, as evidenced by the fact that the suspension was turbid and material sedimented over time. Additionally, phospholipids are known to form vesicles in water, which might diffuse slowly towards the interface[167]. The surface pressure of RPL increased to a final surface pressure of 25 mN/m after 3 hrs of adsorption. WPI showed an immediate surface pressure increase to 8 mN/m, followed by a constant increase to a final value of 20 mN/m. The adsorption of WPI was faster than RPL in the first 70 s, probably due to the low solubility of RPL and slow diffusion of the vesicles. On the other hand, RPL reached higher surface pressures after 70 s, as smaller phospholipids can form a more densely packed interface[114,177]. The interfacial packing efficiency of lipid-like structures is also determined by the chemical structure of the aliphatic tails, as unsaturation

in *cis* configuration decreases the packing density[178]. The WPI-RPL mixture led to a similar surface pressure as pure WPI in the first two s, which is similar to the lag phase of pure RPL. Afterwards, the surface pressure increased to slightly higher values compared to pure WPI, but ended again at the same value as WPI after 10,800 s. This could suggest initial adsorption of WPI at the interface, followed by RPL. As less free interface is available for RPL to adsorb on, the surface pressure did not reach the value of 25 mN/m of pure RPL. To further assess the interface stabilising mechanisms of the WPI-OS mixtures, we performed shear and dilatational rheology on the interface.

Interfacial rheology on whey protein – rapeseed phospholipid stabilised interfaces

The surface shear moduli of interfacial films stabilised by WPI, RPL and WPI-RPL mixtures were measured in a strain sweep using a double wall ring geometry coupled to a rheometer Figure 5.4A.

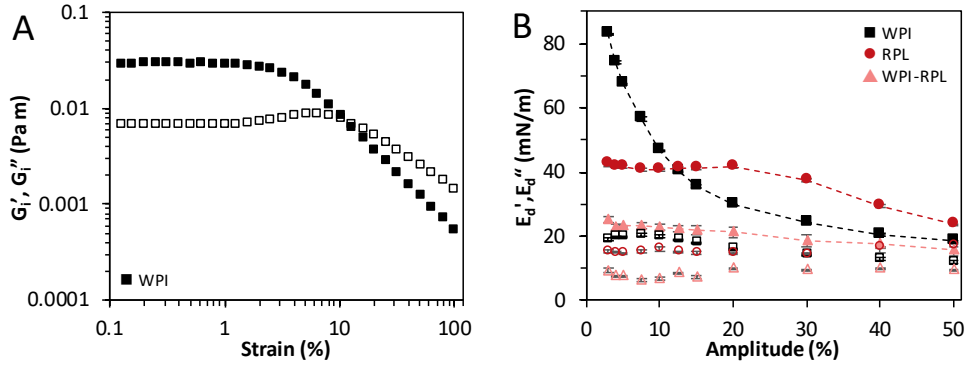

Figure 5.4. (A) The surface shear storage (G_i') and loss (G_i'') moduli as a function of strain of interfacial films stabilised by WPI (black square). (B) The surface dilatational storage (E_d') and loss (E_d'') moduli as a function of amplitude of interfacial films stabilised by WPI (black square), RPL (dark red circle), and WPI-RPL mixtures (light red triangle) in buffer (20 mM PO_4, pH 7.0). Closed symbols show the storage modulus (G_i' or E_d') and open symbols show the loss modulus (G_i'' or E_d''). The averages and standard deviations are the result of at least three replicates.

The WPI-stabilised interface showed a linear viscoelastic (**LVE**) regime up to 1% strain, where the storage (***G_i'***) and loss modulus (***G_i''***) remained constant. The G_i' was found to be higher than the G_i'' in the LVE, resulting in a tanδ of around 0.24, thus suggesting solid-like behaviour. At larger deformations, the response entered the nonlinear viscoelastic (**NLVE**) regime, as the moduli started to decline, revealing that the applied deformation affected the interfacial microstructure, thus resulting in softening behaviour. The *Gi''* had a weak strain overshoot between 3 and 10% strain, which is presumably related to the simultaneous breakdown and formation of new network junctions, due to the collision of clusters. This behaviour is specified as type III nonlinear behaviour, and is commonly found for soft solids[57]. To summarise, the WPI-stabilised air-water interface clearly showed the rheological behaviour of a viscoelastic solid, as was also more elaborately demonstrated in our previous

work[103]. Surface shear experiments were also performed on RPL- and WPI-RPL-stabilised interfaces but resulted in lower torque values than the minimum torque limits of the rheometer. This suggests the formation of a very weak interface with limited in-plane interactions between the molecules at the surface.

A comparable effect is present in the amplitude sweep in dilatational deformations (Figure 5.4B). The WPI-stabilised interface had a surface dilatational elastic modulus (***E_d'***) that decreased from 84 to 20 mN/m with increasing amplitude. This amplitude dependency implies the breakdown of the interfacial microstructure upon applied deformation. Different behaviour can be observed for the RPL-stabilised interfaces, which had a constant E_d' up to 20% amplitude, implying a prolonged linear viscoelastic (**LVE**) regime. At higher deformations, the interfacial microstructure was disrupted, which was reflected in a decrease in elastic modulus. The WPI-RPL mixtures resulted in moduli between 18 and 25 mN/m over the whole range of deformations, which is lower than pure WPI or RPL. The interactions at the interface were further studied by performing frequency sweeps to evaluate the frequency dependence and was quantified using a power-law scaling with frequency, $E_d' \sim \omega^n$. A value of n=0.5 would suggest that the elasticity of the interface is predominantly affected by the exchange of stabiliser between the bulk and interface[144]. The n-values of WPI, RPL and WPI-RPL mixtures were found to be 0.12 ± 0.03, 0.24 ± 0.01, and 0.23 ± 0.03, respectively (Table 5.1). RPL had an increased frequency dependency, which revealed a more mobile interface compared to WPI. This would also suggest increased transfer between bulk and interface for RPL-stabilised interfaces, where the interfacial stabiliser is pushed into the bulk upon compression of the interface, and stabiliser adsorbs upon creation of new surface area in extension. The higher n-value for WPI-RPL compared to WPI also indicate that RPL dominated the rheological properties of the mixtures. The composition of the interface was further examined using Lissajous plots and microstructure imaging.

Table 5.1. An overview of the value of the power-law exponent n, obtained from the dilatational frequency sweeps, for pure WPI, OS, DOS, and mixture-stabilised interfaces. The averages and standard deviations are the result of at least three replicates.

	n-value
WPI	0.12 ± 0.03
OS	0.30 ± 0.01
WPI-OS	0.18 ± 0.03
DOS	0.30 ± 0.03
WPI-DOS	0.27 ± 0.02
RPL	0.24 ± 0.01
WPI-RPL	0.23 ± 0.05

Lissajous plots and interfacial microstructure imaging

To further assess the mechanical and structural properties of the interfacial films, we generated Lissajous plots using the interfacial stress and deformation from the dilatational deformations. Also, we studied the interfacial microstructure by performing atomic force microscopy (**AFM**) on Langmuir-Blodgett (**LB**) films (Figure 5.5). Lissajous plots are proven to be a useful tool in rheology, as they allow for a detailed study of the nonlinearities in the stress response[58,59]. The shear and dilatation moduli in Figure 5.4 are obtained from the first harmonic of the Fourier transformation of the stress signal, which is a suitable method for measurements in the LVE regime. When the response enters the NLVE regime, higher harmonics are present in the stress response (only odd ones in shear, and even and odd ones in dilatation). Higher harmonics are completely neglected in the first harmonic moduli, but their contribution can be analysed in Lissajous plots by plotting the interfacial stress directly versus the deformation. In earlier work, we demonstrated that microstructure imaging of LB films contributes to a better understanding of the behaviour of interfacial layers[103,108,152]. The samples were infused in the subphase of a Langmuir trough filled with buffer. After 3 hrs of waiting time (similar to the waiting time in rheology), the diffusion-based film was compressed and transferred to a substrate, creating an LB Blodgett film.

In our previous work, a phase transition was found to occur around 21 mN/m in the (Langmuir) surface pressure isotherms of WPI[103]. Surface pressure isotherms have been widely studied for Langmuir films stabilised by small molecular weight surfactants[179]. For interfaces stabilised by the latter, the compression state of the interface before the phase transition is called the liquid expanded (**LE**) state, where molecules start increasingly interacting and reorienting to a more densely packed layer upon increasing the degree of compression. The region after the phase transition is referred to as a liquid condensed (**LC**) state[179], where the interfacial stabilisers are compressed into a densely packed interfacial layer. Surface pressure isotherms of the lipids can be observed in Figure A5.1 in the appendix. We produced LB films in the LE and LC state of a WPI-stabilised interfacial layer at surface pressures of 15 and 25 mN/m, respectively[179].

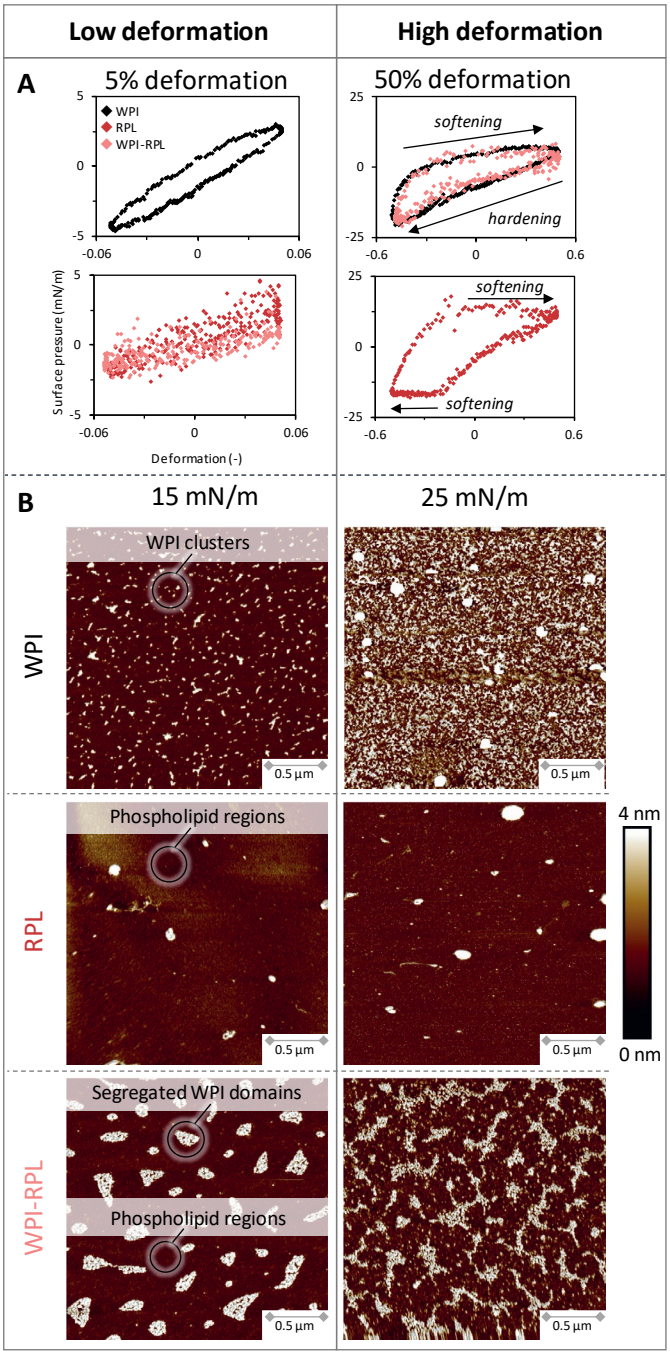

Figure 5.5. (A) Lissajous plots of surface pressure as a function of the applied deformation, obtained from amplitude sweeps of air-water interfacial films stabilised by WPI, RPL, and WPI-RPL mixtures. For clarity, one representative plot is shown for each sample, but comparable plots were obtained on at least three replicates. (B) AFM images of Langmuir-Blodgett films made from RPL and WPI-RPL mixtures. The surface pressure indicates the conditions during film sampling.

The Lissajous plot obtained from the WPI-stabilised interfacial film had a symmetric and narrow shape at 5% deformation (Figure 5.5A), revealing a linear viscoelastic behaviour, where the elastic component dominates the stress response. At higher deformations, such as 50%, the interfacial structure was disrupted, which caused the Lissajous plots to become asymmetric. The asymmetry helps us to understand the interfacial network structure further. If we start at the maximum compression, so at a deformation of -0.50, we can observe a rapid increase in surface pressure, which indicates a predominantly elastic response. Around a deformation of -0.40, the rapid increase becomes more gradual. This point depicts intra-cycle yielding, where the viscous contribution starts dominating, and the interfacial layer starts flowing. The gradual decrease of the slope of the plot afterwards is called intra-cycle strain softening (in extension). The opposite can be observed in compression, as the surface pressure changed steeply to a higher maximum surface pressure (-20 mN/m) compared to the one in extension (7 mN/m). This behaviour is called intra-cycle strain hardening, which can be attributed to concentrating the proteins (as individual molecules or supramolecular structures) on the interface upon compression. As a result, more densely clustered regions will be formed that start jamming at such large deformations.

The jamming of these clusters was nicely depicted in the AFM images in Figure 5.5B, as can be observed as white structures on the WPI film at 15 mN/m (which corresponds to an expanded state). The whey protein clusters were formed due to the segregation of proteins at the interface, driven by attractive interactions. Segregation of proteins occurs continuously on the interface and is reflected in the constant increase of surface pressure after the initial adsorption phase of the proteins. Such long-term processes were found to continue even after more than 12 hrs of ageing of the interface[55,103]. The long time-tail in the adsorption kinetics is often attributed to protein denaturation/unfolding and intra-protein rearrangements[48,49], which seems unlikely, as these long-term processes were also obtained for heat-denatured whey proteins[103]. Therefore, other processes such as protein orientational rearrangements and the earlier described segregation of proteins at the interface are more likely to cause the long-term processes that result in the time-tail[108]. At a higher compression to a surface pressure of 25 mN/m (which corresponds to a higher degree of compression), the WPI interfacial film was densely compressed into a more condensed state, where more clusters can be seen on the AFM film. Here, the clusters seemed to start interacting and jamming, which coincide with the strain hardening in compression in the Lissajous plots at 50% deformation amplitude. From these observations, we conclude that the WPI-stabilised interfaces behave as heterogeneous viscoelastic solids.

The Lissajous plots of the RPL-stabilised interface showed notable differences compared to WPI (Figure 5.5A). The plot at 5% deformation had a symmetric and very narrow loop, which

suggests an almost fully elastic response. The plot for RPL started to display major asymmetries at higher deformations. The plot at 50% deformation had a steep elastic response in extension from -0.50 to -0.20 deformation, followed by intra-cycle yielding around -0.20 deformation. After yielding, nearly constant surface pressure was observed, which indicates intra-cycle strain softening in extension. A minor degree of strain hardening in compression can be observed, followed by strain softening between -0.20 to -0.50 deformation. Phospholipids are known to possess a complex phase diagram, where phase transitions can occur depending on, for instance, the degree of compression of the interfacial layer[179].

The strain softening in compression could be attributed to three different interfacial phenomena: 1. interfacial domains that start to slide over each other; 2. buckling of the interface; or 3. exchange of molecules between bulk and interface. Buckling seems improbable to occur, as this phenomenon requires strong intramolecular interactions between stabiliser molecules at the interface, which, for instance, were earlier observed for saponin-stabilised interfaces[180,181]. Such strong interactions were not observed for RPL in both shear and dilatational rheology. In the surface pressure isotherms from the Langmuir trough (Figure A5.1 in the appendix), RPL showed a phase transition at 36 mN/m, where the slope of the surface pressure isotherm decreases. This point reflected the transition from a liquid expanded (**LE**) to a liquid condensed (**LC**) phase, where the phospholipid layer was densely compressed[179], and is also known as a state where the LE and LC phase co-exist. At such high compressions, some expanded regions started to form more condensed and solid-like structures and resulted in the lower slope in the surface pressure isotherm. This phase transition could explain the strain softening behaviour in the Lissajous plots at 50% deformation, and the formed condensed/solid-like interfacial domains could also start to slide over each other at such high compressions. Another explanation could be the exchange of RPL between the interface and the bulk upon compression and extension of the interfacial area, as the RPL displayed weak in-plane interactions at the interface. AFM images of LB films of RPL showed a flat surface with larger structures (Figure 5.5B) and could correspond to insoluble material or proteinaceous material. The AFM image remained similar at higher compression (to a surface pressure of 25 mN/m), which could imply that material in the flat areas are either pushed into the bulk upon higher compressions (or pushed below the surface, as AFM only analyses the topography), or started to form a more densely compressed layer that might not be visible within the resolution of the AFM.

Mixing WPI and RPL resulted in a Lissajous plot at 5% deformation, which is more tilted towards the horizontal axis than pure WPI (Figure 5.5). This is also reflected in a lower E_d' of the WPI-RPL mixture than pure WPI or RPL-stabilised interfaces. In the AFM image of the LB film at 15 mN/m, more and higher structures are present compared to pure RPL. The

structures are assumed to be segregated domains of WPI, which could be surrounded by phospholipids. The latter formed the continuous phase and dominated the interfacial properties, and this would explain the weak interfaces observed in dilatational and shear rheology. Whey proteins also seem to prevent the phospholipids from forming an interface similar to pure RPL, as the moduli of the mixture were substantially lower compared to either pure WPI or RPL. The partial displacement of proteins from a surface by low molecular weight surfactants was previously demonstrated for milk proteins and Tween 20, a non-ionic surfactant[66,182]. In these studies, AFM images on the interfacial microstructure also demonstrated large surfactant-rich regions that surround domains of milk proteins. They resulted in a decrease in surface moduli compared to pure proteins. At higher compressions, the AFM image corresponding to the film at 25 mN/m displayed disordered domains of whey proteins that seemed to start interacting mutually. The interactions involving whey proteins at WPI at a WPI-RPL-stabilised interface can be observed in the Lissajous plot at 50% deformation, which overlaps with the Lissajous plot of pure WPI. At such high deformations, the RPL is likely to be pushed out of the interface, which would allow the whey proteins in WPI-RPL films to start jamming, thus showing a rheological response similar to that of the film with pure WPI. In summary, the combination of rheology and microstructure imaging on a WPI-RPL mixed interface suggests the formation of whey protein domains, surrounded by a continuous RPL-rich phase.

5.3.3 Whey protein – defatted oleosome mixtures

Adsorption behaviour and interfacial rheology of whey protein – defatted oleosome mixtures

The complexity of the system was increased by studying defatted oleosomes (**DOS**), where the TAGs were removed from the OS. The RPL is a refined extract from the DOS, and the major compositional difference is the presence of membrane proteins in the DOS, as reflected in protein content of 69.5 ± 0.3 % (w/w). We also expect a structural difference between RPL and DOS, as was previously demonstrated for sunflower DOS, which was found to exist as empty membrane shells of OS using scanning electron microscopy[102]. RPL is more likely to be disrupted in the phospholipid refinery process. However, we should be cautious with the assumptions on the DOS structure, as the sunflower DOS were analysed in a dry state, and these empty OS membrane shells could be disrupted upon dissolution in a polar environment. The remaining 30.5% was expected to mainly consist of phospholipids. DOS were previously found to be surface-active, as emulsions could be stabilised by sunflower DOS[102]. As expected, the rapeseed DOS were also surface-active at the air-water interface (Figure 5.6A). The surface pressure induced by DOS was lower compared to that observed with WPI in the first 3 s, and showed a steeper increase afterwards. DOS led to a surface pressure around 31 mN/m after 3 hrs, which was almost twice higher than the final surface

pressure reached with WPI. Mixing of WPI and DOS resulted in higher surface pressures than pure WPI or DOS in the first 500 s of adsorption. Afterwards, the surface pressure followed the curve of pure DOS. It seems that WPI and DOS adsorbed at the interface in the initial phase, but DOS dominated the behaviour after 500 s. The exact composition of the interface was further examined by rheological experiments.

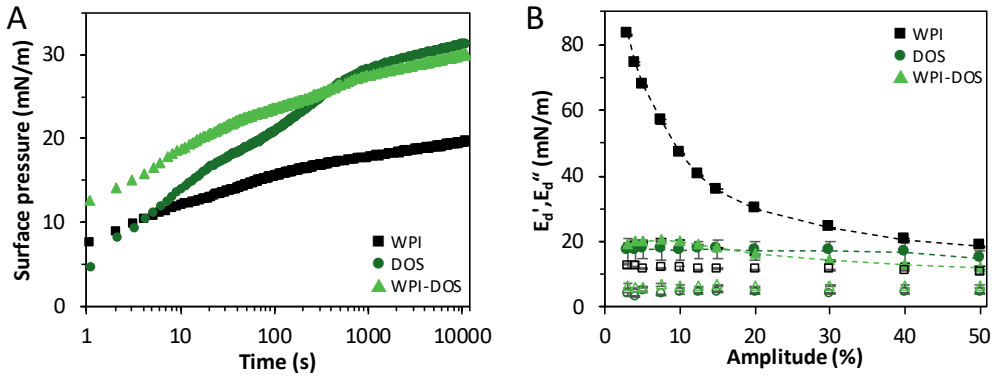

Figure 5.6. (A) Surface pressure as a function of time of interfacial films stabilised by WPI (black square), DOS (dark green circle), and WPI-DOS mixtures (light green triangle) in buffer (20 mM PO_4, pH 7.0). The surface pressure isotherms represent an average from at least three replicates. The standard deviation was below 5%. (B) The surface dilatational storage (E_d') and loss (E_d'') moduli as a function of amplitude of the interfaces mentioned in figure A. Closed symbols show the storage modulus (G_i' or E_d') and open symbols show the loss modulus (G_i'' or E_d''). The averages and standard deviations are the result of at least three replicates.

The DOS-stabilised interface had an E_d' between 19-20 mN/m over the whole range of amplitudes from 2 – 50%, with n=0.30 for the power-law dependence of modulus on frequency (Table 5.1), and indicated a weaker and more mobile interface compared to WPI. The E_d' of WPI-DOS mixtures coincided with that measured for pure DOS, and had a relative high n-value of 0.27. Shear rheology revealed that DOS and WPI-DOS-stabilised interfaces were too weak to be measured accurately, suggesting the formation of a very weak interface with little in-plane interactions between the molecules at the interface, comparable to the RPL-stabilised interface. The dominating behaviour of DOS in adsorption and rheological properties of the WPI-DOS mixture could be related to the displacement of whey proteins by DOS. The combination of Lissajous plots and microstructure imaging could help us further assess the stabilisation mechanism of both components at the air-water interface.

Lissajous plots and interfacial microstructure imaging

The Lissajous plots of DOS-stabilised films showed large differences from those of RPL; an overview of all Lissajous plots can be found in Figure A5.2 in the appendix. The plots of RPL- and DOS-stabilised interfaces at 5% deformation exhibited a narrow ellipsoidal loop (Figure 5.7A).

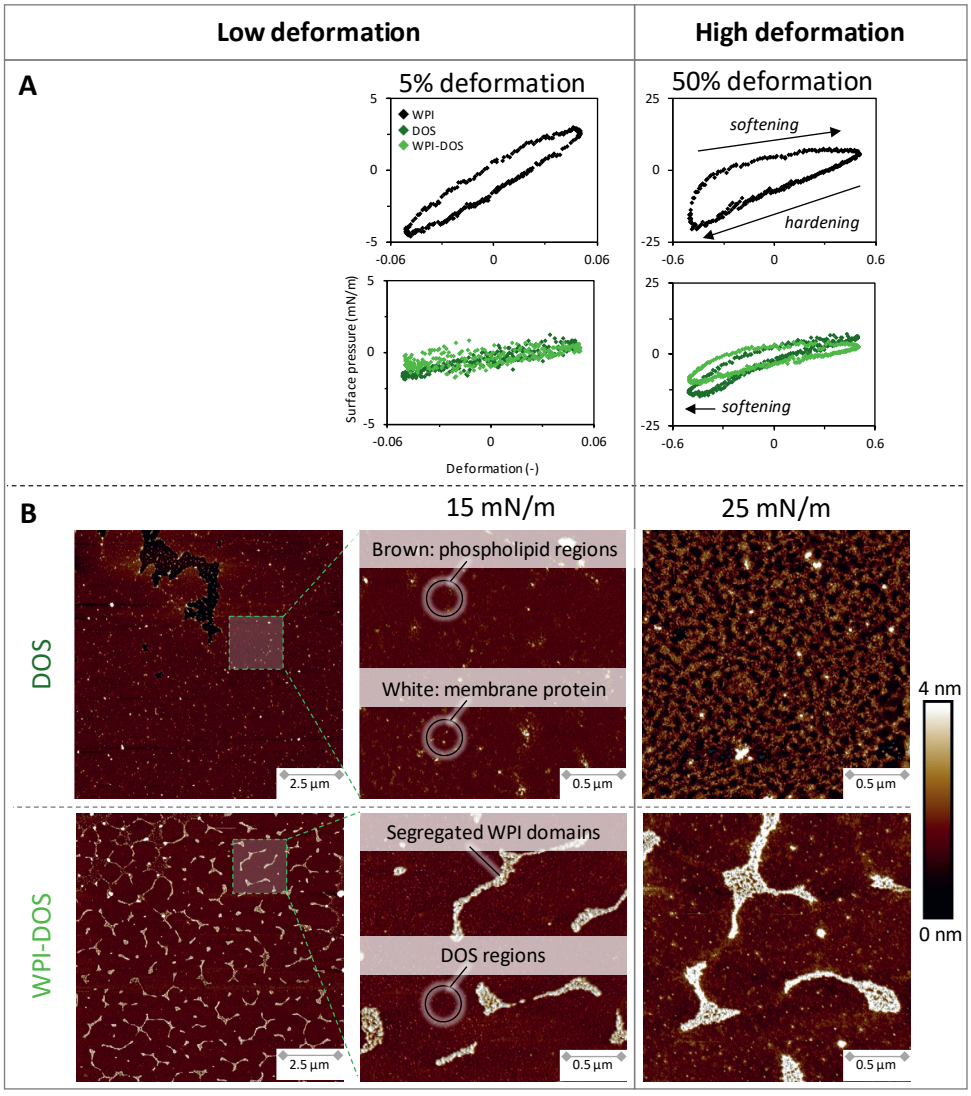

Figure 5.7. (A) Lissajous plots of surface pressure as a function of the applied deformation, obtained from amplitude sweeps of air-water interfacial films stabilised by WPI, DOS, and WPI-DOS mixtures. For clarity, one representative plot is shown for each sample, but comparable plots were obtained on at least three replicates. (B) AFM images of Langmuir-Blodgett films made from DOS and WPI-DOS mixtures. The surface pressure indicates the conditions during film sampling.

At a higher deformation of 50%, the Lissajous plot of the DOS-stabilised films was narrower compared to that obtained for RPL, suggesting a more elastic-dominant behaviour. The Lissajous plot also exhibited strain softening in extension and compression to a lesser extent than the plot of an RPL-stabilised interface. Therefore, we expect the DOS to form a more cohesive interface compared to RPL. AFM images of LB films based on DOS at 15 mN/m showed a rather flat surface with higher structures that could be proteins, as DOS had a

protein content of almost 70% (Figure 5.7B). The presence of membrane proteins became more obvious at a higher compression to a surface pressure of 25 mN/m, where the microstructure became more dense and heterogeneous, as also observed in our previous work for a more diluted WPI system[103]. At such high compression, phospholipids could be pushed out of the surface, which would explain the strain softening between deformations of -0.35 and -0.50 in the Lissajous plot at 50% deformation amplitude.

A WPI-DOS-stabilised interface showed a Lissajous plot at 50% deformation that is even more tilted towards the horizontal axis compared to pure DOS, which indicates an even weaker interface. On the other hand, the strain softening in compression was not observed for WPI-DOS. The AFM image of the LB film at 15 mN/m (Figure 5.7B) showed similar segregated WPI domains as on the WPI-RPL films (Figure 5.5B). The WPI domains could be surrounded by DOS material, such as membrane proteins and phospholipids that dominated the interfacial properties. This would explain the weak interfaces observed in dilatational and shear rheology. At a higher surface pressure of 25 mN/m, the AFM image showed a similar microstructure with segregated whey protein domains. A slight change can be observed in the continuous phase between the domains, as more structures could be observed. The emerging structures could suggest the presence of membrane proteins in this phase, which started to segregate at higher compressions, as demonstrated in the AFM images of pure DOS films at a surface pressure of 25 mN/m. Increased segregation of membrane proteins might be reflected in the absence of the strain softening in compression in the Lissajous plot at 50% deformation amplitude, while the strain softening was present in the (50% deformation) plots of pure DOS-stabilised interfaces. Additionally, whey proteins might contribute to the overall interaction on the WPI-DOS-stabilised interface.

The WPI-DOS and WPI-RPL mixed interface showed the formation of segregated whey protein domains, surrounded by a continuous phase of either DOS (phospholipids and membrane proteins) or RPL (phospholipids). A major difference was the resistance against high compression/deformation, as RPL seemed to be pushed out of the interface, allowing whey proteins to interact, which did not occur for DOS. The higher protein content in DOS could have played a major role in this behaviour. The OS membrane proteins are known to be strongly anchored into the membrane, as membrane proteins form strong hydrophobic and electrostatic interactions with the phospholipids in the interfacial layer[172]. Thus, membrane proteins could prevent the phospholipids in a DOS-stabilised interface from being expelled into the bulk upon (high) compression. In contrast, the expulsion of phospholipids did occur in an RPL-stabilised interface, where substantially fewer membrane proteins were present. A difference in in-plane molecular interactions is reflected in the surface pressure isotherms (Figure A5.1 in the appendix): for the DOS-based films, a change from an LE phase into an LC state without an LE-LC co-existence phase (slope increased after transition

point at 29 mN/m), was observed, whereas the co-existence phase was present for the RPL-based film (slope decreased after transition point at 36 mN/m). The strong interactions between proteins and phospholipids in the DOS is likely to contribute to the transition to a more condensed state upon compression. RPLs also adsorbed more slowly to the interface than whey proteins in the first 70 s. A slow adsorption behaviour would result in the presence of less RPL on the WPI-RPL interface, whereas more DOS might be present on the WPI-DOS interface.

5.3.4 Whey protein – oleosome mixtures

Adsorption behaviour and interfacial rheology of whey protein – oleosomes mixtures

Finally, we increased the complexity of the lipid components by using non-defatted oleosomes (**OS**), and the surface activity of OS, WPI and WPI-OS is shown in Figure 5.8.

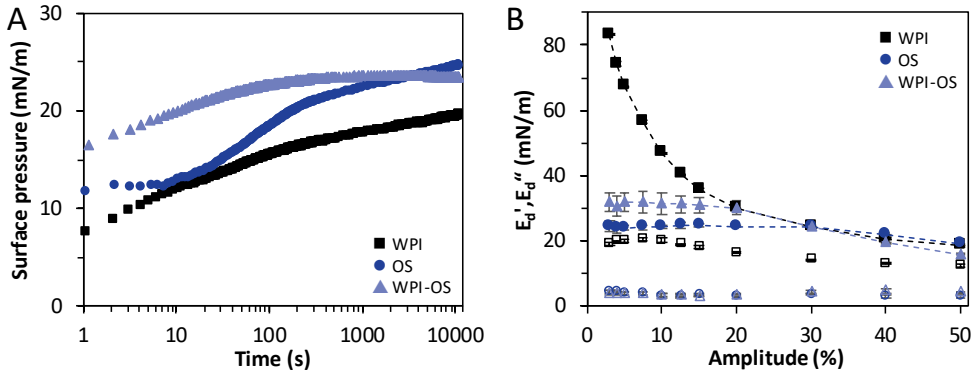

Figure 5.8. (A) Surface pressure as a function of time of interfacial films stabilised by WPI (black square), OS (dark blue circle), and WPI-OS mixtures (light blue triangle) in buffer (20 mM PO_4, pH 7.0). The surface pressure isotherms represent an average from at least three replicates. The standard deviation was below 5%. (B) The surface dilatational storage (E_d') and loss (E_d'') moduli as a function of amplitude of interfacial films stabilised by WPI (black square), OS (dark blue circle), and WPI-OS mixtures (light blue triangle) in buffer (20 mM PO_4, pH 7.0). Closed symbols show the storage modulus (E_d') and open symbols show the loss modulus (E_d''). The averages and standard deviations are the result of at least three replicates.

The OS had an immediate increase of surface pressure, starting at 12 mN/m, and remained constant for about 10 s. Subsequently, the surface pressure increased rapidly for 200 s, followed by a more gradual increase to 25 mN/m after 3 hrs of adsorption time. Several studies already reported a high surface activity and the ability to stabilise interfaces for OS[62,102,169]. Waschatko et al. used Brewster angle microscopy to study the structure of an air-water interface stabilised by soybean OS in a Langmuir trough[62,70]. In this work, a slow initial adsorption phase of OS was observed, similar to our findings in Langmuir trough experiments (data not shown). The slow initial adsorption phase would explain the constant surface pressure in the first 10 s for OS in Figure 5.8, and was followed by a rapid increase that could be related to the rupture of OS at the air-water interface. After the oleosome

rupture, phospholipids, proteins and triacylglycerol (**TAG**) are rearranging and forming phospholipid- and TAG-rich regimes. The interfacial rearrangement phase could explain the slower increase of surface pressure after 200 s in Figure 5.8. For sunflower OS, the rupture of OS was found to depend on the size, as OS larger than 1 µm ruptured at the oil-water interface, while oleosomes with a smaller diameter (< 1 µm) remained intact[102]. The rupture of natural oil storage reservoir structures positioned at an air-water interface has also been demonstrated for low-density lipoproteins (**LDL**) from egg yolk, consisting of a lipid core surrounded by a phospholipid monolayer and membrane proteins[183,184]. The rupture of LDL and spreading of their phospholipids and membrane proteins was referred to as the main contributor to the emulsifying properties of egg yolk[185], thus suggesting a similarly prominent role of oleosome membrane components upon rupture. Mixing WPI and OS resulted in a higher surface pressure increase in the first 3,000 s than pure WPI or OS, and had a final surface pressure of 24 mN/m. A higher surface pressure increase of the mixture suggests the co-adsorption of whey proteins and OS at the air-water interface. The interface stabilising mechanisms of WPI-OS mixtures were further assessed by performing surface rheology.

In surface shear rheology, the OS-stabilised interfaces were too weak to be measured accurately, suggesting the formation of a weak interface with limited in-plane interactions at the interface, as observed for RPL and DOS. We were able to obtain reliable values for the WPI-OS-stabilised interface (see Figure A5.3 in the appendix). The interface stabilised by the WPI-OS mixture had a modulus decrease of almost one order of magnitude, and a higher tanδ in the LVE regime (0.50-0.60) compared to pure whey protein-stabilised interfaces (tanδ = 0.24). The presence of OS caused whey proteins to form weaker and less solid-like interfaces, probably due to the disruption of the whey protein lateral network by the OS adsorbed material.

A comparable effect is present in the amplitude sweep in dilatational deformations (Figure 5.8B). The moduli of OS-stabilised interfaces remained nearly constant over the entire range of amplitudes, and implied the formation of a weak and more stretchable interfacial layer. The whey protein-OS mixture-stabilised interface showed moduli close to those obtained with the pure OS, with an LVE regime up to 20% amplitude, followed by softening at higher deformations. The interactions at the interface were further studied by performing frequency sweeps, which resulted in n-values of 0.30 ± 0.01 and 0.18 ± 0.03 for OS and WPI-OS, respectively (Table 5.1). The moduli of OS-stabilised interfaces showed an increased frequency dependency, which revealed a more mobile interface compared to films obtained with WPI and the WPI-OS mixture. A more mobile interface suggests increased mass transfer between interface and bulk, as observed for DOS and RPL interfaces. The exact interfacial composition was further analysed using Lissajous plots and microstructure imaging.

Lissajous plots and interfacial microstructure imaging

The 5% deformation Lissajous plots of the OS-stabilised interface had a symmetric and narrow loop, again suggesting a dominating elastic response (Figure 5.9A).

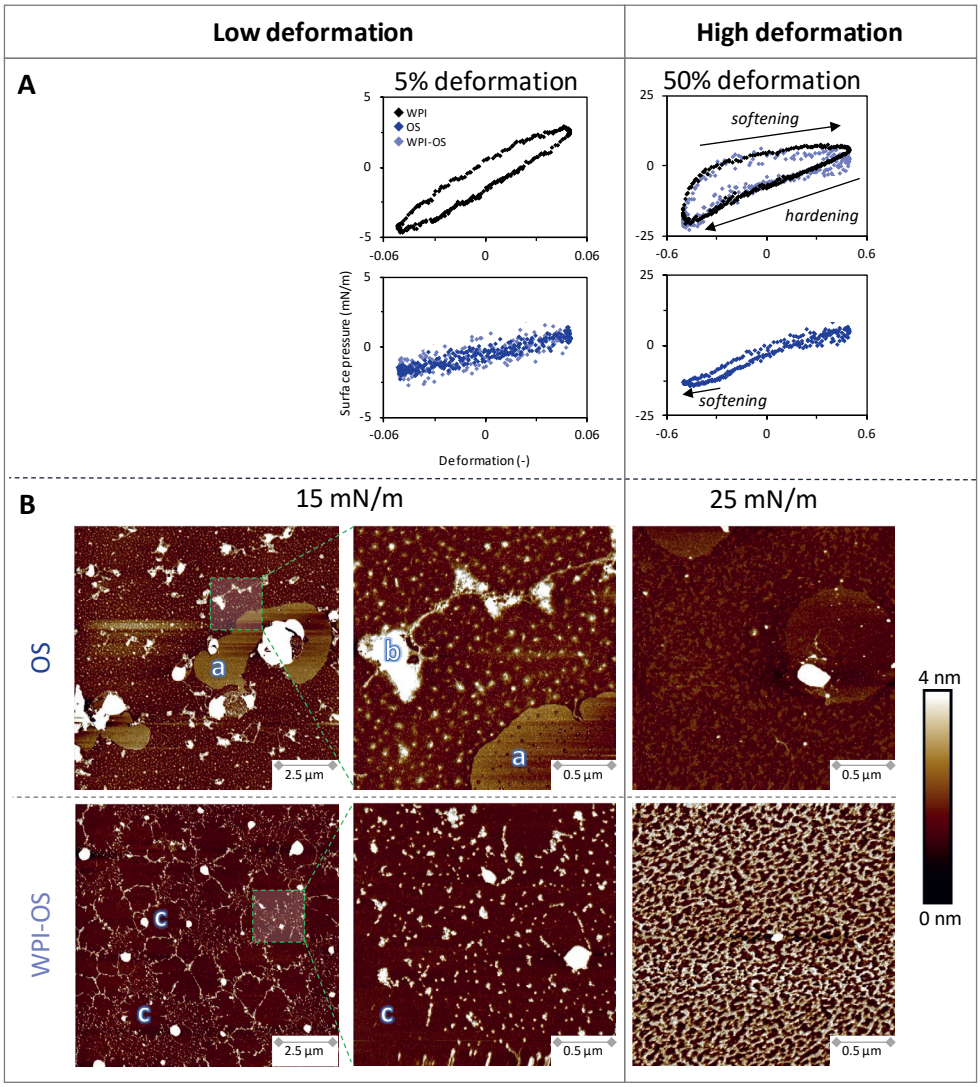

Figure 5.9. (A) Lissajous plots of surface pressure as a function of the applied deformation, obtained during amplitude sweeps of air-water interfacial films stabilised by WPI, OS, and WPI-OS mixtures. For clarity, one representative plot is shown for each sample, but comparable plots were obtained on at least three replicates. (B) AFM images of Langmuir-Blodgett films made from WPI, OS, and WPI-OS mixtures. The surface pressure indicates the conditions during film sampling.

At 50% deformation, the shape of the plot was still narrow, but it exhibited a slight strain softening in compression. The strain softening occurred in the last part of the compression cycle between -0.30 and -0.50 deformation, which is likely to occur due to the exchange of

stabiliser between bulk and interface, as the interface has a high frequency dependence and weak in-plane interactions. The AFM image of the OS-stabilised film at 15 mN/m was found to be highly complex (Figure 5.9B, left). A magnified image of the surface allows us to evaluate the films in more detail (Figure 5.9B, middle). In the images, a large flat and higher area is present (labelled as 'a'), which could be TAG-rich regions, formed after rupturing the OS at the interface. Rupture of the OS should yield fragments of the phospholipid/oleosin membrane, which could be the structures labelled as 'b'. Additionally, many smaller spherical structures between 50-200 nm are present in the film. At this point, we can only speculate about the nature of these structures that could be small OS or phospholipid-protein clusters. The AFM images are in agreement with the observations that larger oleosomes would rupture at an interface[102]. At a higher surface pressure of 25 mN/m, we observe a much flatter surface with fewer structures. Several spherical structures around 1 µm were present, which could be the TAG or phospholipid-rich regime. Overall, most of the structures observed at a surface pressure of 15 mN/m disappeared from the surface. From these images, it seems plausible that material is pushed out of the interface, either into the bulk or into a sub-layer (AFM only studies the topography of the interfacial microstructure and cannot distinguish between these two). The rheological response of OS-stabilised interfaces confirms this scenario since the interfaces were found to be weak and stretchable, and the response was significantly frequency-dependent.

The WPI-OS mixtures led to Lissajous plots similar to OS at a 5% deformation (Figure 5.9A). Interestingly, the plots started to overlap more with those obtained with WPI at larger deformation, which was most pronounced at 50% deformation, as the Lissajous plot obtained with WPI-OS coincided with the plot for WPI. Based on the adsorption isotherms, both whey proteins and OS are present at the interface (Figure 5.8), and can also be observed in the AFM image at 15 mN/m that showed a different structure than for the films made with pure WPI or OS (Figure 5.9B left). These images showed flat regions (labelled as 'c') surrounded by structures that largely resemble the protein clusters of in WPI-based films (see magnified image). The flat regions could be phospholipid- or TAG-rich regimes, formed after rupturing of the oleosomes. Larger structures between 0.2 – 1 µm were also present and were presumed to be intact oleosomes. At a high surface pressure of 25 mN/m, an overall dense structure can be observed. This confirms that the clusters observed at low deformation were whey proteins, which started to jam and interact at a larger compression. Simultaneously, the OS material (TAG or phospholipids) might be pushed out of the interface or into a lower sublayer. Such behaviour is confirmed by the Lissajous plots, where at low deformations, the OS seemed to dominate the response, and the rheological response of the WPI-OS mixture became WPI-dominated at higher deformations. To summarise, the

WPI-OS mixture formed a mixed interface with domains of phospholipid/TAG-rich regimes, surrounded by whey protein clusters.

The interface stabilising behaviour of WPI-OS and WPI-RPL mixed films showed similarities, as the lipids were pushed out upon compression, and whey proteins started to interact, as shown in the rheology, especially at large deformations of 50% deformation amplitude. It seemed that more lipids were pushed out of the WPI-OS films compared to WPI-RPL, as substantially more whey protein clusters were present on the WPI-OS film at higher compression. We attribute such behaviour to the presence of TAG-rich regions at the WPI-OS mixtures, which could be easily pushed into the bulk or below the surface upon compression, as little lateral interaction is expected between the TAGs. If TAGs are pushed into the bulk, we would expect a transition in a colloidal state, as free lipids in a polar phase would be thermodynamically unfavourable. Droplets of TAGs could be stabilised by excess interfacial stabilisers (protein or phospholipids) in the bulk. We should also keep in mind that the membrane material (phospholipids and proteins) was lower in OS compared to DOS or RPL due to the presence of TAGs, as all lipid extracts were standardised on dry matter.

5.3.5 Step-dilatation

The interfacial films stabilised by WPI and rapeseed lipids were further analysed by performing step-dilatations in the drop tensiometer by suddenly expanding the interfacial area by 10%. The sudden expanding step resulted in a relaxation response, which depends on the stiffness and mobility of the formed interfacial layer. The relaxation response was fitted using equation 5.1, which is a combination of a Kohlraus-William-Watts (**KWW**) stretch exponential and a regular exponential term. The KWW model described the relaxation behaviour of the interface, while the second term was included to decouple the ageing of the interface from the relaxation process.

$$\gamma(t) = ae^{-(t/\tau_1)^{\beta}} + be^{-t/\tau_2} + c \quad (5.1)$$

The stretch exponent β and relaxation time τ_1 are reported in Table 5.2. Other values are the characteristic time of the second term τ_1 and fitting parameters a, b, and c, and can be found in Table A5.1 in the appendix.

Table 5.2. The β and τ_1 values for interfaces prepared with WPI, OS, DOS, RPL, and mixtures of WPI-OS, WPI-DOS, WPI-RPL at 10% extension. Other variables can be found in Table S5.1 in the appendix. The averages and standard deviations are the result of at least three replicates.

	β	τ_1 (s)
WPI	0.51 ± 0.05	25.9 ± 2.6
OS	0.56 ± 0.04	11.3 ± 1.5
WPI-OS	0.61 ± 0.04	14.7 ± 4.9
DOS	0.54 ± 0.10	11.3 ± 2.8
WPI-DOS	0.64 ± 0.01	18.5 ± 1.9
RPL	0.58 ± 0.04	10.7 ± 2.1
WPI-RPL	0.60 ± 0.01	11.2 ± 3.6

The stretch exponent β was between 0.51 and 0.64 for all interfaces. A β-value below 1 suggests dynamic heterogeneity in the relaxation response, which could result from local variations in the relaxation kinetics, thus leading to a wide distribution of relaxation times. β-values between 0.52 and 0.68 have been observed for a wide range of protein-stabilised interfaces[103,108,110]. The occurrence of dynamic heterogeneity was closely related to structural heterogeneity of the interfacial microstructure, as also observed for the interfaces studied in this work.

A significant difference was observed in the relaxation times τ_1: RPL-, DOS- and OS-stabilised films showed relaxation times around 11 s, whereas films made of WPI-lipid mixtures showed relaxation times between 11.2 – 18.5 s. The whey protein-stabilised interface had the highest relaxation time of 25.9 s, which was expected as whey proteins formed stiff and solid-like interfacial layers and a low frequency-dependence (n = 0.12) in dilatational deformations (Table 5.1). The pure lipid (RPL, DOS and OS) and WPI-lipid-stabilised interface had lower relaxation times, showing a more mobile interfacial layer, as confirmed by the n-values (0.18-0.30). The more mobile interfaces were also in line with the rheological responses, as the lipid-stabilised interfaces exhibited predominantly elastic responses with weak in-plane interactions. At a step-dilatation of 10% area deformation, the lipids also affected the interfaces stabilised by the WPI-lipid mixtures, as the relaxation times were lower than pure WPI. The WPI-RPL interface had a similar relaxation time around 11 s, suggesting the earlier mentioned dominating rheological behaviour of RPL in WPI-RPL mixtures at low deformation. WPI-OS-stabilised interfaces had a slightly higher relaxation time (15 s) compared to the pure OS-stabilised interface. The slight increase of relaxation time could be due to the whey protein domains on the WPI-OS-stabilised interface that contributed to a slightly increased resistance in the relaxation response. The whey protein

clusters in WPI-OS (Figure 5.9) were also more widely distributed over the interface compared to those in the WPI-RPL system (Figure 5.5), which were segregated into domains. This would cause the whey protein clusters in the WPI-OS-stabilised films to interact at a lower compression than for the WPI-RPL films, which was also shown in the AFM images, as the WPI-OS films at a high compression (25 mN/m, Figure 5.9) showed a much denser structure with more whey protein clusters compared to the WPI-RPL system (Figure 5.5). Finally, the WPI-DOS-stabilised interfaces had a higher relaxation time of 19 s. At a higher compression at 25 mN/m, the AFM image of WPI-DOS films (Figure 5.7) showed more segregated structures than pure DOS-based films, which was also reflected in the disappearance of strain softening in compression in the 50% deformation Lissajous plot of the WPI-DOS-based film. This might imply that whey proteins contribute to the overall interaction on the WPI-DOS-stabilised interface, thereby increasing the relaxation time. In general, we demonstrated that rapeseed lipids largely dominate the interfacial properties of WPI-lipid mixtures.

5.4 Conclusion

In this work, we characterised interfacial films stabilised by whey proteins (**WPI**), rapeseed lipids, and WPI-lipid mixtures. Whey proteins formed stiff interfacial layers that behaved as viscoelastic solids, while rapeseed oleosomes (**OS**) formed weak and stretchable interfacial layers. The adsorption and proposed interface stabilisation mechanisms are shown in Figure 5.10A.

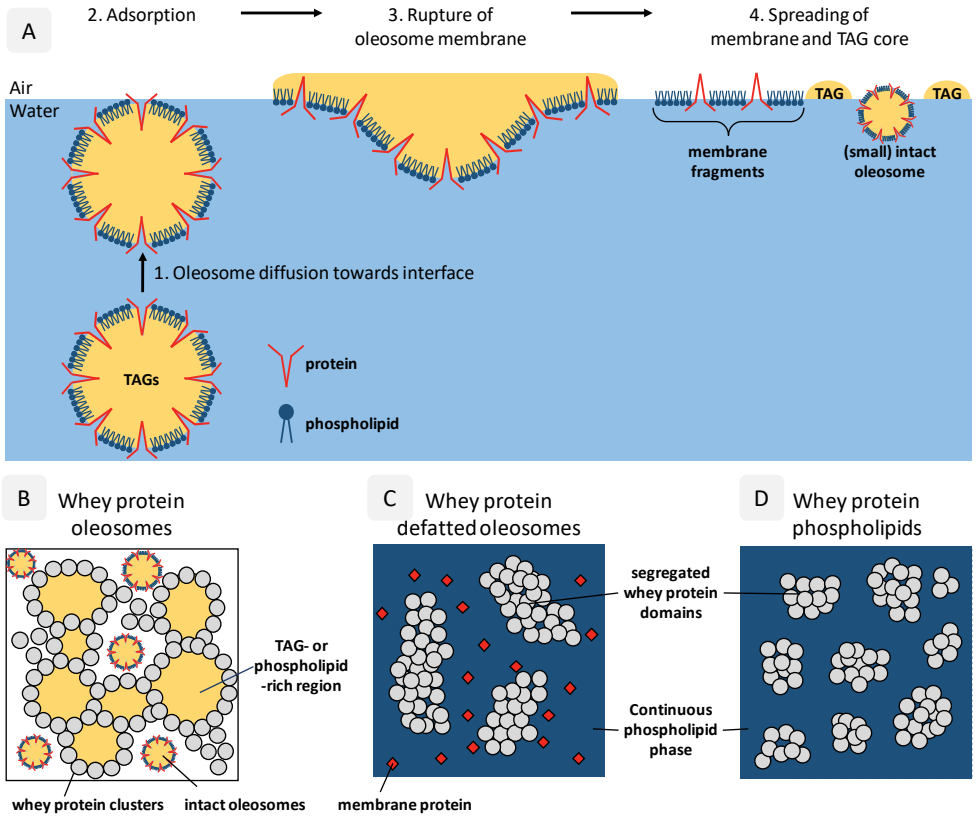

Figure 5.10. (A) Schematic representation of the adsorption and interface stabilisation mechanism of oleosomes. (B-D) Schematic representation (top view) of the interface stabilised by whey protein-lipid mixtures. The components of the illustrations are not to scale.

The OS membrane was found to rupture at the air-water interface, followed by the spreading of the membrane components (phospholipids and proteins) and the triacylglycerol (**TAG**) core. As a result, TAG- and phospholipid-rich regions were formed, as shown in AFM images of Langmuir-Blodgett films. Additionally, the smaller intact OS seemed to be present in the films. Whey proteins and lipids were also used concomitantly, and a proposed schematic representation of the mixed interfaces is shown in Figure 5.10B-D. The AFM images of films made of WPI-OS mixtures showed a mixed interface of WPI and OS, where regions of

phospholipid or TAG from OS were surrounded by clusters of whey proteins (Figure 5.10B). At low deformations in dilatational surface rheology, the OS dominated the surface response, which was visible in the Lissajous plots. At higher deformations, adsorbed whey proteins started jamming, and OS material was pushed out of the interface, which resulted in an overlapping Lissajous plot of pure WPI and WPI-OS films.

The influence of OS membrane components was also studied by incorporating a defatted oleosome (**DOS**) extract and a rapeseed phospholipid extract (**RPL**). Mixtures of WPI and DOS showed a continuous phase of phospholipids or membrane fragments, and domains of segregated whey proteins could be observed (Figure 5.10C). The continuous phase dominated the rheological response over the entire range of tested deformations. The last included sample was RPL. At low deformations, the RPL dominated the rheological response in WPI-RPL mixtures, as the microstructure of the interface was found to coincide with that of the WPI-DOS system (Figure 5.10D). A distinct difference was observed at higher deformations, where whey proteins started to dominate the rheological response, as the protein-rich regions started jamming and interacting, just like with the WPI-OS mixture. It appeared that the presence of OS membrane proteins influences the rheological properties induced by the lipids, probably by interactions with the phospholipids, thus increasing the resistance against deformation. The components in the DOS suspension were more surface-active compared to the RPL ones, and might also have contributed to the increased resistance against deformation in films prepared with WPI-DOS mixtures. From this, we conclude that whey proteins and rapeseed lipids form mixed interfaces. Processing of the lipids can largely influence the composition (protein/phenol/TAG) and the state of the lipids, and these properties determine the interface stabilising properties of the lipid extracts.

Our work provided new insights into the interface stabilising properties of OS and their membrane constituents, especially in a mixture with proteins. The OS seem to possess similar interface stabilising properties as RPL, a widely used emulsifier. Therefore, the properties of both lipid sources in a mixture with proteins were found to be remarkably similar. Therefore, OS could play a role as a more sustainable alternative for phospholipids (lecithin). These findings are an important step to further explore the potential of oleosomes as sustainable ingredients and interface stabilisers in food systems.

5.5 Appendix

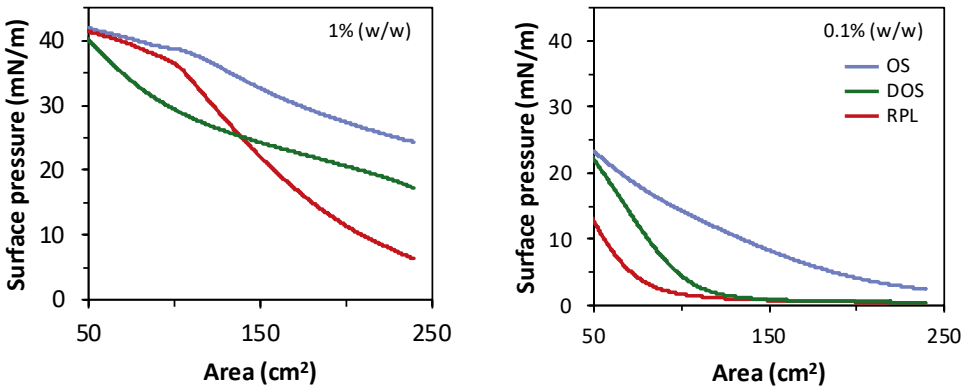

Figure A5.1. Surface pressure isotherms of Langmuir films stabilised by OS, DOS, or RPL, obtained from compression of the films. The films were produced by injecting 0.1 or 1% (w/w) sample at the bottom of the Langmuir trough, followed by 3 hrs of equilibrium time before compression.

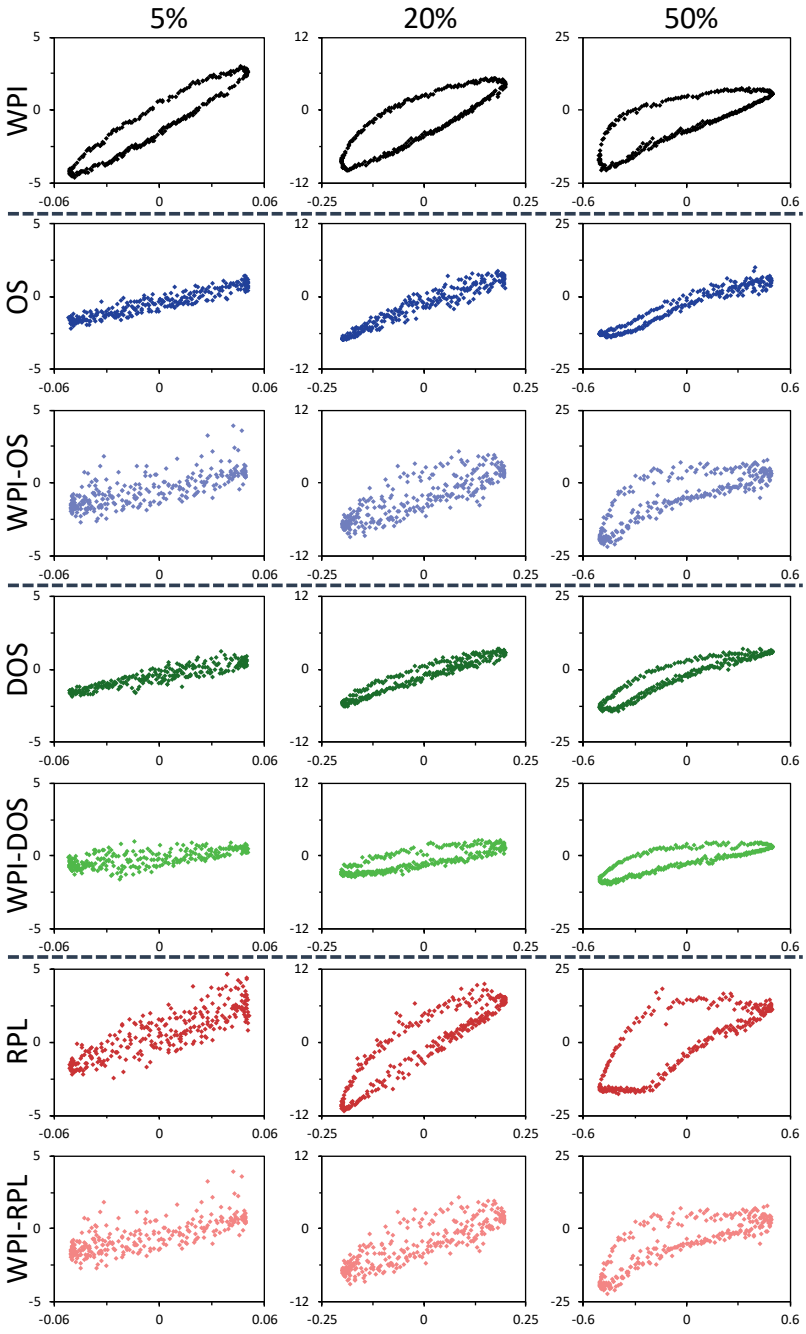

Figure A5.2. Lissajous plots are depicting surface pressure as a function of the applied deformation, obtained from amplitude sweeps of air-water interfacial films prepared with WPI, lipids, and WPI-lipid mixtures. For clarity, one representative plot is shown for each sample, but comparable plots were obtained on at least three replicates.

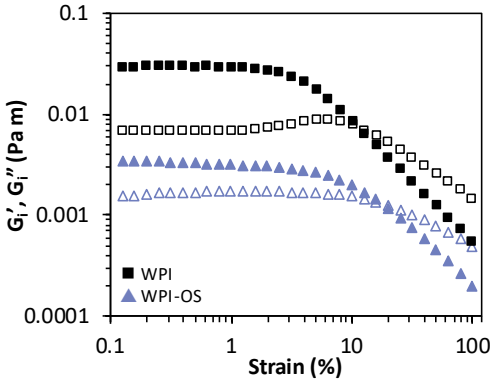

Figure A5.3. The surface shear storage (G_i') and loss (G_i'') moduli as a function of strain of interfacial films stabilised by WPI (black square) and WPI-OS mixtures (light blue triangle) in buffer (20 mM PO_4, pH 7.0). Closed symbols show the storage modulus (G_i') and open symbols show the loss modulus (G_i''). The averages and standard deviations are the result of at least three replicates.

Table A5.1. All variables of equation 5.1 for WPI, lipid, and WPI-lipid stabilised interfaces. The average and standard deviations are the result of at least three replicates.

	a	b	c	β	τ_1	τ_2
WPI	5.0 ± 0.7	2.3 ± 0.2	53.1 ± 0.4	0.51 ± 0.05	27.4 ± 6.7	638 ± 175
OS	1.2 ± 0.3	0.5 ± 0.1	45.0 ± 0.9	0.56 ± 0.04	11.3 ± 1.5	1002 ± 215
DOS	1.4 ± 0.2	0.4 ± 0.1	36.5 ± 0.5	0.54 ± 0.06	11.3 ± 2.8	693 ± 327
RPL	3.8 ± 0.4	0.7 ± 0.1	46.6 ± 0.1	0.58 ± 0.04	10.7 ± 2.1	392 ± 49
WPI-OS	2.1 ± 0.4	0.5 ± 0.1	45.9 ± 0.2	0.61 ± 0.04	14.7 ± 4.9	399 ± 75
WPI-DOS	2.0 ± 0.2	0.9 ± 0.2	47.5 ± 4.2	0.64 ± 0.03	18.5 ± 1.9	415 ± 254
WPI-RPL	3.5 ± 0.6	0.9 ± 0.2	48.9 ± 0.4	0.56 ± 0.02	11.2 ± 3.6	410 ± 54

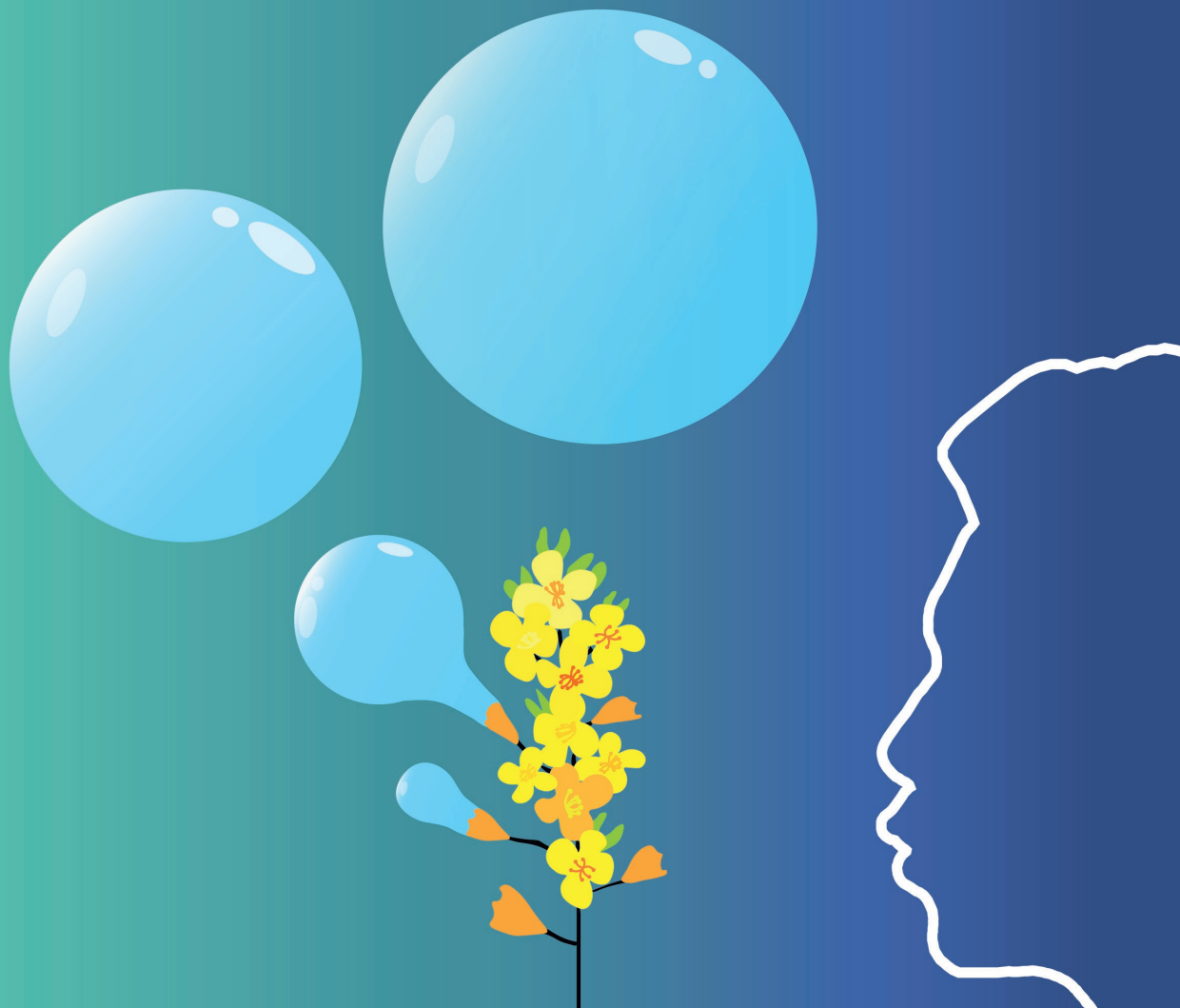

Chapter 6

Interfacial and foaming properties of rapeseed protein – oleosome mixtures

Submitted as:
Yang, J., Berton-Carabin, C. C., Nikiforidis, C. V., van der Linden, E., & Sagis, L. M. C.
Air water interfaces and foams stabilised by rapeseed protein and oleosome mixtures.

Abstract

There is an increasing interest to apply oleosomes (plant oil storage organelles) as natural oil droplets in food systems. Lipids are usually known to be detrimental for protein-stabilised foams due to the weakening of interactions between adsorbed proteins, or by forming oil bridges between two protein surfaces. Both mechanisms can lead to film rupture, and thereby destabilise protein-stabilised foams. Little is known about the influence of oleosomes on protein-stabilised interfaces and foams. Therefore, these properties were studied for rapeseed protein–rapeseed oleosome mixtures at various protein concentrations and ratios. At 0.1 and 0.2% (w/w) protein content, oleosomes were found to co-adsorb with proteins at the interface, followed by rupture of oleosomes and release of triacylglycerols and phospholipids. This led to weaker in-plane interactions between adsorbed proteins. As a result, the foamability and foam stability of protein-oleosome systems were substantially lower compared to systems made with pure proteins. At 0.5 and 1.0% (w/w) protein content, the rapeseed proteins were found to dominate the interfacial properties. At such high concentrations, the proteins formed a dense solid-like layer, which prevented the oleosomes from co-adsorbing at the interface. Also, in foam systems at high protein concentrations, the proteins seemed to outcompete the oleosomes for the interface, leading to higher foam stability. Here, we have demonstrated that the detrimental influence of oleosomes on protein-stabilised interfaces and foams can be controlled by varying the amount of oleosomes and rapeseed proteins in the mixture, which is a promising outcome to further utilise oleosomes in aerated food systems.

6.1 Introduction

Oilseeds are widely cultivated for oil production, and are essential in a healthy human diet[186,187]. Examples of such plant crops are soybean, sunflower seed and rapeseed. Their oil is generally extracted by pressing, followed by an organic solvent-based extraction step[188,189]. Such processing disrupts the naturally occurring oil reservoirs in plants, known as oleosomes, oil bodies, or lipid droplets[22,102,190]. Oleosomes are natural oil droplets (diameter 0.2 – 10.0 µm) of triacylglycerols (**TAG**), which are surrounded by a protective monolayer of phospholipids with anchored membrane proteins, mostly oleosins (Figure 6.1)[22,23,165,166]. Oleosomes can be extracted without physical disruption by aqueous mild purification methods[175], and possess exceptional high chemical and physical stability against lipid oxidation and droplet coalescence[25–28].

Despite the exceptional properties of oleosomes, the food industry, instead of using them as such, creates "artificial" oil droplets by emulsifying the oleosome-derived oil with emulsifiers. If the use of intact oleosomes for food applications could be facilitated, the processing steps of oil extraction and oil droplet formation can be avoided. Therefore, oleosomes can play an important role in the sustainable food transition, in applications such as natural emulsions in liquid/solid foods, or even as a functional component in oil structuring[22,169,171].

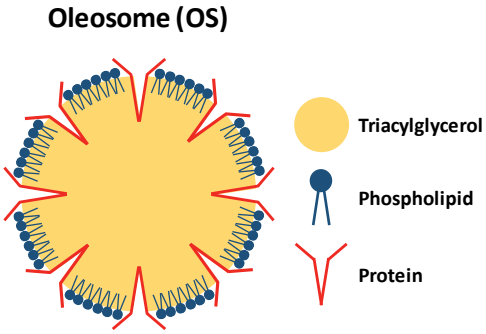

Figure 6.1. Schematic overview of the oleosome structure. The components in the illustration are not to scale.

The aforementioned food applications are obvious for oleosomes, but oils/lipids could also be applied as a functional ingredient in other systems, such as foams, which is the focus of this work. Foams are air bubbles entrapped in continuous liquid or solid matrices, such as milk foams and ice cream[191]. In food foam systems, the air-water interface is often stabilised by proteins that form stiff and viscoelastic solid-like interfacial layers[47,152], which is an important attribute in forming stable foams[48,174,192]. Polar lipids, such as phospholipids, can compete with proteins for the interface, forming mixed interfaces, or even displace the

proteins from the interface[61,106,116]. As a result, the proteins are impaired in the formation of strong interfacial layers, which may lead to poor foaming properties[68]. Also, the TAGs in the oleosome core can act as anti-foaming agents in the thin films by bridging two air bubbles, and thereby inducing coalescence of the air bubbles[71,72].

However, the interfacial behaviour of oleosomes is different from that of free lipids, as both phospholipids and TAGs are enclosed in the colloidal structure of the oleosomes. For soybean oleosomes, a slow initial adsorption phase was demonstrated in a Langmuir trough, due to the relatively slow diffusion towards the air-water interface. After approaching the air-water interface, oleosomes were able to adsorb at the interface, followed by rupture of the phospholipid/protein membrane[62,70]. The different components started to phase separate into TAG-rich and membrane-rich regions, which we also demonstrated in our previous work by studying the topography of the Langmuir-Blodgett films[193]. In our previous work, oleosome-stabilised air-water interfaces were weaker and more mobile compared to protein-stabilised interfaces, due to weak in-plane interactions. Desorption and adsorption of interfacial material were observed upon compression and expansion of the interfacial area. Mixing of whey proteins and oleosomes formed a mixed interface, where whey proteins surrounded the TAG-rich regions. When oleosomes were present, they dominated the rheological response of the mixed interfaces.

The influence of oleosomes on the protein interfacial layer was not clearly observed in the foaming properties of mildly-purified rapeseed protein extracts, which contained about 8% (w/w) oleosomes[152]. A defatted rapeseed protein extract had similar foaming properties as a non-defatted protein extract, thus indicating that oleosomes at this concentration did not hamper protein foaming properties. However, the previous studies were limited to one protein-to-oleosome ratio, and were performed at relatively low bulk concentrations (<0.2% w/w) compared to real food systems. At different absolute amounts of proteins and different protein-oleosome ratios, it is not yet clear which component would dominate the functional properties of the total mixture.

Therefore, we aim to investigate rapeseed protein and oleosome mixtures for their interfacial and foaming properties at various bulk concentrations and protein-to-oleosome ratios. Oleosomes and proteins were extracted from rapeseeds, and systematically mixed. The rapeseed protein-oleosome mixtures were studied by surface dilatational rheology, and microstructure imaging by performing atomic force microscopy on Langmuir-Blodgett films. Finally, the mixtures were characterised for their foaming properties. A comprehensive study on the effect of oleosomes on protein-stabilised foams provides new insights on the necessity of purifying proteins from oleosomes, and further expands the possibilities for using oleosomes as a sustainable ingredient in foods.

6.2 Experimental section

6.2.1 Materials

Untreated Alizze rapeseeds were purchased from a local seed producer. All chemicals (Sigma-Aldrich, USA) were used as received. Ultrapure water (MilliQ Purelab Ultra, Germany) was used in all experiments.

6.2.2 Sample preparation

Rapeseed protein extraction

Rapeseed protein concentrate (**RPC**) was prepared with the method of Ntone et al.[43]. Dehulled rapeseed kernels were soaked for 4 hrs at pH 9.0 in a rapeseed-to-water ratio of 1:8 (w:w). Afterwards, the mixture was blended for 2 min at max speed in a kitchen blender (Waring Commercial, 400 W, USA) to obtain a rapeseed slurry, and the solids were removed using a twin-screw press. The pH of the liquid extract was re-adjusted to 9.0 after the completion of each previously mentioned step. The supernatant was centrifuged for 30 min at 10,000xg (4 °C), which resulted in a three-layer system: a cream layer on top, a pellet with solids, and a middle layer containing the soluble proteins and other solutes. The middle layer was recovered and diafiltrated over a 5-kDa membrane to remove minerals, sugars and free phenols. The diafiltrated sample was freeze-dried, which yielded a mildly purified RPC. The protein extract was further purified to obtain the soluble fraction at the studied conditions by dispersing 10% (w/w) mildly purified RPC in 20 mM sodium phosphate buffer (pH 7.0). The dispersion was adjusted to pH 7.0 and stirred overnight at 4 °C. Afterwards, the dispersion was centrifuged twice for 30 min at 16,000xg (20 °C) and filtered over a 0.22 µm syringe filter. The supernatant was freeze-dried for further analysis and labelled as rapeseed protein concentrate (RPC).

Oleosomes extraction

A rapeseed slurry was produced, as mentioned in the previous paragraph. The pH of the slurry was adjusted to 9.0, and the slurry was passed through a cheesecloth to remove the solids. The pH was adjusted once more to 9.0, and the sample was centrifuged for 30 min at 10,000xg (4 °C). The cream layer was resuspended in ultrapure water at a 1:5 (w/v) ratio, stirred for 15 min and centrifuged for 30 min at 10,000xg (4 °C). A second re-dispersion step was performed with 20 mM sodium phosphate buffer (pH 7.0), followed by another centrifugation step. The final cream layer containing oleosomes was recovered and diluted with buffer based on dry matter content. Large aggregated clusters of oleosomes were broken up by a high-speed mixing step of 30 s at 5,000 rpm with a T25 Ultra-turrax (IKA, Germany). A preservative (sodium azide) was added to the oleosome extract (**OS**), and the sample was used in experiments for a maximum of 5 days while stored at 4 °C.

Compositional analysis

The protein content was measured in a Flash EA 1112 Series Dumas (Interscience, The Netherlands). The nitrogen content of the samples was obtained, which was converted into a protein content using a conversion factor of 5.7[100]. These measurements were performed in triplicate. The oil content was determined by drying the samples overnight at 60 °C, followed by solvent (petroleum ether) extraction for 6 hrs in a Soxhlet. The oil content was calculated by weighing the initial sample and the oil in the collection flasks. The measurements were performed in duplicate.

Dissolving samples

RPC was dissolved in 20 mM sodium phosphate buffer (pH 7.0) at protein concentrations ranging from 0.1 to 2% (w/w), and the sample was stirred for 4 hrs at room temperature. The OS were diluted in the same buffer to concentrations ranging from 0.002 to 2% (w/w). RPC-OS mixtures were prepared by mixing pure RPC and OS in a 1:1 (v:v) ratio.

6.2.3 Determination of adsorption behaviour and surface dilatational properties

The air-water interfacial properties were investigated using drop tensiometers. A profile analysis tensiometer PAT-1M (Sinterface Technologies, Germany) was used to perform time and frequency sweeps. A hanging droplet with an area of 20 mm^2 was created at the tip of a needle, and the shape of the droplet was analysed and fitted with the Young-Laplace equation to calculate the surface tension. The droplet was always equilibrated for 3 hrs before performing any deformation of the droplet area. Frequency sweeps were performed by increasing the oscillatory deformation frequency from 0.002 – 0.1 Hz with a fixed amplitude of 3%. An automated drop tensiometer (ADT, Teclis, France) was used to perform amplitude sweeps, and the ADT was operated similarly to the PAT-1M. A major difference was the droplet size, which had an area of 15 mm^2 in the ADT. The droplet was again subjected to 3 hrs of waiting time before performing the amplitude sweep, where the amplitude was increased from 2 to 50% at a fixed frequency of 0.02 Hz. All measurements were performed at least in triplicates at 20 °C. The amplitude sweep was further analysed by plotting Lissajous plots of the surface pressure ($\Pi = \gamma - \gamma_0$) over the deformation ($(A-A_0)/A_0$). Here, γ and A are the surface tension and area of the deformed interface, γ_0 and A_0 are the surface tension and area of the non-deformed interface. Lissajous plots were made from the middle three oscillations of each amplitude cycle.

6.2.4 Preparation of Langmuir-Blodgett films

Langmuir-Blodgett films of RPC-OS mixtures

A Langmuir trough (KSV NIMA/Biolin Scientific Oy, Finland) was used to produce Langmuir-Blodgett (**LB**) films of interfacial films stabilised by RPC and RPC-OS mixtures. Samples with

RPC contained 0.1% (w/w) protein, and the protein-oleosome mixtures had RPC concentrations varying from 0.05 to 0.1% (w/w) and OS concentrations varying from 0.001 to 0.05% (w/w). The Langmuir trough was filled with 20 mM phosphate buffer (pH 7.0), and 200 µL of sample solution was injected at the bottom of the trough with a gas-tight syringe. A 3 hr waiting step was necessary to allow adsorption of the surface-active material at the interface, and the surface pressure was measured with a Wilhelmy plate (platinum, perimeter 20 mm, height 10 mm). Afterwards, the interfacial film was compressed with Teflon barriers moving at a speed of 5 mm/min to a target surface pressure of 21 mN/m. The surface pressure was kept constant, while the interfacial layer was deposited on a freshly cleaved mica sheet (Highest Grade V1 Mica, Ted Pella, USA) at a withdrawal speed of 1 mm/min. All films were produced in duplicate and dried in a desiccator.

Langmuir-Blodgett films to study potential displacement of RPC-proteins by OS

The Langmuir trough was similarly prepared and operated as described in the previous paragraph. A major difference is the separate introduction of RPC and OS. First, 200 µL of 0.01 to 0.1% (protein w/w) RPC solutions were spread on top at the surface using a gas-tight syringe. The interfacial layer was equilibrated for 30 min, and afterwards, the layer was compressed until a target surface pressure of 5, 10, 15, 20, or 25 mN/m. The target surface pressure was maintained by constantly compressing the interface, until the surface pressure was constant without further compression. Afterwards, 100 µL of OS extract was injected at the bottom of the trough, i.e., below the RPC-stabilised film. The concentration was determined by the surface area of the Langmuir film, which was varied for each replicate, as 0.001% of OS/100 µL was injected per cm^2 of surface area. Oleosomes were found to diffuse and adsorb at the interface after roughly 1 hr. Therefore, an adsorption time of 1.5 hrs was applied after infusion of the OS in the subphase. Finally, Langmuir-Blodgett films were produced, as described in the previous section. All films were prepared in duplicate and dried in a desiccator before analysis.

6.2.5 Determination of interfacial microstructure by AFM

The topography of the LB films was analysed with atomic force microscopy (**AFM**, MultiMode 8-HR, Bruker, USA) in tapping mode using a Scanasyst-air model non-conductive pyramidal silicon nitride probe (Bruker, USA) with a normal spring constant of 0.40 N/m and a lateral scan frequency of 0.977 Hz. The films were scanned over an area of 2 x 2 μm^2 with a lateral resolution of 512 x 512 $pixels^2$. At least two locations were scanned on the films to ensure good representativeness.

6.2.6 Determination of foaming properties

The foaming ability of the samples was analysed by whipping using an aerolatte froth (Aerolatte, UK) connected to an overhead stirrer. Aliquots of 15 mL solution were whipped

for 2 min at 2,000 rpm in plastic tubes (ø = 3.4 cm), and the top and the bottom of the foam were directly marked on the tube. The difference was measured using a ruler, and a foam volume was calculated with the tube diameter. From the foam volume, the overrun (%) was calculated by dividing the foam volume (mL) by the liquid volume (15 mL) times 100. The foam stability of the samples was analysed in a Foam scan (Teclis, France). Foams with a volume of 400 mL were produced from 40 mL of sample in a glass cylinder (ø = 6 cm) by sparing nitrogen gas through a metal frit (27 µm pore size, 100 µm distance between centres of pores, square lattice) at a gas flow rate of 400 mL/min. A camera monitored the foam volume until half of the foam volume decayed, and this time point is also known as the foam volume half-life time. The machine was equipped with an SLR lens to record detailed images of air bubbles, which were analysed using DIPlip and DIPimage image analysis software (TU Delft, the Netherlands) to quantify the average air bubble size. All experiments were performed at least in triplicate at room temperature.

6.3 Results and discussion

6.3.1 Protein and oleosome extraction

Rapeseed proteins, napin and cruciferin, were extracted with a mild-purification method to obtain a rapeseed protein concentrate (**RPC**) that retained the native protein structure and had a protein content of 77.8 ± 1.9% (w/w)[43,152]. The protein purity increased by roughly 6% compared to a previously produced RPC in our earlier work[152], as a filtration step with a 0.22 µm cut-off was added in this work. The filtration step (partly) removed oleosome (**OS**) flocculates between 2 and 300 µm. The obtained OS extract contained 88.5 ± 3.8 % (w/w) oil and 7.2 ± 0.3% (w/w) protein and had a droplet size distribution between 0.2 – 20.0 µm with a $d_{3,2}$ of 0.8 µm[193]. The RPC and OS were mixed to obtain rapeseed protein concentrations of 0.1, 0.2, 0.5, and 1.0 % (w/w), and OS was mixed to obtain protein-to-OS (w/w) ratios of 100:1, 10:1, and 1:1.

6.3.2 Interfacial properties of rapeseed protein – oleosome mixtures

Adsorption behaviour

The adsorption behaviour of RPC, OS, and RPC-OS mixtures at an air-water interface was studied (Figure 6.2), and the protein bulk concentration of RPC was varied between 0.1 – 1.0% (w/w), while OS was added to obtain a 10:1 RPC-to-OS ratio. This ratio was chosen, as a comparable ratio was found in the mildly-derived RPC in our previous work[152].

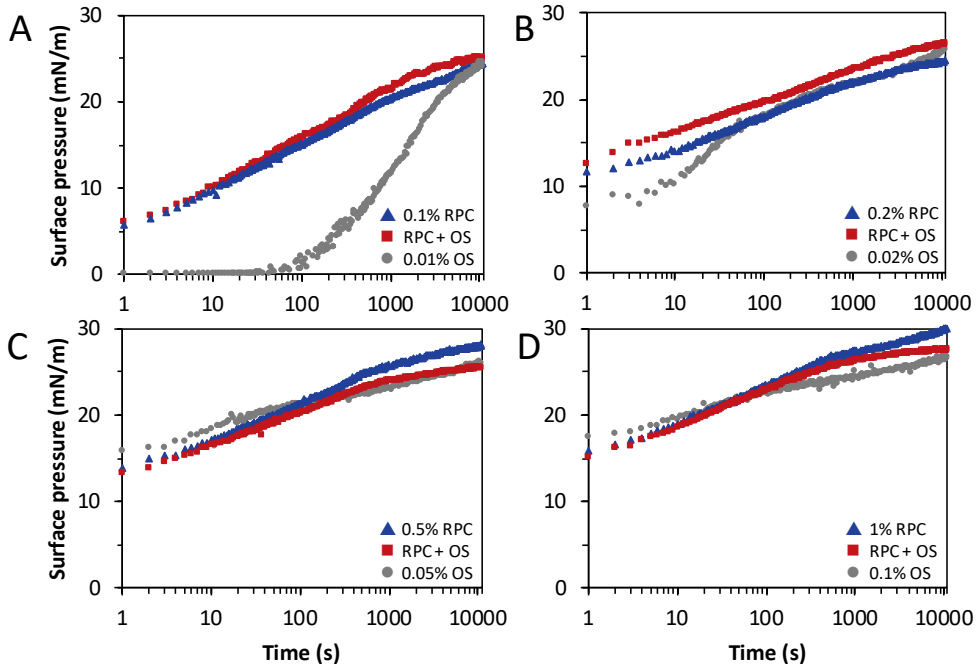

Figure 6.2. Surface pressure as a function of time of interfacial films stabilised by RPC (blue triangles), OS (grey circles), and RPC-OS mixtures (red squares) in buffer (20 mM PO_4, pH 7.0). The concentrations of RPC and OS are shown in the legend of each graph, and these concentrations are also applied in the RPC-OS mixtures. The surface pressure isotherms represent an average of at least three replicates. The standard deviation was below 5%.

Pure RPC at all concentrations led to an immediate increase of surface pressure with values between 5 – 15 mN/m at 1 s, followed by a continuous increase to values up to 30 mN/m after 3 hrs of adsorption. The OS had a different behaviour at lower concentrations, such as 0.01% (w/w) OS (Figure 6.2A). For this sample, a lag time was observed in the first 50 s, showing that the amount of stabiliser on the interface is insufficient to increase the surface pressure. Afterwards, the surface pressure increased rapidly to similar values as with the 0.1% (w/w) RPC after 3 hrs. The adsorption behaviour of OS is different from that of rapeseed proteins, as OS are larger structures, and thus have a lower diffusion rate towards the interface. The OS can rupture after adsorption, followed by spreading of the membrane (made of phospholipids and proteins) and triacylglycerol (**TAG**) core over the interface[70]. These phenomena are shown in the adsorption isotherm of 0.02% (w/w) OS, where a slow adsorption phase in the first 10 s was followed by a rapid increase up to 70 s due to OS adsorption. After 70 s, the slope decreased due to OS rupture and rearrangements of the components at the interface. At higher concentrations of 0.05 and 0.10% (w/w) OS (Figure 6.2C & D), OS adsorbed at a higher rate, comparable to that observed with pure RPC. The findings at higher OS concentrations should be interpreted with caution, as impurities in the

OS extract, such as storage proteins and phenols, could significantly contribute to the adsorption behaviour.

Mixing RPC and OS showed two types of behaviour, and the first type is present in Figure 6.2A & B. In Figure 6.2A, the RPC-OS (0.10% RPC – 0.01% w/w OS) adsorption kinetics coincided with that of the pure RPC up to 50 s, indicating adsorption of mainly rapeseed proteins, which is expected, as pure OS showed a lag phase in this period. After 50 s, the slope measured for the RPC-OS mixture was higher than pure RPC, suggesting a contribution of OS, as the pure OS curve also showed an increase of surface pressure from this time point. Such co-adsorption is also found for a higher concentration (0.20% RPC – 0.02% w/w OS), as the mixture led to a higher surface pressure than with pure RPC or OS. The surface pressure kinetics at higher concentrations (0.5% RPC – 0.05% OS & 1% RPC – 0.1% w/w OS) showed a distinctly different behaviour, as the curve of the mixtures first followed the pure RPC curve in the initial ±300 s. Afterwards, the slope of the mixtures was lower compared to pure RPC. At such high concentrations, the RPC and OS seemed to start competing for the interfacial area, perhaps leading to a partial displacement of RPC. An alternative explanation could be that at these higher concentrations, the components segregate after adsorption (2D phase-separation), leading to a heterogeneous interfacial microstructure. The structure and mechanical properties of the interfacial film were further assessed by performing rheological experiments.

Surface dilatational rheology

The surface dilatational moduli of interfacial films stabilised by RPC and RPC-OS mixtures were obtained from an amplitude sweep using drop tensiometry (Figure 6.3). At all RPC concentrations (0.1 – 1% w/w), rapeseed protein-stabilised interfacial films showed a decline of storage modulus (***E_d'***) from 42 – 60 mN/m (2% deformation) to 22 – 24 mN/m (30% deformation) with increasing amplitude, indicating the presence of a nonlinear viscoelastic (**NLVE**) regime. Amplitude-dependent moduli suggest an increased disruption of the interfacial structure at higher deformations. The amplitude-dependence of E_d' in combination with a substantially lower loss modulus (***E_d''***) indicates the formation of a viscoelastic solid-like layer. Formation of such interfaces was previously demonstrated for rapeseed proteins at both air-water and oil-water interfaces[43,152]. In this previous work, we also observed a decrease of surface moduli upon increasing protein bulk concentration, which we attributed to the presence of non-proteinaceous components, such as phenols and oleosomes. A similar trend was also found in this work, where the E_d' decreased with higher RPC concentrations. Interfacial films stabilised by OS had a distinctly different rheological behaviour, as the E_d' were low and nearly independent of the applied deformation. OS-stabilised interfaces were more mobile with an increased mass exchange between bulk and

interface upon deformation[193]. This behaviour was associated with the low in-plane interactions between the interfacial stabiliser at an OS-stabilised interface.

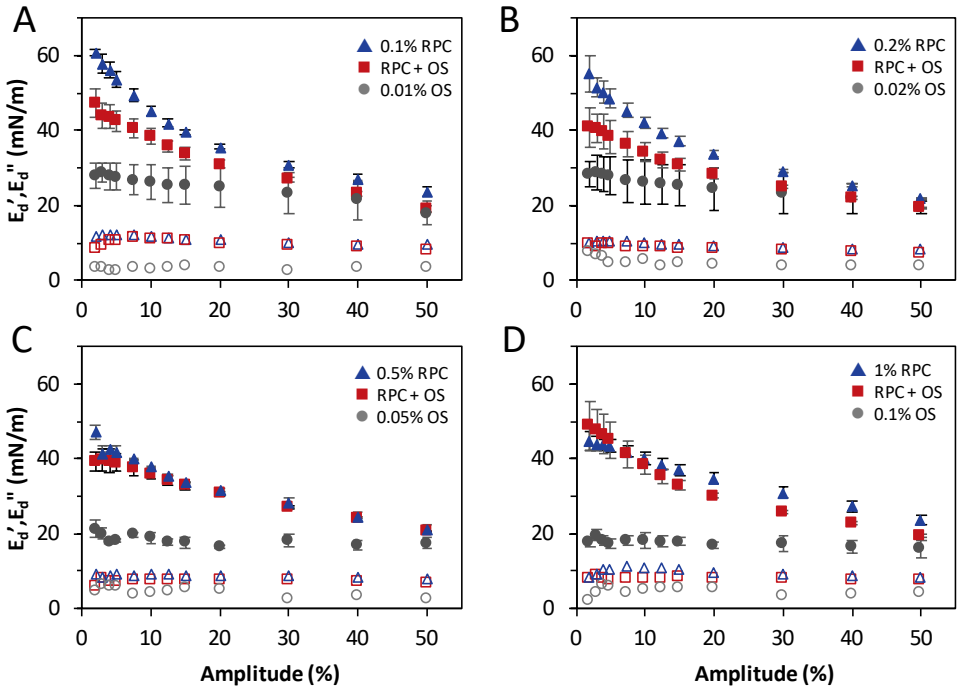

Figure 6.3. The surface dilatational storage (E_d') and loss (E_d'') moduli as a function of the deformation amplitude for interfacial films stabilised by RPC (blue triangles), OS (grey circles), and RPC-OS mixtures (red squares) in buffer (20 mM PO_4, pH 7.0). The concentrations of RPC and OS are shown in the legend of each graph, and these concentrations are also present in the RPC-OS mixtures. The closed symbols depict the storage modulus (E_d'), and open symbols depict the loss modulus (E_d''). The averages and standard deviations are the result of at least three replicates.

The mixtures led to different behaviour depending on the total protein content. At a fixed protein content of 0.1 and 0.2% (w/w) (Figure 6.3A & B), the RPC-OS-stabilised interfaces had lower E_d' than pure RPC-stabilised ones. The moduli decreased due to the presence of OS in the bulk, and most likely at the air-water interface. A different influence of the OS was observed at higher concentrations (0.5 and 1% w/w) (Figure 6.3C & D), as the moduli of interfaces stabilised by RPC-OS mixtures coincided remarkably with those of pure RPC-stabilised interfaces. This implies a less detrimental effect of OS on the rheological properties of the RPC-stabilised interface at higher protein concentrations, at a constant RPC-to-OS ratio. The interactions between the interfacial stabilisers were further examined by constructing Lissajous plots.

Lissajous plots

The dilatational surface moduli obtained from amplitude sweeps are calculated from the intensity and phase shift of the first harmonic of the Fourier transform of the surface stress signal. Only incorporating the first harmonic results in neglecting the contributions of higher-order harmonics present in the surface stress signal in the NLVE regime, caused by disruptions of the interfacial microstructure at large deformations. The contribution of higher harmonics was previously analysed by constructing Lissajous plots, where the surface stress is plotted against applied deformation[58]. Previously, Lissajous plots were demonstrated as a useful tool to analyse the contribution of higher-order harmonics that are generated at large deformations[103,117,152].

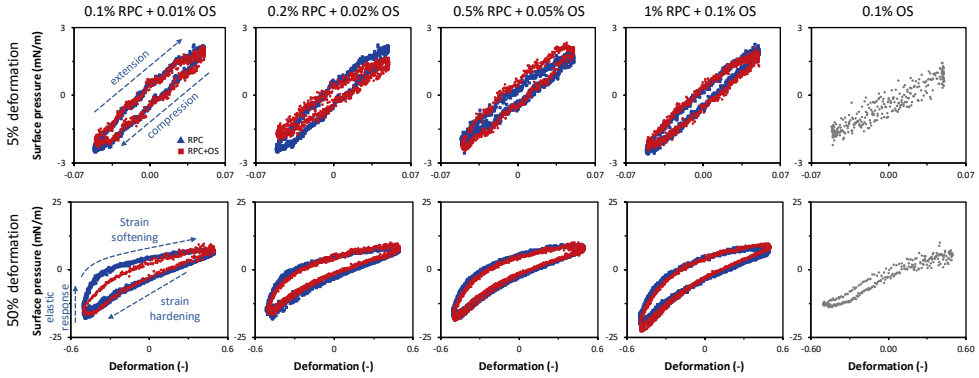

Figure 6.4. Lissajous plots of surface pressure as a function of the applied deformation, obtained from amplitude sweeps of air-water interfacial films stabilised by RPC (blue triangles), OS (grey circles), and RPC-OS mixtures (red squares). For clarity, one representative plot is shown for each sample, but comparable plots were obtained on at least three replicates.

The results of the amplitude sweep were transformed into Lissajous plots and are depicted in Figure 6.4. All Lissajous plots at 5% deformation amplitude showed narrow and symmetric ellipses, suggesting an interfacial layer where the elastic component dominated the stress response. By increasing the deformation amplitude to 50%, the Lissajous plots became asymmetric due to disruption of the interfacial microstructure. At such large deformations, higher-order harmonics are generated that are well illustrated by the shape of Lissajous plots. Several rheological phenomena are present in the plots and are highlighted in the 50% deformation plot of a 0.1% RPC-stabilised interface. At the start of the extension cycle (at -0.50 deformation, bottom-left corner), we observed a steep increase in surface pressure (nearly vertical) as a result of a predominantly elastic response. Afterwards, the steep increase was followed by a phase with a decreasing slope, showing a gradual (intra-cycle) strain softening of the interfacial microstructure upon further extension of the interfacial area. Here, the elastic component started to diminish, and the viscous component started dominating the response, implying that the interfacial microstructure started flowing.

A distinct behaviour can be examined in compression of the interface, as the surface pressure increased steeply to a higher maximum surface pressure (-18 mN/m) compared to the value in extension (+6 mN/m), which is known as intra-cycle strain hardening. Strain hardening was previously attributed to the concentration of adsorbed proteins upon compression. As a result, dense protein clusters would form and start jamming[103]. The depicted rheological behaviour suggests the formation of a viscoelastic solid-like layer by RPC, probably due to strong in-plane interactions between rapeseed proteins at the air-water interface. Interestingly, the initial elastic response became less evident at higher protein concentrations (at 50% deformation), and the plots also became slightly narrower. This would imply slightly weakened in-plane interactions between proteins at such the higher protein concentrations (≥0.5% w/w).

The OS-stabilised interface showed a substantially narrower Lissajous plot at 50% deformation compared to RPC. The plot also revealed a slight strain softening in compression that we previously related to the pushing out of interface stabiliser into the bulk, due to weak in-plane interactions between molecules at the OS-stabilised interface. In previous work, rupture of OS was demonstrated at the air-water interface, leading to a heterogeneous interface with TAG-rich regions and membrane fragments. Especially phospholipids and TAGs are known to largely hamper interactions between other stabilisers at the interface, thus weakening the interfacial layer, which was demonstrated for protein interfaces[68,72,114,194].

The Lissajous plot showing 50% deformation of an interfacial film stabilised by a 0.1% (w/w) RPC – 0.01% (w/w) OS mixture was considerably narrower compared to the plot for pure RPC at 0.1% (w/w), implying the formation of a weaker layer due to impaired in-plane interactions among adsorbed proteins. Such changes of rheological behaviour in the presence of OS imply the interference of phospholipids and TAG of OS (after rupture) on the layer formation of rapeseed proteins, which by itself formed stiff and viscoelastic solid-like layers. Similar behaviour was observed in whey protein-OS mixtures, as the OS weakened the interactions between whey proteins by forming large phospholipid/TAG-rich regions at the interface, leading to 2D phase separation of proteins and lipids at the interface[193]. Also, pure phospholipids and surfactants are known to form concentrated and laterally segregated regions at the interface, thereby reducing the protein interactions at the interface[61,63,66].

At higher protein concentrations, OS had a limited effect on the rheological properties of the RPC-OS-stabilised interface. From 0.5% (w/w) RPC onwards, the OS-protein mixtures led to nearly overlapping Lissajous plots compared to pure RPC. The detrimental effect of OS on a protein-stabilised interface is concentration-dependent (at a fixed RPC-to-OS ratio), and might be related to the findings in the adsorption behaviour (Figure 6.2). At lower

protein concentrations of 0.1 and 0.2% (w/w), we demonstrated co-adsorption of both rapeseed proteins and OS, whereas the adsorption of rapeseed proteins seemed to be more predominant at higher protein concentrations of 0.5 and 1.0% (w/w). A mixed interface after co-adsorption (0.1 and 0.2% RPC) could increase the weakening effect of OS on the rapeseed proteins' connectivity in the interfacial layer, whereas an interface with more RPC (0.5 and 1.0% RPC), thus less OS, would result in less decrease in moduli. To summarise, OS can negatively influence the in-plane interactions of adsorbed rapeseed proteins, leading to weaker interfacial layers. This behaviour is concentration-dependent, as RPC is more dominant at higher concentrations (>0.2% w/w).

6.3.3 Interfacial microstructure

Imaging the interfacial microstructure can contribute to a better understanding of the rheological properties of RPC-OS mixture-stabilised interfacial layers. Interfacial films were produced in a Langmuir trough by injecting RPC-OS mixtures with various ratios at the bottom of the trough and allowing them to diffuse towards and adsorb at the interface (schematic overview in Figure 6.5). Langmuir-Blodgett (**LB**) films were produced, and the topography of the dried films was analysed using atomic force microscopy (**AFM**) (Figure 6.5). There is a narrow concentration range of RPC and OS that could be injected into the trough to induce co-adsorption. As a result, a fixed ratio with various protein concentrations could not be studied, but the RPC-to-OS ratio and the total amount of stabiliser were varied.

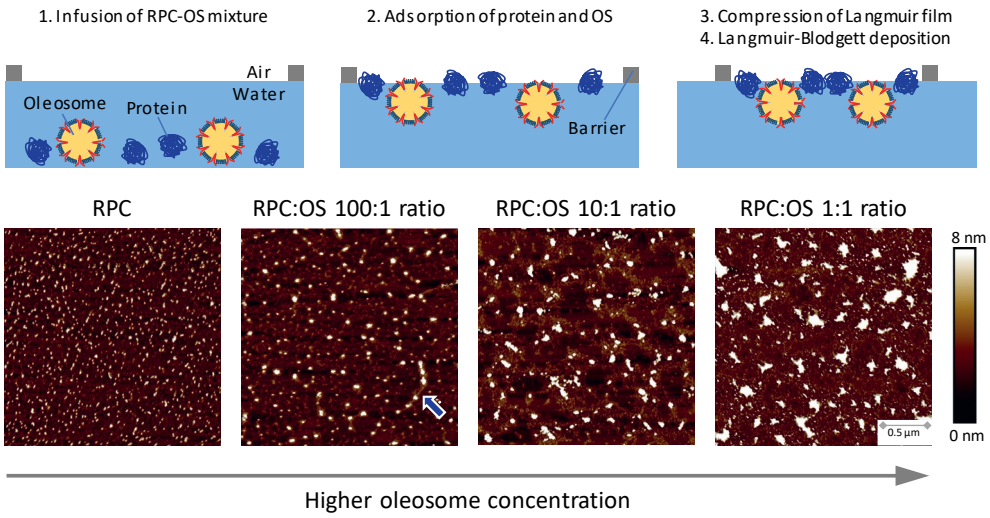

Figure 6.5. A schematic overview of the production of Langmuir-Blodgett films and the AFM images of the films made from RPC and RPC-OS mixtures. The films were produced at a target surface pressure of 21 mN/m. The images are representative of at least four scans on two independently produced films. The blue arrow indicates long strand-like structures, which are membrane fragments of disrupted oleosomes.

The topography of pure RPC showed many white structures, which are thicker regions on the film, and were previously identified as protein-dense regions[103,152]. The protein regions (or clusters) are either pre-existing aggregates in the protein material, or are possibly formed because of attractive interactions between the proteins that result in protein segregation[103]. Jamming of protein-dense regions is responsible for the strain hardening in compression in the Lissajous plots (Figure 6.4). The addition of OS in a 100:1 RPC-to-OS ratio resulted in a film with larger protein-dense regions. By carefully examining the film, long strand-like structures can be observed (see arrow in Figure 6.5). The strand-like structures were previously identified as membrane fragments of disrupted oleosomes[193]. Similar structures were observed earlier on RPC-stabilised films that were made from unfiltered RPC[152]. In the current work, the RPC was filtered over 0.22 μm to remove OS, which resulted in fewer strand-like structures.

Increasing the OS content to a 10:1 RPC-to-OS ratio showed a different topography, as larger structures and flat areas can be observed. The large structures could be intact oleosomes or large protein-dense regions. The flat areas are likely TAG- or phospholipid-rich regions, as demonstrated for pure OS and whey protein-OS mixed interfaces[70,193]. A similar topography can be observed by further increasing the OS concentration to a 1:1 RPC-to-OS ratio, as flat regions are still present at the surface. A minor difference between the current work and the one performed on whey protein-OS mixtures is the larger structures at the surface, which could be the formation of large domains of RPC proteins or (intact) OS structures. The presence of intact OS is a noticeable finding, as OS are known to rupture at an air-water interface[70]. On the other hand, the rupture of sunflower OS at oil-water interfaces was previously found for larger sunflower OS (>1 μm)[102]. The smaller sunflower OS (<1 μm) remained intact in the oil-water systems, and the rapeseed OS on our LB films (Figure 6.5) were in a small size range (<0.25 μm). This could imply that the large OS ruptured, leading to the formation of the flat lipid-rich regions, whereas the smaller ones remained intact at the interface. At lower RPC-to-OS ratio's (i.e. higher OS content), more OS are present in the bulk, which would explain the presence of more intact OS on the LB films.

In conclusion, the co-adsorption of rapeseed proteins and OS resulted in the formation of mixed interfaces, where the OS formed lipid-dense regions between rapeseed proteins. Such 2D-phase separation would lead to weaker in-plane interactions among adsorbed proteins. This was also observed in the dilatational surface rheology, especially for the mixtures at lower protein concentrations (0.1% RPC – 0.01% OS & 0.2% RPC – 0.02% w/w OS) (Figure 6.4).

6.3.4 Adsorption behaviour of oleosomes on rapeseed protein interfaces

In this section, we evaluated the interfacial behaviour as shown for the RPC-OS mixtures at higher protein concentrations (0.5% RPC – 0.05% OS & 1.0% RPC – 0.1% w/w OS). In the adsorption behaviour (Figure 6.2) of these samples, the RPC seemed to dominate the initial adsorption phase. Also, in the surface dilatational rheology (Figure 6.4), the rapeseed proteins dictated the mechanical properties of the RPC-OS mixtures. From these results, we hypothesised that OS might not be able to adsorb after the formation of a rapeseed protein-stabilised interfacial film. This hypothesis was investigated by creating LB films in a sequential manner, and a schematic overview of the process is shown in Figure 6.6A.

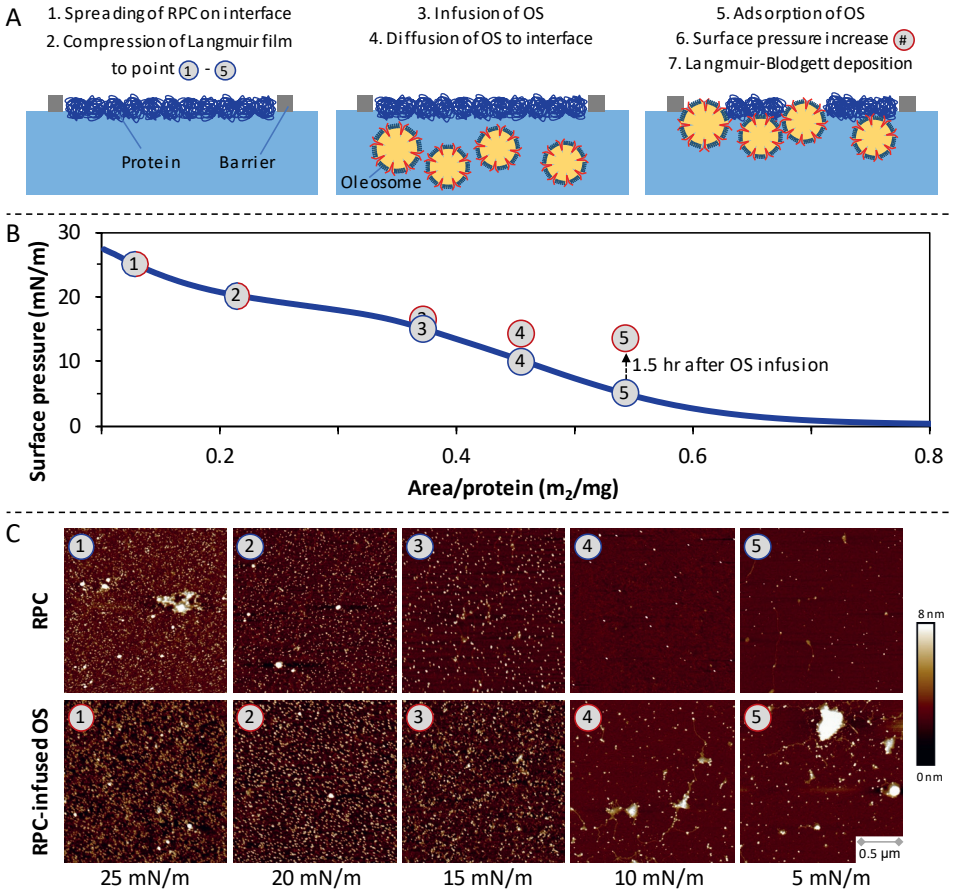

Figure 6.6. (A) A schematic overview of the production of the Langmuir-Blodgett (LB) films. (B) Surface pressure isotherm of an RPC-stabilised film. RPC-stabilised interfaces were produced at one of the five marked points (blue circles), and OS suspension was next infused in the subphase to study potential adsorption/displacement. After allowing the OS to diffuse towards the interface, the surface pressure increase is shown by the red circles. The Langmuir films were then deposited on a solid substrate to create LB films. (C) AFM scans of these films are shown, and the numbers correspond to the different compression states indicated on the surface pressure isotherm. Pure RPC films were also included for comparison purposes. The isotherm is an average of two replicates, and the error was below 5%. Each image is representative of at least four scans on two independently produced films.

First, a surface pressure isotherm of rapeseed proteins was produced by spreading the RPC solution at the surface of the subphase in the Langmuir trough (Figure 6.6B). The isotherm showed an increase of surface pressure upon compression. Here, we observe the formation of an increasingly condensed layer upon compression. Five different compression states, varying from 5 – 25 mN/m, were chosen. After the production of the layers, an OS suspension was infused in the subphase, below the RPC-stabilised Langmuir film. The OS were allowed to diffuse and potentially adsorb at the interface, and, afterwards, Langmuir-Blodgett films were created.

AFM images of the films stabilised with pure RPC, and with RPC and infused OS are shown in Figure 6.6C. The pure RPC-stabilised films show the previously mentioned white structures, which are segregated protein-dense regions. When increasing the surface pressure from 5 to 25 mN/m, thus also increasing the protein surface concentration, more protein-dense regions can be observed. At the highest compression states corresponding to 20 and 25 mN/m, we observed the formation of highly dense and heterogeneous structures, which was previously also highlighted for whey protein and rapeseed protein-stabilised interfaces[103,152]. The formation of such a dense and heterogeneous microstructure was the result of strong in-plane interactions between proteins, which led to the formation of a heterogeneous viscoelastic solid-like interfacial film.

The introduction of OS in the subphase resulted in a different microstructure on the LB films (Figure 6.6C) and in a shift of the surface pressure. For the 5, 10 and 15 mN/m RPC-stabilised interfaces, the surface pressure increased to 13.6, 13.3, and 15.7 mN/m, respectively (Figure 6.6B). The RPC-stabilised interfacial films at 20 and 25 mN/m remained constant upon the introduction of OS. From these surface pressure increases, we can assume that adsorption of OS occurred when the rapeseed protein-related surface pressure reaches only 5, 10 or 15 mN/m. The presence of intact OS is also clearly visible on the RPC-OS films at 5 and 10 mN/m, as larger structures (100-300 nm) can be observed. Also, more long strand-like structures were present, which were previously identified as membrane fragments upon disruption of the larger OS[193]. At 15 mN/m, no clear visible alterations were present after the introduction of OS. A minor amount of OS could have adsorbed, as the surface pressure increased from 15.0 to 15.7 mN/m, but this was not detected in the topography of the LB films. Further increasing the compression state of the RPC-stabilised interface to 20 or 25 mN/m resulted in RPC-OS films that were comparable with the pure RPC films. This observation, combined with the constant surface pressure after the introduction of OS, indicates that OS could not adsorb at the interface. Also, OS did not seem to attach as a sublayer beneath the rapeseed protein-stabilised interface, as the formation of such layers would normally result in clear alterations of the film topography, and thus be visible in AFM images.

The OS were thus not able to adsorb at the air-water interface when rapeseed proteins formed a condensed interfacial layer. Conversely, they did adsorb at a preformed RPC-stabilised interface at lower compression states (≤15 mN/m). We could argue that a loosely covered interface results in weaker in-plane interactions at these lower surface pressures, thus allowing OS to adsorb and probably rupture and spread at the interface. These findings imply that rapeseed proteins can outcompete OS for the air-water interface, and avoid the OS from adsorbing, if the proteins can form a dense solid-like interfacial layer. This proposed mechanism is also reflected in the mechanical properties (Figure 6.4) of RPC-OS mixture-stabilised interfaces (0.5% RPC – 0.05% OS & 1.0% RPC – 0.1% w/w OS), where the rapeseed proteins dictated the rheological behaviour. Another interesting point is the entrapment of phospholipids in the colloidal structure of the OS. Phospholipids can be detrimental for a protein-stabilised interface, may displace proteins from the interface[72,167]. In the present case, the lipid molecules in the OS did not have such an effect, probably because they are trapped in the OS structure.

6.3.5 Foaming properties of rapeseed protein – oleosome mixtures

The foaming properties of three RPC-to-OS ratios (100:1, 10:1, 1:1) were studied at fixed protein concentrations between 0.1 – 1.0% (w/w) (Figure 6.7). A wide range of RPC-to-OS ratios was studied to evaluate the effect of OS on RPC-stabilised foams at various OS concentrations. First, the foaming ability was studied by measuring the overrun and average air bubble size. The overrun was expressed as the foam volume over the initial liquid volume. RPC-stabilised foams had high overruns between 372 – 384% (Figure 6.7A). Increasing the OS concentration to a 100:1 RPC-to-OS ratio resulted in lower overruns for foams with protein concentrations ranging from 0.1 – 0.5% (w/w) compared to pure RPC, whereas the RPC-OS mixture with 1.0% (w/w) protein had a similar overrun as a pure 1.0% (w/w) RPC foam. The detrimental effect of OS was higher at lower protein concentrations. Such a trend was also present by further increasing the OS concentration to a 10:1 and 1:1 RPC-to-OS ratio, as the overrun increased at higher protein content at the same RPC-to-OS ratio. The addition of OS (from 100:1 to 1:1 ratio) initiated a decrease in foam overrun at each concentration, but the detrimental effect was less marked at higher protein concentrations.

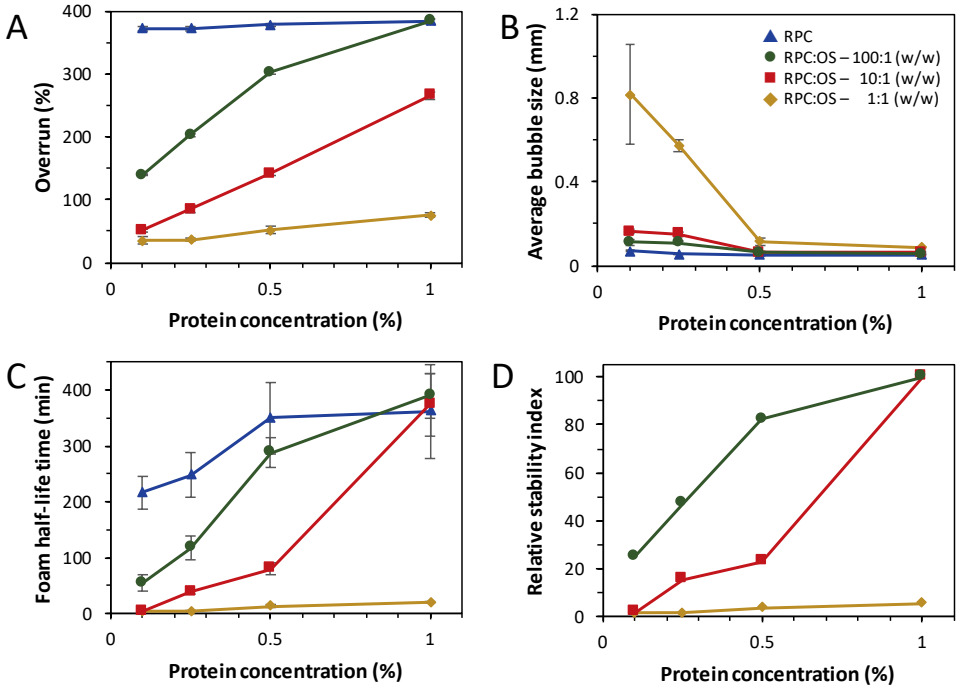

Figure 6.7. The overrun (A), average bubble size (B, diameter), volume half-life time (C), and relative stability index (D) of foams stabilised by RPC and RPC-OS mixtures. The line drawn through points is to guide the eye. Averages and standard deviations are the result of at least three replicates.

A similar trend was also observed in the average air bubble size (Figure 6.7B), as the bubble size became larger when increasing OS concentration (100:1 to 1:1 ratio). At 0.1% (w/w), the largest increase of air bubble size could be observed, which increased from 0.07 (pure RPC) to 0.82 mm (1:1 ratio), whereas increasing the protein concentration to 1.0% (w/w) resulted in an increase from 0.05 mm to 0.09 mm. Also, the OS hampered the air bubble formation more at lower protein concentrations. From the interfacial rheology experiments, it was obvious that OS reduced the in-plane interactions among adsorbed proteins, which are required for proteins to form stiff and solid-like layers around air bubbles. As a result, the formed interfaces were weaker, leading to a collapse of air bubbles already during the foam formation, thus resulting in larger air bubbles at the moment of recording. We also attempted to create foams using pure OS solutions with bulk concentrations ranging from 0.01 – 1.0% (w/w), but no foams could be created. The absence of foamability by OS is most likely attributed to the formation of a weak and incohesive interfacial layer due to the rupture and spreading of free TAGs and phospholipids. The presence of free lipids was previously found to be detrimental to the protein connectivity at the interface, thus largely reducing the foaming properties of proteins[68,71,193].

The presence of OS also affected the foam stability, which was evaluated by determining the time point where half of the foam volume decays, also known as the foam volume half-life time (Figure 6.7C). RPC-stabilised foams had half-life times increasing from 216 min at 0.1% (w/w) to 362 min at 1.0% (w/w) protein bulk concentration, and the addition of OS to RPC resulted in a decrease in foam half-life times. To directly compare the influence of OS on RPC-stabilised foams, a relative stability index was calculated by dividing the half-life time of an RPC-OS-stabilised foam over the half-life time of a pure RPC-stabilised foam at the same protein concentration times 100 (Figure 6.7D). At the lowest protein concentration of 0.1% (w/w), the relative stability index decreased to 25.2 at a 100:1 ratio and even further to 1.6 at a 1:1 ratio. The foam stabilised with 1.0% (w/w) protein had a relative stability index of 100 at 100:1 and 10:1 ratio, suggesting no negative influence of OS. The influence of OS on foam stability of RPC was more detrimental at lower protein concentrations at each ratio, and also by increasing OS concentration (100:1 to 1:1 ratio).

The interfacial rheology experiments showed the formation of weaker protein layers with reduced connectivity due to the presence of free TAGs and phospholipids after OS rupture, thus decreasing foaming ability and stability. Lipid droplets are also known to play a destabilising effect in the thin films between the interfacial layers of two neighbouring air bubbles. One of the proposed anti-foaming mechanisms is bridging by the droplet in the thin film, where the droplet connects the films on two air bubbles. Afterwards, the surface material around to droplet can spread and replace the proteins on the film. At this point, the thin film is connected by an unstable oil bridge, which can cause film rupture[71,72]. OS seem to behave as anti-foaming agents in the early stages of foam preparation, as OS can influence the air bubble size and foam overrun. The formation of larger air bubbles is correlated to lower foam stability, as the entrapped liquid in the foam is lower and gas diffusion through the films is higher compared to foams with smaller air bubbles.

The anti-foaming effect of OS is the highest at low protein concentrations (0.1 and 0.2%), where the protein film is probably less dense due to lower protein concentrations. It is likely that the OS can perform film bridging in these conditions and also adsorb at the interface, followed by spreading and film rupture, as shown by rheology (Figure 6.4) and microstructure imaging (Figure 6.6). These techniques also showed the formation of an RPC-dominated interface at higher protein concentrations. As a result, the negative effect of OS on foam/air bubble formation and stability decreased. Additionally, we could argue that OS might be trapped between the air bubbles, as observed for hydrophilic particles[195]. The entrapment of the hydrophilic OS in lamellae and plateau borders could prevent the rupture at the interface, thus protecting the protein-stabilised interface and foam from destabilising. However, the 'protective' effect of a stiff and dense protein layer reduced at higher OS concentrations, even at a high fixed RPC concentration of 1.0% (w/w), where more

extensive film-bridging could occur. At these concentrations, the rapeseed proteins might not be able to outcompete the higher number of OS for the interface, or more extensive film-bridging could occur.

6.4 Conclusion

In this work, the influence of oleosomes (**OS**) on rapeseed protein concentrate (**RPC**)-stabilised interfacial films and foams were investigated. At low protein concentrations (0.1 and 0.2% w/w), RPC and OS co-adsorb at the interface, resulting in a weaker interfacial layer than that formed with pure RPC. The OS can unfold at the interface, and their lipid components (phospholipids and TAGs) can spread and decrease the connectivity between the adsorbed proteins (Figure 6.8A). As a result, the foaming ability and stability of RPC decreases in the presence of OS at these conditions. The OS are probably able to adsorb and rupture due to a loosely packed protein interface.

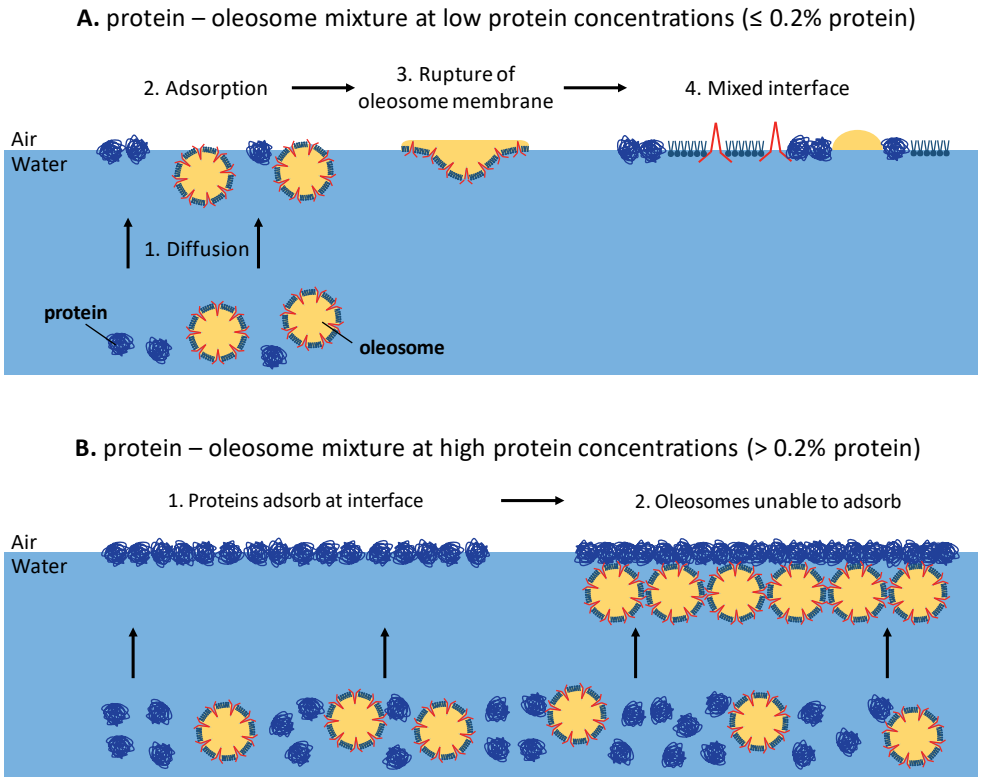

Figure 6.8. A schematic representation of the proposed interface stabilisation mechanism of rapeseed protein concentrate (RPC) – oleosome (OS) mixtures at protein concentrations of (A) ≤0.2% and (B) >0.2% (w/w).

At higher protein concentrations (0.5 and 1.0% w/w), rapeseed proteins dominate the interfacial properties, and OS have a less detrimental effect on the foaming properties compared to the situation at a low protein concentration. By infusing an OS suspension beneath a pre-formed RPC-stabilised Langmuir film (Figure 6.8B), we demonstrated that OS are not able to adsorb at such an interface when the rapeseed proteins have readily formed

a dense layer with a surface pressure of >15 mN/m. At higher enough concentrations, the rapeseed proteins thus outcompete the OS interfacial localisation. This interface stabilisation mechanism could protect the protein foams from the detrimental effect of OS. However, at high OS concentrations and relative amount (RPC:OS ratio of 1:1), OS act as effective anti-foaming agents, since the foam stability was reduced by more than 98% compared to the pure RPC-stabilised systems.

In summary, we have demonstrated that the influence of OS on RPC interfacial and foaming properties can be tuned by changing the RPC-to-OS ratio or the absolute amount of stabiliser up to a certain degree. The relationship between foaming properties and the concentration of bulk material is promising for the application of OS in aerated food systems. OS could be co-extracted with plant proteins or separately introduced as a sustainable ingredient and lipid source. The utilisation of oleosomes should be further explored in both academia and the food industry, as oleosomes can play an important role in the production of healthy and sustainable food products.

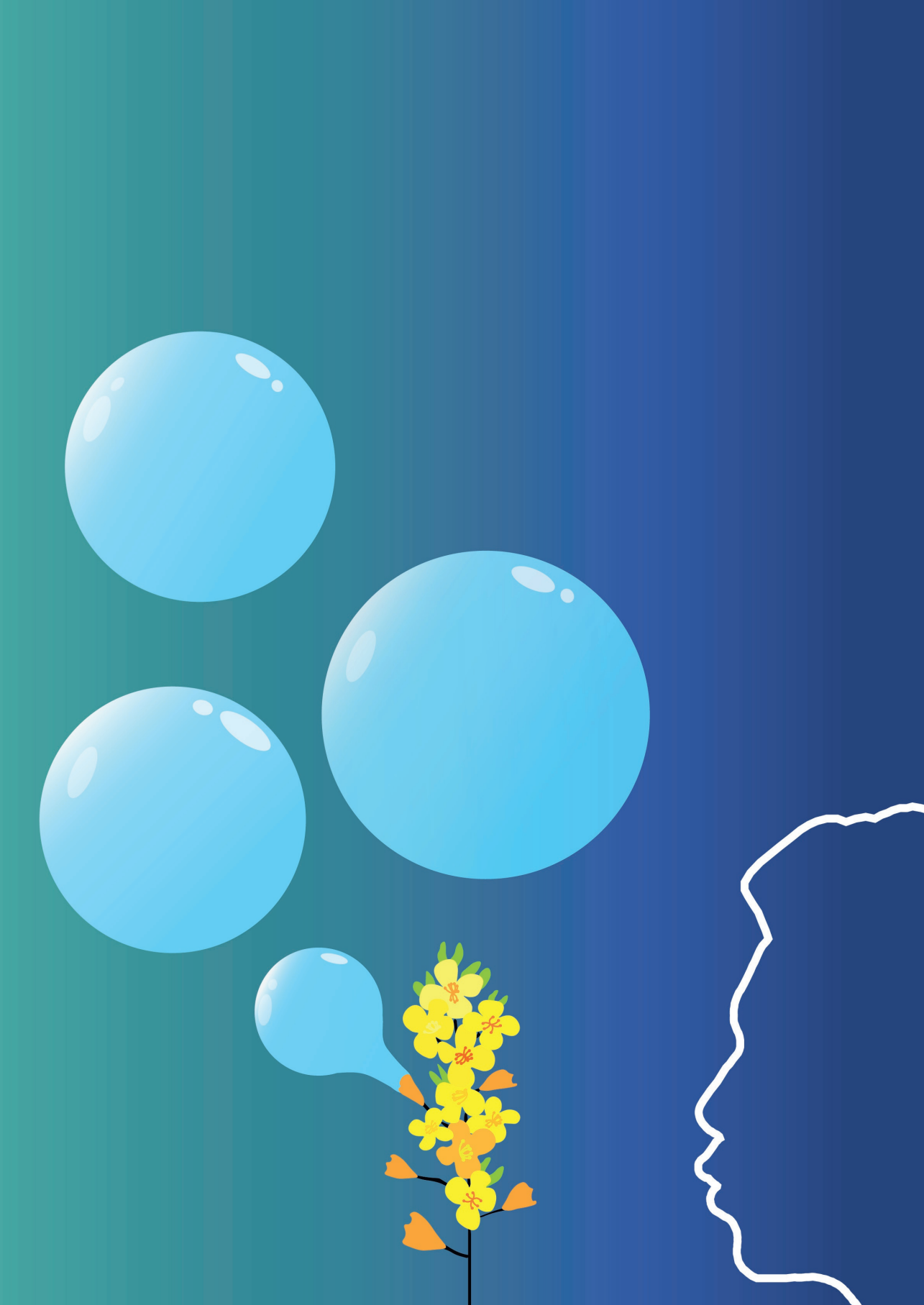

Chapter 7

General discussion

7.1 Introduction

The aim of this thesis was to study the contribution of non-proteinaceous components to the interfacial and foaming properties of mildly derived plant protein extracts by using a multi-length scale approach, which was performed for specific components in research **chapters 2–6**. In this chapter, the main results of the research chapters are summarised and are discussed together (Figure 7.1). Subsequently, the specific findings are interlinked to the composition and structural properties of plant protein extracts in general. This will help us relate the composition of the protein extracts, which is determined by the extraction method, to the macroscopic functional properties (i.e. foaming properties). Additional findings on the role of protein composition in protein extracts will also be examined. Finally, we will carefully review the limitations in current studies and methodologies, and provide recommendations for further research in the field of interface science and plant protein functionality.

7.2 Main results of this thesis

First, rapeseed was used as a plant protein source to produce a mildly derived plant protein extract (rapeseed protein concentrate, **RPC**), which contains non-proteinaceous components, such as phenols and lipids. The whole mixture was investigated in **Chapter 2** for its interfacial and foaming properties. The first step in this chapter was an extensive compositional analysis, where we found a protein content of 71.7% and a lipid content of 8.3%. The mild fractionation method extracted both napin (albumin) and cruciferin (globulin). The RPC was able to form viscoelastic solid-like interfacial layers, which became weaker and more stretchable at increasing bulk concentration. We suspected the lipids to play a key role in reducing the formation of cohesive interfacial layers by proteins, especially when increasing the RPC concentration, thus increasing the absolute lipid content. These lipids exist as oleosomes in rapeseeds, which are extracted into the RPC. To study the influence of the lipids, the RPC was defatted by organic solvent extraction to obtain a defatted RPC (**DRPC**). We still found a decrease in interfacial layer strength when increasing the concentration of DRPC. In AFM images of Langmuir-Blodgett films, we revealed the presence of non-proteinaceous components in the form of long strand-like structures. In **Chapter 5**, the exact nature of these strands was evaluated, which are likely to be fragments of the oleosome membrane after disruption. Even though the interfacial layer became weaker and less cohesive at higher concentrations, the RPC and DRPC can form foams with similar air bubble sizes and foam stabilities. This suggested a limited detrimental effect of lipids on foam stability in the mildly derived rapeseed protein extracts. The influence of non-proteinaceous components was more elaborately investigated in **Chapters 4 – 6**.

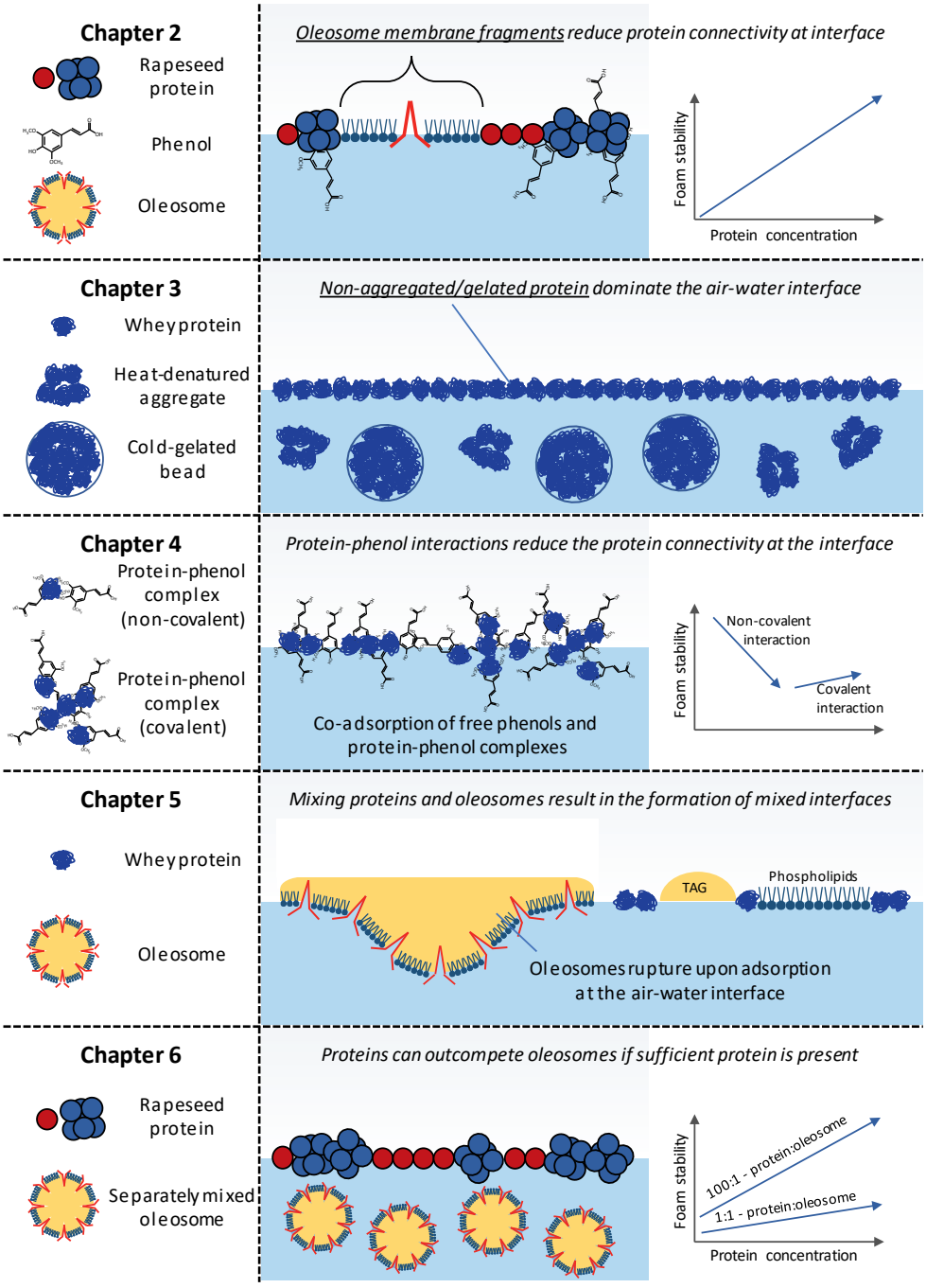

Figure 7.1. Graphical overview of the main findings.

Prior to performing an in-depth study on the non-proteinaceous components, we considered the state of aggregation of the proteins in **Chapter 3**, as plant proteins often exist in a larger aggregated state in the available commercial ingredients. Such aggregates are most likely induced by specific steps in the protein extraction method, which leads to soluble and insoluble aggregates. More details about potential protein aggregation due to processing will be discussed in further sections. In this chapter, whey protein isolate was used as a model protein source, as these proteins have been well-characterised for their physicochemical and interfacial properties. Whey proteins (diameter: 2 – 10 nm) were processed into heat-denatured aggregates (20 – 100 nm), and the aggregates were cold-gelated into larger whey protein beads (150 – 350 nm). Whey proteins and the aggregates were found to form densely clustered networks with strong in-plane interactions at the air-water interface, while the beads were not able to stabilise the interface. Surprisingly, the smaller non-aggregated or non-gelated material in the beads was found to dominate the interfacial properties, which is probably also occurring in the whey protein aggregate system. Smaller and more surface-active material tends to outcompete the larger aggregated structures for the interface. At the same time, larger aggregate sizes lead to a decrease in surface activity. Such behaviour could also occur in plant protein extracts, which are usually moderately to highly aggregated.

Aggregation of proteins can also occur due to chemical interactions with phenols, and this effect was elaborately studied in **Chapter 4**. Whey proteins were mixed with the main rapeseed phenol, sinapic acid. In this chapter, whey proteins were selected as the phenols in the RPC were difficult to remove without causing protein denaturation. Sinapic acid was found to interact non-covalently with whey proteins, which led to increased surface activity. On the other hand, the non-covalent binding on the proteins reduced the in-plane interactions of proteins at the interface, thus forming a weaker interfacial layer. These effects in surface activity and interfacial layer strength were even more pronounced when the mixtures were oxidised to induce covalent protein-phenol interactions. The increased surface activity resulted in smaller air bubble sizes, and the weaker interfacial layers after protein-phenol interaction led to an immense decrease in foam stability. These findings are important to understand the influence of plant protein extraction on protein-phenol interactions, which will be more extensively examined later in this general discussion.

The influence of oleosomes on the interfacial properties of proteins was investigated in **Chapters 5 & 6**. In **Chapter 5**, we continued using the whey protein model system, which we mixed with rapeseed oleosomes. Oleosomes were found to rupture after adsorption at the air-water interface, followed by spreading and rearranging of the triacylglycerol (**TAG**) core and membrane material consisting of phospholipids and proteins. Mixtures of oleosomes and whey proteins resulted in co-adsorption of both components, and interfacial microstructure analysis revealed TAG/phospholipid-rich regions that were surrounded by

whey proteins. The TAG/phospholipid-rich regions were pushed out upon compression, followed by interaction and jamming of the whey proteins, as demonstrated by dilatational rheology. The complexity of the oleosome-stabilised interface was reduced by removing the TAGs by solvent defatting, which yielded defatted oleosomes. Additionally, the proteins in the oleosome membrane contributed to increased resistance against deformation. The absence of the membrane proteins resulted in a phospholipid layer with little in-plane interactions. As a result, the phospholipids were pushed out of the interface upon compression.

The influence of oleosomes on the protein interface and foaming properties was further studied in **Chapter 6**, where oleosomes were mixed with RPC in various RPC:oleosome ratios and various protein concentrations. The influence of oleosomes on the interfacial properties depended on the RPC:oleosome ratio, as oleosomes dominated the interfacial properties at low protein concentrations. At these conditions, the oleosomes and proteins were found to co-adsorb. Here, the oleosomes were found to disrupt at the air-water interface, which led to weaker interfacial layers, and also lower foamability and stability compared to systems stabilised by pure protein. At higher protein concentrations or higher RPC:oleosome ratios, the proteins started to outcompete the oleosomes for adsorption at the air-water interface. The result is a rapeseed protein dominated interface, where oleosomes are unable to adsorb. This led to limited or no detrimental effect of oleosomes on protein interface and foam stabilising properties. The findings on the influence of oleosomes on protein interfaces (**Chapter 5 & 6**) yield an essential insight regarding the presence of lipids in plant protein extracts, which will be elaborately discussed in further sections.

7.3 The focus of current plant protein research

First, an overview of plant protein-related studies published in research articles in the peer-reviewed journal of *Food Hydrocolloids, Food Science and Technology and Food Research International* in 2020, with a special focus on their extraction processes is given in Figure 7.2.

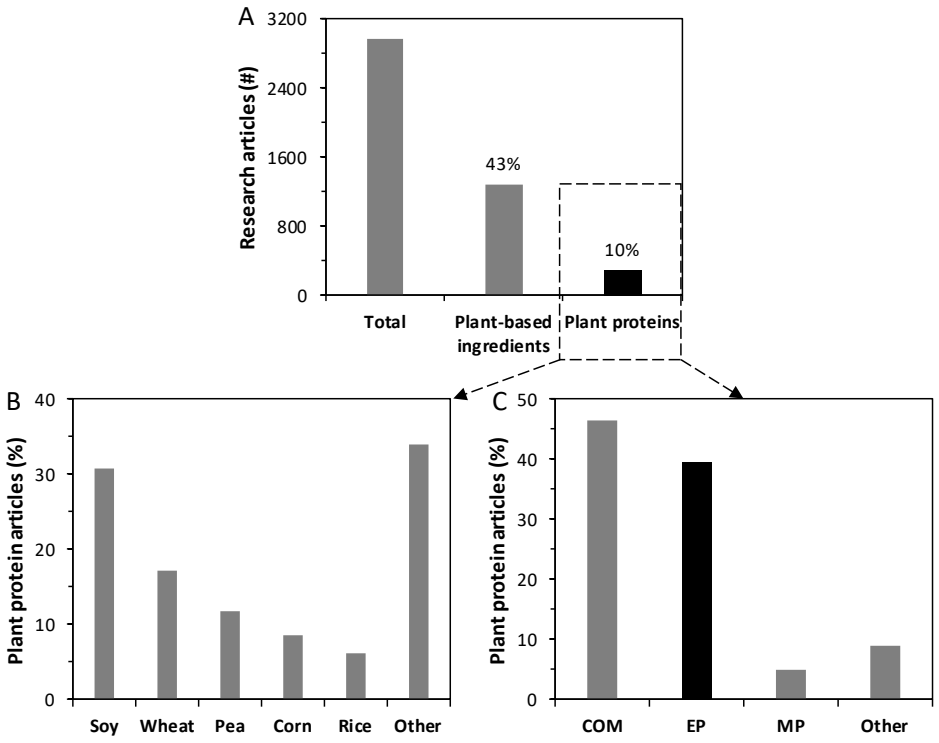

Figure 7.2. (A) Topic category overview of Food Hydrocolloids, Food Science and Technology and Food Research International articles from 2020. (B) Overview of top 5 studied plant protein sources. (C) Overview of plant protein extract acquisition. Abbreviations: COM: commercial, EP: extensive purified, MP: mildly purified.

This reveals an overwhelming interest in plant-based ingredients (43%), and 10% of the research articles are focused on plant-based proteins. About two-thirds of the plant protein functionality studies deal with the three most investigated sources: soybean, wheat, and pea. About 34% of the plant protein studies focus on other ingredients, including specific local plant sources and upcoming sources, such as rapeseed, sunflower seed, and algae. A majority of these sources were obtained commercially (46%). The second-largest group (40%) was obtained using (wet) extensive purification methods, which generally consist of an alkaline protein extraction combined with isoelectric point precipitation. The commercial protein isolates were assumed to be obtained with an extensive extraction method, as protein purities were often >80%. Another point of attention is the overestimation of the

protein content, as high nitrogen conversion factors around 6.25 are often used, while a lower conversion factor ranging from 5.2-5.8 is more appropriate for proteins from plant sources[196]. Substantially fewer studies focused on mild and more sustainable extraction methods, where isoelectric point precipitation or other harsh processing were not performed.

Plant protein research is largely focused on obtaining protein extracts with high purity using extensive protein processing. Such a methodology has several disadvantages, which we will discuss later in this chapter. Simultaneously, we will show how mild purification methods can be utilised to overcome the drawbacks of extensive protein purification. To fully evaluate the functional properties of an extraction process, we performed a multi-length scale approach. The protein extraction process determines the composition and structural properties of the extracts, which can be attributed to the macroscopic functionality using the multi-length scale approach. By using such research tools, we can directly link processing to functional properties and, thereby, provide design rules for optimal and more sustainable extraction processes to obtain protein extracts with promising functionality.

7.4 Plant protein purification: extensive versus mild purification

The first experimental study in this project dealt with the comparison between an extensively (**eRPC**) and mildly (**mRPC**) derived RPC. The exact extraction method of the eRPC was not known as it is a commercial extract, but the method is assumed to be extensive. The eRPC is probably extracted from defatted rapeseed meal, a side-stream from rapeseed lipid extraction, using alkaline extraction, followed by isoelectric point precipitation of the proteins[11]. An alkaline extraction at high pH (>10) is expected, as the eRPC had a much darker brown colour compared to the mRPC (data not shown). Such a colour difference is probably the result of phenol oxidation[43], where highly reactive quinones are formed with the ability to covalently bind to proteins[160]. The covalent phenol-protein interaction in the eRPC could have led to aggregation, which was reflected in the larger particle size in dynamic light scattering (Figure 7.3A). The eRPC showed protein aggregates between 50–1000 nm, while the mRPC only showed proteins between 5–10 nm. Please bear in mind that the shown size distributions are obtained from the soluble fraction after centrifugation. Larger (insoluble) aggregates/particles were neglected in this analysis. Other processing steps may also lead to protein aggregation, such as isoelectric point precipitation[38,39], or heating in solvent-defatting or spray-drying[40,197]. These steps were avoided in the mild purification process. In a preliminary study, we attempted to perform an isoelectric point precipitation step on the mRPC. After centrifugation, the pellet with precipitated proteins was less soluble, probably due to protein aggregation, thus suggesting a negative impact of this processing step on protein properties.

The interfacial and foaming properties of both RPCs were also compared. First, the soluble fraction of the RPCs was extracted and freeze-dried. This would allow the standardisation based on soluble protein, which is a more accurate comparison between the two RPCs. Here, we found a major difference in protein extractability at pH 7.0, where 40.6% of the proteins could be extracted from the eRPC, and 58.0% from the mildly derived one. A lower extractability of the eRPC was expected, as protein aggregation could lead to a loss of solubility[198]. Protein aggregation can influence the interfacial properties, which is shown in Figure 7.3B & C. The eRPC showed a slower increase in surface pressure than the mildly derived one, which can most likely be attributed to larger protein aggregates in eRPC than the substantially smaller proteins in the mRPC. Also, an immense difference was found in the surface rheological properties, as the layer formed with eRPC showed nearly amplitude independent surface dilatational moduli (18 to 16 mN/m), while the layer formed with mRPC had higher moduli with a strong amplitude dependence (49 to 26 mN/m).

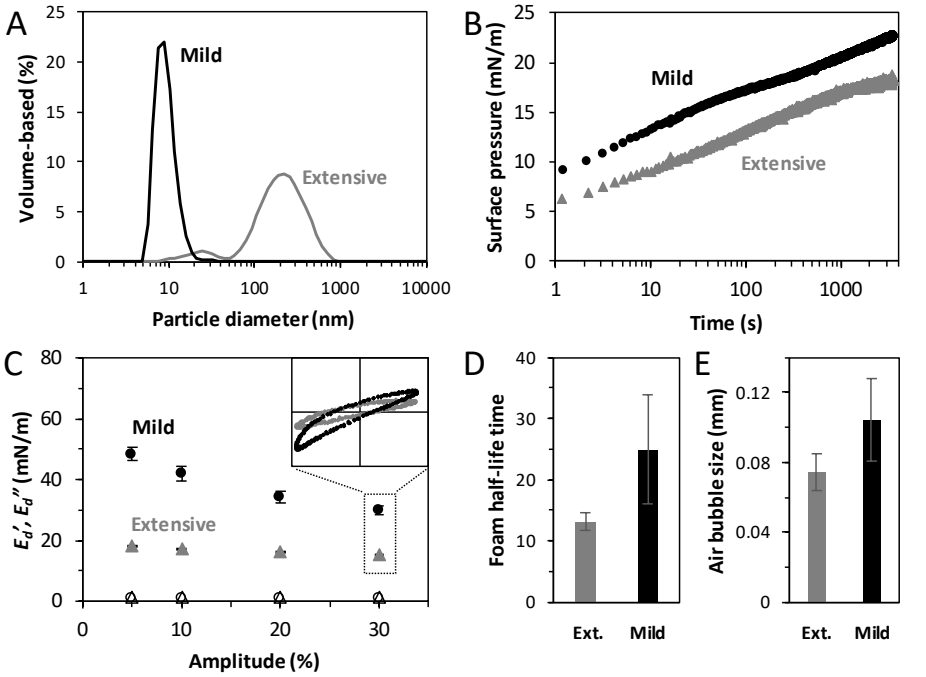

Figure 7.3. (A) Particle size distribution of mildly (mRPC, black) and extensively derived (eRPC, grey) RPC. (B) The surface pressure expressed over time of interfacial film stabilised by both RPCs. (C) The surface dilatational moduli expressed over deformation amplitude of both RPCs (ω = 0.02 Hz). The closed symbols depict the storage modulus E_d', and the open symbols depict the loss modulus E_d''. Lissajous plots of the 30% deformation with surface pressure over deformation were plotted in the insert in panel C. The foam half-life time (D) and average air bubble size (E) of both RPCs were also shown. All samples had 0.1% (w/w) protein content and were prepared in 20 mM PO_4-buffer at pH 7.0. All experiments were performed in at least triplicates, and a representative size distribution is shown in A, while averages and standard deviations are shown in B–E.

In the Lissajous plot (Figure 7.3C), we observe the formation of a much weaker and stretchable interface by the eRPC. In **Chapter 3**, we produced whey protein beads in a comparable size range as the protein aggregates in the eRPC. The interfacial properties of eRPC are in line with those found for whey protein beads, which formed weaker and more mobile interfaces, especially compared to their constituents, native whey proteins. Aggregation to such size ranges (>100 nm) seemed to largely reduce the proteins' ability to adsorb and interact at the air-water interface.

The eRPC also led to the lowest foam stability, which is intimately related to the formation of weaker interfacial films due to aggregate formation. Our mRPC showed substantially better interface and foam stabilising properties compared to eRPC. On the other hand, the eRPC formed about 30% smaller air bubbles, which was unexpected, as this concentrate showed a lower surface activity (Figure 7.3B). Non-proteinaceous components in the mRPC could affect the air bubble formation and stabilisation by proteins. In the next sections, we will elaborately review the contribution of the non-proteinaceous components to the structural and functional properties of plant protein extracts.

7.5 Influence of non-proteinaceous components in plant protein extracts on the structural and functional properties of proteins

In this thesis, we focused on two abundantly present non-proteinaceous components in plant crops that are also known to influence the molecular, interfacial, and foaming properties of proteins. These components are phenols and lipids, and the type of extraction process largely determines their occurrence in the extract, molecular state, interaction with proteins, and influence on the protein functional properties. A possible influence of non-proteinaceous components in the mildly derived RPC was demonstrated in **Chapter 2**, where the interfacial layers became weaker and more easily stretchable at higher protein concentrations. An increase in protein concentration also results in more phenols and lipids, which could have interfered with the protein interactions at the interface. The effect of phenols and lipids on the protein interfacial and foaming properties were extensively evaluated in **Chapters 4–6** and will be further discussed in the following sections.

7.5.1 Phenols

Phenols can exist in three states in a phenol-protein mixture: 1. Unbound state, 2. Non-covalently bound with proteins, 3. Covalently bound state with proteins[73]. A diafiltration step can effectively remove unbound phenols, as an earlier study showed a phenol decrease by 57% (based on dry matter) in rapeseed[43]. Our mildly derived RPC still contained about 2.1% (w/w) phenols, which are likely bound phenols, and could influence protein functionality. Therefore, we attempted to remove phenols, which is commonly performed using alcohol solvents[37,75]. However, this process led to a loss of protein solubility, up to 78.8% for

cruciferin. The comparison between RPC and a dephenolised/modified RPC would be invalid. Hence, we chose to use a model, phenol-free protein system, whey protein isolate (**WPI**), which was systematically mixed with the main rapeseed phenol, sinapic acid (**SA**), to study the influence of unbound and (non)covalently bound phenols in **Chapter 4**.

In the WPI-SA model system, unbound phenols co-adsorbed with the proteins at the interface, and reduced in-plane interactions between proteins. A similar effect was found when phenols were both non-covalently and covalently bound to the proteins. Binding on the protein surface most likely led to changes in protein surface properties, which resulted in higher surface activity but weaker protein layers. Covalent phenol-protein interactions were induced by overnight phenol oxidation at alkaline pH, leading to phenol-protein aggregates, and caused the formation of weaker interfacial layers compared to pure WPI. The weaker interfacial layers ultimately resulted in lower foam stability after the addition of phenols. However, there are several differences between the studied WPI-SA system and the mildly derived RPC. In **Chapter 4**, we focused on a low protein:phenol ratio of 1:10, and for this ratio, a most pronounced effect could be observed, while a substantially lower amount of phenols is present in the RPC (protein:phenol ratio 33:1). Additionally, we only studied one type of phenol in **Chapter 4**, whereas multiple phenols are known to be present in RPC[12]. Therefore, it is difficult to directly compare the outcome from the WPI-SA system with the RPC one. To fully understand the influence of phenols in the RPC, the phenols in the RPC were oxidised overnight at pH 10.0 to induce covalent phenol-protein interactions. The oxidised RPC (**RPCox**) was evaluated for its interface and foam stabilising properties (Figure 7.4).

The presence of a lower amount of phenols in the RPCox was not as detrimental for the interfacial and foaming properties in comparison to an oxidised WPI-SA mixture with a substantially higher phenol:protein ratio. A higher phenol content could result in larger phenol-protein aggregates, as more phenols are available to covalently bind to proteins. Also, the whey and rapeseed proteins differ largely, as whey protein mainly consists of β-lactoglobulin with a molecular weight of 18.4 kDa and often exists in dimeric form[137]. Rapeseed proteins consist of napin, which has a comparable size, but also cruciferin, which often forms tri- or hexamers, with molecular weights ranging between ~150–300 kDa[176]. It is worth mentioning that these quaternary structures and molecular sizes are often found at neutral pH, and the protein conformations, especially quaternary structure, are known to depend on pH and ionic strength[11,20]. Cruciferin was previously found to possess a compact protein structure, which might prevent large alterations due to phenol binding[21]. On the other hand, the structural conformation of β-lactoglobulin, the main whey protein, was described to partially destabilise by loss of secondary protein structures after non-covalent phenol binding within the hydrophobic protein core[155]. Previously, it was revealed that the

protein structure alteration by a phenol is also affected by the type of protein[83]. The exact mechanism behind the different outcomes has not been extensively investigated and should be addressed in future studies to understand the influence of phenols on (plant) proteins. Nonetheless, 2.1% (w/w) phenols in the RPC did not seem to negatively influence the interfacial and foaming properties after phenol oxidation. Of course, we were unable to evaluate the influence of phenols in the RPC before oxidation, as a phenol-free RPC without altered protein solubility/structure could not be obtained.

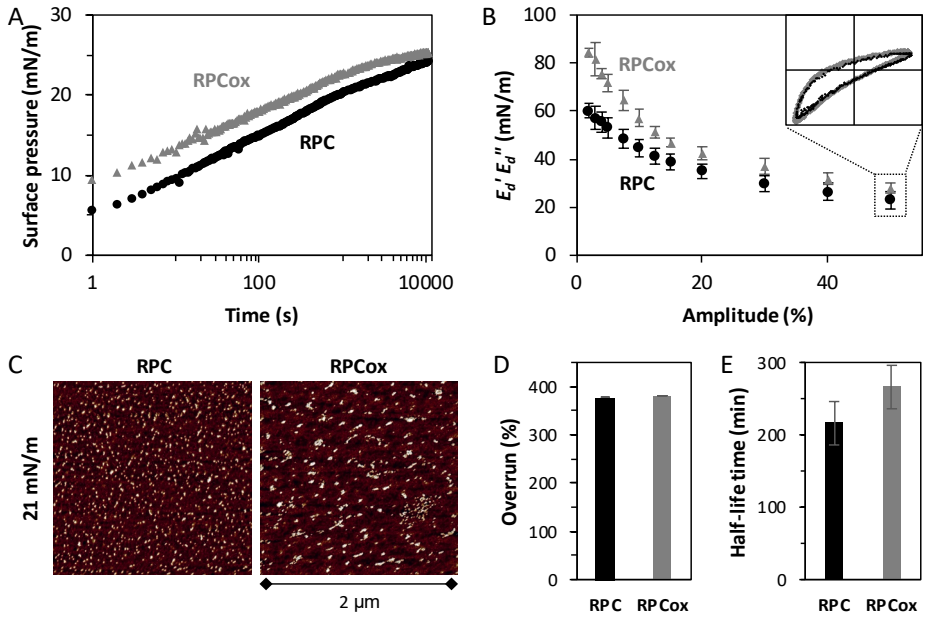

Figure 7.4. (A) Surface pressure as a function of time of an air-water interfacial film stabilised by RPC (filtered over 0.22 µm) or oxidised RPC (RPCox). (B) The surface dilatational moduli as a function of deformation amplitude of both RPC-stabilised layers (ω = 0.02 Hz). The closed symbols depict the storage modulus E_d', and the open symbols depict the loss modulus E_d''. Lissajous plots of the 50% deformation, showing surface pressure over deformation, are shown in the insert in panel B. (C) AFM images of Langmuir-Blodgett films made of both RPCs at a sampling surface pressure of 21 mN/m. The foam overrun (D) and foam volume half-life time (E) of both samples were also shown. All samples had 0.1% (w/w) protein content and were prepared in 20 mM PO_4-buffer at pH 7.0. All experiments are performed in at least duplicate, and representative images shown in C, while averages and standard deviations are shown in A, B, D, and E.

Whereas phenols in the RPC did not influence the interfacial and foaming properties of the proteins, other important ingredient properties could be affected. Oxidised phenols often cause undesired colour formation, such as a dark brown RPC[31,154]. Another example is sunflower seeds, where protein-phenol complexes cause the protein extract to turn dark green[199]. The phenol-protein interaction can also occur with saliva proteins in the mouth during ingestion, which is known to initiate a dry and puckering mouthfeel, called astringency[12,30]. Bitterness is another undesired effect of phenols, which should be evaluated for mildly derived extracts in further studies. A final drawback of phenol-protein interactions

is nutritional, as phenol-protein aggregates could have a lower digestibility than pure proteins[200]. Therefore, unbound phenols should be removed as much as possible during plant protein extraction by, for instance, filtration. Phenol oxidation in a protein extract involves many drawbacks and should be avoided, especially by preventing protein extraction at extreme alkaline pH, as phenol oxidation is largely accelerated in such conditions.

7.5.2 Lipids

The intensity of protein purification can largely affect the lipid content, as was observed for the mildly derived RPC with a lipid content between 20–30%, due to the absence of an extensive defatting step. The lipids (i.e. TAGs, polar lipids and free fatty acids) exist in their natural state, the oleosomes. They can be co-extracted with proteins, due to the presence of hydrophilic phospholipid headgroups and membrane protein domains on the oleosome surface[22]. A majority of the oleosomes were separated in the cream layer after centrifugation, but smaller oleosomes were more difficult to remove and remained in the soluble phase with the proteins. In **Chapter 5**, the influence of rapeseed oleosomes on the interfacial properties of whey proteins was evaluated. The oleosome membrane ruptured upon adsorption at the air-water interface. As a result, the core and membrane material spread over the interface, leading to weak and mobile interfacial films[70]. In mixtures, oleosomes and whey proteins were found to form a mixed interface, where oleosomes dominated the rheological properties at small deformations. The formation of an oleosome-dominated interface could largely reduce the in-plane interactions among adsorbed proteins, thus negatively influencing the foaming properties of the mildly derived RPC.

Therefore, the RPC was defatted, and the non-defatted and defatted RPCs were compared for their interfacial and foaming properties (**Chapter 2**). Interestingly, the defatted RPC showed slightly stronger interfaces than the non-defatted RPC, but very comparable foaming properties. The presence of oleosomes in RPC did not seem to hamper the foaming properties, whereas oleosomes can largely affect the in-plane protein interactions at the interface. When studying the interfacial microstructure, we found strand-like structures in the Langmuir-Blodgett films of both RPCs. From **Chapter 5**, we suspect these long structures to be oleosomes membrane fragments. In the non-defatted RPC, these fragments are formed after oleosome rupture. Fragments are also present in the defatted RPC, as the solvent defatting removes the TAG core, while the oleosome membrane components remain in the RPC[102]. The remaining membrane components, comprising phospholipids and membrane proteins, in the defatted RPC might also have influenced the foaming properties, leading to similar results as the non-defatted one.

The contradicting results between **Chapter 2** and **5** led to the follow-up study (**Chapter 6**), where RPC was carefully defatted by additional centrifugation and filtration to remove

oleosomes. The obtained RPC was systematically mixed with oleosomes at various RPC:oleosome ratios and RPC concentrations. In **Chapter 6**, we discovered that oleosomes dominated the interfacial and foaming properties at low RPC:oleosome ratios, leading to poor foaming properties. At higher protein concentrations, the RPC dominated the interface by out-competing the oleosomes from the interface. This led to a limited or no detrimental effect of oleosomes on RPC foaming properties. This would also explain the increased foaming properties of RPC in **Chapter 2**, as the foamability and stability increased with higher RPC concentrations, while the RPC:oleosome ratio was constant. We have demonstrated that oleosomes can act as anti-foam ingredients in protein foams, but the detrimental effect can be reduced by varying the protein:oleosome ratio and/or the absolute amount of protein in the mixture. On the other hand, the anti-foaming properties of oleosomes should also be embraced as an interesting attribute for applications, such as 'natural' anti-foaming agents.

The mildly derived RPC is suitable as a foaming ingredient, even though lipids are present. The colloidal state of the lipids also plays a role in the interfacial properties, as the TAGs and phospholipids are 'trapped' in an oleosome. These components can only hamper the strength and cohesiveness of the protein-stabilised interface, if oleosomes reach the interface and release lipids (TAGs and phospholipids) by unfolding. The colloidal structure could avoid the components from reaching the interface. It is known that free TAGs or phospholipids can largely affect the interfacial properties by reducing protein connectivity or displacing proteins[68,72], which might occur in extensively derived protein concentrates. In the defatting step, the TAG core is extracted by solvent extraction, leaving the oleosome membrane, thus phospholipids, in the defatted meal. Phospholipids may end up in the plant protein extract and negatively influence the interfacial and foaming properties of the plant proteins.

Additionally, defatting is mainly performed on plant protein extracts from oil-rich seeds, such as soybean, sunflower seed, and rapeseed. Plant sources with marginal lipid contents, such as legumes, are generally not defatted before protein extraction. Therefore, such plant protein extract could contain lipids, such as demonstrated for pea protein extract with lipid concentrations between 1.0 and 4.0% (w/w)[45,201,202]. Another point for attention is the chemical stability of the TAGs inside the oleosomes, as plant TAGs consist of a broad mixture of fatty acids, including unsaturated ones. The latter could become oxidised, which leads to undesired components concerning odour and flavour. It is difficult to modify the fatty acid composition of oleosomes, which is a drawback with regard to chemical stability. Therefore, the chemical stability of oleosomes should be carefully addressed before the large-scale utilisation of oleosomes.

7.6 Protein composition in plant protein extracts

As mentioned in the general introduction, a mild protein extraction method yields a protein concentrate with both albumins and globulins, as the isoelectric point precipitation step is excluded. Normally, this step separates the albumins and other solutes from the globulins, and the latter is processed into an extensively purified protein extract. The conventional wet extraction process creates a large side stream with albumins, which is generally discarded. An example is the production of the most commonly utilised and extensively purified plant protein extract, which is soy protein isolate. The production of 1 ton soy protein isolate yields 20 tons of waste stream with about 0.3% (w/v) protein[203]. Therefore, the protein transition from the animal- to plant-derived proteins is mainly focused on globulins, which we show in Figure 7.5, where globulins are the most extensively investigated proteins (49%) in plant protein studies (*Food Hydrocolloids, Food Science and Technology, and Food Research International,* 2020).

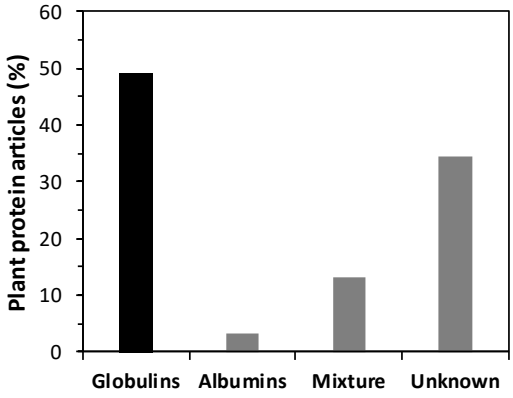

Figure 7.5. Overview of studied plant proteins in Food Hydrocolloids, Food Science and Technology, and Food Research Internationa articles from 2020. Glutelins and prolamins were excluded from this overview.

About 80% of the articles with unknown protein composition were commercial extracts, which are most likely globulin-dominated extracts. Albumins have received little attention with regard to functional properties. We tried to separate (albumin) napin and (globulin) cruciferin by isoelectric point precipitation, but this always led to a substantial loss of protein solubility for cruciferin. This effect was less strong for three other protein sources: mung bean (**MB**), Bambara groundnut (**BGN**) and yellow pea (**PEA**). We managed to extract albumin- (**ALB**) and globulin-rich (**GLOB**) extracts from these three sources (see gel electrophoresis scan in Figure 7.6).

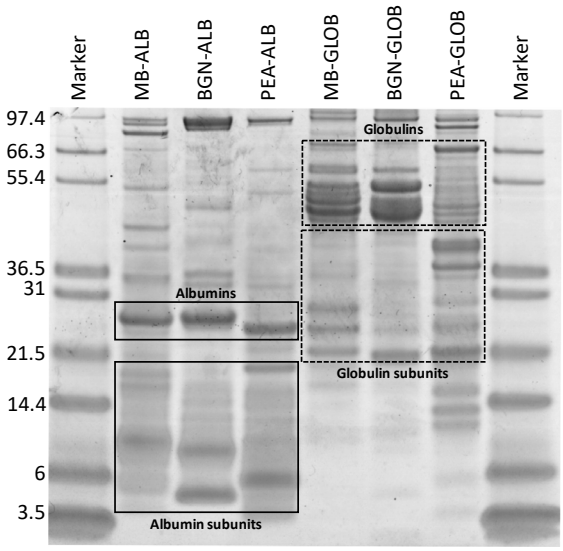

Figure 7.6. SDS-PAGE profile under reducing conditions of mung bean (MB), Bambara groundnut (BGN), and pea (PEA) albumin-rich (ALB) or globulin-rich (GLOB) extracts. A molecular weight marker is included, and the corresponding molecular weights (kDa) are indicated on the outer lanes.

Albumins are generally smaller proteins (14 – 53 kDa)[204] compared to globulins (170 – 385 kDa), which we demonstrated in our gel electrophoresis scan (Figure 7.6). Another generic difference in this study is the zeta-potential at pH 7.0, ranging between -3.3 to -2.0 mV for albumins and -14.8 to -10.3 mV for globulins. These molecular properties can influence the interfacial properties of the plant proteins. The results of an amplitude sweep for both albumin- and globulin-stabilised interfaces are shown in Figure 7.7.

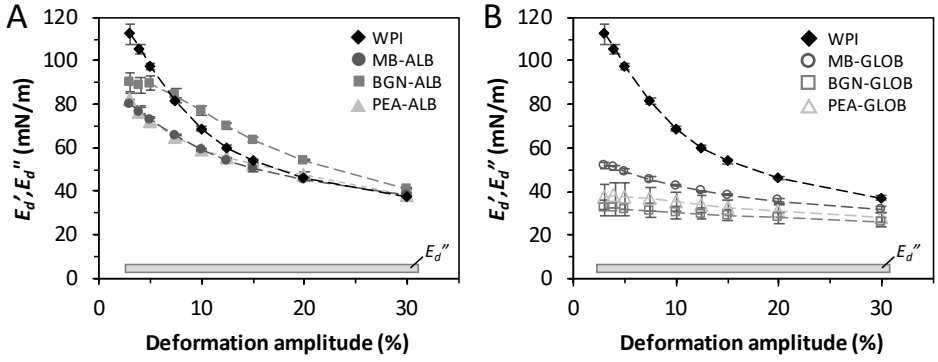

Figure 7.7. The surface dilatational moduli against deformation amplitude of whey protein isolate (WPI), mung bean (MB), Bambara groundnut (BGN), and pea (PEA) albumin-rich (ALB) or globulin-rich (GLOB) extract-stabilised interfaces (ω = 0.02 Hz). The dilatational storage moduli (E_d') are depicted as symbols with a dotted line as a guide for the eye. The dilatational loss moduli (E_d'') of all interfaces are labelled with the grey bar. All samples had 0.1% (w/w) protein content and were prepared in 20 mM PO_4-buffer at pH 7.0. The symbols are described in the legends. Averages and standard deviations were obtained from at least three replicates.

Here, we showed higher and more amplitude-dependent moduli for albumin- than for globulin-stabilised interfacial films. Albumins were able to form stiff, dense and solid-like interfaces, very similar to a whey protein-stabilised film, as shown in AFM and Lissajous plots (data not shown), while globulins form weak and more easily stretchable interfacial films. The smaller protein could allow more proteins to fit on the surface, which can also closely approach each other due to a low net-protein charge. Such behaviour could lead to strong in-plane interactions at the interface, resulting in the formation of stiff viscoelastic solid-like interfaces. Globulins are larger than albumins and also possess a higher net electrostatic charge. As a result, globulins could only form less dense, thus weaker, interfacial layers, as demonstrated in AFM (data not shown).

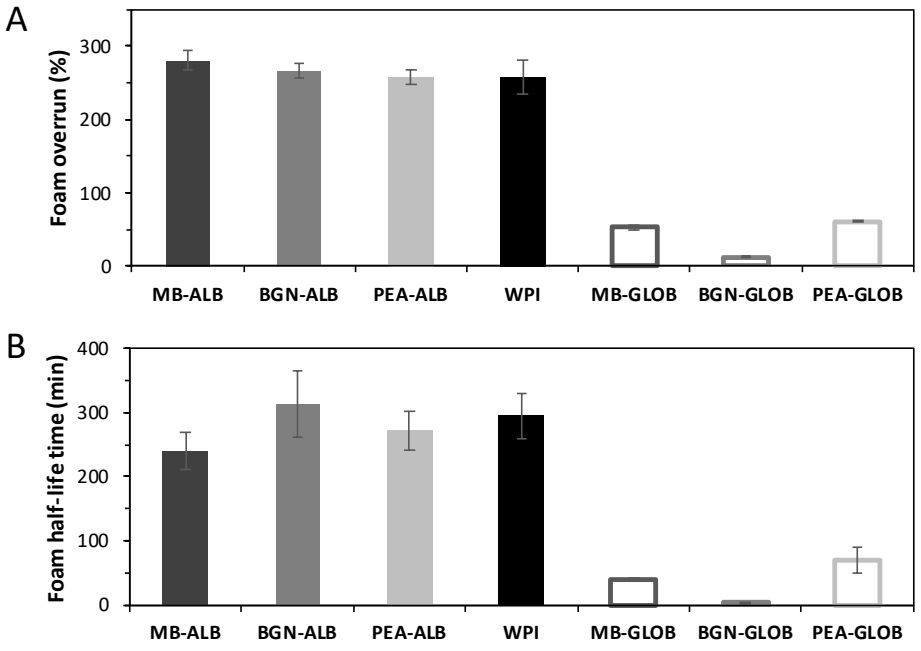

Figure 7.8. The foam overrun (A) and foam half-life time (B) of whey protein isolate (WPI), mung bean (MB), Bambara groundnut (BGN) and pea (PEA) albumin-rich (ALB) or globulin-rich (GLOB) extract-stabilised foams. The protein concentration of all samples was 0.1% (w/w), and samples were prepared in 20 mM PO_4-buffer at pH 7.0. The averages and standard deviations were obtained from at least three replicates.

Consequently, the formation of stiff interfacial layers resulted in superior foaming properties for albumins with high foam overruns and stability, similar to those of whey protein-stabilised foams (Figure 7.8). In contrast, globulins showed substantially lower foamability and foam stability, which we could relate to the formation of weaker interfacial layers around the air bubbles. Albumins have highly promising foaming properties, while this protein fraction is generally discarded. The main reason for this disposal is the presence of other

solutes in the side stream additional to albumins, such as phenols, sugars and minerals, but also anti-nutritional components (e.g. lipoxygenases and phytic acid)[35]. These components can be removed by filtration[204] or inactivated by heating, fermentation or germination[205]. Another drawback of some albumins is the potential to trigger allergenic responses[36], which should be carefully evaluated before applying specific albumins as food ingredients. Nonetheless, albumins show significant potential as a food ingredient with regard to foaming. On the other hand, albumins from BGN and PEA were found to provide limited flocculation stability in emulsions, whereas globulins were more successful in emulsion stabilisation (data not shown). We can relate this to the lower protein net-charge of albumins, which is reflected in a lower surface charge of the oil droplets, leading to increased droplet flocculation. For rapeseed proteins, it was demonstrated that (albumin) napin and (globulin) cruciferin stabilise the interface synergistically. Napin adsorbs rapidly at the oil-water interface, while the cruciferin attaches as a layer around the droplet and provides stability against droplet flocculation. Albumins might also play an important role in emulsion stabilisation in mixture with globulins.

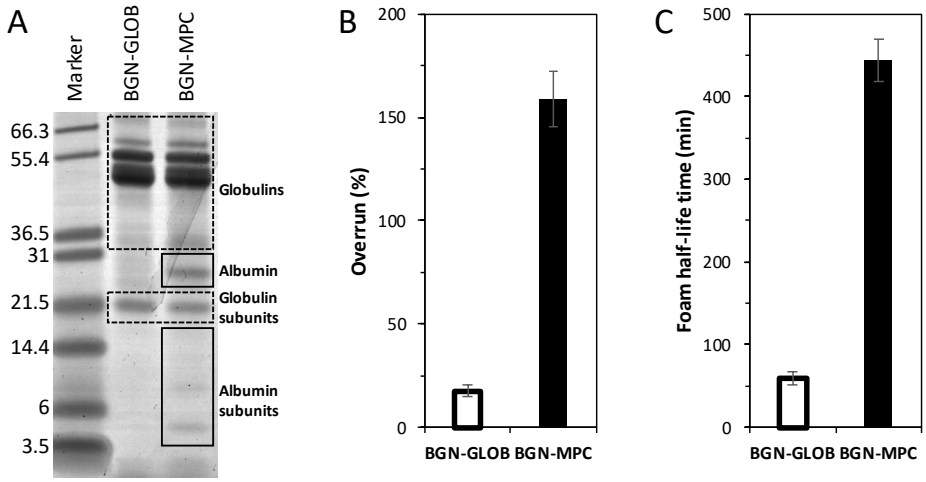

Figure 7.9. (A) SDS-PAGE profile under reducing conditions of Bambara groundnut (BGN) globulin-rich extract (GLOB) and mildly derived protein concentrate (MPC). A molecular marker is included, and the corresponding molecular weights (kDa) are indicated on the left. The foam overrun (B) and stability (C) of the BGN-GLOB and -MPC at 1% (w/w) protein content are also shown. All samples were prepared in 20 mM PO_4-buffer at pH 7.0. The averages and standard deviations were obtained from three replicates.

The side stream containing albumins could be utilised to create protein extracts with good foaming properties, but albumins can also be included in a mildly derived plant protein extract, such as the RPC studied in this thesis. To fully evaluate the method, we used the mild extraction method on BGN to produce a BGN-mildly derived protein concentrate (**MPC**), which was compared to an extensively extracted concentrate with mainly globulins (BGN-GLOB) (Figure 7.9A). A major difference between the BGN-MPC and -GLOB is the presence

of albumins and 10.8% (w/w) lipids in the MPC. We produced foams from both samples and found tremendously higher foam overrun and stability for the BGN-MPC compared to BGN-GLOB (Figure 7.9B & C). We could attribute the increased foaming properties to the presence of albumins in the MPC, or the absence of the isoelectric point precipitation step in the MPC production. This process step was previously linked to the formation of largely aggregated globulins and ultimately resulted in a loss of protein solubility[38]. We could argue that the globulins in the MPC are more soluble and also less aggregated than the ones in the GLOB sample, thus contributing to the foaming properties. Here, we proved that the mild protein extraction process in our work is suitable for multiple sources to obtain ingredients for foam, but also emulsion stabilisation. The albumins seem to play an important role in the foaming properties, and the presence of non-proteinaceous components does not affect the foaming properties.

7.7 Design rules for mild plant protein extraction methods

Based on the findings in this thesis, we would like to discuss and formulate design rules for mild plant protein extraction methods. The design rules could contribute to more sustainable production of plant protein extracts with high functionality. Current plant protein functionality research mainly focuses on extensive processing to obtain protein extracts with high purity, as the presence of non-proteinaceous components is widely assumed to hamper protein functionality. Therefore, this project was initiated with a research question: "To what extent is protein purification necessary?".

To answer this question, we produced a mildly derived rapeseed protein extract, which showed much better interfacial and foaming properties compared to a commercially or extensively derived rapeseed protein extract (Figure 7.3). Extensive processing seemed to induce protein aggregation, which led to poor functional properties. Afterwards, we focused on the non-proteinaceous components phenols and lipids. From **Chapter 4**, we conclude that unbound phenols should be removed as much as possible, and alkaline pH-induced phenol oxidation should be limited. The latter can be induced during the initial protein dissolution step, which is commonly performed at high alkaline pH (up to 13)[12,13] to increase globulin extractability. Ironically, the aim to obtain a higher protein extraction yield also leads to more phenol oxidation, thus forming more and larger phenol-protein aggregates with limited functional properties. Protein-phenol interactions would also lead to challenges in product colour and sensory properties. Therefore, phenol oxidation should be avoided by finding a balance between protein extraction yield and phenol oxidation. Protein extraction yield can also be increased by increasing ionic strength, or phenol oxidation could be reduced by adding antioxidants or inhibitors.

In this thesis (**Chapter 5 & 6)**, we also focused on the lipids, which were present in the form of oleosomes in the mildly derived protein extract. We demonstrated how their colloidal state determines the influence of lipids (i.e. TAGs and phospholipids) on protein functionality (**Chapter 5**) and also the concentration of both lipids and proteins (**Chapter 6**). The presence of oleosomes in the mildly derived protein extract did not influence the protein foaming properties (**Chapter 2**). Oleosomes might trap the TAGs and phospholipids in their structure, thus in the bulk, and prevent these lipids from reaching the interface. Therefore, the natural colloidal structure of plant lipids (oleosomes) should remain intact upon plant protein extraction.

Another major difference between the mildly and extensively derived protein concentrate is the protein composition. The conventional extensive protein extraction method mainly extracts the globulins and discards the side-streams containing albumins. Therefore, the plant protein transition in the food industry and academia is a plant globulin transition. An advantage of mild purification is the inclusion of albumins, which possess foaming properties as good as those of dairy proteins. By co-extracting both albumins and globulins, we were able to create higher and more stable foams compared to an extensively derived protein extract with mainly globulins. Also, there seems to be a synergy between rapeseed albumins and globulins in emulsions[50]. Additionally, in gelled systems, a mildly derived pea protein extract formed stiffer gels than an extensively derived one[41]. In the latter case, the processing probably played a more substantial role, as more extensive purification led to the formation of large aggregates by globulins, and resulted in the formation of weaker gels. The culprit of this protein alteration is most likely the isoelectric point precipitation step, which was previously found to alter the protein structure and solubility[38,39,206]. Therefore, isoelectric point precipitation should be avoided in protein extraction, which is, for instance, not included in our mild purification extraction method.

For a long time, more sustainable and mild purification methods were neglected due to the presence of non-proteinaceous components. Sustainability and functionality were argued to be conflicting, but we proved the opposite. The conventional wet extraction method is harming protein structure and functionality, whereas mild purification is able to retain protein nativity to a certain extent. Also, the presence of non-proteinaceous components was found to be negligible with regard to protein functionality. Next to a sustainability gain, mild purification also possesses a functionality gain. The field of food science and industry should further explore the possibilities of mild protein extraction methods. The current focus on producing protein ingredients with high protein purities has to be abandoned, while the new aim should focus on obtaining ingredient mixtures with good functional properties. Additionally, we usually try to produce an all-purpose protein ingredient with good gelling, foaming and emulsifying properties. We could also consider performing targeted

purification/fractionation of proteins (albumins or globulins, or a mixture) to obtain protein extracts with specific functional properties instead.

In this thesis, we were able to link specific steps of plant protein extraction processes to the molecular properties of the protein extracts. Simultaneously, the molecular properties explained the macroscopic properties, which were bridged by the mesoscopic scale, the interface properties. By applying this multi-length scale approach, we demonstrated the contribution of non-proteinaceous components in mildly derived protein extracts, which can be present under several conditions, as mentioned in this section. Therefore, we present mild purification as a tool to achieve more sustainable plant protein ingredients with promising and target functional properties.

7.8 Outlook and recommendations

Plant protein research is a major topic in food science. Each of these studies usually focuses on one or several plant sources, often with the aim to show interesting/promising functional properties. However, most studies apply slight differences in protein extraction methods or analysis of functional properties. These differences complicate relevant comparisons between studies, whereas we should start focusing on unravelling the general properties of plant proteins. Such recurring properties could be linked to protein functionality and will accelerate the advances in the plant protein transition. At this point, plant proteins are commonly compared to animal-derived proteins in terms of molecular and functional properties. This comparison is performed as animal proteins have been more extensively studied, but both proteins have very different roles in their original systems. Therefore, we should aim to better understand the plant proteins, and make good use of their intrinsic properties, instead of comparing them to animal ones. Future studies should aim to investigate multiple plant protein sources with a systematic methodology, thereby revealing plant protein (molecular) properties that contribute to good functional properties.

On the other hand, it is also important to understand why plant proteins are not able to provide the desired functional properties, as such understanding could allow for the application of targeted modifications, such as enzymatic hydrolysis and addition of functional groups, but also the addition of other functional ingredients. Another important note is involving other scientific fields in the plant protein transition in foods. For instance, plant science, which has studied plant proteins and non-proteinaceous plant ingredients extensively, thus acquired a vast amount of knowledge on plant-based ingredients. Both fields should collaborate, and an example topic could be investigating the influence of growing conditions of plant crops on the composition of protein extracts, thus on protein functionality. Such insights would allow the modification of the source material, which has not received much attention yet. Collaborations between plant and food science would yield promising insights on plant protein functionality research from a food perspective.

Another focus in plant protein functionality studies should be the contribution of non-proteinaceous components in the plant protein extracts. Non-proteinaceous components, such as lipids and phenols, are generally present in plant protein extracts, especially in mildly derived extracts, but also extensively derived extracts may still contain substantial amounts of non-protein components. The impact of these components has not been extensively examined, and these systems are often considered too complicated for accurate analysis. In this thesis, we have indeed encountered multiple challenges in studying protein – phenol or lipid mixtures. Nonetheless, the system conditions or methodology could always be optimized, which allowed us to produce accurate and reproducible results. With the current methodological and technical advances, we should aim to investigate more complex

plant mixtures. The focus should also be on finding generalities in mixtures, which could, for instance, explain the differences in phenol-protein aggregation between whey and rapeseed proteins in this work.

In this thesis, we provided a methodology to study the earlier mentioned complex plant mixtures: a multi-length scale approach. The first step in this approach is a compositional analysis, which is key information to understand the larger-scale properties of the entire mixture. The next step is studying the molecular properties of the components, such as chemical structure, size, hydrophobicity, and intermolecular interactions. The intermediate length scale is the mesoscopic one, and for multiphase systems, such as foams and emulsions, this is the interface. The largest length scale is the macroscopic properties, such as gelling, emulsifying and foaming. The strength of the multi-length scale approach is effectively bridging the molecular and macroscopic length scale by the mesoscopic one. At this length scale, the interfacial properties were analysed in our work by a combination of nonlinear rheology and microstructure imaging. The applied deformations in the dilatational deformations in this work were mostly in the nonlinear regime. In the majority of interfacial studies, only one deformation amplitude is evaluated with dilatational rheology, while studying the amplitude dependence (in the nonlinear viscoelastic regime) with amplitude sweeps yields a more accurate insight on the material properties of the interface. We also recommend the analysis of oscillatory deformations using Lissajous plots. In this work, we have proven the usefulness of these figures, as more details are exposed when studying the raw signal of the deformations compared to only evaluating surface moduli. Needless to say, Lissajous plots are also an adequate tool to analyse nonlinearities in surface shear and bulk rheology.

A strong addition to rheological properties is the evaluation of the interfacial microstructure. We performed such analysis by producing Langmuir-Blodgett films of the interfacial layers, which can be analysed by atomic force or scanning electron microscopy. An insight into the microstructure assisted us distinctly in understanding the rheological properties of the interfacial layers. A combination of interfacial rheology and microstructure imaging is a powerful toolset to reveal the interfacial properties, especially of mixed systems. Such tools enable us to further explore the secrets of the interface, which is a crucial link in the multi-length scale approach. In this thesis, we proved the usefulness of such an approach, especially in systems that are considered too complicated for analysis. This toolset is key in linking molecular properties to macroscopic functionalities, allowing us to link the degree of protein purification to molecular, interfacial, and foaming properties. Our approach can substantially expand the knowledge on plant protein functionality and thereby accelerate the protein transition.

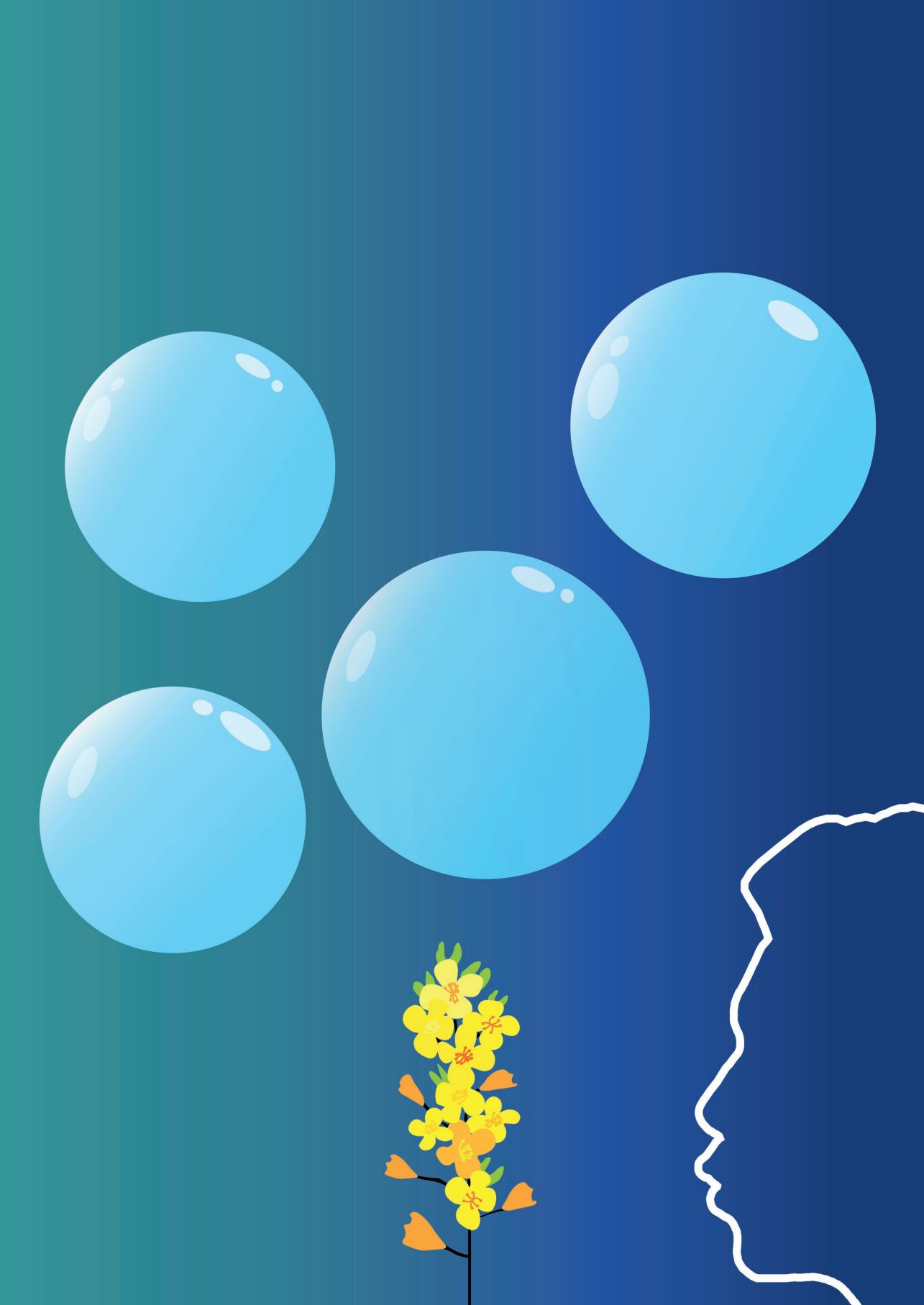

References

1. Tripathi, A. D., Mishra, R., Maurya, K. K., Singh, R. B. & Wilson, D. W. *Estimates for world population and global food availability for global health*. *The Role of Functional Food Security in Global Health* (Elsevier Inc., 2018). doi:10.1016/B978-0-12-813148-0.00001-3
2. Poore, J. & Nemecek, T. Reducing food's environmental impacts through producers and consumers. *Science (80-.).* **360**, 987–992 (2018).
3. FAO. *The state of the world's land and water resources for food and agriculture*. (2011). doi:http://www.fao.org/3/a-i1688e.pdf
4. Ellis, E. C., Goldewijk, K. K., Siebert, S., Lightman, D. & Ramankutty, N. Anthropogenic transformation of the biomes, 1700 to 2000. *Glob. Ecol. Biogeogr.* **19**, 589–606 (2010).
5. Arjen Y. Hoekstra. The water footprint of food. 4 (2008).
6. Friel, S. *et al.* Public health benefits of strategies to reduce greenhouse-gas emissions: food and agriculture. *Lancet* **374**, 2016–2025 (2009).
7. Aiking, H. & de Boer, J. The next protein transition. *Trends Food Sci. Technol.* **105**, 515–522 (2018).
8. Stehfest, E. *et al.* Climate benefits of changing diet. *Clim. Change* **95**, 83–102 (2009).
9. Worldwide oilseed production in 2019/2020, by type. *US department of Agriculture* (2020).
10. Aider, M. & Barbana, C. Canola proteins: Composition, extraction, functional properties, bioactivity, applications as a food ingredient and allergenicity - A practical and critical review. *Trends Food Sci. Technol.* **22**, 21–39 (2011).
11. Wanasundara, J. P. D. Proteins of brassicaceae oilseeds and their potential as a plant protein source. *Crit. Rev. Food Sci. Nutr.* **51**, 635–677 (2011).
12. Naczk, M., Amarowicz, R., Sullivan, A. & Shahidi, F. Current research developments on polyphenolics of rapeseed/canola: A review. *Food Chem.* **62**, 489–502 (1998).
13. Thiyam, U., Claudia, P., Jan, U. & Alfred, B. De-oiled rapeseed and a protein isolate: Characterization of sinapic acid derivatives by HPLC-DAD and LC-MS. *Eur. Food Res. Technol.* **229**, 825–831 (2009).
14. Osborne, T. B. *The vegetable proteins*. *Longmans green and co* (1924).
15. Chéreau, D. *et al.* Combination of existing and alternative technologies to promote oilseeds and pulses proteins in food applications. *OCL - Oilseeds fats, Crop. Lipids* **41**, (2016).
16. Karaca, A. C., Low, N. & Nickerson, M. Emulsifying properties of chickpea, faba bean, lentil and pea proteins produced by isoelectric precipitation and salt extraction. *Food Res. Int.* **44**, 2742–2750 (2011).
17. Shevkani, K., Singh, N., Kaur, A. & Rana, J. C. Structural and functional characterization of kidney bean and field pea protein isolates: A comparative study. *Food Hydrocoll.* **43**, 679–689 (2015).
18. Perera, S., McIntosh, T. & Wanasundara, J. Structural Properties of Cruciferin and Napin of Brassica napus (Canola) Show Distinct Responses to Changes in pH and Temperature. *Plants* **5**, 36 (2016).
19. Gonzalez-Perez, S., Vereijken, J. M., van Koningsveld, G. A., Gruppen, H. & Voragen, A. G. J. Physicochemical Properties of 2S albumins and the corresponding protein isolate from Sunflower (Helianthus annuus). *Food Chem. Toxicol.* **70**, C98–C103 (2005).
20. Gonzalez-Perez, S. & Vereijken, J. M. Sunflower proteins: overview of their physicochemical, structural and functional properties. *J. Sci. Food Agric.* **87**, 2173–2191 (2007).
21. Nietzel, T. *et al.* The native structure and composition of the cruciferin complex in brassica napus. *J. Biol. Chem.* **288**, 2238–2245 (2013).
22. Nikiforidis, C. V. Structure and functions of oleosomes (oil bodies). *Adv. Colloid Interface Sci.* **274**, 102039 (2019).
23. Frandsen, G. I., Mundy, J. & Tzen, J. T. C. Oil bodies and their associated proteins, oleosin and caleosin. *Physiol. Plant.* **112**, 301–307 (2001).
24. Tzen, J. T. C. & Huang, A. H. C. Surface structure and properties of plant seed oil bodies. *J. Cell Biol.* **117**, 327–335 (1992).
25. Karkani, O. A., Nenadis, N., Nikiforidis, C. V. & Kiosseoglou, V. Effect of recovery methods on the oxidative and physical stability of oil body emulsions. *Food Chem.* **139**, 640–648 (2013).
26. Kapchie, V. N., Yao, L., Hauck, C. C., Wang, T. & Murphy, P. A. Oxidative stability of soybean oil in oleosomes as affected by pH and iron. *Food Chem.* **141**, 2286–2293 (2013).
27. Ding, J. *et al.* Thermally treated soya bean oleosomes: the changes in their stability and associated proteins. *Int. J. Food Sci. Technol.* **55**, 229–238 (2020).

28. Ding, J. *et al.* The physicochemical properties and gastrointestinal fate of oleosomes from non-heated and heated soymilk. *Food Hydrocoll.* **100**, 105418 (2020).
29. Romero-Guzmán, M. J., Köllmann, N., Zhang, L., Boom, R. M. & Nikiforidis, C. V. Controlled oleosome extraction to produce a plant-based mayonnaise-like emulsion using solely rapeseed seeds. *Lwt* **123**, 109120 (2020).
30. Shahidi, F. & Senadheera, R. *Encyclopedia of Food Chemistry: Protein–Phenol Interactions*. *Encyclopedia of Food Chemistry* **2**, (Elsevier, 2019).
31. Cai, R., Arntfield, S. D. & Charlton, J. L. Structural changes of sinapic acid during alkali-induced air oxidation and the development of colored substances. *JAOCS, J. Am. Oil Chem. Soc.* **76**, 757–764 (1999).
32. Naczk, M., Oickle, D., Pink, D. & Shahidi, F. Protein Precipitating Capacity of Crude Canola Tannins: Effect of pH, Tannin, and Protein Concentrations. *J. Agric. Food Chem.* **44**, 2144–2148 (1996).
33. Keppler, J. K., Schwarz, K. & van der Goot, A. J. Covalent modification of food proteins by plant-based ingredients (polyphenols and organosulphur compounds): A commonplace reaction with novel utilization potential. *Trends Food Sci. Technol.* **101**, 38–49 (2020).
34. Sari, Y. W., Mulder, W. J., Sanders, J. P. M. & Bruins, M. E. Towards plant protein refinery: Review on protein extraction using alkali and potential enzymatic assistance. *Biotechnol. J.* **10**, 1138–1157 (2015).
35. Chua, J. Y. & Liu, S. Q. Soy whey: More than just wastewater from tofu and soy protein isolate industry. *Trends Food Sci. Technol.* **91**, 24–32 (2019).
36. Souza, P. F. N. The forgotten 2S albumin proteins: Importance, structure, and biotechnological application in agriculture and human health. *Int. J. Biol. Macromol.* **164**, 4638–4649 (2020).
37. González-Pérez, S., Vereijken, J. M., Van Koningsveld, G. A., Gruppen, H. & Voragen, A. G. J. Formation and stability of foams made with sunflower (Helianthus annuus) proteins. *J. Agric. Food Chem.* **53**, 6469–6476 (2005).
38. Kornet, C. *et al.* Yellow pea aqueous fractionation increases the specific volume fraction and viscosity of its dispersions. *Food Hydrocoll.* **99**, 105332 (2020).
39. Jiang, J., Chen, J. & Xiong, Y. L. Structural and emulsifying properties of soy protein isolate subjected to acid and alkaline pH-shifting processes. *J. Agric. Food Chem.* **57**, 7576–7583 (2009).
40. Geerts, M. E. J., Nikiforidis, C. V., van der Goot, A. J. & van der Padt, A. Protein nativity explains emulsifying properties of aqueous extracted protein components from yellow pea. *Food Struct.* **14**, 104–111 (2017).
41. Kornet, R. *et al.* Less is more: Limited fractionation yields stronger gels for pea proteins. *Food Hydrocoll.* **112**, 106285 (2021).
42. L'Hocine, L., Boye, J. I. & Arcand, Y. Composition and functional properties of soy protein isolates prepared using alternative defatting and extraction procedures. *J. Food Sci.* **71**, (2006).
43. Ntone, E., Bitter, J. H. & Nikiforidis, C. V. Not sequentially but simultaneously: Facile extraction of proteins and oleosomes from oilseeds. *Food Hydrocoll.* **102**, 105598 (2020).
44. Karefyllakis, D., Octaviana, H., van der Goot, A. J. & Nikiforidis, C. V. The emulsifying performance of mildly derived mixtures from sunflower seeds. *Food Hydrocoll.* **88**, 75–85 (2019).
45. Pelgrom, P. J. M., Boom, R. M. & Schutyser, M. A. I. Functional analysis of mildly refined fractions from yellow pea. *Food Hydrocoll.* **44**, 12–22 (2014).
46. Berton-carabin, C. C., Sagis, L. & Schroën, K. Formation , Structure , and Functionality of Interfacial Layers in Food Emulsions. *Annu. Rev. Food Sci. Technol.* **9**, 551–87 (2018).
47. Narsimhan, G. & Xiang, N. Role of Proteins on Formation, Drainage, and Stability of Liquid Food Foams. *Annu. Rev. Food Sci. Technol.* **9**, 45–63 (2018).
48. Dickinson, E. Adsorbed protein layers at fluid interfaces: Interactions, structure and surface rheology. *Colloids Surfaces B Biointerfaces* **15**, 161–176 (1999).
49. Beverung, C. J., Radke, C. J. & Blanch, H. W. Protein adsorption at the oil/water interface: Characterization of adsorption kinetics by dynamic interfacial tension measurements. *Biophys. Chem.* **81**, 59–80 (1999).
50. Ntone, E. *et al.* Adsorption of rapeseed proteins at oil / water interfaces . Janus-like napins dominate the interface. *J. Colloid Interface Sci.* **583**, 459–469 (2021).
51. Wierenga, P. A., Meinders, M. B. J., Egmond, M. R., Voragen, F. A. G. J. & Jongh, H. H. J. de. Protein Exposed Hydrophobicity Reduces the Kinetic Barrier for Adsorption of Ovalbumin to the Air-Water Interface. *Langmuir* **19**, 8964–8970 (2003).
52. Sagis, L. M. C. & Scholten, E. Complex interfaces in food: Structure and mechanical properties.

Trends Food Sci. Technol. **37**, 59–71 (2014).

53. Bos, M. A. & van Vliet, T. Interfacial rheological properties of adsorbed protein layers and surfactants: a review. *Adv. Colloid Interface Sci.* **91**, 437–471 (2001).
54. Foegeding, E. A. & Davis, J. P. Food protein functionality: A comprehensive approach. *Food Hydrocoll.* (2011). doi:10.1016/j.foodhyd.2011.05.008
55. Rühs, P. A., Scheuble, N., Windhab, E. J. & Fischer, P. Protein adsorption and interfacial rheology interfering in dilatational experiment. *Eur. Phys. J. Spec. Top.* **222**, 47–60 (2013).
56. Rullier, B., Novales, B. & Axelos, M. A. V. Effect of protein aggregates on foaming properties of β-lactoglobulin. *Colloids Surfaces A Physicochem. Eng. Asp.* **330**, 96–102 (2008).
57. Hyun, K., Kim, S. H., Ahn, K. H. & Lee, S. J. Large amplitude oscillatory shear as a way to classify the complex fluids. *J. Nonnewton. Fluid Mech.* **107**, 51–65 (2002).
58. Ewoldt, R. H., Hosoi, A. E. & McKinley, G. H. New measures for characterizing nonlinear viscoelasticity in large amplitude oscillatory shear. *J. Rheol. (N. Y. N. Y).* **52**, 1427–1458 (2007).
59. Sagis, L. M. C., Humblet-Hua, K. N. P. & van Kempen, S. E. H. J. Nonlinear stress deformation behavior of interfaces stabilized by food-based ingredients. *J. Physics-Condensed Matter* **26**, 9 (2014).
60. Bykov, A. G. *et al.* Surface dilational rheological properties in the nonlinear domain. *Adv. Colloid Interface Sci.* **222**, 110–118 (2015).
61. Zhang, H., Cui, G. & Li, J. Morphological investigation of mixed protein/phospholipid monolayers. *Colloids Surfaces A Physicochem. Eng. Asp.* **201**, 123–129 (2002).
62. Waschatko, G., Junghans, A. & Vilgis, T. A. Soy milk oleosome behaviour at the air-water interface. *Faraday Discuss.* **158**, 157–169 (2012).
63. Glomm, W. R., Volden, S., Halskau, Ø. & Ese, M. H. G. Same system-different results: The importance of protein-introduction protocols in Langmuir-monolayer studies of lipid-protein interactions. *Anal. Chem.* **81**, 3042–3050 (2009).
64. Crawford, N. F. & Leblanc, R. M. Serum albumin in 2D: A Langmuir monolayer approach. *Adv. Colloid Interface Sci.* **207**, 131–138 (2014).
65. Zou, Y. *et al.* Tunable assembly of hydrophobic protein nanoparticle at fluid interfaces with tannic acid. *Food Hydrocoll.* **63**, 364–371 (2017).
66. Mackie, A. R., Gunning, A. P., Wilde, P. J. & Morris, V. J. Orogenic Displacement of Protein from the Air/Water Interface by Competitive Adsorption. *J. Colloid Interface Sci.* **210**, 157–166 (1999).
67. Morris, V. J. *Atomic force microscopy (AFM) and related tools for the imaging of foods and beverages on the nanoscale*. *Nanotechnology in the Food, Beverage and Nutraceutical Industries* (Woodhead Publishing Limited, 2012). doi:10.1016/B978-1-84569-739-6.50005-8
68. Wilde, P. J. *et al.* Destabilization of beer foam by lipids: Structural and interfacial effects. *J. Am. Soc. Brew. Chem.* **61**, 196–202 (2003).
69. Maldonado-Valderrama, J. & Patino, J. M. R. Interfacial rheology of protein–surfactant mixtures. *Curr. Opin. Colloid Interface Sci.* **15**, 271–282 (2010).
70. Waschatko, G., Schiedt, B., Vilgis, T. A. & Junghans, A. Soybean Oleosomes Behavior at the Air – Water Interface. *J. Phys. Chem. B* **116**, (2012).
71. Denkov, N. D. Mechanisms of foam destruction by oil-based antifoams. *Langmuir* **20**, 9463–9505 (2004).
72. Denkov, N. D. & Marinova, K. G. Antifoam effects of solid particles, oil drops and oil–solid compounds in aqueous foams. in *Colloidal Particles at Liquid Interfaces* 383–444 (2006). doi:10.1017/CBO9780511536670.011
73. Xu, L. & Diosady, L. L. Interactions between canola proteins and phenolic compounds in aqueous media. *Food Res. Int.* **33**, 725–731 (2000).
74. Czubinski, J. & Dwiecki, K. A review of methods used for investigation of protein–phenolic compound interactions. *Int. J. Food Sci. Technol.* **52**, 573–585 (2017).
75. Das Purkayastha, M. *et al.* Physicochemical and functional properties of rapeseed protein isolate: Influence of antinutrient removal with acidified organic solvents from rapeseed meal. *J. Agric. Food Chem.* **62**, 7903–7914 (2014).
76. Wei, Z., Yang, W., Fan, R., Yuan, F. & Gao, Y. Evaluation of structural and functional properties of protein-EGCG complexes and their ability of stabilizing a model β-carotene emulsion. *Food Hydrocoll.* **45**, 337–350 (2015).
77. Yang, W., Liu, F., Xu, C., Yuan, F. & Gao, Y. Molecular interaction between (-)-epigallocatechin-3-gallate and bovine lactoferrin using multi-spectroscopic method and isothermal titration calorimetry. *Food Res. Int.* **64**, 141–149 (2014).
78. Cao, Y., Xiong, Y. L., Cao, Y. & True, A. D. Interfacial properties of whey protein foams as

influenced by preheating and phenolic binding at neutral pH. *Food Hydrocoll.* **82**, 379–387 (2018).

79. Cao, Y. & Xiong, Y. L. Interaction of Whey Proteins with Phenolic Derivatives Under Neutral and Acidic pH Conditions. *J. Food Sci.* **82**, 409–419 (2017).
80. Zhang, H. *et al.* Interaction of milk whey protein with common phenolic acids. *J. Mol. Struct.* **1058**, 228–233 (2014).
81. Jia, Z. *et al.* Effect of covalent modification by (-)-epigallocatechin-3-gallate on physicochemical and functional properties of whey protein isolate. *LWT - Food Sci. Technol.* **66**, 305–310 (2016).
82. Karefyllakis, D., Salakou, S., Bitter, J. H., van der Goot, A. J. & Nikiforidis, C. V. Covalent Bonding of Chlorogenic Acid Induces Structural Modifications on Sunflower Proteins. *ChemPhysChem* **19**, 459–468 (2018).
83. Pringent, S. V. E., Voragen, A. G. J., Visser, A. J. W. G., van Koningsveld, G. A. & Gruppen, H. Covalent interactions between proteins and oxidation products of caffeoylquinic acid (chlorogenic acid). *J. Sci. Food Agric.* **87**, 2502–2510 (2007).
84. Rodríguez, S. D., von Staszewski, M. & Pilosof, A. M. R. Green tea polyphenols-whey proteins nanoparticles: Bulk, interfacial and foaming behavior. *Food Hydrocoll.* **50**, 108–115 (2015).
85. Rullier, B., Axelos, M. a V, Langevin, D. & Novales, B. β-Lactoglobulin aggregates in foam films: Correlation between foam films and foaming properties. *J. Colloid Interface Sci.* **336**, 750–755 (2009).
86. Jiang, J., Zhang, Z., Zhao, J. & Liu, Y. The effect of non-covalent interaction of chlorogenic acid with whey protein and casein on physicochemical and radical-scavenging activity of in vitro protein digests. *Food Chem.* **268**, 334–341 (2018).
87. Lamminen, M., Halmemies-Beauchet-Filleau, A., Kokkonen, T., Vanhatalo, A. & Jaakkola, S. The effect of partial substitution of rapeseed meal and faba beans by Spirulina platensis microalgae on milk production, nitrogen utilization, and amino acid metabolism of lactating dairy cows. *J. Dairy Sci.* **102**, 7102–7117 (2019).
88. Krause, J. P. & Schwenke, K. D. Behaviour of a protein isolate from rapeseed (Brassica napus) and its main protein components - Globulin and albumin - At air/solution and solid interfaces, and in emulsions. *Colloids Surfaces B Biointerfaces* **21**, 29–36 (2001).
89. Wu, J. & Muir, A. D. Comparative structural, emulsifying, and biological properties of 2 major canola proteins, cruciferin and napin. *J. Food Sci.* **73**, 210–216 (2008).
90. Cheung, L., Wanasundara, J. & Nickerson, M. T. Effect of pH and NaCl on the Emulsifying Properties of a Napin Protein Isolate. *Food Biophys.* **10**, 30–38 (2014).
91. Cheung, L., Wanasundara, J. & Nickerson, M. T. The Effect of pH and NaCl Levels on the Physicochemical and Emulsifying Properties of a Cruciferin Protein Isolate. *Food Biophys.* **9**, 105–113 (2014).
92. Larré, C. *et al.* Characterisation and foaming properties of hydrolysates derived from rapeseed isolate. *Colloids Surfaces B Biointerfaces* **49**, 40–48 (2006).
93. Tan, S. H., Mailer, R. J., Blanchard, C. L., Agboola, S. O. & Day, L. Gelling properties of protein fractions and protein isolate extracted from Australian canola meal. *Food Res. Int.* **62**, 819–828 (2014).
94. Tan, S. H., Mailer, R. J., Blanchard, C. L. & Agboola, S. O. Emulsifying properties of proteins extracted from Australian canola meal. *LWT - Food Sci. Technol.* **57**, 376–382 (2014).
95. Bérot, S., Compoint, J. P., Larré, C., Malabat, C. & Guéguen, J. Large scale purification of rapeseed proteins (Brassica napus L.). *J. Chromatogr. B* **818**, 35–42 (2005).
96. Malabat, C., nchez-Vioque, R. I. S., Rabiller, C. & Gu guen, J. Emulsifying and foaming properties of native and chemically modified peptides from the 2S and 12S proteins of rapeseed (Brassica napus L.). *J. Am. Oil Chem. Soc.* **78**, 235–242 (2001).
97. Aluko, R. E. & McIntosh, T. Electrophoretic and functional properties of mustard seed meals and protein concentrates. *JAOCS, J. Am. Oil Chem. Soc.* **81**, 679–683 (2004).
98. Aluko, R. E., McIntosh, T. & Katepa-Mupondwa, F. Comparative study of the polypeptide profiles and functional properties of Sinapis alba and Brassica juncea seed meals and protein concentrates. *J. Sci. Food Agric.* **85**, 1931–1937 (2005).
99. Estrada, P. D. *et al.* Protein Oxidation in Plant Protein-Based Fibrous Products: Effects of Encapsulated Iron and Process Conditions. *J. Agric. Food Chem.* **66**, 11105–11112 (2018).
100. Fetzer, A., Herfellner, T. & Eisner, P. Rapeseed protein concentrates for non-food applications prepared from pre-pressed and cold-pressed press cake via acidic precipitation and ultrafiltration. *Ind. Crops Prod.* **132**, 396–406 (2019).
101. Nikiforidis, C. V. *et al.* Purified oleosins at air-water interfaces. *Soft Matter* **9**, 1354–1363 (2013).
102. Karefyllakis, D., Van Der Goot, A. J. & Nikiforidis, C. V. The behaviour of sunflower oleosomes at the interfaces. *Soft Matter* **15**, 4639–4646 (2019).

103. Yang, J., Thielen, I., Berton-Carabin, C. C., van der Linden, E. & Sagis, L. M. C. Nonlinear interfacial rheology and atomic force microscopy of air-water interfaces stabilized by whey protein beads and their constituents. *Food Hydrocoll.* **101**, 105466 (2020).

104. Jaishankar, A. & McKinley, G. H. Power-law rheology in the bulk and at the interface: quasi-properties and fractional constitutive equations. *Proc. R. Soc. A* **469**, 20120284–20120284 (2012).

105. Chen, M. & Sagis, L. M. C. The influence of protein/phospholipid ratio on the physicochemical and interfacial properties of biomimetic milk fat globules. *Food Hydrocoll.* **97**, 105179 (2019).

106. Waninge, R. *et al.* Competitive adsorption between β-casein or β-lactoglobulin and model milk membrane lipids at oil-water interface. *J. Agric. Food Chem.* **53**, 716–724 (2005).

107. Watts, C. & Davies, E. Non-Symmetrical Dielectric Relaxation Behaviour Arising from a Simple Empirical Decay Function. *Trans. Faraday Soc.* **66**, 80–85 (1969).

108. Sagis, L. M. C. *et al.* Dynamic heterogeneity in complex interfaces of soft interface-dominated materials. *Sci. Rep.* **9**, 1–12 (2019).

109. Felix, M., Yang, J., Guerrero, A. & Sagis, L. M. C. Effect of cinnamaldehyde on interfacial rheological properties of proteins adsorbed at O/W interfaces. *Food Hydrocoll.* **97**, 105235 (2019).

110. Cicuta, P. Compression and shear surface rheology in spread layers of β-casein and β-lactoglobulin. *J. Colloid Interface Sci.* **308**, 93–99 (2007).

111. Klafter, J. & Shlesinger, M. F. On the Relationship among Three Theories of Relaxation in Disordered. *Proc. Natl. Acad. Sci. U. S. A.* **83**, 848–851 (1986).

112. Berton-Carabin, C., Genot, C., Gaillard, C., Guibert, D. & Ropers, M. H. Design of interfacial films to control lipid oxidation in oil-in-water emulsions. *Food Hydrocoll.* **33**, 99–105 (2013).

113. Sah, B. K. & Kundu, S. Modification of hysteresis behaviors of protein monolayer and the corresponding structures with the variation of protein surface charges. *Colloids Surfaces B Biointerfaces* **159**, 696–704 (2017).

114. Maldonado-Valderrama, J. & Patino, J. M. R. Interfacial rheology of protein-surfactant mixtures. *Curr. Opin. Colloid Interface Sci.* **15**, 271–282 (2010).

115. Campbell, G. M. & Mougeot, E. Creation and characterisation of aerated food products. *Trends Food Sci. Technol.* **10**, 283–296 (1999).

116. Dickinson, E. Mixed biopolymers at interfaces: Competitive adsorption and multilayer structures. *Food Hydrocoll.* **25**, 1966–1983 (2011).

117. Humblet-Hua, N.-P. K., van der Linden, E. & Sagis, L. M. C. Surface rheological properties of liquid–liquid interfaces stabilized by protein fibrillar aggregates and protein–polysaccharide complexes. *Soft Matter* **9**, 2154–2165 (2013).

118. Langevin, D. Rheology of Adsorbed Surfactant Monolayers at Fluid Surfaces. *Annu. Rev. Fluids Mech.* **46**, 47–65 (2014).

119. Pickering, S. U. Pickering: Emulsions. *J. Chem. Soc.* **91**, 2001–2021 (1907).

120. Dickinson, E. Food emulsions and foams : Stabilization by particles. *Curr. Opin. Colloid Interface Sci.* **15**, 40–49 (2010).

121. Berton-Carabin, C. C. & Schroën, K. Pickering emulsions for food applications: background, trends, and challenges. *Annu. Rev. Food Sci. Technol.* **6**, 263–97 (2015).

122. Wu, J. *et al.* Pickering emulsions stabilized by whey protein nanoparticles prepared by thermal cross-linking. *Colloids Surfaces B Biointerfaces* **127**, 96–104 (2015).

123. Destribats, M., Rouvet, M., Gehin-Delval, C., Schmitt, C. & Binks, B. P. Emulsions stabilised by whey protein microgel particles: towards food-grade Pickering emulsions. *Soft Matter* **10**, 6941–54 (2014).

124. Shimoni, G., Levi, C. S., Tal, S. L. & Lesmes, U. Food Hydrocolloids Emulsions stabilization by lactoferrin nano-particles under in vitro digestion conditions. *Food Hydrocoll.* **33**, 264–272 (2013).

125. Chen, M. *et al.* Interfacial properties, thin film stability and foam stability of casein micelle dispersions. *Colloids Surfaces B Biointerfaces* **149**, 56–63 (2017).

126. Dhayal, S. K., Delahaije, R. J. B. M., de Vries, R. J., Gruppen, H. & Wierenga, P. A. Enzymatic cross-linking of α-lactalbumin to produce nanoparticles with increased foam stability. *Soft Matter* **11**, 7888–7898 (2015).

127. Liu, F. & Tang, C.-H. Emulsifying Properties of Soy Protein Nanoparticles: Influence of the Protein Concentration and/or Emulsification Process. *J. Agric. Food Chem.* **62**, 2644–2654 (2014).

128. Sarkar, A. *et al.* In vitro digestion of Pickering emulsions stabilized by soft whey protein microgel particles: influence of thermal treatment. *Soft Matter* **12**, 3558–69 (2016).

129. van Leusden, P. *et al.* Strength of microbeads for the encapsulation of heat sensitive,

hydrophobic components. *Food Hydrocoll.* **56**, 318–324 (2016).

130. Beaulieu, L., Savoie, L., Paquin, P. & Subirade, M. Elaboration and characterization of whey protein beads by an emulsification/cold gelation process: Application for the protection of retinol. *Biomacromolecules* **3**, 239–248 (2002).
131. Wan, Z., Yang, X. & Sagis, L. M. C. Contribution of Long Fibrils and Peptides to Surface and Foaming Behavior of Soy Protein Fibril System. *Langmuir* **32**, 8092–8101 (2016).
132. Butré, C. I., Wierenga, P. a. & Gruppen, H. Effects of ionic strength on the enzymatic hydrolysis of diluted and concentrated whey protein isolate. *J. Agric. Food Chem.* **60**, 5644–5651 (2012).
133. Paques, J. P., Van der Linden, E., Van Rijn, C. J. M. & Sagis, L. M. C. Alginate submicron beads prepared through w/o emulsification and gelation with CaCl2 nanoparticles. *Food Hydrocoll.* **31**, 428–434 (2013).
134. Vandebril, S., Franck, A., Fuller, G. G., Moldenaers, P. & Vermant, J. A double wall-ring geometry for interfacial shear rheometry. *Rheol. Acta* **49**, 131–144 (2010).
135. van Kempen, S. E. H. J., Schols, H. A., van der Linden, E. & Sagis, L. M. C. Non-linear surface dilatational rheology as a tool for understanding microstructures of air/water interfaces stabilized by oligofructose fatty acid esters. *Soft Matter* **9**, 9579 (2013).
136. Betz, M., Josef, H., Fuchs, T. & Kulozik, U. Swelling behaviour, charge and mesh size of thermal protein hydrogels as influenced by pH during gelation. *Soft Matter* **8**, 2477–2485 (2012).
137. Aymard, P., Durand, D. & Nicolai, T. The effect of temperature and ionic strength on the dimerisation of β-lactoglobulin. *Int. J. Biol. Macromol.* **19**, 213–221 (1996).
138. Erickson, H. P. Size and shape of protein molecules at the nanometer level determined by sedimentation, gel filtration, and electron microscopy. *Biol. Proced. Online* **11**, 32–51 (2009).
139. Richtering, W. Responsive emulsions stabilized by stimuli-sensitive microgels: Emulsions with special non-pickering properties. *Langmuir* **28**, 17218–17229 (2012).
140. Winter, H. H. & Mours, M. Rheology of Polymers Near Liquid-Solid Transitions. *Neutron Spin Echo Spectrosc. Viscoelasticity Rheol.* **134**, 165–234 (1997).
141. Sollich, P. Rheological constitutive equation for a model of soft glassy materials. *Phys. Rev. E - Stat. Physics, Plasmas, Fluids, Relat. Interdiscip. Top.* **58**, 738–759 (1998).
142. Precha-Atsawanan, S., Uttapap, D. & Sagis, L. M. C. Linear and nonlinear rheological behavior of native and debranched waxy rice starch gels. *Food Hydrocoll.* **85**, 1–9 (2018).
143. Mermet-Guyennet, M. R. B. *et al.* LAOS: The strain softening/strain hardening paradox. *J. Rheol. (N. Y. N. Y).* **59**, 21–32 (2015).
144. Lucassen, J. & Van Den Tempel, M. Dynamic measurements of dilational properties of a liquid interface. *Chem. Eng. Sci.* **27**, 1283–1291 (1972).
145. Böttcher, S., Keppler, J. K. & Drusch, S. Mixtures of Quillaja saponin and beta-lactoglobulin at the oil/water-interface: Adsorption, interfacial rheology and emulsion properties. *Colloids Surfaces A Physicochem. Eng. Asp.* **518**, 46–56 (2017).
146. Schröder, A., Berton-Carabin, C., Venema, P. & Cornacchia, L. Interfacial properties of whey protein and whey protein hydrolysates and their influence on O/W emulsion stability. *Food Hydrocoll.* **73**, 129–140 (2017).
147. Davis, J. P., Doucet, D. & Foegeding, E. A. Foaming and interfacial properties of hydrolyzed β-lactoglobulin. *J. Colloid Interface Sci.* **288**, 412–422 (2005).
148. Rühs, P. A., Affolter, C., Windhab, E. J. & Fischer, P. Shear and dilatational linear and nonlinear subphase controlled interfacial rheology of β-lactoglobulin fibrils and their derivatives. *J. Rheol. (N. Y. N. Y).* **57**, 1003–1022 (2013).
149. Phillips, J. C. Stretched exponential relaxation in molecular and electronic glasses. *Reports Prog. Phys.* **59**, 1133–1207 (1996).
150. Gunning, A. P. *et al.* Atomic Force Microscopy of Interfacial Protein Films. *J. Colloid Interface Sci.* **183**, 600–602 (1996).
151. Tan, S. H., Mailer, R. J., Blanchard, C. L. & Agboola, S. O. Extraction and characterization of protein fractions from Australian canola meals. *Food Res. Int.* **44**, 1075–1082 (2011).
152. Yang, J. *et al.* Foams and air-water interfaces stabilised by mildly purified rapeseed proteins after defatting. *Food Hydrocoll.* **112**, 106270 (2020).
153. Tan, S. H., Mailer, R. J., Blanchard, C. L., Agboola, S. O. & Day, L. Gelling properties of protein fractions and protein isolate extracted from Australian canola meal. *Food Res. Int.* **62**, 819–828 (2014).
154. Naczk, M., Amarowicz, R. & Shahidi, F. Role of phenolics in flavor of rapeseed protein products. *Dev. Food Sci.* **40**, 597–613 (1998).
155. Li, X. *et al.* Characterization the non-covalent interactions between beta lactoglobulin and selected phenolic acids. *Food Hydrocoll.* **105**, 105761 (2020).

156. Jin, X. L. *et al.* Characterization of hydroxycinnamic acid derivatives binding to bovine serum albumin. *Org. Biomol. Chem.* **10**, 3424–3431 (2012).

157. von Staszewski, M., Pizones Ruiz-Henestrosa, V. M. & Pilosof, A. M. R. Green tea polyphenols-β-lactoglobulin nanocomplexes: Interfacial behavior, emulsification and oxidation stability of fish oil. *Food Hydrocoll.* **35**, 505–511 (2014).

158. Xu, L. & Diosady, L. L. Removal of phenolic compounds in the production of high-quality canola protein isolates. *Food Res. Int.* **35**, 23–30 (2002).

159. Seczyk, L., Swieca, M., Kapusta, I. & Gawlik-Dziki, U. Protein–phenolic interactions as a factor affecting the physicochemical properties of white bean proteins. *Molecules* **24**, 1–24 (2019).

160. Ozdal, T., Capanoglu, E. & Altay, F. A review on protein-phenolic interactions and associated changes. *Food Res. Int.* **51**, 954–970 (2013).

161. Kroll, J., Rawel, H. M. & Rohn, S. Reactions of Plant Phenolics with Food Proteins and Enzymes under Special Consideration of Covalent Bonds. *Food Sci. Technol. Res.* **9**, 205–218 (2003).

162. Miao, S. & Mao, L. DSC Application to Characterizing Food Emulsions. in *Differential Scanning Calorimetry Applications in Fat and Oil Technology* 243–272 (CRC, 2014). doi:10.1201/b17739-14

163. Ali, H., Alli, I., Ismail, A. & Kermasha, S. Protein-phenolic interactions in food. *Eurasian J. Anal. Chem.* **7**, 123–133 (2012).

164. Lech, F. J., Delahaije, R. J. B. M., Meinders, M. B. J., Gruppen, H. & Wierenga, P. A. Identification of critical concentrations determining foam ability and stability of β-lactoglobulin. *Food Hydrocoll.* **57**, 46–54 (2016).

165. Tzen, J. T. C. Integral Proteins in Plant Oil Bodies. *ISRN Bot.* **2012**, 1–16 (2012).

166. Tzen, J. T. C., Cao, Y. Z., Laurent, P., Ratnayake, C. & Huang, A. H. C. Lipids, proteins, and structure of seed oil bodies from diverse species. *Plant Physiol.* **101**, 267–276 (1993).

167. Pichot, R., Watson, R. L. & Norton, I. T. Phospholipids at the interface: Current trends and challenges. *Int. J. Mol. Sci.* **14**, 11767–11794 (2013).

168. Geerts, M. E. J., Mienis, E., Nikiforidis, C. V., van der Padt, A. & van der Goot, A. J. Mildly refined fractions of yellow peas show rich behaviour in thickened oil-in-water emulsions. *Innov. Food Sci. Emerg. Technol.* **41**, 251–258 (2017).

169. Ishii, T. *et al.* Interfacial and emulsifying properties of crude and purified soybean oil bodies. *Food Struct.* **12**, 64–72 (2017).

170. Zielbauer, B. I. *et al.* Soybean oleosomes studied by small angle neutron scattering (SANS). *J. Colloid Interface Sci.* **529**, 197–204 (2018).

171. Iwanaga, D. *et al.* Extraction and characterization of oil bodies from soy beans: A natural source of pre-emulsified soybean oil. *J. Agric. Food Chem.* **55**, 8711–8716 (2007).

172. Deleu, M. *et al.* Interfacial properties of oleosins and phospholipids from rapeseed for the stability of oil bodies in aqueous medium. *Colloids Surfaces B Biointerfaces* **80**, 125–132 (2010).

173. Wanasundara, J. P. D., McIntosh, T. C., Perera, S. P., Withana-Gamage, T. S. & Mitra, P. Canola/rapeseed protein-functionality and nutrition. *Ocl* **23**, D407 (2016).

174. Yang, J. *et al.* Air-water interfacial and foaming properties of whey protein - sinapic acid mixtures. *Food Hydrocoll.* **112**, 106467 (2021).

175. Romero-guzman, M. J., Louis, L. J., Kyriakopoulou, K., Boom, R. M. & Nikiforidis, C. V. Efficient single-step rapeseed oleosome extraction using twin-screw press. **276**, (2020).

176. Wanasundara, J. P. D., Abeysekara, S. J., McIntosh, T. C. & Falk, K. C. Solubility differences of major storage proteins of brassicaceae oilseeds. *JAOCS, J. Am. Oil Chem. Soc.* **89**, 869–881 (2012).

177. McClements, D. J. & Gumus, C. E. Natural emulsifiers — Biosurfactants, phospholipids, biopolymers, and colloidal particles: Molecular and physicochemical basis of functional performance. *Adv. Colloid Interface Sci.* **234**, 3–26 (2016).

178. Hildebrandt, E., Nirschl, H., Kok, R. J. & Leneweit, G. Adsorption of phospholipids at oil/water interfaces during emulsification is controlled by stress relaxation and diffusion. *Soft Matter* **14**, 3730–3737 (2018).

179. Kaganer, V. M., Hohwald, H. & Dutta, P. Structure and phase transitions in Langmuir monolayers.pdf. *Rev. Mod. Phys.* **71**, 779–819 (1999).

180. Giménez-Ribes, G., Habibi, M. & Sagis, L. M. C. Interfacial rheology and relaxation behavior of adsorption layers of the triterpenoid saponin Escin. *J. Colloid Interface Sci.* **563**, 281–290 (2020).

181. Golemanov, K., Tcholakova, S., Denkov, N., Pelan, E. & Stoyanov, S. D. Remarkably high surface visco-elasticity of adsorption layers of triterpenoid saponins. *Soft Matter* **9**, 5738 (2013).

182. Mackie, A. & Wilde, P. The role of interactions in defining the structure of mixed protein-

surfactant interfaces. *Adv. Colloid Interface Sci.* **117**, 3–13 (2005).

183. Dauphas, S., Beaumal, V., Riaublanc, A. & Anton, M. Hen egg yolk low-density lipoproteins film spreading at the air - water and oil - water interfaces. *J. Agric. Food Chem.* **54**, 3733–3737 (2006).
184. Dauphas, S. *et al.* Structure modification in hen egg yolk low density lipoproteins layers between 30 and 45 mN/m observed by AFM. *Colloids Surfaces B Biointerfaces* **54**, 241–248 (2007).
185. Anton, M. Egg yolk: Structures, functionalities and processes. *J. Sci. Food Agric.* **93**, 2871–2880 (2013).
186. Damude, H. G. & Kinney, A. J. Enhancing plant seed oils for human nutrition. *Plant Physiol.* **147**, 962–968 (2008).
187. Lin, L. *et al.* Evidence of health benefits of canola oil. *Nutr. Rev.* **71**, 370–385 (2013).
188. Tasan, M., Gecgel, U. & Demirci, M. Effects of storage and industrial oilseed extraction methods on the quality and stability characteristics of crude sunflower oil (Helianthus annuus L.). *Grasas y Aceites* **62**, 389–398 (2011).
189. Danlami, J. M., Arsad, A., Zaini, M. A. A. & Sulaiman, H. A comparative study of various oil extraction techniques from plants. *Rev. Chem. Eng.* **30**, 605–626 (2014).
190. Abdullah, Weiss, J. & Zhang, H. Recent advances in the composition, extraction and food applications of plant-derived oleosomes. *Trends Food Sci. Technol.* **106**, 322–332 (2020).
191. Damodaran, S. Protein Stabilization of Emulsions and Foams. *J. Food Sci.* **70**, R54–R66 (2005).
192. Foegeding, E. A., Luck, P. J. & Davis, J. P. Factors determining the physical properties of protein foams. *Food Hydrocoll.* **20**, 284–292 (2006).
193. Yang, J., Waardenburg, L. C., Berton-carabin, C. C., Nikiforidis, C. V. & van der Linden, E. Chapter 5 - mixed interfaces stabilised by whey protein - rapeseed lipid mixtures. *This thesis*
194. Caro, A. L., Niño, M. R. R. & Patino, J. M. R. The effect of pH on structural, topographical, and rheological characteristics of β-casein-DPPC mixed monolayers spread at the air-water interface. *Colloids Surfaces A Physicochem. Eng. Asp.* **332**, 180–191 (2009).
195. Aveyard, R., Beake, B. D. & Clint, J. H. Wettability of spherical particles at liquid surfaces. *J. Chem. Soc. - Faraday Trans.* **92**, 4271–4277 (1996).
196. Mariotti, F., Tomé, D. & Mirand, P. P. Converting nitrogen into protein - Beyond 6.25 and Jones' factors. *Crit. Rev. Food Sci. Nutr.* **48**, 177–184 (2008).
197. Wang, T. Soybean Processing. in *Encyclopedia of Grain Science* (ed. Wrigley, C.) 159–168 (Elsvier, 2004).
198. Nicolai, T., Britten, M. & Schmitt, C. β-Lactoglobulin and WPI aggregates: Formation, structure and applications. *Food Hydrocoll.* **25**, 1945–1962 (2011).
199. Wildermuth, S. R., Young, E. E. & Were, L. M. Chlorogenic Acid Oxidation and Its Reaction with Sunflower Proteins to Form Green-Colored Complexes. *Compr. Rev. Food Sci. Food Saf.* **15**, 829–843 (2016).
200. Duodu, K. G., Taylor, J. R. N., Belton, P. S. & Hamaker, B. R. Factors affecting sorghum protein digestibility. *J. Cereal Sci.* **38**, 117–131 (2003).
201. Swanson, B. G. Pea and lentil protein extraction and functionality. *J. Am. Oil Chem. Soc.* **67**, 276–280 (1990).
202. Chavan, U. D., McKenzie, D. B. & Shahidi, F. Functional properties of protein isolates from beach pea (Lathyrus maritimus L.). *Food Chem.* **74**, 177–187 (2001).
203. Wang, L., Wu, Z., Zhao, B., Liu, W. & Gao, Y. Enhancing the adsorption of the proteins in the soy whey wastewater using foam separation column fitted with internal baffles. *J. Food Eng.* **119**, 377–384 (2013).
204. Lu, B. Y., Quillien, L. & Popineau, Y. Foaming and emulsifying properties of pea albumin fractions and partial characterisation of surface-active components. *J. Sci. Food Agric.* **80**, 1964–1972 (2000).
205. Samtiya, M., Aluko, R. E. & Dhewa, T. Plant food anti-nutritional factors and their reduction strategies: an overview. *Food Prod. Process. Nutr.* **2**, 1–14 (2020).
206. Wang, S. *et al.* pH-induced conformational changes and interfacial dilatational rheology of soy protein isolated/soy hull polysaccharide complex and its effects on emulsion stabilization. *Food Hydrocoll.* **109**, 106075 (2020).

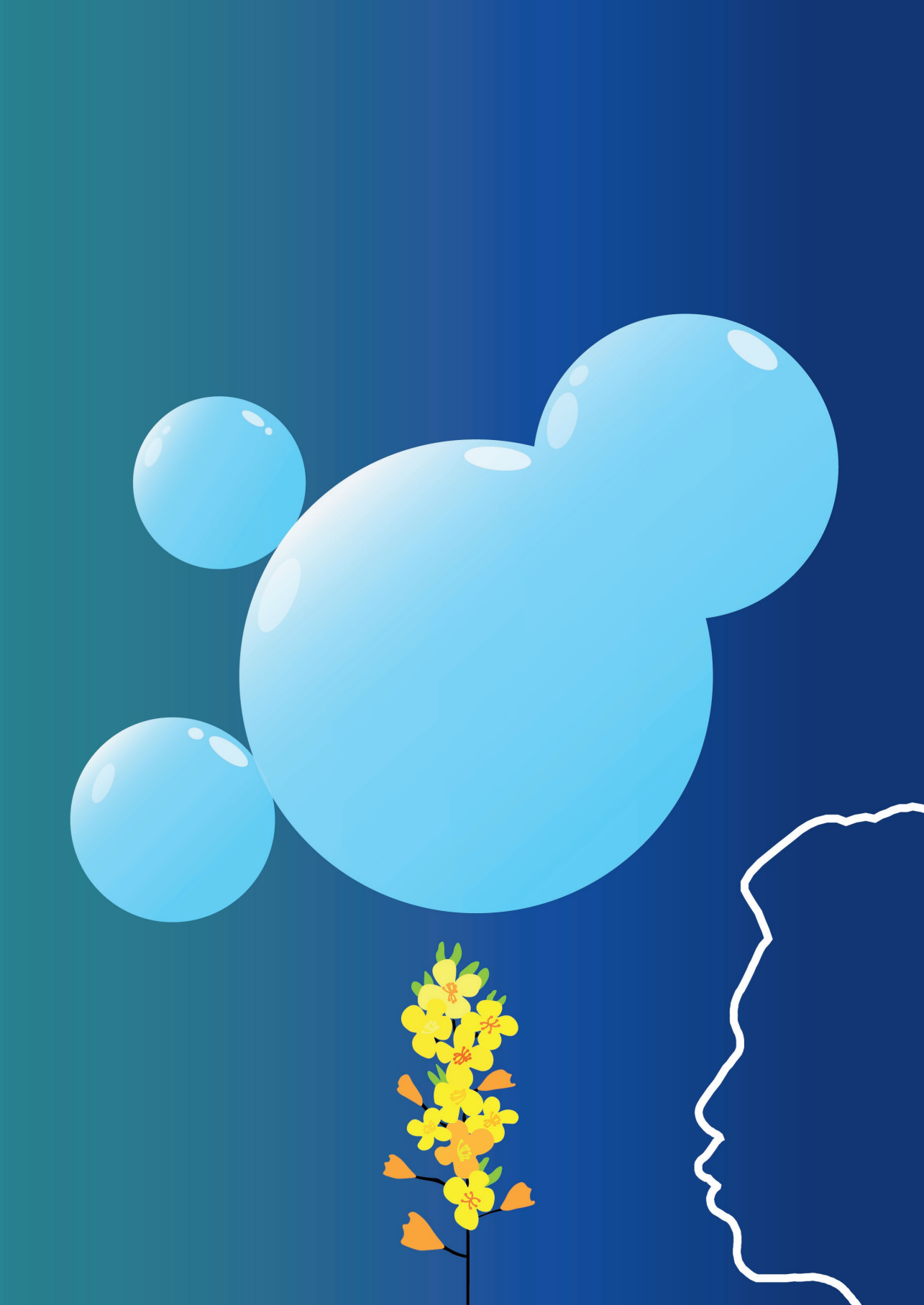

Summary

Sustainable food production is a necessity to meet the increasing demand for food by an increasing world population. A major trend is the protein transition from animal- to plant-derived proteins. As a result, the interest in plant proteins from both industry and academia has been rapidly increasing. Prior to the utilisation of these ingredients, plant proteins must be extracted from the plant or crop. The most common extraction processes are extensive processes with many processing steps, require copious amounts of water and energy, and generate substantial amounts of waste streams. There are also indications that such processing might alter plant protein functional properties, for example, through denaturation of the protein structure and formation of insoluble aggregates. A solution could be milder and more sustainable processes, but less processing leads to protein extracts with lower protein purity due to the presence of more non-proteinaceous components, such as lipids and phenols. The aim of this thesis was to investigate the contribution of these non-proteinaceous components to the interfacial and foaming properties of mildly derived plant protein extracts.

In **Chapter 1**, we discussed the various components in plant crops. Rapeseed was chosen as a model system for our study, as the seeds are high in protein, lipids and phenols. We discussed the conventional/extensive wet extraction method, which is generally performed by protein extraction at an alkaline pH, followed by isoelectric point precipitation to obtain a protein-rich pellet. In our work, we proposed a mild purification method with the requirement of fewer resources and processing steps. Additionally, an introduction was given on the applied toolset in this work, which is a multi-length scale approach, where molecular properties are linked to macroscopic foam properties by an intermediate length scale, also known as the mesoscopic scale. The bridging length scale was extensively studied by characterising the interfacial properties using a combination of nonlinear surface rheology and microstructure imaging. In more detail, the nonlinear contributions in the rheological responses of the interfacial layers were evaluated by constructing Lissajous plots of the surface stress over the applied deformation. The interfacial microstructure was characterised by creating Langmuir-Blodgett films, which were subsequently analysed using atomic force microscopy (**AFM**). With this toolset, we studied complicated mixtures containing protein and non-proteinaceous components, such as lipids and phenols.

In Chapter 2, we first studied the molecular, interfacial and foaming properties of the whole mixture, which was a mildly derived rapeseed protein concentrate (**RPC**), containing 71.7% (w/w) proteins, 8.3% (w/w) lipids, and 2.1% (w/w) phenols. Also, both albumins and globulins of rapeseed were present in the RPC. The RPC formed stiff and viscoelastic solid-like interfacial layers, as shown by nonlinear surface rheology. The stiffness of the RPC-

stabilised interfacial films reduced at higher bulk concentrations, probably due to non-proteinaceous components. This was also demonstrated by the presence of long strands on AFM images of the RPC-stabilised Langmuir-Blodgett films. Therefore, a defatted RPC was produced to evaluate the contribution of the lipids. The interfacial layers were slightly stiffer after defatting, but the foaming properties of both non-defatted and defatted RPC were remarkably comparable. The lipids in the RPC did not have a detrimental effect on the foaming properties, which could be attributed to their colloidal structure, as the lipids exist in the form of oleosomes. These natural lipid droplets are storage organelles of plant oils with a triacylglycerol (**TAG**) core, surrounded by an interfacial layer with phospholipids and membrane proteins. An advantage of mild purification is the extraction of intact oleosomes, which are normally disrupted in the defatting step in the conventional protein extraction process. The exact role of the oleosomes on protein interface and foam stabilising properties was further evaluated in **Chapter 5** and **6**.

Prior to comprehensive studies on the non-proteinaceous components, the aggregation state of the proteins was studied in **Chapter 3**, as plant proteins can exist in a largely aggregated state. Here, we studied native whey proteins (diameter 2 – 10 nm), which were heat-denatured into aggregates (20 – 100 nm), and, finally, cold-gelated into larger whey protein beads (150 – 350 nm). Native whey proteins formed stiff and heterogeneous viscoelastic solid-like layers at the air-water interface, as whey proteins can form densely clustered networks with strong in-plane protein-protein interactions. Increasing the aggregated state to heat-denatured aggregates led to lower surface activity, but a similar rheological behaviour compared to native proteins. In the beads system, smaller non-aggregated or non-gelated constituents were found to dictate the interfacial properties, as smaller and more surface-active material seemed to outcompete the larger aggregated structures for adsorption at the air-water interface. The dominance of smaller non-aggregated material probably also occurred in the heat-denatured aggregate system, as smaller material was found to dominate the Langmuir-Blodgett films. Aggregation of proteins seems to impair the interfacial properties, as the surface activity and in-plane interactions of adsorbed material decreases. Such behaviour may occur in plant protein extracts, as processing steps, such as pH-shifts and heating, can induce protein aggregation, which was carefully discussed in further chapters.

Protein aggregation can also be chemically induced by phenol-protein interactions, which was investigated in **Chapter 4**. A phenol-free protein system is required to study phenol-protein interactions. However, phenols could not be removed from rapeseed proteins without inducing protein denaturation and insolubility. Therefore, a model system was studied using whey proteins and sinapic acid, the most abundantly present phenol in rapeseed. Sinapic acid can interact non-covalently with whey proteins, leading to higher surface activity of the

phenol-protein complex compared to the pure protein. A drawback of such interactions is a weaker interfacial layer, as sinapic acid reduced the in-plane interactions between the proteins. The interfacial layer became even weaker after oxidation of the phenols to a highly reactive form, called quinones. As demonstrated in AFM, these quinones interacted covalently with proteins and cross-linked multiple proteins into large aggregates. Consequently, foaming properties were altered, as phenol-protein interactions led to smaller air bubble sizes, due to higher surface activity. On the other hand, the foams had lower stability, as phenol-protein interactions impaired the in-plane protein interactions at the interface. Understanding the role of phenols on proteins is crucial to examine the contribution of these non-proteinaceous components in plant protein extracts. For example, plant proteins are generally extracted at (extreme) alkaline pH to increase protein solubility. From this chapter, we could expect an accelerated phenol oxidation step at such alkaline pH, leading to the formation of quinones, thereby suggesting the potential formation of phenol-protein aggregates.

In **Chapter 5** and **6**, another major component in our mildly derived RPC was evaluated, namely the oleosomes. First, we studied a model system with whey proteins and rapeseed oleosomes (**Chapter 5**). By microstructure imaging, the oleosomes were found to rupture after adsorption at the air-water interface. Subsequently, the TAG core, phospholipids and membrane proteins started spreading and rearranging at the interface. Oleosomes and whey proteins were found to co-adsorb at the air-water interface, and lipid-rich regions were formed that were surrounded by whey protein clusters. The result was a weak and more easily stretchable interfacial film at low dilatational deformations. At higher deformations, lipids were expelled out of the interface. As a result, proteins started interacting and dominating the rheological behaviour. Additionally, the oleosome membrane proteins were found to be strongly anchored in a continuous phospholipid phase. These membrane proteins largely increased the resistance against deformation of an air-water interfacial layer stabilised by oleosome phospholipids and membrane proteins. Removal of the membrane proteins resulted in a phospholipid layer with little lateral interactions, leading to expulsion of the stabilisers upon compression of the interfacial film.

The findings of the model system in **Chapter 5** were explored for mixtures containing our mildly derived RPC and additional oleosomes (**Chapter 6**). Here, we created mixtures with various RPC to oleosome ratios and also varied the protein concentrations. At low rapeseed protein concentrations (<0.2% w/w), oleosomes and proteins were found to co-adsorb, resulting in an oleosome dominated interface. This led to reduced connectivity between the rapeseed proteins, thus resulted in weaker interfacial layers. At higher protein concentrations or higher protein to oleosome ratios (i.e. fewer oleosomes), the proteins started to dominate the interfacial properties. A similar relationship was revealed for the

foaming properties, as oleosomes have the potential to substantially reduce foamability and foam stability of rapeseed proteins-stabilised foams. Here, the detrimental effect of oleosomes was also reduced, when more proteins were present in the mixture. We discovered by a displacement experiment in a Langmuir trough that oleosomes could not adsorb at the air-water interface, if proteins had formed a sufficiently dense and solid-like layer. This indicates the ability of protein to outcompete the oleosomes for adsorption at the air-water interface, which is largely dictated by the mixing ratios of oleosomes and proteins, and also affects interface and foam stabilising properties.

Finally, in **Chapter 7**, we reviewed the findings of all chapters, and discussed the advantages and drawbacks of mildly derived plant extracts. The phenols and lipids in our RPC did not seem to largely affect the interfacial and foaming properties of the rapeseed proteins. Oleosomes were probably entrapping TAGs and phospholipids in their colloidal structure. This would prevent the adsorption of the lipids at an interface, thus protecting the adsorbed protein layer from the detrimental effect of lipids. Another advantage of mild processing is the co-extraction of both plant albumins and globulins, as in the conventional extraction process, globulins are mainly extracted, while albumins are discarded. Here, we evaluated the potential of albumins as excellent foam stabilisers, similar to dairy proteins, while globulins were revealed to be poor foam stabilisers. Albumins could positively contribute to a protein mixture, such as in our mildly derived RPC. From the findings in this thesis, we formulated three design rules to obtain plant protein extracts with promising functional properties:

1. Phenol oxidation should be avoided, especially at (extreme) alkaline pH;
2. Lipids can be present in the protein extract as long the natural colloidal structure is intact;
3. Isoelectric point precipitation of proteins should be avoided.

The findings in this thesis could only be achieved by performing the earlier described multi-length scale approach. Bridging the molecular and foaming properties by characterising the interfacial properties was highly effective. Here, we have shown a powerful combination of nonlinear surface rheology and microstructure imaging, which allowed us to unravel the composition and mechanical properties of interfaces stabilised by complex mixtures. This toolset is key in linking properties on all these various length scales to the protein purification process. Our approach is suitable to expand the knowledge on plant protein functionality, thereby contributing to the protein transition.

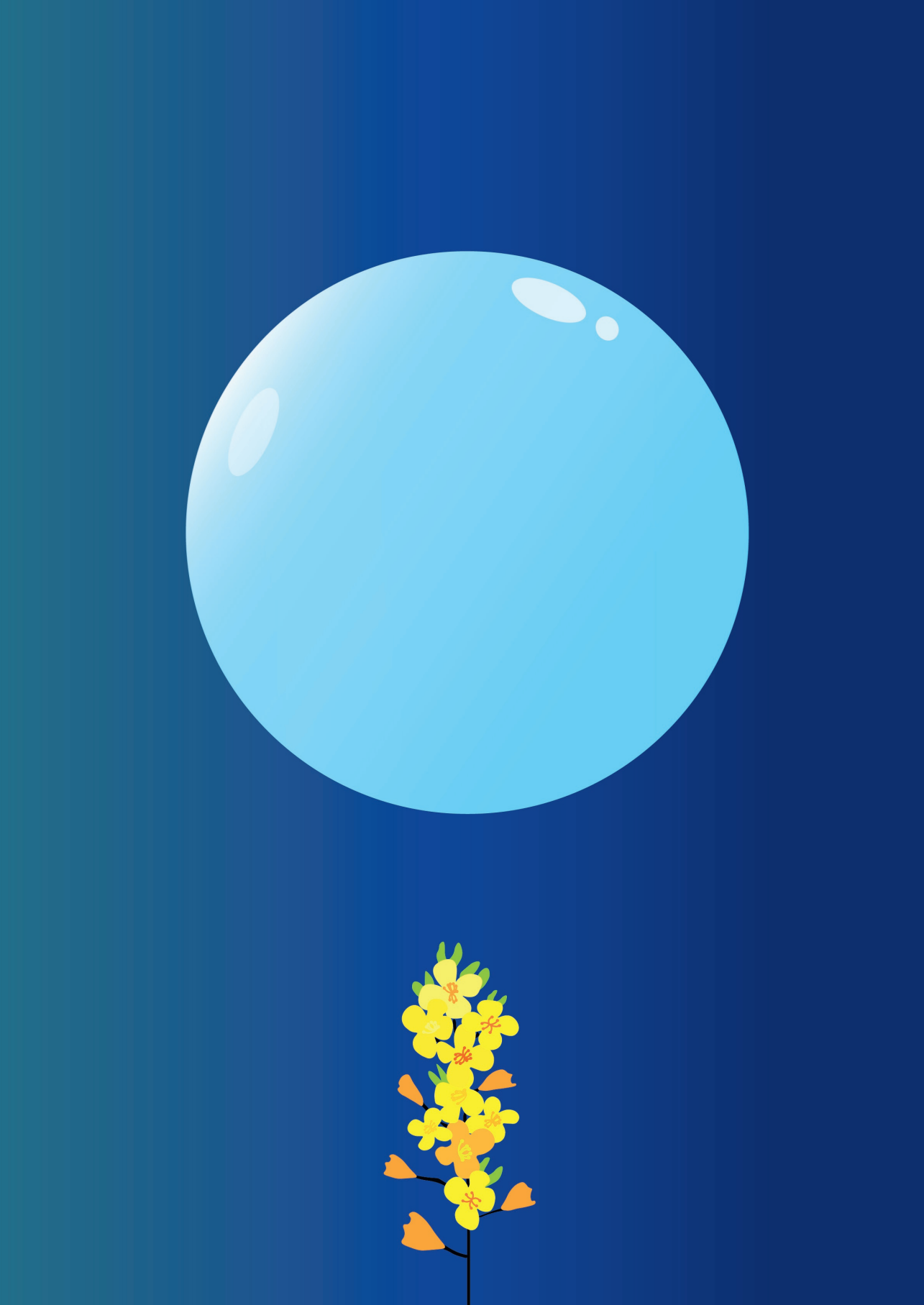

Acknowledgement

I never thought four years could pass at such a rapid pace. It was an amazing journey. There was happiness, there were exciting moments, and sometimes there was hardship. Nonetheless, I enjoyed every moment of it, and am happy and proud of the result. Of course, I could not have done it alone, as many contributed to my PhD project.

First of all, I want to thank my supervisors: Leonard, Claire, Costas & Erik. It was a big team, and each of you supplemented outstanding expertise to this thesis. All four of you helped me and taught me so much. Leonard, you were my direct supervisor, and I would like to thank you for your guidance. From you, I learned the tricks of the trade of interface science, but also the skills of an independent and critical scientist & thinker. Also, I appreciate your open-door policy, as I could always knock on your door for burning questions. Many thanks for your confidence in my abilities and many (side-project) ideas, and for providing me with the freedom and guidance in executing the ideas. Claire, thank you for your efforts and valuable criticism. From the beginning, I noticed that you had a slightly different angle compared to the rest of the team and a strong attention to detail. Combining these traits sometimes led to many comments and track changes on manuscripts. I was slightly overwhelmed at first, but I am grateful for the effort and learned immensely from it. As a result, I am also giving feedback to students and peers in a similar fashion. Costas, I enjoyed our many discussions. You always had the answer I needed to design an experiment or explain points in a manuscript. In addition, thank you for introducing and guiding me through the field of oleosomes, which are remarkable structures. Erik, you always managed to motivate me by highlighting my achievements, and more importantly, by putting findings and results in a broader perspective. This substantially increased the quality of the manuscripts and, of course, this thesis. It really was a pleasure working with all of you, and I am sure we will meet again in the future.

Next, I would like to thank my colleagues at Food Physics. Els, Miranda, Harry, Roy and Floris are the core of a good functioning group. Thank you for the help on countless matters, such as introductions, hunts for chemicals, and so much more! And now the PhDs/postdocs. First, my office Y0025/Y0010: Pauline, Yuan, Joon, Cai, Melika, Qi, Aref and Zhihong. I had a good time in our office with our great talks and practical jokes (such as covering all my desk and stuff with aluminium foil). We were each other's first hotline for help, and also chair decorators for each other's birthdays! Also, thanks to Annika, Arianne, Belinda, Bo, Cai[2], Claudine, Dengfeng, Evelen, Gerard, Joon, Lei, Luka, Manolo, Marco, Monica, Naomi, Ninna, Parisa, Pauline, Phillipp, Raisa, Remco, Suraj, Tijs, Wenjie, Xiangyu, Xiao and Xilong for the good times at coffee/lunch breaks, trips and in the lab. Special thanks to Xilong, Wenjie, Remco, Manolo, Gerard, Evelen, Dengfeng and Claudine. I enjoyed our direct

collaboration in the projects, which led to fruitful insights and findings. A shoutout to Belinda, my karaoke buddy. We need to sing again soon. Elke thank you for alle borrels & gezelligheid. Aref & Lei, double thanks for being my paranymphs!

Then my students: Thiemo, Vera, Hao, Iris, Sarah, Maria, Leonie, Tjitske, Annemiek, Kees, Ralf, Qixin, Babet, Anteun. Thank you all for your efforts during your thesis projects. All of you contributed to my project, and I also learned much from you. It was a pleasure working with you.

For the past four years, I did not only stayed within the boundaries of our lab. I ran around the building and campus, using many different techniques and machinery. Therefore, I would like to thank the technicians and all others involved in the groups FBR, FCH, FPE, FQD, and PCC. Joanne, thank you for helping us initiate the asparagus project!

A PhD can be a lonely job on your own island, but this was not the case for me, as I was part of a TiFN project. With other PhD's we were an archipelago, where all the PhD islands were connected. Eleni, Simha, Maud, Emma, Remco, Dana and Marius, thank you for the great experience in our big project. I liked how we were closely involved in each other projects and the great willingness to help each other! Special thanks to Emma, my interface buddy. We simultaneously started as newcomers to interface science and assisted each other to master many techniques.

The TiFN project did not only consist of PhDs, as many others were involved: Marcel, Irene, Mira, Jan, Martha and Jacqueline. Special gratitude to Helene. Thank you so much for the help with the protein extractions. I also appreciate the involvement of the industrial partners; thank you all for the discussions.

Of course, friends outside work have supported me innumerable times, too many persons to mention. Thanks to the Club8, Bestuur, Sprint, Leidse boys, C8 coaches! I would like to highlight a few individuals. Rosita & Floor, the Wageningen survivors, I enjoyed the many bike trips and dinners we had. Sander & Michel, the Drakar achterblijvers in Wageningen (en omgeving). Thank you for the many coffee meetings we had. Abel, my (almost) neighbour, and also fellow PhD. I appreciate the coffee and long walks through the forest, especially during the lockdowns. Vera, we didn't meet much these 4 years, but I enjoyed our many WhatsApp conversations about the ups and downs of your PhD project! Jelmer, my friend and temporary roommate, we always have a good time & I could always empty my thoughts with you. Kenneth, one of my oldest friends. Thanks for the good times and support. I also have had a mouse arm for three years, and I would not have been able to finish my PhD in time without the many massages of Mike, bedankt!

My dear brother Jimmy. Food is what binds us, and food is what we did. Thank you for the many breakfast, lunches and dinners we had. I might have eaten over 1,000 pieces of sushi these four years.

妈妈爸爸，谢谢你们这么多年的养育和无限的支持。

My love, Carol. You enlightened my life during these years. You were my mental support, practice audience for presentations, proof-reader, reviewer, graphic design advisor, and so much more. Thank you for your help and love. I look forward to our future adventures.

About the author

Jack Yang was born on the 10th of October in Dordrecht, the Netherlands. In 2010, he started the Bachelor programme of Food Technology at the Wageningen University and Research (WUR) in the Netherlands. The programme included a thesis project on the extraction and purification of cashew nut allergens. In the academic year of 2013/2014, Jack paused his study programme for a board year at the student rowing club Argo in Wageningen. He continued into a Master programme in Food Technology with the specialisation of Ingredient Functionality at the WUR. The topic of his Master thesis was the interfacial and foaming properties of whey protein-peptide and β-lactoglobulin mixtures. Afterwards, the MSc programme was concluded with an internship at the Unilever R&D centre in Vlaardingen, the Netherlands, which was on techno-functional properties of plant proteins. In 2017, Jack was hired as a PhD candidate, and his project was part of a larger TiFN consortium called 'Sustainable Ingredients'.

Email: jack.yang9210@gmail.com

List of publications

First authorships

This thesis

Yang, J., Thielen, I., Berton-Carabin, C. C., van der Linden, E., & Sagis, L. M. C. (2020). Nonlinear interfacial rheology and atomic force microscopy of air-water interfaces stabilized by whey protein beads and their constituents. *Food Hydrocolloids*, *101*, 105466

Yang, J., Faber, I., Berton-Carabin, C. C., Nikiforidis, C. V., van der Linden, E., & Sagis, L. M. C. (2020). Foams and air-water interfaces stabilised by mildly purified rapeseed proteins after defatting. *Food Hydrocolloids*, *112*, 106270.

Yang, J., Lamochi Roozalipour, S. P., Berton-Carabin, C. C., Nikiforidis, C. V., van der Linden, E., & Sagis, L. M. C. (2021). Air-water interfacial and foaming properties of whey protein - sinapic acid mixtures. *Food Hydrocolloids*, *112*, 106467.

Yang, J., Waardenburg, L. C., Berton-Carabin, C. C., Nikiforidis, C. V., van der Linden, E., & Sagis, L. M. C. (2021). Air-water interfacial behaviour of whey protein and rapeseed oleosome mixtures. ***Submitted.***

Yang, J., Berton-Carabin, C. C., Nikiforidis, C. V., van der Linden, E., & Sagis, L. M. C. (2021). Air water interfaces and foams stabilised by rapeseed protein and oleosome mixtures. ***Submitted***.

Other works

Yang, J., Kornet, R., Diedericks, C. F., Yang, Q., Berton-Carabin, C. C., Nikiforidis, C. V., Venema, P., van der Linden, E., & Sagis, L. M. C. Rethinking plant protein extraction: albumins – an excellent foaming ingredient. **In preparation.**

Yang, J. Diedericks, C. F., de Wit, A., Venema, P., van der Linden, E., & Sagis, L. M. C. Improving foaming and emulsifying properties of Bambara groundnut proteins by using extensive and mild aqueous extraction methods to obtain the most functional protein composition. ***In preparation.***

Kornet, R.*, **Yang, J.***, Venema, P., van der Linden, E., & Sagis, L. M. C. Optimizing foaming and emulsifying properties by tailored fractionation of pea protein. ***In preparation.***

Yang, J.*, Xia, W.*, Botma, T., Sagis & L. M. C. Selective proteolysis of β-conglycinin as a tool to increase air-water interface and foam stabilising properties of soy proteins. ***In preparation.***

Gimenez-Ribes, G.*, **Yang, J.***, He, Q. & Sagis, L. M. C. Rheological properties of whey protein and escin mixtures – plasticisers on the air-water interface. ***In preparation.***

Yang, J.*, Gimenez-Ribes, G.*, He, Q. & Sagis, L. M. C. Saponin escin – an excellent foam stabiliser in mixture with whey proteins as explained by interfacial rheology. ***In preparation.***

Yang, J.*, Yang, Q.*, Waterink, B., Venema, P., van der Linden, E. & Sagis, L. M. C. Interfacial and foaming properties of various mung bean protein extracts obtained by various extraction methods. ***In preparation.***

Yang, Q.*, **Yang, J.***, Waterink, B., Venema, P., van der Linden, E. & Sagis, L. M. C. Mung bean protein colloids created by coacervate formation - a novel and excellent foam stabiliser explained by a comprehensive study on their interface and foam stabilising properties. ***In preparation.***

Yang, J*, Delahaije, R. J. B. M.*, Sagis, L. M. C., Impact of sedimenting silica beads on pendant drop measurements. ***In preparation.***

Shared first authorship: ∗

Co-authorships

Felix, M., **Yang, J.**, Guerrero, A., & Sagis, L. M. C. (2019). Effect of cinnamaldehyde on interfacial rheological properties of proteins adsorbed at O/W interfaces. *Food Hydrocolloids*, *97*, 105235.

Sagis, L. M. C., Liu, B., Li, Y., Essers, J., **Yang, J.**, Moghimikheirabadi, A., Hinderink, E.B.A. , Berton-Carabin, C.C.… Schroen, K. (2019). Dynamic heterogeneity in complex interfaces of soft interface-dominated materials. *Scientific Reports*, *9*(1), 1–12.

Peng, D., Jin, W., Arts, M., **Yang, J.**, Li, B., & Sagis, L. M. C. (2020). Effect of CMC degree of substitution and gliadin/CMC ratio on surface rheology and foaming behavior of gliadin/CMC nanoparticles. *Food Hydrocolloids*, *107*, 105955

Garcia-Moreno, P. J., **Yang, J.**, Gregeren, S., Jones, N., Berton-Carabin, C.C., Sagis, L. M.C., Hoffmann, S. Marcatili, P.… Jacobsen, C. (2021) The structure, viscoelasticity and charge of potato peptides adsorbed at the oil-water interface determine the physicochemical stability of fish oil-in-water emulsions. *Food Hydrocolloids,*

De Groot, A., **Yang, J.**, Sagis, L. M. C., The potential of white asparagus waste streams as air-water interface and foam stabilising ingredient after mild protein purification. ***In preparation***

De Groot, A. **Yang, J.**, Sagis, L. M. C., An in-depth analysis of the dilatational rheological response of protein-stabilised interfaces. ***In preparation***

Overview of completed training activities

Discipline specific courses		
Rheology course	Wageningen, the Netherlands	2018
AERC Rheology course	AERC, Online	2021
Conferences and Symposia		
Rheology workshop[1]	Wageningen, the Netherlands	2017-2018
17th Food Colloids conference[1]	Leeds, United Kingdom	2018
16th IACIS conference[1]	Rotterdam, the Netherlands	2018
1st Oil Body Conference[1]	Wageningen, the Netherlands	2018
Edible Soft Matter workshop[1]	Le Mans, France	2019
8th ISFRS conference[1]	Zürich, Switzerland	2019
33th EFFoST conference[2]	Rotterdam, the Netherlands	2019
Nizo Plant Protein conference[2]	Nizo, Online	2020
34th EFFoST conference	EFFoST, Online	2020
Conference S&T for Meat Analogues	Wageningen, Online	2021
Oil Body symposium[1]	Wageningen, Online	2021
AERC conference[1]	AERC, Online	2021
General courses		
Competence assessment	WGS, the Netherlands	2017
VLAG PhD week	VLAG, the Netherlands	2017
Philosophy and ethics in Food Science	VLAG, the Netherlands	2018
Teaching and supervising thesis students	WGS, the Netherlands	2018
Scientific writing	WGS, the Netherlands	2018
Posters and pitching	WGS, the Netherlands	2018
Reviewing a scientific paper	WGS, the Netherlands	2018
Storytelling	WGS, the Netherlands	2018
Effective behaviour in your professional surroundings	WGS, the Netherlands	2018
Scientific artwork	WGS, the Netherlands	2019
Infographics and iconography	WGS, the Netherlands	2019
Adobe InDesign	WGS, the Netherlands	2019
PhD workshop carousel	VLAG, the Netherlands	2019
Presenting with impact	WGS, the Netherlands	2020
Popular Science Writing	WGS, the Netherlands	2021
Career orientation	WGS, the Netherlands	2021
Other activities		
Preparation of research proposal	Wageningen, the Netherlands	2017
PhD study trip[1,2]	Singapore and Indonesia	2018
Weekly group meetings at FPH[1]	Wageningen, the Netherlands	2017-2021
Quarterly project TiFN/partner meetings[1,2]	Wageningen, the Netherlands	2017-2021

Oral[1] or poster[2] presentations

Colophon

This research formed part of a project that was organised by TiFN, a public-private partnership on precompetitive research in food and nutrition, and executed under its auspices. The public partners were responsible for the study design, data collection and analysis, decision to publish, and preparation of the manuscript. The private partners Danone, Fromageries Bel, Pepsico, Unilever have contributed to the project through regular discussions. Co-funding for the project was obtained from the Netherlands Organisation for Scientific Research (NWO) and the Top-Consortium for Knowledge and Innovation Agri&Food (TKI).

Financial support from Wageningen University and TiFN for performing this research as well as for printing this thesis is gratefully acknowledged.

Cover design: Jack Yang

This thesis was printed by Proefschriftmaken (80 copies)